NOVEMBER, 1951

Journal of METALS

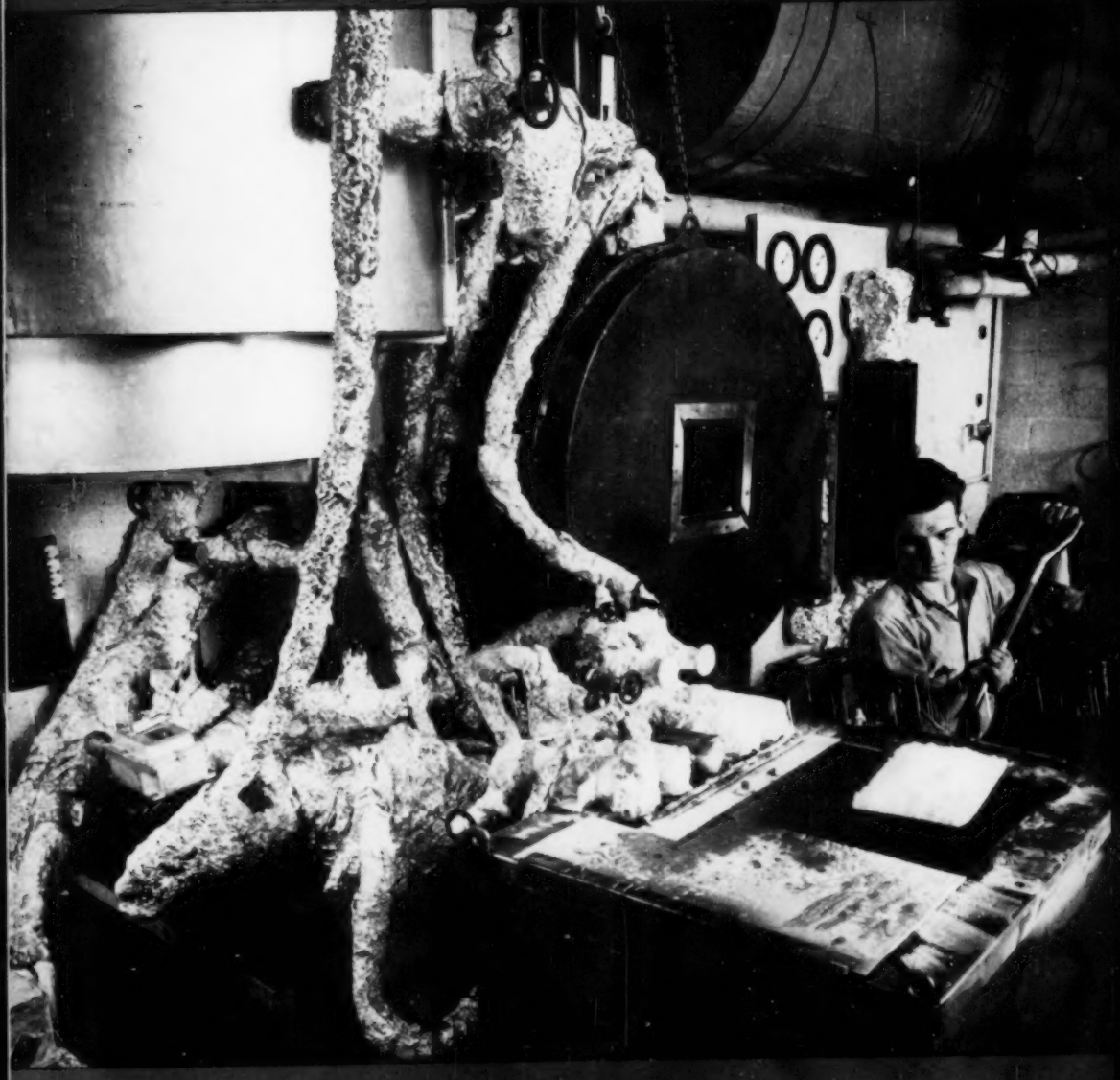

November JOURNAL OF METALS Highlights:

"Hot Workability of Stainless Steel Improved by Adding Cerium and Lanthanum" - p. 973

"Effect of Rare-Earth Metals on the Properties of Extruded Magnesium" - p. 987

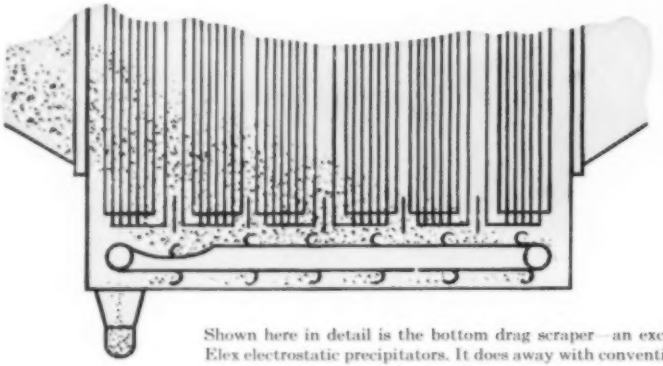

Let's be practical about precipitators

Shown here in detail is the bottom drag scraper—an exclusive feature of Koppers-Elex electrostatic precipitators. It does away with conventional hoppers and simplifies operation by removing dust continuously.

Continuous dust removal

is just one of the many advantages you get with

Koppers-Elex Electrostatic Precipitators

IN ADDITION to high recovery rates, Koppers-Elex electrostatic precipitators offer you *continuous dust removal*. The Koppers exclusive drag scraper operating on a flat bottom replaces the conventional type hopper—with its trouble of dust build-up and clogging. Dust is fed from the precipitator at a uniform rate which simplifies disposal or storage.

Other features of Koppers-Elex precipitators include separately energized multiple series fields which provide maximum collection of very fine particles. This same feature protects your investment in still another way since the outage of one field does not halt the gas-cleaning action of the precipitator.

To get maximum recovery and effective nuisance abatement, specify Koppers-Elex electrostatic precipitators. For the metallurgical field Koppers has two distinct designs: the dry dust precipitator for hearth, flash, fluidized roasters, etc. . . . and the acid mist precipitator for secondary cleaning.

IF YOU HAVE A GAS-CLEANING PROBLEM, write and outline the details for us to review. There is no obligation. Just address your letter to: KOPPERS COMPANY, INC., *Precipitator Dept.*, 361 Scott St., Baltimore 3, Maryland.

PERFORMANCE GUARANTEED!

Koppers engineers protect your investment in an electrostatic precipitator by guaranteeing both the recovery or gas-cleaning *efficiency* and the *residual content* left in the gas after cleaning. Koppers-Elex electrostatic precipitators are designed, engineered, fabricated, erected, and guaranteed *under one contract* by Koppers Company, Inc.

KOPPERS

Koppers-Elex ELECTROSTATIC PRECIPITATORS

Journal of METALS

VOL. 3, NO. 11 NOVEMBER, 1951

Published to provide a continuing, authoritative, and up-to-date record of technological, engineering, and economic progress in all branches of the metals industry by the
Metals Branch
American Institute of Mining and Metallurgical Engineers, Inc.
29 West 39th Street, New York 18

THOMAS E. LLOYD
Manager of Publications
Editor, Journal of Metals

A. S. COHAN Associate Editor

D. G. GARRETT MARGARET BAGG
Assistant Editors

GRACE PUGSLEY Production Manager

W. J. SEWING Asst. Prod. Mgr.

METALS BRANCH COUNCIL
C. C. Long Chairman
E. O. Kirkendall Secretary
R. M. Brick IMD Chairman
T. L. Joseph ISD Chairman
O. C. Ralston EMD Chairman
M. Gensamer D. S. Eppelsheimer
H. K. Work Evan Just

TECHNICAL PUBLICATIONS COMMITTEE
J. I. Laudermilk Chairman
E. J. Kennedy, Jr. Secretary

AUXILIARY PUBLICATIONS COMMITTEE CHAIRMEN
M. Gensamer Institute of Metals Div.
A. G. Forrest Iron & Steel Div.
J. Glosser Extract. Metal Div.

JAMES A. STANGARONE
Advertising Manager

B. C. SNELL
Regional Manager, Pittsburgh
1110 McDonald Place, Sewickley, Pa.

The AIME Publishes:
Journal of Metals
Mining Engineering
Journal of Petroleum Technology

COVER

Jet engine accessories, such as fuel pumps, control mechanisms, and metering devices must work even at temperatures as low as —67°F. In the test pictured at Westinghouse Aviation Gas Turbine Div., Philadelphia, super-cold alcohol is circulating through the engine's fuel pump, which is installed in the windowed black cylinder in the center. Crinkled aluminum foil, pressed in place by hand, is used to insulate the pipes that control the flow of fuel. Dry ice is being shoveled into a cold-chest containing a tank of fuel to be sent through the pump under test.

NEWS

Journal of Metals Reporter	971	New Products	961A
"Drift of Things"	972	AIME News	1077
Employment Service	962	Coming Events	1078
Meet the Authors	959	Personals	1079

TECHNICAL FEATURES

Hot-Workability of Stainless Steel Improved by Adding Cerium and Lanthanum — C. B. Post, D. G. Schaffstall, H. O. Beaver — 973

Solid Solution Alloys of Mg with Li and In — W. R. Hibbard, Jr., A. L. Kearney, W. H. Hawley, Jr., E. C. Burke — 978

Refractory Coatings Upgrade Mild Steel — 980

TRANSACTIONS

Work Hardening-Reannealing Cycle of Pure Silver — M. Balicki, G. Leeds — 981

Effect of Rare-Earth Metals on the Properties of Extruded Magnesium — T. E. Leontis — 987

Preferred Orientation in Zirconium — R. K. McGeary, B. Lustman — 994

Grain Growth and Recrystallization Characteristics of Zirconium — F. J. Dunkerley, F. Pledger, V. Damiano, J. Fulton — 1003

Chromium-Nickel Phase Diagram — D. S. Bloom, N. J. Grant — 1009

Free Energy of Formation of Cementite and the Solubility of Cementite in Austenite — L. S. Darken, R. W. Gurry — 1015

Habit Phenomenon in the Martensitic Transformation — E. S. Machlin, M. Cohen — 1019

Metallographic Techniques for Austenite Grain Size of Steels in the As-Cast State — E. A. Loria — 1029

Low Sulphur Steel from High Sulphur Raw Materials and Fuel — F. L. Robertson, C. H. Bacon, J. W. Till — 1031

Discussion—Extractive Metallurgy Div. — 1045

Discussion—Iron and Steel Div. — 1047

Discussion—Institute of Metals Div. — 1056

Published the first day of each month by the American Institute of Mining and Metallurgical Engineers, Inc., 29 West 39th Street, New York 18, N. Y. Telephone: PEnnsylvania 6-9220. Subscription $8 per year for non-AIME members in United States and North, South and Central America; $9, foreign; $6 for AIME members, or $4 additional in combination with a subscription to "Mining Engineering" or "Journal of Petroleum Technology". Single copies, 75 cents; special issues, $1.50 . . . The AIME is not responsible for any statement made or opinion expressed in its publications. . . .
Copyright 1951 by the American Institute of Mining and Metallurgical Engineers, Inc. . . .
Registered cable address, AIME New York . . . Indexed in Engineering Index, Industrial Arts Index and Chemical Abstracts . . . Reentered as second-class matter Sept. 21, 1949, at the post office at New York, N. Y., under the Act of March 3, 1879. Additional entry established at Manchester, N. H.

THE MORGAN
AIR EJECTOR
gives the draft you want
quickly . . inexpensively

You do not have to invest a fortune in foundations and stacks to exhaust gases from furnaces and boilers, or to discharge acid or other fumes.

It has been proven many times that a Morgan Air Ejector will do the job better and at far less cost.

Write us and let us explain in detail.

CCC-16

MORGAN CONSTRUCTION CO.

WORCESTER, MASSACHUSETTS

ROLLING MILLS • MORGOIL BEARINGS • WIRE MACHINERY
COMBUSTION CONTROL • PRODUCER GAS MACHINE

HOW IT OPERATES

Cool air is directed upward through the venturi throat, creating a powerful suction in the stack. Superheated gases, fumes, etc., are drawn out without passing through the fan. The gases are mixed with cool air and discharged at low temperature to the atmosphere.

MEET THE AUTHORS

M. BALICKI

L. S. DARKEN

R. W. GURRY

C. H. BACON

J. W. TILL

M. Balicki (p. 981) was born in Poland, and was associated with University of Mining and Metallurgy at Cracow after his graduation. With the onset of war, he escaped from Cracow in 1939 and joined the Polish Army in France. With the fall of France, he managed to get to England, where he did research at Swansea University College, until recalled to London to act as professor of metallurgy for the Polish Board of Technical Studies. Now professor of metallurgical engineering at Polytechnic Institute of Brooklyn, he holds membership in AIME, ASM, and numerous societies here and abroad. An ardent sportsman, he likes skiing, mountain climbing, rowing, and won the 1938 championship of Poland in single and double sculls.

R. K. McGeary (p. 994) received his B.S. and M.S. degrees from University of Pittsburgh. After graduation he started in the Westinghouse Electric Corp. student training program, and is now senior scientist in the Atomic Power Div. He enjoys sports as a participant and as a spectator.

L. S. Darken (p. 1015) graduated from Hamilton College and received his Ph.D. degree from Yale University. A physical chemist in the United States Steel Co. Research Laboratory, he has contributed over a dozen papers to the Institute. Bowling and bridge are the hobbies of this member of AIME, ACS, N.Y. Academy of Sciences, and Sigma Xi.

R. W. Gurry (p. 1015) is associated with the Research Laboratory of United States Steel Co. of Kearney, N. J. He was awarded B.S. and Ph.D. degrees by Union College and Yale University respectively. A member of ACS, his hobbies are music, gardening, and sailing.

E. A. Loria (p. 1029), senior engineer at Carborundum Co., Niagara Falls, was formerly associated with Mellon Institute of Industrial Research and Carnegie-Illinois Steel Corp. This author of over 25 technical papers belongs to AIME, ASM, and AFS.

C. H. Bacon (p. 1031), born in Essex, England, was educated at Cambridge University. Previously associated with Ford Motor Co. in England, he is now metallurgist, refractories technologist, and openhearth furnace metallurgist for John Summers & Sons Ltd., Hawarden Bridge Steelworks, Shotton, Chester, England. Photography and sailing are the pastimes of this member of the British Iron & Steel Inst., and Ceramic Society.

F. L. Robertson (p. 1031) was born in Glasgow, Scotland, and graduated from Glasgow University. He has been connected with the Brown-Firth Research Laboratories, Steel Co. of Japan, Blochairn Steelworks, Shelton Iron, Coal, and Steel Co. Ltd., and is now steelmaking consultant to John Summers & Sons Ltd. He commanded the 52nd (Lowland) Div. Signals from 1929 to 1934, and retired with the rank of Brevet Colonel.

J. W. Till (p. 1031) was born in Wednesbury, Staffs, England, and studied at Stafforshire County Technical College and London City Guild Institute. Now technical assistant to steelmaking consultant, John Summers & Sons Ltd., he was formerly with Birchley Rolling Mills Ltd., Stewarts & Lloyds Ltd., and Cloverdale Steel Works, Scotland. A member of the British Iron & Steel Institute and Institution of Metallurgists, his hobbies are literature, model making, social service, and technical lecturing.

T. E. Leontis (p. 987) received M.E., M.S., and S.D. degrees from Stevens Institute of Technology and Carnegie Institute of Technology. He has been associated with Vanadium Corp. of America, Stevens and Carnegie Institutes of Technology, Dow Chemical Co., and is now metallurgist for the AEC at a plant built under Dow Chemical Co. supervision. This member of AIME and ASM has been a previous contributor to Institute publications.

V. Damiano (p. 1003), a graduate of the University of Pennsylvania, is research assistant and candidate for an M.S. degree at that school. A student associate of AIME, his hobbies are photography and golf.

PROFESSIONAL SERVICES

Limited to AIME members, or to companies that have at least one AIME member on their staffs. Rates $40 per year per inch.

MAX STERN
Consulting Engineer
Expert for Scrap Recovery and Shipwrecking — Modernization of Plants and Yards for Ferrous and Nonferrous Metal Scrap
150 Broadway New York 7, N. Y.

ST & CO. INC.
ENGINEERS
CONSULTANTS
METALLURGISTS
Small Jobs Welcomed
SAM TOUR & CO., INC.
Laboratories and offices
44 Trinity Place, New York 6, N. Y.
Testing—Certifying
American Standards
Testing Bureau, Inc.

R. S. DEAN LABORATORIES, INC.
Consulting, Research Development Chemistry, Electrochemistry, & Metallurgy Laboratory Research on a Contract Basis
5810—47TH AVENUE AP-2821
RIVERDALE, MD.

LEWIS B. LINDEMUTH
Consulting Engineer
140 CEDAR STREET, NEW YORK 6, N. Y.
STEEL PRODUCTION
DESIGN · OPERATION · CONSTRUCTION · METALLURGY

Bailey EQUIPMENT

PIG CASTING MACHINES

Ruggedly constructed for low-cost service, this machine is completely self-contained. If necessary it can be moved by crane and erected wherever needed. Once it is set in place, only an electrical connection is necessary for operation. Bailey Stationary Wheel design eliminates 80% of the moving parts of the conventional type. Capacities, 3 tons per hour to 50 tons per hour. Lengths, 15 ft. to 100 ft. in multiples of 5 ft. The standard Bailey machine for blast furnaces is made in lengths of 100 to 250 feet as required.

CLAY GUN

Best results and safety in plugging blast furnace tapping holes are obtained with the Bailey Clay Gun. A powerful electrically-driven piston assures unfailing performance. The special Bailey Lever Action forces the nose of the gun forward with positive accuracy. A powerful, motor-driven screw provides the piston pressure necessary to maintain long tapping holes.

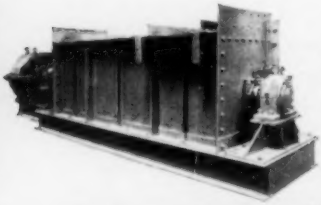

PUG MILLS

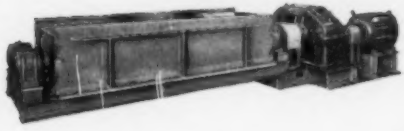

Service records of up to twenty years continuous operation prove the soundness of Bailey Pug Mill design and construction. Types for either Dust Catcher or Sintering Plant service, single or double shaft, direct or rope drive. Bailey Pug Mills can be built to any required capacity.

In addition to the equipment shown here, Bailey offers the following items:

- **Cinder Notch Stopper**
- **Blast Furnace Cold Blast Valve**
- **Blast Furnace Blow-off Valve**
- **Check and Snort Valves**
- **Mixer and Check Relief Valve**
- **Blast Furnace Stove Checker**
- **Fabricated Steel Stove Bottom**
- **Precision Table Feeder**
- **Ladle Skulling Hook**
- **Check Valve for Cold Blast Main**

BRINGS *Safety* AND *Efficiency*

to ***STEEL MILL OPERATIONS***

Recognized throughout the iron and steel producing industry for dependability and highest quality, Bailey equipment meets the vigorous requirements of many vital operations. Some of the principal items of Bailey equipment are shown on these pages.

BAILEY GOGGLE VALVES

MECHANICAL TYPE

Bailey Goggle Valves provide a tight, positive seal for shutting off gas mains in emergencies or for repairs. They operate by a powerful clamping force which is applied equally at all points around the disc periphery. Regardless of time between operations, they open or close instantly. Sizes from 6" to 72", totally enclosed if desired.

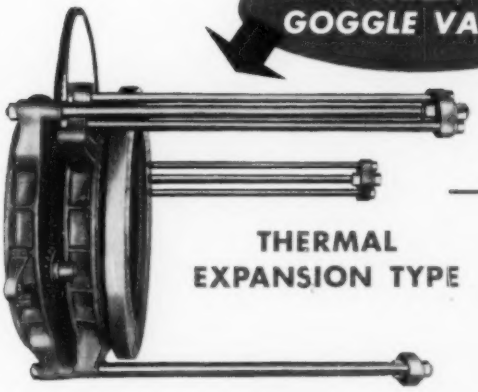

THERMAL EXPANSION TYPE

The Bailey Thermal Expansion type Goggle Valve is operated by the linear expansion and contraction of the three sets of tubes spaced around the rigid steel flange. When steam is passed into the tubes, thermal expansion of the tubes frees the goggle plate. When the steam is removed, contraction closes the flanges against the goggle plate. Diameters of 36" to 120"

WILLIAM M. **Bailey** COMPANY

ENGINEERS

LEADERSHIP THROUGH QUALITY

1221 BANKSVILLE ROAD **PITTSBURGH 16, PA**

New Products

New Products | New Literature | New Services

For Further Information or Literature on any Product, Fill in the Coupon and Send to JOURNAL OF METALS
Students are Requested to Apply Directly to Manufacturers for Bulletins and Information

1—STRATOSPHERE CHAMBER: This stratosphere chamber, designed and built by *Tenney Engineering, Inc.*, will duplicate atmospheric pressures at all heights from sea level to 70,000 ft, temperatures from 185°F to —85°F. The chamber is 18x14x28 ft. A perfect seal of door and chamber is obtained by air cylinders located at each corner of the door to exert the required pressure, and 12-in. steel channel sections set on 12-in. centers within all outside surfaces provide reinforcement against external pressure when the vacuum system is in operation.

2—INDUSTRIAL GAMMA TUBE: A stainless steel tube especially designed for industrial process control procedures using gamma rays and for cosmic ray counting has been developed by *Tracerlab, Inc.* The fill gas used is helium with an organic quench and the tube has a recovery time of approximately 200 microsec. Overall dimensions of the standard tube are 15¼x1 in. OD.

3—POWER BRUSHES: Power brushes manufactured by *Osborn Mfg. Co.* remove heat treat scale and prepare the strip surface for name etching. These two operations were formerly done by machines having six brushing heads. However, improvements have enabled the manufacturer to reduce to a two-station automatic machine that does both operations simultaneously. The cutting tool strip is pulled through the brushes at 50 fpm and the brushes rotate at 3450 rpm.

4—NYLON VALVE SEATS: Small seats machined from nylon rod supplied by the *Polymer Corp.*, are made for use in oxygen, hydrogen and helium regulators, as well as for high pressure aircraft check valves.

5—SUSPENSION ARM: A 4000-lb capacity fork truck equipped with a special ram type suspension arm has reduced keg handling time by more than 75 pct. Formerly, 500 to 800-lb kegs of electrolytic nickel were hauled by hand truck and stood on end without being stacked. Now, they are picked up four at a time by the special arm and grippers, hauled at speeds up to 5 mph and stacked four and five high. *Mercury Mfg. Co.*

6—FLUORESCENCE ANALYSIS UNIT: This new unit incorporates design improvements to facilitate rapid qualitative and quantitative analysis of constituents in metals, alloys, minerals, ores, and chemical mixtures. It is in production at *North American Philips Co.* and it employs a wide range vertical goniometer with a sweep radius of 170 mm. The unit operates at potentials up to 50 kv peak and at current values up to 50 ma.

7—INDUCTION FURNACE: A new 60-cycle induction furnace for heating nonferrous metals and some applications of steel has been developed by *Loftus Engineering Corp.* The process involves a transformer that converts balanced 3-phase power into 2-phase operation. Two closely interlaced coils, leading off this 2-phase line surround the billet and provide all the characteristics of uniformity and through penetration of single phase heating.

8—AUTOMATIC FEED ROUTER: An automatic, electronically controlled power feed router and skin mill has been introduced by *Onsrud Machine Works, Inc.* A 39 hp motor supplies power for routing aluminum stock of 1 in. or more in thickness. It also handles skin milling of large aluminum pieces used to form wings. A 40 hp, 5400 rpm direct-driven liquid cooled motor provides all the power necessary for tough milling work. Three table widths are available for routing or skin mill applications with bed lengths furnished in multiples of 15-ft sections plus 7 ft for conveyor.

9—WATERLESS HAND CLEANER: When rubbed into the skin, this cleaner turns to a liquid and loosens dirt, grime, rubber cement, paint, etc. Manufactured by *Boyer-Campbell Co.*, it contains a good solvent, buffered by emollient oils, petrolatum and soothing lanolin to protect the skin.

10—AIR SCREW DRIVERS: A line of cushion clutch air screw drivers in three sizes for general manufacturing operations has been announced by *Ingersoll-Rand.* These screw drivers have adjustable exhaust deflectors permitting operators to direct the exhaust air as desired. Thirty-eight sizes are available for all speeds and capacities.

11—CONDENSIFIER: A device that removes water, oil, sludge, and other foreign materials from compressed air is a new development of *Hankison Corp.* It combines in a single unit a dehydrating device, mechanical filter and self-purging trap. It is recommended for purifying and dehydrating compressed air used in combustion and process control; in soaking pit, blast furnace and open hearth control; and in operating boilers, and sand blast and laboratory equipment.

12—DESICCATOR: A new desiccator used effectively for storage of either hot or cold crucibles in a size range from No. 000 to 3, or of metallurgical, biological, and chemical samples up to 3x5½ in. has been announced by *Bethlehem Apparatus Co., Inc.*

13—CORROSION PREVENTION: A method of preventing rust and corrosion of metal parts in the presence of air and moisture is provided by VPI crystals. A slightly volatile amine nitrite, it is now available from *Shell Oil Co.* Being slightly volatile at atmospheric temperatures, VPI gives off vapors that are carried by convection and diffusion to all surfaces of the metal, where they condense to provide a thin protective layer. It will also arrest corrosion at any advanced stage. When using VPI, ventilation of the enclosure in which parts are stored should be kept to a minimum to insure the maximum protection period, and the parts should be no further than 2 ft from the VPI source.

Journal of Metals
29 West 39th St.
New York 18, N. Y.

November

Please send me
- More Information ☐
- Free Literature ☐
- Price Data ☐

on items indicated

1	2	3	4	5	6	7	8	9	10
11	12	13	14	15	16	17	18	19	20
21	22	23	24	25	26	27	28	29	30
31	32	33	34	35	36	37	38	39	40

Name _____ Title _____
Company _____
Street _____
City and Zone _____ State _____

Free Literature

20—EXPANSION JOINTS: New catalog containing over 78,000 possible combinations of bellows type expansion joints has been published by *Solar Aircraft Co.* These assemblies are manufactured in sizes from ½ in. pipe size to 75 in. pipe size covering a complete line of pressures from vacuum to 1000 lb. They are fabricated from stainless steel and a variety of heat and corrosion-resisting alloys.

21—HYDRAULIC VALVES: Catalog 203 lists all standard hydraulic valves offered in industry. Available from *Rivett Lathe & Grinder, Inc.*, working drawings and specifications are furnished for each model and size valve. Also described are 25 models of oil pilot valves for remote control of main 4-way valves.

22—ANNIVERSARY BOOKLET: Booklet available from *United Engineering & Foundry Co.* highlights company's progress during 50 years since organization and its position in the industry today.

23—POWER CONVERSION UNITS: Brochure on metallic rectifier power conversion units is now obtainable from *General Electric Co.* Bulletin GEA-5658 describes the features of the equipment, application, and operation. A specification guide for GE dc power supplies and exciters is also included, as well as complete rating charts and dimensions.

24—POTENTIOMETERS: To describe design and construction features of high-precision Wenner potentiometers, *Leeds & Northrup Co.* has issued a revised catalog. Low range instrument and high range are discussed and a listing of recommended accessory equipment is included.

25—ELECTRONIC TUBE: Booklet devoted to industrial electronic and special purpose tubes has been published by *Milo Radio & Electronics Corp.* Designed for industrial use, the booklet furnishes complete technical specifications on special purpose electronic tubes used in various industrial applications.

26—NICKEL ALLOYED CAST IRONS: Applications and comparative service data in many industrial fields are presented in 36-p bulletin from *International Nickel.* High or low controlled expansion, magnetic or nonmagnetic properties and resistance to thermal shock add variety to its usefulness.

27—SOLENOID VALVES: Catalog 710, *Hauck Mfg. Co.*, describes solenoid valves for dependable shut-off on oil pressures up to 300 psi heavy grades as well as light fuel oils, oil temperatures up to 250°F and both UL and FM approval. The rotating cam feature provides a shearing and wiping action to clear away foreign particles in the oil and insure shut-off of oil without leakage.

28—METAL FABRICATION: Booklet available from *Electro Chemical Co.* illustrates many of the precision parts turned out by the firm. Production of parts varying in size from miniature watch dial to panels a yard long, with draws up to 5 in. deep, is permitted with presses ranging from 5 to 600 tons.

29—LIQUID LEVEL CONTROLLERS: Specification sheet 412-2 issued by *Minneapolis-Honeywell Regulator Co.* covers internal float and external float cage liquid level controllers used to maintain liquid level in surge tanks, feedwater heaters, etc. The sheet gives pertinent specification data such as sizes, construction, materials, ratings, and complete dimensions for mounting.

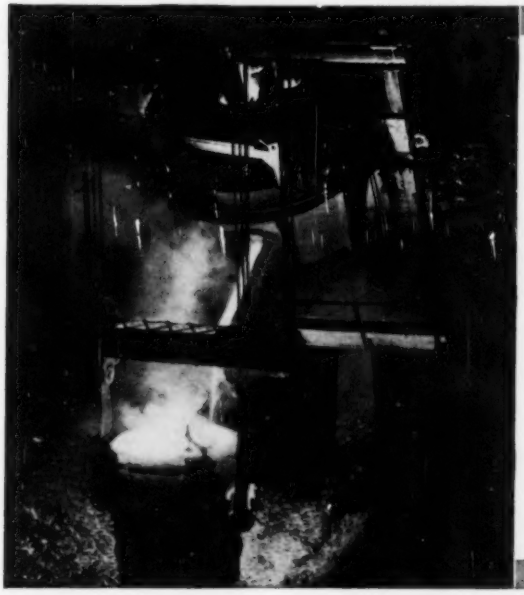

Heroult

ELECTRIC MELTING FURNACE

. . . as ever, the dependable furnace for the production of high-grade stainless, alloy and rimming steels.

Removable roof of new design now available for the larger furnaces.

AMERICAN BRIDGE COMPANY
General Offices: Frick Building, Pittsburgh, Pa.

Contracting Offices in New York, Philadelphia, Chicago, San Francisco and other principal cities
United States Steel Export Company, New York

USS AMERICAN BRIDGE
UNITED STATES STEEL

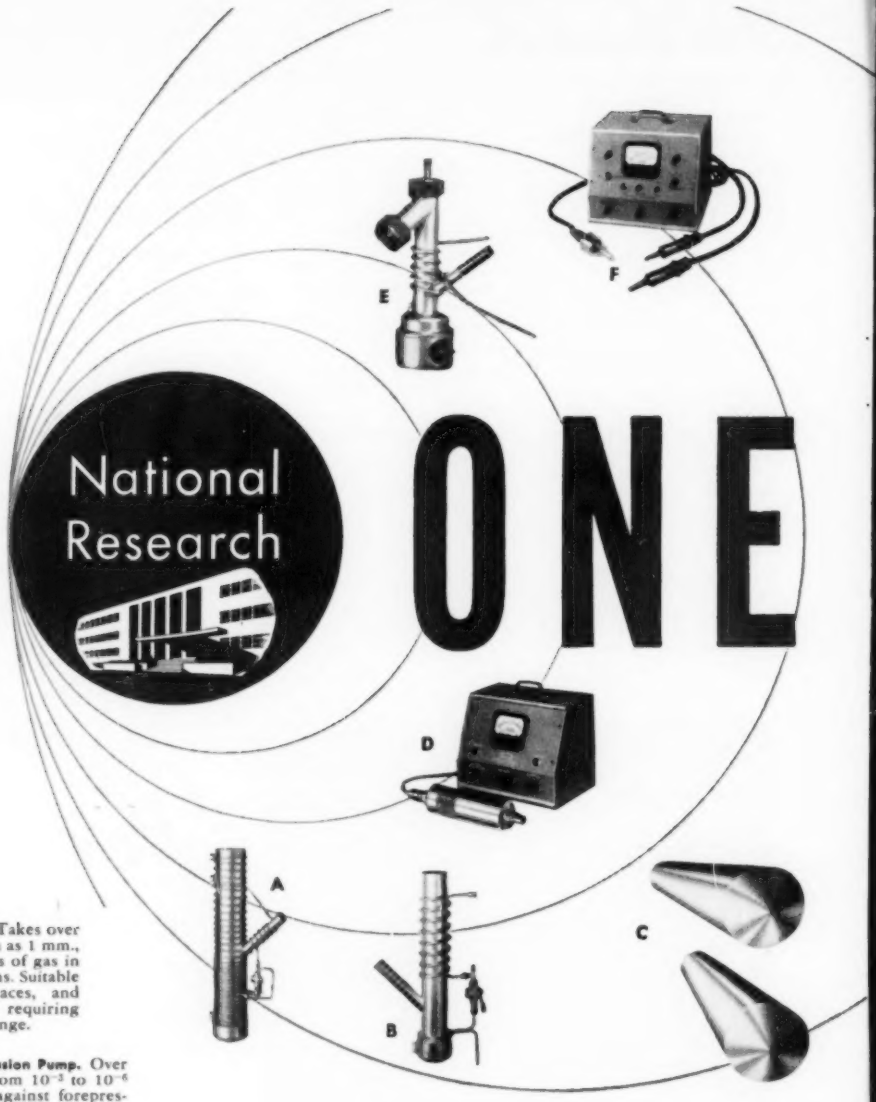

(A) B-4 Booster Pump. Takes over at forepressures as high as 1 mm., handling large amounts of gas in range of 1 — 30 microns. Suitable for evaporators, furnaces, and other vacuum systems requiring high capacity in this range.

(B) H-2-P Purifying Diffusion Pump. Over 50 liters per second from 10^{-3} to 10^{-6} mm. range. Operates against forepressures as high as 0.300 mm. Blank-off 2×10^{-7} mm.

(C) Gas Free High Purity Metals. Copper, nickel, cobalt and iron. Special melts on request. Ingot weights up to 600 pounds.

(D) Alphatron* Vacuum Gauge. Accurate gauging from 10 mm. to 1 micron. A rugged metal ionization type instrument which can be adapted for recording, controlling, gas filling, and leak detection.

(E) B-1 Booster Pump. A small pump designed for rotary exhaust equipment used in miniature and subminiature tube production. Useful where a small pump is required to quickly obtain pressures in the region of one micron.

(F) Type 710 Thermocouple-Ionization Gauge Control. One instrument for scientific and industrial vacuum gauging. Incorporates two thermocouple gauges (1 — 1000 microns) and one ionization gauge (10^{-3} mm. to 10^{-8} mm. Hg. range) in one control. Automatic input regulation and protective circuit.

(G) Standard Vacuum Furnace. A versatile packaged unit to melt, pour, heat treat, degas, sinter, and anneal under high vacuum or controlled atmospheres. Temperatures up to 2000° C.

(H) Vacuum Seals. For introducing motion, power, or connecting gauges.

(I) High Vacuum Valves. Available in sizes ⅛" to 16". Low rate of leak.

(J) Vacuum Fusion Gas Analyzer. Analyzes metals and alloys, including titanium, for combined or dissolved oxygen, nitrogen, and hydrogen.

(K) Type 701 Thermocouple Gauge Control. A light, portable instrument for vacuum testing in range 1 — 1000 microns. Compact and rugged.

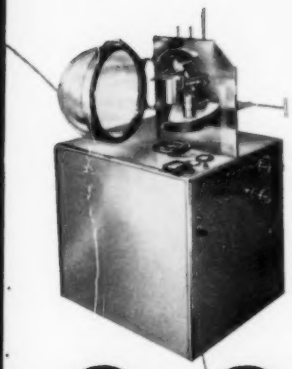

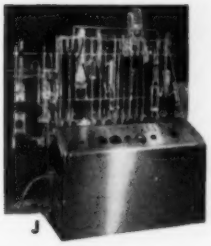

SOURCE!

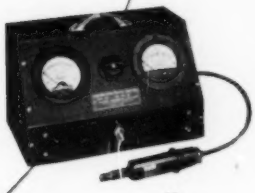

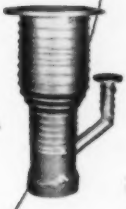

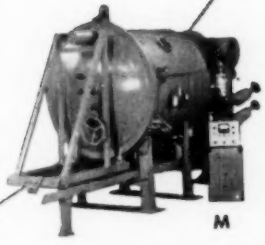

with a COMPLETE LINE *of* HIGH VACUUM EQUIPMENT

You may be using one or two of our products without realizing that at this one source you have available such a full line of high vacuum equipment.

You will find a unique quality in most of these products. They were created to "ideal" specifications drawn up by *manufacturers* who, in many cases, never dreamed we could fulfill their exacting requirements. The products are meeting these requirements day after day on production lines.

Let us supply all your high vacuum equipment needs. You will gain the benefits of a single source of supply plus the high standards of performance designed into National Research products. Write us for further details. National Research Corporation, Memorial Drive, Cambridge, Mass.

(L) H-16-P Purifying Diffusion Pump. Over 10,000 CFM in 10^{-5} range. Suitable for cyclotrons, commercial coating units, and other equipment demanding high pumping speed.

(M) Evaporators. Standard models from laboratory unit to high capacity tank type units.

*Reg. U. S. Pat. Off.

INDUSTRIAL RESEARCH
PROCESS DEVELOPMENT
HIGH VACUUM ENGINEERING
AND EQUIPMENT

METALLURGY
DEHYDRATION
DISTILLATION COATING
APPLIED PHYSICS

National Research Corporation

Seventy Memorial Drive, Cambridge, Massachusetts

Advertisement

ELECTROMET Data Sheet

A Digest of the Production, Properties, and Uses of Steels and Other Metals

Published by Electro Metallurgical Company, a Division of Union Carbide and Carbon Corporation, 30 East 42nd Street, New York 17, N. Y. • In Canada: Electro Metallurgical Company of Canada, Limited, Welland, Ontario

How VANADIUM improves engineering steels and helps conserve critical alloys

In these critical times when many alloying materials are scarce, you may be able to use vanadium to good advantage. Steels alloyed with vanadium meet most of the mechanical specifications for low-alloy engineering and structural steels. In fact, vanadium can often be used in engineering steels to replace at least part, if not all, of certain alloys now in critical supply.

The metallurgy of vanadium is well known. Small additions of vanadium—0.10 to 0.30 per cent—can be used effectively to give steel extra strength, toughness, and resistance to fatigue and wear. It improves engineering steels by increasing their yield strength without sacrificing ductility. The uniformly fine grain size of vanadium-bearing steels makes them tough and resistant to abrasion, fatigue, and impact.

Better Mechanical Properties

In the following table are typical analyses for carbon-vanadium and chromium-vanadium steels that are suitable for most applications where low-alloy, high-strength steels are required. The carbon-vanadium steel is compared with plain-carbon steel; and the chromium-vanadium steel, with chromium-molybdenum steel. Note the excellent properties of the vanadium-bearing steels.

Fig. 1 – Vanadium increases the strength, toughness, and wear resistance of engineering steels for many machine parts, such as this large crankshaft.

Improves Cast Iron

A small addition of vanadium, usually from 0.10 to 0.25 per cent, refines the grain of cast iron, and materially increases its strength and hardness. Moreover, vanadium may be used in cast iron to replace at least part, if not all, of certain alloys that are now in short supply.

Vanadium in Rimmed Steel

An addition of approximately 1 lb. of vanadium per ton of steel produces non-aging characteristics in a rimmed steel. These non-aging properties, together with improved deep-drawing characteristics and the good surface inherent in rimmed steels, make these steels of particular interest at the present time.

Grades of Ferrovanadium

ELECTROMET produces ferrovanadium containing 50 to 55 per cent vanadium for the production of vanadium-bearing steels and irons. The alloy is produced in three grades with maximum 0.20, 0.50, or 3.00 per cent carbon and maximum 1.50, 2.00, and 8.00 per cent silicon, respectively. Each grade is specially adapted to fill the different requirements of iron- and steel-making.

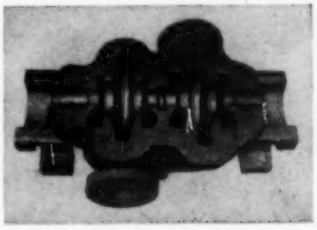

Fig. 2—Steel and iron castings treated with small additions of vanadium have high ductility and greater toughness and impact resistance.

Write for a copy of the booklet, "ELECTROMET Products and Service," which gives helpful information about the use of ferrovanadium and other alloying metals that ELECTROMET supplies. The booklet may be obtained from any ELECTROMET office: in Birmingham, Chicago, Cleveland, Detroit, Los Angeles, New York, Pittsburgh, or San Francisco. In Canada: Welland, Ontario.

Properties of Vanadium Steels Compared With Other Engineering Steels

Typical Analysis, %	Carbon Steel	Carbon-Vanadium Steel	Chromium-Molybdenum Steel	Chromium-Vanadium Steel
Vanadium	—	0.16	—	0.16
Carbon	0.50	0.49	0.50	0.50
Manganese	0.71	0.77	0.80	0.79
Silicon	0.19	0.15	0.30	0.31
Chromium	—	—	0.95	0.98
Molybdenum	—	—	0.20	—
Annealed and Furnace-Cooled				
Tensile Strength, psi	90,600	100,000	100,000	99,500
Yield Point, psi	48,900	66,000	50,000	64,100
Elongation in 2 in., %	23.3	25.0	23.0	28.4
Reduction of Area, %	37.8	49.1	45.0	59.0
Izod Impact, ft.-lb.	13.5	26.0	17.0	44.0
Quenched and Tempered				
Tensile Strength, psi	134,900	134,500	232,000	232,800
Yield Point, psi	110,800	128,000	214,500	224,200
Elongation in 2 in., %	18.3	18.3	10.0	10.4
Reduction of Area, %	54.1	56.6	39.0	43.1
Izod Impact, ft.-lb.	54.0	65.0	12.0	12.0

The term "Electromet" is a registered trademark of Union Carbide and Carbon Corporation

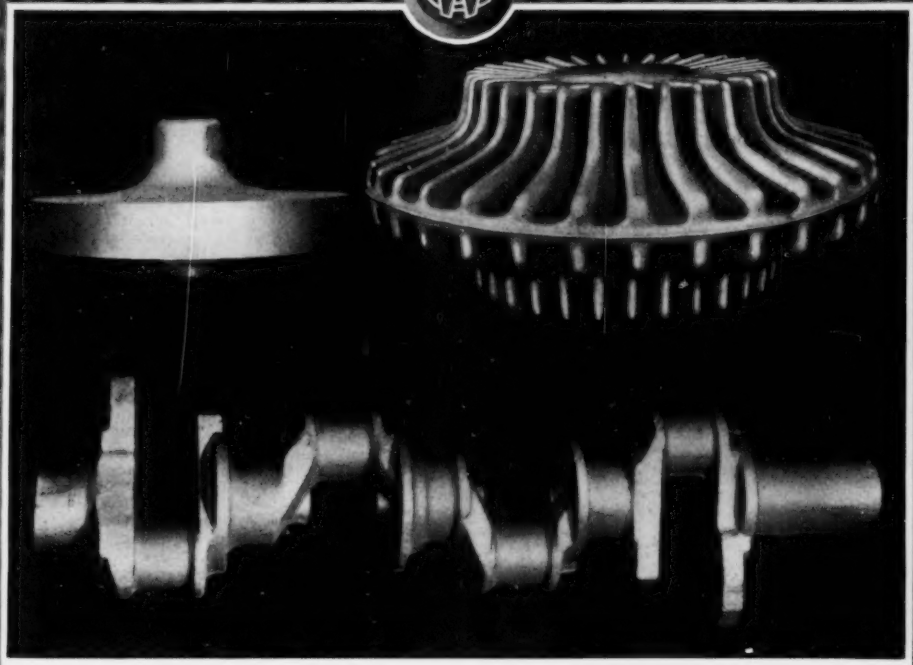

Wyman-Gordon—specialists in the vital forgings of the internal combustion engine since its inception—is today the largest producer of crankshafts for the automotive industry and of all types of forgings for the aircraft industry. Be it crankshafts and other vital forgings for the piston type engines or turbine wheels and impellers for turbo jets—there is no substitute for Wyman-Gordon experience.

Standard of the Industry for More Than Sixty Years

WYMAN-GORDON

FORGINGS OF ALUMINUM • MAGNESIUM • STEEL

WORCESTER, MASSACHUSETTS

HARVEY, ILLINOIS DETROIT, MICHIGAN

— Personnel Service —

THE following employment items are made available to AIME members on a non-profit basis by the Engineering Societies Personnel Service, Inc., operating in cooperation with the Four Founder Societies. Local offices of the Personnel Service are at 8 W. 40th St., **New York 18;** 100 Farnsworth Ave., **Detroit;** 57 Post St., **San Francisco;** 84 E. Randolph St., **Chicago 1.** Applicants should address all mail to the proper key numbers in care of the New York office and include 6c in stamps for forwarding and returning application. The applicant agrees, if placed in a position by means of the Service, to pay the placement fee listed by the Service. AIME members may secure a weekly bulletin of positions available for $3.50 a quarter, $12 a year.

POSITIONS OPEN

Engineers. (a) Engineer to solve corrosion problems in process equipment and plant maintenance, for work in laboratory or plant to help select proper metals, plastics or protective coatings. One to two years' experience, with college degree. Salary open. (b) Senior Engineer to solve corrosion problems in process and plant maintenance by proper metal selection, protective coatings, plastics, fabrication procedure. Five to ten years' experience plus B.S. or M.S. in chemical, metallurgical or mechanical engineering. Salary open. Positions with well established consumer products industry. Location, New Jersey. Y6089.

Product Development Engineer, 28 to 40 with engineering degree, some experience in industrial marketing, for post emergency product development. Company is equipped to do a wide variety of metal fabrication work including press work, metal finishing and assembly; has a large machine shop, engineering design and drafting organization. Salary open. Location, Ohio. Y6087-CD.

Chemist with experience on metal analysis covering aluminum, bronze and steel for commercial testing laboratory. Salary, $3900 to $5200 a year. Location, New York. Y6081.

Engineers for company making cutting tools and dies by powder metallurgy methods. Will work with present personnel in surveying and evaluating present production processes, adapting research results to production and conducting production scale research and development. (a) Materials Engineer with metallurgical degree, to analyze material failures and specify materials for development and production applications. (c) Process Engineer with chemical degree, to evaluate, improve metal powder process methods and equipment. Location, Pennsylvania. Y6044.

Chemists, Chemical Engineers and Metallurgists, B.S., M.S., Ph.D., for process design, development and pilot plant, analytical laboratory and plant technical service. Position offers opportunity to become familiar with latest developments in ore processing, metal refining and fabrication. Salary open. Location, southern Ohio. Y-6042-D.

General Plant Superintendent, 35 to 40, preferably mechanical engineering education, with full knowledge of heat treating, metallurgy, stamping and piercing dies, and shearing and forming for manufacturers of perforated metals. Location, northern New Jersey. Y6027.

Salesmen, 2, with experience and knowledge of heat treatment and metallurgy of tool steels, to sell Swedish steels. Territories, one for northern Ohio and one for southern California. Y6020.

Engineers. (a) Welding Engineer, with 5 to 7 years' experience, to head department and direct research on all types of joining of aluminum. (b) Engineer, 1 to 3 years' experience, to conduct experimental work on soldering. (c) Physical Metallurgist, M.S. or Ph.D. with outstanding ability, preferably with 3 to 5 years' experience, to conduct investigations on aluminum base alloys. (d) Phys-

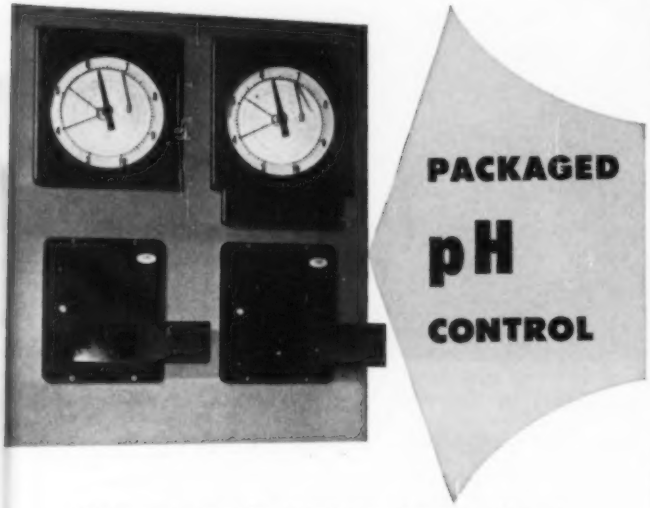

AN increasing number of producing plants are taking advantage of the inherent features of the *ElectroniK* Potentiometer in this packaged panel for pH measurement and control . . . for these two important operations:

FOR PLATING

- *It holds correct acidity at proper tank level.*
- *With instant corrective action, it assures ideal bath conditions at all times.*
- *It provides an accurate and permanent record.*

FOR WASTES TREATMENT

- *It governs the addition of chemicals, in exactly the right amount.*
- *It helps insure compliance with stream pollution laws, furnishes an accurate and permanent record.*
- *It saves time of operating personnel.*

Complete information is available in new Catalog No. 15-16 . . . "pH and Conductivity Recorders and Controllers." Write for your copy today. MINNEAPOLIS-HONEYWELL REGULATOR CO., *Industrial Division*, 4573 Wayne Ave., Philadelphia 44, Pa.

MINNEAPOLIS
Honeywell
Brown Instruments

ical Metallurgist, no experience required. (e) Metallurgist, or chemical engineer, B.S. or M.S., with 5 to 7 years' practical experience in metal finishing, preferably aluminum, for development and technical service work in plating, chemical coating, brightening, etc. (f) Engineer or Chemist, B.S. or M.S., with training or experience in paint technology for the investigation of paint and lacquer finishes for aluminum. (g) Testing Engineer, 5 to 7 years' experience, to conduct and direct all phases of mechanical testing. (h) Metallurgical Process Engineer, B.S., 3 to 5 years' experience, to conduct research work on melting, ore dressing, calcination, etc. (j) Metallurgist or Electrochemist, with 3 to 5 years' experience, for fundamental corrosion research on aluminum. Apply by letter giving full details. Location, Washington State. S-1331.

Concentrator Metallurgist, 30 to 35, graduate in ore dressing with practical experience, to take charge of laboratory testing for large mining company. Spanish helpful. Three year contract, transportation, living quarters. Location, South America. Y6010.

Metallurgist for research work in the field of metal coatings. Salary, $4600 to $6400 a year depending upon qualifications. Location, Washington, D. C. Y6001.

Junior Engineer, metallurgical or chemical graduate, to do analysis, make physical tests, covering materials, heat treatment, coatings, etc. Salary, $3900 to $4420 a year. Location, Connecticut. Y5997(b).

Engineering Draftsman with experience, to lay out and detail metal working machinery for canning and metal products fields. Salary, $3900 to $4940 a year. Location, New York. Y5995.

Metallurgist with B.S. degree in metallurgy or metallurgical engineering, and at least six months' professional experience in metallurgy. Will be responsible for conducting X-ray, Gamma-ray, Magnaflux and Zyglo examinations of castings, weldments, and forgings to determine the suitability for naval use. Salary to start $3825 a year. Location, Pennsylvania. Y5992.

Supervisor, metallurgy and metallurgical engineering, M.S. Met. or Met. Eng., 35 to 45. Must have had eight or more years in broad program of industrial research in practical application. Will supervise all metallurgical and metallurgical engineering functions. Company will pay placement fee. Salary, $7000 to $9000 year. Location, Michigan. T8206(b).

Assistant to President, graduate engineer, 40 or over. Must have had

(Continued on page 968)

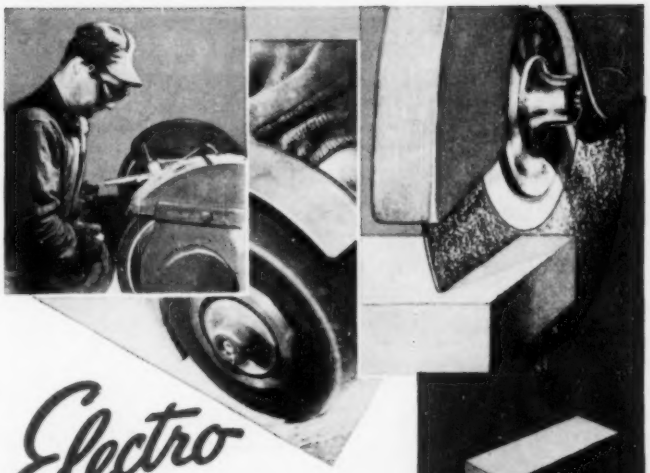

Electro agrees:

It's Take-Off That Pays Off

Whatever the *theory* of wheel quality, it's take-off that pays off. Currently, competitive tests prove that Electro Wheels, *engineered to the job,* are 45% more effective!

As grinding problems and practices become more and more individual, production executives realize more and more that only those wheels that are engineered for specific purposes under individual conditions, are wholly satisfying.

Permission to survey the possibilities as to whether comparable efficiencies and economies can be achieved for you, will place you under no obligation whatever. Phone, write or wire. We'll get a competent Field Engineer to you quick!

Electro SINCE 1919

Resin Bonded
ABRASIVE WHEELS FOR
•
CUTTING-OFF
•
PRECISION GRINDING
•
SNAGGING
•
GRINDING WHEEL MANUAL 645 AND SPEED CALCULATOR

Free on Request
Write For Them *NOW!*

Plants: Buffalo, N. Y. Cap-de-la-Madeleine, P. Q. Canada · Regional Warehouse: Los Angeles 58, Cal.

3 GOOD TECHNICIANS IN YOUR LABORATORY

"MULTIPLE UNIT"
TEMPERING FURNACE
For Temperatures to 1250° F.
A high speed centrifugal fan located in the rear of the heating chamber supplies rapid and uniform heating. Shelves and baffle are easily removed. Write for Bulletin LAB- 1049.

"MULTIPLE UNIT"
MUFFLE FURNACE
For Temperatures to 1850° F.
For drying precipitates, ash determinations, fusions, ignitions, heating metals and alloys, enameling, heat treating, and experimental test work. Available in four standard sizes. Write for Bulletin LAB-849.

HEVI DUTY
"G-05-PT" FURNACE
For Temperatures to 2600° F.
Designed for operation at high temperature with or without a protective atmosphere. Heating elements are silicon carbide rods extending across the chamber, above and below the refractory muffle. Write for Bulletin LAB- 250.

HEVI DUTY ELECTRIC COMPANY
LABORATORY FURNACES **MULTIPLE UNIT** ELECTRIC EXCLUSIVELY
MILWAUKEE 1, WISCONSIN

at least ten years' experience industrial heat treating furnaces. Duties will be to follow up design, supervise engineering department and assist sales department in design and customer contact work. Must have knowledge of steel plant operations. Salary, $9000 or better. Some traveling. Location, Chicago, R8216.

Welding Engineer. Must have had two or more years' experience in arc or resistance welding around electronic equipment, and knowledge of electronic circuits. Will set up welding standards in resistance or arc welding projects and train personnel. Company may pay part of placement fee. Salary up to $600 per month. Location, western Chicago suburb. R8168(a).

Maintenance Engineer. Must have had five or more years' experience in maintenance and repair of welding equipment, and knowledge of welding equipment maintenance. Will handle inert arc welding, ac arc welding, resistance welding and dc generating equipment. Will also handle normal electrical maintenance of manufacturing plant. Company may pay part of placement fee. Salary up to $700 per month. Location, western Chicago suburb. R8168(b).

Recent Chemical or Metallurgical Engineering Graduates for work in connection with a prospecting program. Excellent opportunity for advancement. Location, Florida. Y6013.

WANTED: Bound Volume, 1938 edition, *Transactions*, Iron & Steel Division, AIME.

Box K-16
JOURNAL OF METALS

WANTED—MELTING DEPARTMENT SUPERINTENDENT

Immediate opening for person having experience in electric arc furnace melting of tool, high speed, stainless, and specialty steels in long-established mill in Pittsburgh district. Should have considerable practical experience, technical background, and ability for handling men. Reply giving complete record of experience, qualifications, age, and references.

Box K-17
JOURNAL OF METALS

Industrial Notes . . . . .

• $296 million will be spent by Westinghouse Electric Corp. for expansion to increase the company's productive capacity by 50 pct. This is the second such program undertaken, the first having cost $150 million.

• **Union Carbide & Carbon Corp. will operate the new Uranium-235 production plant at Paducah, Ky., under agreement with AEC. Already operating three Oak Ridge atomic energy installations, it will operate the Paducah and the Oak Ridge gas diffusion plants under a single organization centered at Oak Ridge. The plant at Paducah cost $500 million.**

• United Carbon, Inc., Charleston, W. Va., is completing a $2 million oil base furnace black plant at Franklin, La., the capacity of which is expected to be over 30 million lb per year.

• *$5 million will be spent by American Welding & Mfg. Co. for additions and equipment at its Warren, Ohio, plant. The plant produces aircraft parts, including coated nozzle boxes, turbine casings, exhaust cones and stainless steel and titanium welded ring assemblies.*

• Harbison-Walker Refractories Co., Pittsburgh, is negotiating for the Warm Springs, Calif., plant of Laclede Christy Co., Chicago. The acquisition will be handled by a West Coast subsidiary and will permit the company to enter a wider field of production of basic and silica refractories.

• H. K. Porter Co., Pittsburgh, has purchased Buffalo Steel Co., Tonawanda, N. Y., which produces about 70,000 tons a year of reinforcing bars, agricultural shapes, fence posts, light angles, merchant bars, and similar light steel products.

• *Combined Metals Reduction Co., announced that it will build a new ferromanganese plant at the Henderson, Nev., magnesium plant owned by the Government. The new plant will cost about $1¼ million.*

• Vulcan Mold & Iron Co., Latrobe, Pa., is planning construction of foundry for production of ingot molds at Riverside, N. J., and is completing a new ingot mold foundry at Lansing, Ill.

• Bridgeport Thermostat Co., a division of Robertshaw-Fulton Controls Co., will build a $1 million plant near Milford, Conn.

• *Budd Co., Philadelphia, will erect a $6 million machining, welding, and painting plant for tank hulls and turrets under subcontract from Chrysler Corp.*

• Wallander Fabricant Steel Co., New York, is planning a $1 million plant near the Hudson River in North Albany, N. Y.

• **Reserve Mining Co., owned jointly by Republic, Armco, and National Steel Corp.'s will spend more than $75 million on a beneficiating plant for producing high grade iron ore from magnetic taconites. The plant will be 55 miles east of Duluth, Minn.**

• Thompson Products, Inc., has acquired Antenna Research Laboratory, Columbus, Ohio. Thompson is building up an electronics division, and will set up facilities for large scale production of antennas at the new plant.

• **By 1954, General Electric Co.'s capital expansion program since World War II will reach a total cost of nearly $1 billion. Research and development costs amount to about $100 million a year, and the number of plants owned by the company has increased from 37 in 1939 to 114 today.**

As sure as the coming of Spring

. . . you will switch to MOLYBDENUM High Speed Steel

The increased usage of Molybdenum high speed steel is based on:

its merits,
its easy availability,
its lower cost.

You can save tungsten for uses where it is really needed. Don't delay, the switch is easy.

All the facts you need in this FREE BOOKLET.

Climax Molybdenum Company
500 Fifth Avenue · New York City

Please send your FREE BOOKLET
"MOLYBDENUM HIGH SPEED STEELS"

Name .....
Position .....
Company .....
Address .....

JM-11

MOLY

HS 11

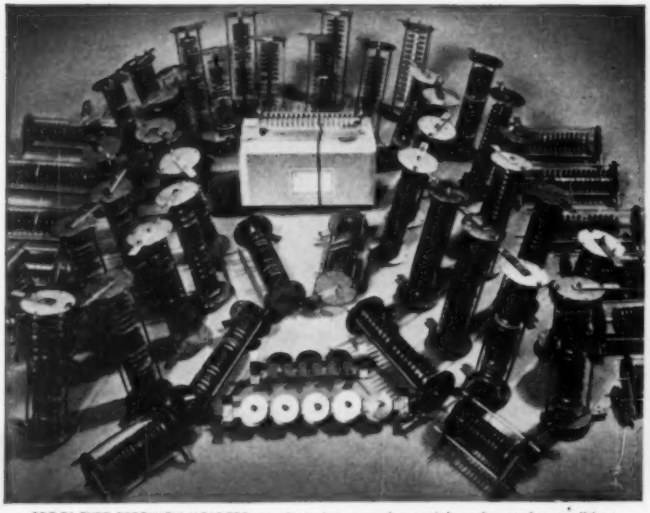

SPOOL-TYPE SPECIMEN HOLDERS permit testing several materials under service conditions without risk of mechanical damage. Specimens make no contact with each other or with plant equipment . . . thus, galvanic effects are prevented.

ASSEMBLING A CORROSION TEST SPOOL. Specimens are machined to specified dimensions, and expose exactly 0.5 sq. dm. when mounted for test.

Help for solving your INDUSTRIAL CORROSION PROBLEMS...

Available for solving your specific problem is a vast amount of information on industrial corrosion.

Acquired and catalogued by The International Nickel Company's Corrosion Engineering Section, this fund of data is constantly being increased.

Valuable information is obtained in various ways...for instance, by cooperative field tests in which specimens are exposed to actual plant operating conditions. Also, by fundamental investigations in the laboratory and by tests that duplicate, so far as practical, existing or expected conditions where plant tests are impractical.

A great deal of important data comes from INCO's large scale marine testing stations at Kure Beach and Harbor Island, and from stations having industrial and rural atmospheres. In addition, technical literature, reports, and manufacturer bulletins contribute useful information.

Our files contain data from more than 2,000 plant tests on some 40,000 metal and alloy specimens. All information is tabulated on standard forms, and a punch card key sort system facilitates finding specific data.

We freely provide the Corrosion Data Work Sheet, illustrated, for presenting your specific problems.

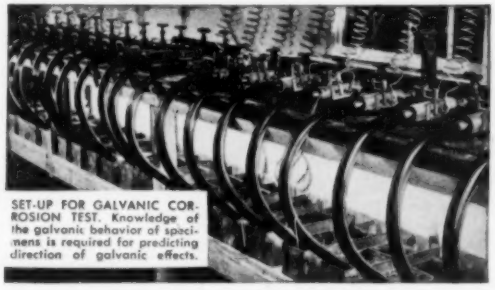

SET-UP FOR GALVANIC CORROSION TEST. Knowledge of the galvanic behavior of specimens is required for predicting direction of galvanic effects.

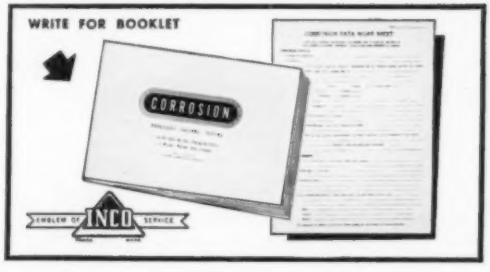

Whenever you need assistance in solving a corrosion problem, our Corrosion Engineering Section will gladly cooperate with you. A free copy of the new booklet entitled "Corrosion" may help you defeat corrosive attacks...write for it now.

THE INTERNATIONAL NICKEL COMPANY, INC. 67 WALL STREET NEW YORK 5, N. Y.

American Smelting & Refining broke ground recently for a new Central Research Laboratory at South Plainfield, N. J. The lab will have about 75 individual laboratories for basic studies on gold, silver, lead, copper, zinc, antimony, cadmium, and other metals produced by the company. One important project will be the development of new uses for a number of byproducts, notably arsenic and such metals as indium, thallium, and tellurium.

Reserve Mining Co. has started construction of a 2,500,000 tons per year beneficiating plant for producing high grade iron ore from magnetic taconite. The plant will cost upwards of $75 million, and operation will begin in late 1955 or early 1956. It is on the north shore of Lake Superior about 55 miles east of Duluth. Provision is being made to enlarge the plant as needed to a 10 million tons per year plant. To operate at 2,500,000 tons per year, 7,500,000 tons of taconite will be required. Republic, Armco, and National Steel Corps. are partners in Reserve Mining Co., and Oglebay-Norton & Co. manages the firm.

Containers made from low carbon hot rolled steel plate, utilizing rolled flanges and rubber rings for moisture and air seals, are being used to protect jet engines from damage in shipping and eliminate frequent inspections for corrosion. Engines are rubber mounted in the cans, can withstand total immersion in water, and drops of 36 in. without damage.

Allis-Chalmers Mfg. Co. will do about 90 pct of the manufacturing operations on the Pratt & Whitney T-34 turbo-prop engines, producing and assembling the gas turbine engines which will be tested by P&W at East Hartford, Conn. T-34's were developed in collaboration with the Navy and will be used for the Air Force's new Douglas giant transports.

Bohn Aluminum & Brass Corp., Detroit, will operate the production and experimental aluminum forging and extrusion plant owned by the Government at Adrian, Mich. Bohn built and operated the plant during World War II, but in 1948 it was turned over to Gerity-Michigan Corp., and later to Reynolds Metals Co.

Plans call for shipment of about 3 million tons a year of Brazilian iron ore into the Pittsburgh, Pa., district. One of the main sources is Ita Bira Mountain, with about 100 million tons of ore visible. The ore runs about 69 pct iron.

Bureau of mines describes a successful production process for 99.9 pct pure electrolytic manganese from low grade ore by use of a chloride electrolyte. While the chloride process is more difficult and expensive to operate than the sulphate process, it is believed to have certain advantages that will overcome these difficulties.

Norton Co., has developed highly improved and efficient techniques of grinding titanium commercial alloys, one of the major fabricating production problems in handling these alloys.

U. S. Steel Corp. has just put into operation rotary sintering and Dwight-Lloyd sintering equipment at its taconite concentration plant in Minnesota. Comparative studies of costs, end-products, and other factors of sinter produced by these two methods will be studied.

THE DRIFT OF THINGS

by Edward H. Robie

NOT often do we refer in these columns to what is going on in Washington. Several other organizations cover affairs in the national capital satisfactorily and we confess that their reports make pretty tough reading for us. The lighter stories about Washington appeal to us more, such as the one in the September issue of *Pay Dirt*, about the small mine operator who put in a hectic week going from one office to another trying to get things done. The most unusual thing that happened, he said, was when he took out a blonde the last evening he was there. Following dinner he asked for special favors, and she slapped him in the face. "You know," he said, "that was the first definite answer I had had in all that week."

But we do feel that Jim Boyd's exit from the Washington scene is worthy of note. Dr. Boyd was appointed director of the Bureau of Mines four years ago, succeeding Dr. R. R. Sayers. John L. Lewis took violent exception to his appointment and for some time one of Colorado's Senators blocked his confirmation. As a result he served without compensation for two years. Not long ago he was made head of the Defense Minerals Administration, though still keeping his title as director of the Bureau. He is reported to have differed with Interior Secretary, Oscar L. Chapman, on several matters, including payment of subsidies to mineral producers and the synthetic fuels program. He was therefore relieved of his duties and Dr. W. C. Schroeder became acting administrator. Also, many of the DMA powers were transferred to a still newer organization, the Defense Materials Procurement Agency, headed by Jess Larson. Mr. Larson has asked Howard I. Young to become his deputy in charge of the Agency's metals and minerals section, with Simon D. Strauss and Alan Bateman as advisers. Then, on Oct. 1, President Truman announced the resignation of Dr. Boyd as director of the Bureau of Mines. He has found what should be a much happier home with the Kennecott Copper Corp., which he joined Oct. 16 in an executive capacity.

Probably some political sagacity, and a willingness to follow administration policies, are required of a bureau chief in Washington, making the climate inauspicious for an independent and objective thinker and doer. However, we can at least hope that when a new head for the Bureau of Mines is chosen, he will be a man of professional stature rather than primarily a political appointee.

The Chemical Society's 75th

As this is written, in October, New York is the scene of the American Chemical Society's Diamond Jubilee celebration. Four years ago—one year late, for the AIME was founded in 1871—the AIME had a similar celebration. Our official representative at the Chemical Society's 75th birthday, Carleton C. Long, presented for us an engrossed scroll of greeting which read: "The American Institute of Mining and Metallurgical Engineers extends its most cordial congratulations to the American Chemical Society upon having so successfully attained the seventy-fifth anniversary of its founding. The Institute is proud that its roll contains the names of many members of the Society who have attained world-wide distinction in our related fields, and who have added substantially to our national industrial progress. May the Society in the future raise still further the high scientific and technical level of the chemical industry for which it is so largely responsible."

The Society now has more than 66,000 members, of whom 16,000 are chemical engineers. It is the largest scientific society in the world. It embraces 20 professional divisions, indicating the wide scope of the chemical industry. Really, almost every manufacturing industry in the country depends to a considerable extent on chemistry, as do many of the professions as well, conspicuously that of medicine. At the New York meeting 720 technical papers were presented at 129 sessions, covering 80 general subjects of scientific interest.

Ore and Near Ore

Some 8 years ago the Bureau of Mines and Geological Survey decided to classify ore reserves into *measured ore*, *indicated ore*, and *inferred ore*. The definitions were stated in the October 1943 issue of *Mining and Metallurgy*. Now comes an inquiry from England as to whether these classifications ever were accepted by mining men in this country. We referred the question to a prominent mining geologist, who writes in part as follows:

"We use these terms in our own reports but my experience with mining companies indicates that most of those in the westerr United States follow the old nomenclature in recording their ore reserves. Also, most of the annual reports hold to the old terms—developed (proved) ore, etc. One company qualifies further by classing ore reserves as 'fully developed ore'. An official of one of our larger companies, the American Smelting & Refining Co., said that his company uses the old terms around its operations because the operators are more familiar with them, but when dealing with the U. S. Government they are forced to use the new terms. He believed the new terms would gradually replace the old because of the insistence of the U. S. Government, if for no other reason. The Defense Minerals Administration requires the use of the terms *measured*, *indicated*, and *inferred* ore in all petitions submitted to that office.

"My own opinion is that the changeover, so far as our mining companies are concerned, will take a little time in spite of obvious advantages in the new definitions."

More Peeves

In the June issue we spoke of some words and phrases that got under our skin a bit. Robert A. Laurence, from Knoxville, Tenn., voices "a loud and hearty amen. I wish you had included two of my pet peeves: 'finalize' (to complete or finish) and 'foreseeable future.' (At what point does the unforeseeable future begin—five minutes from now, five days, five weeks, or five months?) But wasn't it President Harding who thought up 'normalcy,' for the 1920 campaign?" Yes, it surely was; we gave the credit to Coolidge.

Hot-Workability of Stainless Steel Improved by Adding Cerium and Lanthanum

By C. B. Post,

D. G. Schoffstall and H. O. Beaver

ONE of the more general problems in some grades of stainless steel manufacture is the production of consistently malleable ingots. The hot-workability of any particular stainless grade determines to a large extent its availability as bars, sheets, strip, plates, and other commercial wrought products.

Considerable work has been done on this problem of hot-workability but published data are rare because the problem is difficult to study by laboratory techniques. The variables known to affect the problem, such as melting practice, ingot size, rolling temperatures, etc. are complex and do not lend themselves to exact technical data treatment.

For some years Carpenter Steel Co., Reading, Pa., has been investigating variables that affect hot-workability of stainless steels to improve the hot-workability of those steels where some measure of hot-workability presently exists, and to impart hot-workability to stainless alloys previously considered to be non-hot-workable.

The rare-earth elements are an effective agent in promot ng and improving the hot-workability of austenitic chromium-nickel and high alloyed stainless steels when added as an alloying element. The effect of this alloy agent can be exceptionally marked in some alloys where the metal is converted into a commercial wrought product from a metal previously considered to be non-hot-workable. In other metals, the effect will be to improve the existing hot-workability as evidenced by better ingot-to-billet yields, less billet preparation, and better hot-rolled strip surfaces. The results by alloying rare-earth metals in these high alloyed stainless steels are described elsewhere.* The term *rare-earth elements* refers principally to cerium, lanthanum and those other rare-earth metals commonly associated together in *misch-metal*.

To present the data on a systematic basis, variables known to affect hot-workability must be reviewed so that the inherent ductility of the alloy can be separated from other variables of a mechanical or physical nature. Some of these variables known to influence hot-workability are as follows:

1—Stiffness: Stainless steels as a class are high in alloy content. The austenitic stainless alloys are generally higher in alloy content than the ferritic grades. As a group, stainless steels are noted to be stiffer in the rolling mills or under the hammer than conventional low alloy or carbon steels. This is primarily because of higher alloy content, which, even at more elevated temperatures, causes the steel to resist deformation. Starting with iron or SAE 1010 as the most easily deformed grade of steel, the SAE alloy steels would come next in stiffness, followed by the ferritic grades of stainless such as AISI Types 403, 410, 416, and 430, followed by the austenitic 18-8 grades of stainless such as Type 302 and 304. Alloys stiffer than this latter type would include the 18-8 grades with molybdenum such as Type 316 and 317, the high-chromium high-nickel alloys such as Type 310, followed by various specialized alloys such as Inconel (80 pct Ni-20 pct Cr), and the so-called super-alloys currently used in jet power units.

Hot-workability will not be concerned with stiffness of the alloy provided the alloy is ductile. The stiffness

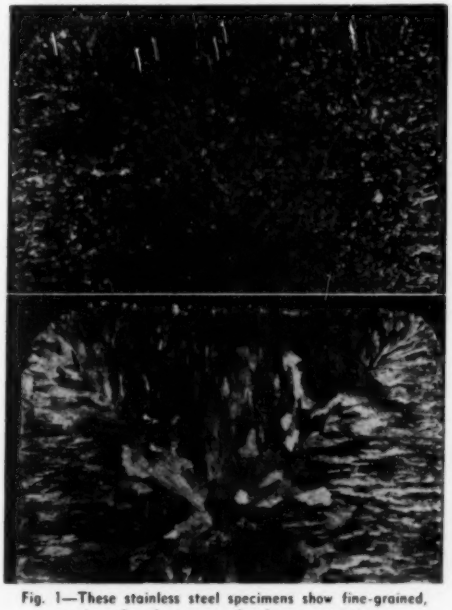

Fig. 1—These stainless steel specimens show fine-grained, equi-axed and pronounced columnar structures.

* U. S. Patent 2,553,330, C. B. Post and D. G. Schoffstall, assigned to the Carpenter Steel Co., Reading, Pa.

C. B. Post, D. G. Schoffstall, and H. O. Beaver are in the Metallurgical Dept., Carpenter Steel Co., Reading, Pa. **This paper will be presented at the Electric Furnace Steel Conference, Iron and Steel Div., AIME, Dec. 6-8, 1951.**

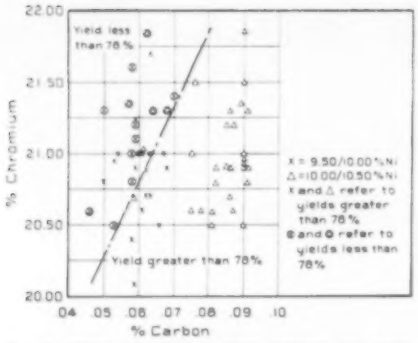

Fig. 2—Effects of carbon-chromium balances are shown here on prepared rolled billet yields, Type 308 stainless.

makes the alloy more difficult to deform by demanding more power from the rolling mill or from the hammer. Provided enough power can be brought to bear upon a ductile alloy, it can be made to flow as easily as one of the lower alloy grades.

2—Ingot Structure: In some grades of high alloyed steels a pronounced columnar structure is obtained in ingots, illustrated in Fig. 1. Two conditions are illustrated, one is a fine grained equi-axed center condition in the ingots, while the other shows large columnar grains. The ferritic grades, especially Type 430 or types where no transformation exists between the metal solidification point and room temperature, are prone to show the columnar type of grain structure. Some grades of austenitic alloys can show these columnar grains, especially if cast on the hot side. Ingot structures have been observed for a number of years in the austenitic types but it cannot be definitely claimed that the columnar type of structure causes any particular trouble in rolling or hammering, provided the alloy is ductile. However, experiments segregated this effect as much as possible.

3—Heating Conditions at Mill or Hammer: The heating of stainless steels for rolling or hammering requires, in general, higher temperatures and better control of temperatures than is required on the low alloy steels. Furthermore, the allowable hot working range for most individual types of stainless steels is generally limited to less than 150°F in breaking down the ingot structure. These temperatures are generally in the range of 2000° to 2300°F and represent the lowest temperature at which the alloy becomes soft enough to be handled on the conventional rolling mills and hammers, while the upper range of temperatures is determined by grain boundary effects such as melting or collapse of the grain boundaries. The correct heating procedure and temperatures for stainless steels cannot be over-emphasized. Numerous cases of austenitic alloys have been observed where heating temperature and cogging procedure must be prescribed within such narrow limits as to make its production impractical because the alloy was inherently hot-short. The same alloy made to be more ductile can stand wider liberties in the heating temperature and handling procedure at the mill. In this sense it is granted that a poor heating job at a mill or hammer can ruin or make unusable a worthwhile good heat of stainless steel, but it is also true that no amount of care in heating or in heating procedure can make malleable a heat of steel that is inherently non-ductile.

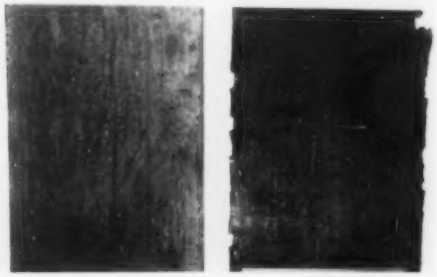

Fig. 3—Shown here is the effect of free delta ferrite on the rolling behavior of Types 316 and 316X, hot-rolled 7¾x 0.148-in. strip. Left shows Type 316; right shows Type 316X with 30 pct delta ferrite in the austenitic matrix.

4—Hot-Shortness: This is the variable which is believed to overshadow all foregoing variables in importance. Hot-shortness or non-ductility can be the result of several causes. The first cause in stainless steel melting that can produce pronounced hot-shortness is contamination with elements such as lead, tin, silver, etc. At present, nothing can be done to overcome this type of hot-shortness caused by tramp elements except better selection of scrap. Another important cause is the furnace melting procedure on hot-shortness. For instance, in melting Type 316 considerable nickel oxide and molybdenum oxide can be used in the charge. If insufficient carbon is present in the charge to combine with the oxygen from the nickel oxide and molybdenum oxide, the heat will be exceptionally wild when melted-in, and consequently will be hard to handle in the refining period. Such heats are likely to show a pronounced tendency for hot-shortness in rolling mills or hammers. If sufficient carbon is incorporated into the charge to take care of the oxygen, the heat will melt-down in a normal manner (not excessively wild) and will yield ductile metal. It is thought that this action comes about because of the hearth picking up considerable amounts of oxygen from the oxidizing period when insufficient carbon is present to boil out the oxygen. This oxygen which is picked up by the hearth remains into the refining period so that the melter is faced with deoxidizing the metal and deoxidizing the hearth. Another important factor in determining the hot-shortness of stainless steel, especially of the austenitic grades containing nickel, chromium, molybdenum, etc., is the correct chemical balance in the alloy. This chemical balance influences primarily the amount of high temperature ferrite and austenite that will be present at the rolling temperatures. A completely austenitic alloy in general will be rolled or hammered better at a higher temperature than a completely ferritic alloy. It is thought that when some ferrite is present with the austenite, the ferrite acts as zones of weakness between the austenitic grains; and if the alloy is heated to the correct temperature for austenite, the ferrite collapses at these temperatures. If enough ferrite is present, the alloy will tear apart at the mill or hammer. For a ferritic alloy, small amounts of austenite will cause the opposite effect. That is, the austenite will be stiffer than the ferrite matrix at the rolling temperature normally used for the ferrite, and if too much austenite is present the alloy is too stiff to flow well at the lower temperature and stress or strain cracks will appear, especially, on edges of strip or sheets. Fig. 2 shows the effect of carbon and chromium at 9.50 to 10.50 pct Ni on the prepared billet yields of Type 308. Lower carbons in Type 308 causes lower yields, unless the lower carbons are offset by a lower chromium content at constant nickel. Enough is known about this effect to state that the lower carbons cause a ferritic-austenitic mixture at rolling temperatures. Consequently, if an austenitic element like carbon is decreased, then this decrease must be balanced by a decrease in one of the ferrite-forming elements, such as chromium. Fig. 3 shows the effect of 30 pct ferrite in the austenite matrix of Type 316 on the appearance of hot-rolled strip. In this case the carbon, chromium and molybdenum contents of the two samples shown in

Fig. 3 are approximately the same. The principal difference is that the regular sample of Type 316 shown on the left in Fig. 3 contains about 12 pct Ni, while the sample on the right, Type 316X, contains about 9.50 pct Ni. In this case the appearance of a substantial quantity of ferrite in the austenitic matrix is caused by a decrease in the amount of an austenite-forming element, such as nickel.

Forgeability Evaluation

To isolate these hot working variables so that an intelligent study can be made of this hot working problem, it is necessary to devise some testing procedure with each heat. Such a test would have little to do with determining the heating conditions and heating temperatures at the mill or hammer, since these procedures are best set up based upon general experience and detailed studies of heats when they are first taken on for manufacture. Also, the test should not be concerned too much with the problem of stiffness, since this again is determined by the alloy content and can be handled in a general manner by judicious use of experience. For instance, high cobalt contents such as 10 or 20 pct in a chromium-nickel stainless steel means that the alloy is going to be stiffer than the conventional grade of 18-8 or Type 316; and the proper ingot size and billet size for the rolling mills can be generally determined by past experience. The test should differentiate clearly between hot-shortness as determined by the foregoing chemical variables and the possibility of hot-shortness caused by ingot structure. Such a test could be made using a chill cast structure so that the question of ingot structure could be differentiated from the inherent hot-workability of the alloy. If the chill cast test showed the alloy to be ductile and ingots were not ductile, then it would be necessary to look to ingot structure to determine a possible reason.

At Carpenter Steel Co., a cone test as shown in Fig. 4 was used. One or more cone tests are cast with each heat of stainless steel under study. If not much is known of the steel, the cone test will lead to the correct rolling or forging temperature. This is determined by heating up the cones to various temperatures and forging them on a hammer. The forging procedure is as follows:

After the cone is heated to the correct temperature it is placed on the die of the hammer (a 1½ ton hammer has been used in the experimental work), and a light tap is given the cone to seat it well on its base. Then a full blow of the hammer is given to the cone so that the truncated portion is driven down into the base and spread as shown in Fig. 5. An examination of the periphery of the cone allows an estimation of the hot-workability of the alloy.

In the case of ferritic stainless alloys cases have been found where the cone test will show the alloy to be ductile but ingots are almost completely non-ductile. Investigation on this effect has shown pronounced columnar grain sizes in the ingots with subsequent large grain sizes at the rolling temperatures. In the case of high-chromium steels such as 25 to 30 pct Cr, these large grains can cause the steel to be very notch brittle, even at rolling temperatures, so that scabs can initiate checks and cracks on the billet. The steel also will have little strength in going through a diamond pass because of these large grains tearing on the sharp corners of the diamond.

In the case of austenitic stainless alloys, experience with the cone test has shown that if the ductility of the metal is satisfactory as measured by the cone test, then the metal will behave satisfactory in either rolling or hammering. There has not been a case where the cone test showed an austenitic alloy to be ductile that ingots have not been ductile. This is probably because austenitic alloys have a much narrower range of freezing than the ferritic alloys, and when the ingots start to freeze the ingot freezes fast; whereas in ferritic alloys the ingots will behave somewhat like iron or steel and will exhibit all defects of ingotism that can be found in steel ingots.

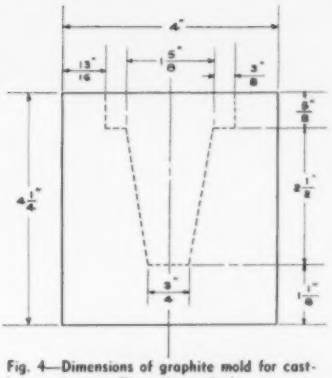

Fig. 4—Dimensions of graphite mold for casting cone test. Dimensions of the cone are given by inside dashed lines.

It would seem that from correlations of this cone test with hot working of ingots that the ingot structure of austenitic alloys has little effect on the resulting hot-workability. If there is any effect, it is of a secondary nature and in most melt shops the problem of hot-workability is much more severe than would be accounted for on the basis of ingot structures. The work that follows is concerned only with austenitic stainless grades, and the cone test gives a measure of the hot-shortness as influenced by the chemical balance, contamination caused by tramp elements, influence of melting practice, and influence of any element such as rare-earth metals on the resulting hot ductility. The answer in the case of austenitic stainless steels will be fairly clear cut and will be capable of duplication in other shops.

Effect of Rare Earths

First experiments had to do with the effect of misch metal alloy addition on the forgeability of austenitic chrome-nickel steels containing nitrogen. One of the early steels for experimentation was an austenitic valve steel of the following nominal composition: C, 0.20 pct; Cr, 21.00 pct; Ni, 11.00 pct; W, 3.00 pct; and N, 0.20 pct. Experience with this steel had shown that without nitrogen additions, the steel could be forged and rolled without too much difficulty and could be satisfactorily fabricated into automotive exhaust valves. The introduction of nitrogen to increase the hot-hardness brought along several manufacturing problems, principally having to do with hot-shortness of the alloy on hammering or rolling. The hot-shortness was studied by means of the cone test and no improvement could be made in melting practice to make this analysis commercially hot-workable. The introduction of misch metal brought some surprising results on the hot ductility of the analysis. Fig. 6 shows

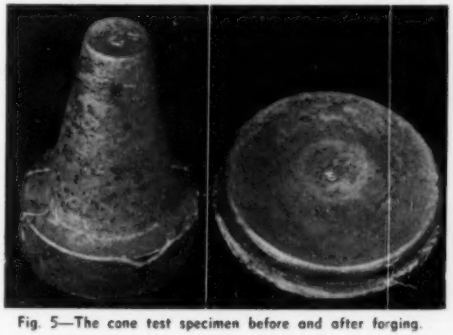

Fig. 5—The cone test specimen before and after forging.

Fig. 6—Forged 3½-in. squares of 21-12 WN steel. The upper two billets had no misch metal additions; and the lower four billets had misch metal additions of 2 lb per ton.

the appearance of billets, 3½ in. square made from the same Ajax high frequency heat in which several ingots were cast without the introduction of misch metal, followed by several ingots after an alloy addition of misch metal equivalent to 2 lb per ton. Fig. 7 shows the hot forged cone test specimens corresponding to these two parts of the heat. A comparison of the appearance of the cone test specimens illustrates the appearance of ductile and non-ductile steels on the cone test as compared with their appearance in forged or rolled billets. The percentage yield from ingots to

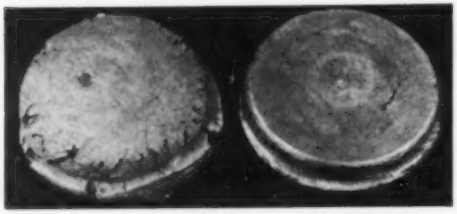

Fig. 7—Forged cones of 21-12 WN steel demonstrate the effect of misch metal additions. The cone at left had no additive, while that on the right had misch metal added at rate of 2 lb per ton.

prepared billets ready for rolling is an important economic figure for steel mill operations. In the case of the 21-12WN valve steel, the misch metal alloyed steels showed an average increase in prepared billet yields of about 15 pct over what had been obtained without the use of misch metal.

Another grade of steel on which early experiments were conducted was a sulphuric acid corrosion resistant steel of the following nominal composition: 0.10 pct (max) C; 2.00 pct Mn; 1.00 pct Si; 19.50 pct Cr; 23.00 pct Ni; 3.50 pct Mo; and 1.50 pct Cu. This

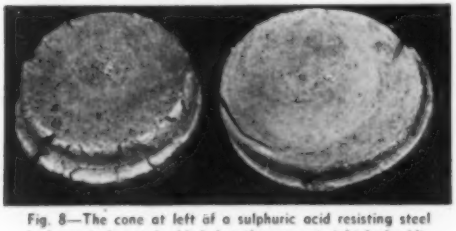

Fig. 8—The cone at left of a sulphuric acid resisting steel had no misch metal added; but the cone at right had additions corresponding to 12 lb per ton, showing 0.12 to 0.18 pct cerium plus lanthanum in analysis.

steel was of the general class of chrome-nickel-molybdenum-copper steels especially designed for resisting sulphuric acid. Steels of this grade have been available for many years as castings, but attempts to hot work steels into the form of wrought products have been unsuccessful (as evidenced by the lack of available stocks of this grade of steel in the form of wrought products.) In this particular analysis the addition of misch metal to the Ajax furnace in quantities equivalent to 6 lb per ton converted an otherwise unworkable steel into a ductile alloy capable of being handled by commercial mill practices to make forgings, bars, hot and cold rolled strip, plates and sheets. The alloy containing no misch metal is completely non-commercial as far as the manufacture into wrought products is concerned; whereas the alloy containing cerium is inherently ductile and can be handled on commercial mill units. In the case of this particular grade of corrosion resisting stainless steel, the yields from ingots to prepared billets increased by a factor of about 30 pct, which means the difference of an unworkable alloy as compared to one fitting into the mill schedule.

The effect of misch metal was next studied on a higher alloyed grade of sulphuric acid resisting steel represented by the following nominal composition: 0.08 pct (max) C; 1.00 pct Mn; 1.00 pct Si; 20.00 pct Cr; 28.00 pct Ni; 2.50 pct Mo; and 3.50 pct Cu. In this case the alloy with an addition of 12 lb of misch metal per ton, leading to cerium contents of about 0.10 pct and lanthanum contents of about 0.08 pct, is completely hot-workable and able to be rolled into bars, strip and slab ingots converted to plates. Fig. 8 shows upset cones and Fig. 9 shows the appearance of billets with and without cerium and it is apparent that the alloy containing cerium and lanthanum is a completely commercial product; whereas the alloy made without cerium or lanthanum is completely non-ductile.

The cone test enables considerable experimentation to be done on austenitic stainless steels regarding this question of hot ductility or hot-workability because of the good correlation of the hot working of the cone with the behavior in ingots. This makes it possible to study a variety of melting practices and analyses by means of the cone test to obtain the best possible analysis balance, and in the case of misch metal, cerium and lanthanum contents necessary to obtain the most ductile metal. For instance, each particular analysis requires some experimentation to determine the correct amount of cerium and lanthanum to be incorporated in the metal. This is not so apparent in the low alloyed steels of the 18-8 variety, such as Type 304, 316 or 317, but it is apparent in the higher alloyed grades—especially with the higher nickel contents. This is illustrated by the following experiments.

Table I shows some of the analyses studied to illustrate the effect of nickel on the resulting initial range of cerium and lanthanum necessary to obtain the best hot-working properties. These analyses were all

Fig. 9—These 4¾-in. square billets forged from 9⅝-in. ingots were from the same melts as cone tests shown in Fig. 8. Good billets correspond to good cones.

Table I. Analysis of Heats Studied to Illustrate the Critical Relationships Between Nickel, Cerium, and Lanthanum Contents

ALLOY → / BASE ANALYSIS: PCT ↓		A	B	C	D	E
Carbon		0.048	0.056	0.059	0.050	0.062
Manganese		1.14	1.09	0.97	0.91	0.89
Silicon		0.96	0.95	0.96	0.81	0.79
Phosphorus		0.004	0.013	0.004	0.006	0.012
Sulphur		0.010	0.013	0.007	0.008	0.016
Chromium		10.04	10.12	19.43	9.90	10.35
Nickel		67.58	59.13	49.64	30.28	9.96
Molybdenum		19.20	16.01	4.20	8.04	7.74
Cone A	Ce	None	None	None	None	None
	La	None	None	None	None	None
Cone B	Ce	0.057	0.025	0.020	0.014	0.020
	La	0.031	0.011	0.010	0.019	0.014
Cone C	Ce	0.048	0.033	0.038	0.030	0.041
	La	0.024	0.016	0.021	0.026	0.031
Cone D	Ce	0.098	0.054	0.079	0.087	0.041
	La	0.059	0.029	0.056	0.078	0.042
Cone E	Ce	0.208	0.161	0.163	0.131	0.110
	La	0.133	0.108	0.270	0.113	0.066
Cone F	Ce	0.32	0.238	0.195	0.169	0.102
	La	0.22	0.173	0.217	0.160	0.057
Cone G	Ce			0.52	0.39	0.42
	La			0.48	0.39	0.41
Cone H	Ce			0.59	0.57	0.58
	La			0.58	0.55	0.57
Cone I	Ce			0.30	0.66	0.84
	La			0.30	0.62	0.84
Cone J	Ce			0.70	0.72	1.27
	La			0.63	0.58	0.74
Cone K	Ce				1.03	1.03
	La				0.70	0.72

melted in a 60 lb high frequency furnace, using virgin charges to eliminate any questions of scrap contamination. The heats were deoxidized with CaSi in accordance with past experience in melting comparable grades of steel. A series of cones were cast, the first set containing no cerium or lanthanum. The next set was cast after an addition of misch metal equivalent to 2 lb per ton, the following set after an additional addition making a total misch metal addition equivalent to, say, 4 lb per ton, etc. The cones were then forged at the best forging temperature of the alloy, generally in the range 2050° to 2150°F, optical pyrometer temperature read on the die just after the first light blow to seat the cone on the die. Figs. 10, 11, 12, 13 and 14 illustrate the appearance of these cones containing variable amounts of cerium and lanthanum, and Fig. 15 is a chart showing quantitatively this effect

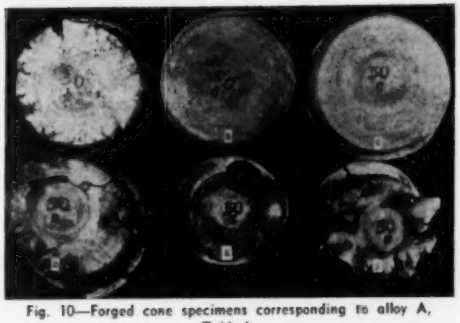

Fig. 10—Forged cone specimens corresponding to alloy A, Table I.

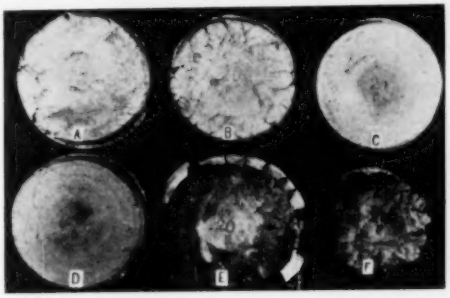

Fig. 11—Forged cone specimens corresponding to alloy B, Table I.

of nickel on the resulting critical range of cerium and lanthanum necessary to improve hot-workability.

At any given nickel content, the critical range of cerium and lanthanum necessary to achieve the best hot working properties can be narrower than the outside range shown in Fig. 15. For instance, Fig. 16 shows the appearance of upset cones for 0.10 pct C (max), 30 pct Ni, 20 pct Cr, and 4 pct Mo with variable misch metal additions. The critical range of cerium and lanthanum is shown to be 0.06 to 0.49 pct Ce + lanthanum corresponding to cones C, D, E and F.

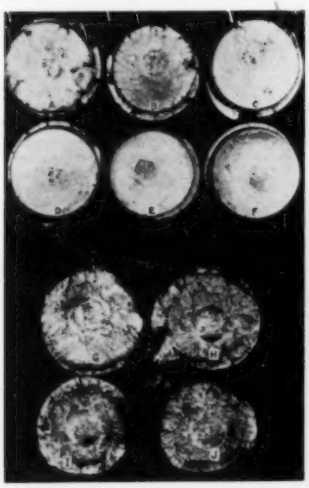

Fig. 12—Forged cone specimens corresponding to alloy C, Table I.

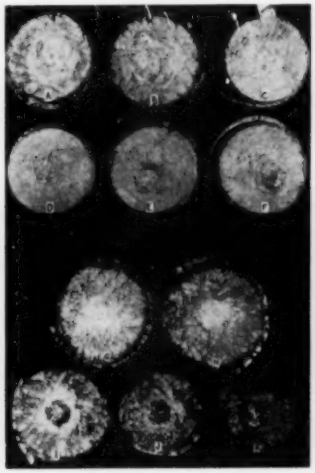

Fig. 13—Forged cone specimens corresponding to alloy D, Table I.

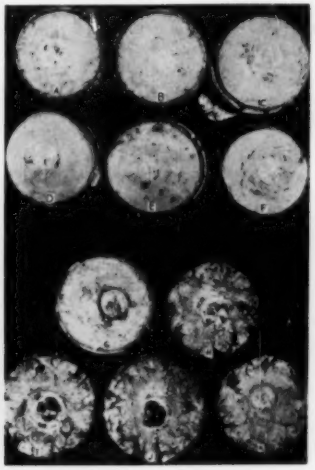

Fig. 14—Forged cone specimens corresponding to alloy E. Table I.

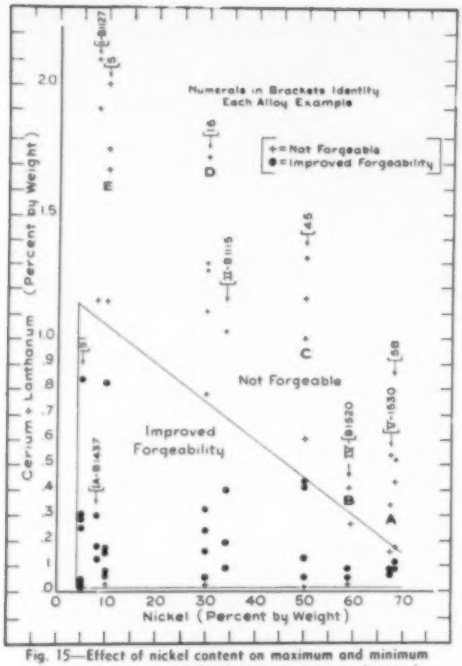

Fig. 15—Effect of nickel content on maximum and minimum amounts of cerium and lanthanum to improve hot-workability in Cr-Ni-Mo stainless alloys.

Increasing the molybdenum content to 12 pct requires a more restricted range of cerium and lanthanum to achieve the best hot working properties. This is shown in Fig. 17 for an analysis of 0.10 pct C (max), 30 pct Ni, 20 pct Cr and 12 pct Mo when the critical range of cerium + lanthanum is shown to be 0.13 to 0.32 pct Ce + lanthanum, corresponding to cones D and E.

The conclusion to be drawn from these experiments is that the nickel content of austenitic stainless steels containing elements of the group, chromium, molybdenum and tungsten determines the minimum and maximum amounts of cerium and lanthanum necessary to obtain improvements in hot-working (see Fig. 15), but for any analysis the critical cerium and lanthanum contents necessary to improve hot-working can be narrower and will fall within these preferred ranges, depending on the analysis being considered. Here experience or an actual experiment with the cone test will indicate the correct cerium and lanthanum range for best hot working properties.

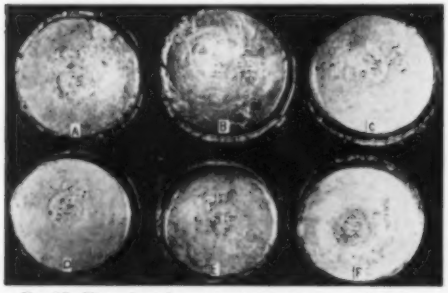

Fig. 16—These forged cone specimens are of an alloy containing 0.10 pct (max) carbon, 30 pct nickel, 20 pct chromium and 4 pct molybdenum. Cones C, D, E, and F show a marked improvement in forgeability over cones A and B.

The exact mechanism of misch metal (cerium, lanthanum, etc.) in promoting the hot-workability of these alloys has not yet been determined. In the course of experiments the various ranges of analyses which will be benefited by rare-earth additions have been established. It can be stated also with assurance the concentration of rare-earths necessary to improve the hot-ductility of the various alloys, but in spite of intensive investigation no clear explanation can be given of the deoxidation effects or benefits of the rare-earth additions. There appears to be little doubt that some of the benefits obtained are the result of a certain amount of deoxidation in the bath, which is accompanied by a marked increase in the fluidity of the molten metal. Since the effect obtained depends mainly on the alloy content of rare-earths, it is considered satisfactory to use the alloy content of rare-earths as a measure of the final results without a definite explanation of the deoxidation properties.

The examples up to this point have been concerned with showing the effect of misch metal in high-frequency melted Ajax steels because smaller melts, particularly on these types of alloys, are most suitably adapted to experimental study and application. The general conclusions from these experiments in high-frequency melted Ajax steel can be transferred to steels melted in the basic electric arc furnace. Certain modifications regarding the proper rare-earth content will be noticed in comparing Ajax with basic electric arc metal, but the effect of misch metal on the hot-workability of arc melted steel can be as marked as Ajax melted steels.

As an example of arc melting, Type 316 is ordinarily taken to have the following analysis range: 0.10 pct (max) C; 0.70 pct (max) Mn; 1.00 pct (max) Si; 16.00 to 18.00 pct Cr; 10.00 to 14.00 pct Ni; and 2.00 to 3.00 pct Mo. This grade of steel is hot-workable and is available in all the standard wrought products. At its best, this grade is somewhat more difficult to hot work and preparation losses generally exceed those for Type 302 or Type 304. Different heats can show varying grades of hot-workability, ranging from those heats partially scrapped at the mill and those requiring heavy billet preparation losses to those exhibiting the standard behavior of this grade. Fig. 18 shows two 4 in. rounds, two $4\frac{3}{4}$ in. rounds, and two $6\frac{3}{8}$ in. squares, hot rolled and pickled billets from a 12-ton arc melted heat of Type 316 analyzing: 0.060 pct C; 1.75 pct Mn; 17.55 pct Cr; 0.47 pct Si; 12.36 pct Ni; and 2.49 pct Mo. The misch metal was added to the ladle in an amount corresponding to 2 lb per ton. These billets were hot rolled direct from a $9\frac{5}{8}$ in. square 1000 lb ingot on a fixed pass 22-in. mill. The ingots were heated in an oil-fired continuous heating furnace, reaching the rolling temperature of 2350°F in the furnace, optical pyrometer temperature 2120°F at the mill. The appearance of these billets on the surface is as good as any rolling of the standard 18-8 grades of

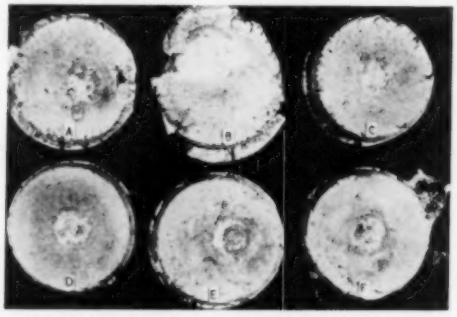

Fig. 17—These are forged cone specimens of a 0.10 pct carbon, 30 pct nickel, 20 pct chromium, and 12 pct molybdenum alloy. Forgeability of cones D and E is better than of cones A, B, C, and F.

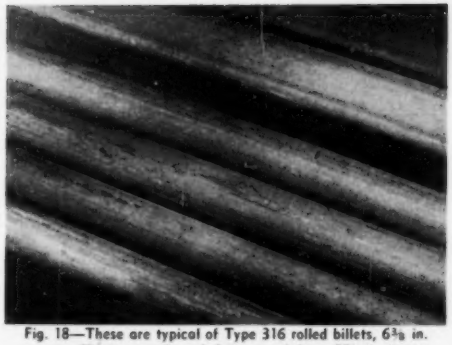

Fig. 18—These are typical of Type 316 rolled billets, 6⅜ in. square, 4¾ in. round, and 4 in. round from 9⅝-in. ingots when 2 lb of misch metal per ton of steel are added to the ladle of basic electric-arc furnace metal.

steel. Prepared billet yields for this heat of steel were 5 pct more than what was considered standard.

Fig. 19 shows a truckload of hot rolled slabs, Type 316, made by rolling 9⅝ in. ingots direct to slabs. The heat was alloyed with 2 lb of misch metal per ton, the steel analyzing 0.011 pct Ce and 0.011 pct La. The slabs were then prepared and rolled to strip 7¾ x 0.148 in. Fig. 20 shows the appearance of the hot rolled strip coil. Note the appearance of the edges. There is no sign of corner checking and the edges are as good as those obtained on Type 430 and Type 304. The yield from ingot weight to hot rolled strip weight increased 6.8 pct on the addition of misch metal in amounts of 2 lb per ton addition made in the ladle from basic electric arc metal.

Another grade of arc melted stainless normally considered difficult to hot work is a grade designated by Carpenter as Type 316X. This has the following nominal composition: 0.06 pct C; 1.75 pct Mn; 0.40 pct Si; 18.00 pct Cr; 9.25 pct Ni; and 2.25 pct Mo. The nickel content for the chromium and molybdenum contents is relatively low. This causes about 30 pct ferrite in the austenitic structure and up until the addition of misch metal the alloy was considered non-hot-workable. The addition of 8 lb of misch metal per ton to this analysis melted in the Ajax or 4 lb per ton in the arc furnace enables ingots to be roll cogged direct to slabs or round or square billets for rerolling into strip. In this case, cerium and lanthanum contents of 0.020 pct and more lead to a commercial product, whereas the alloy without misch metal is not, and was not, obtainable in wrought products.

Another example of the effect of misch metal on improving the hot working properties in a standard grade is that of Type 310. This grade has the following composition limits: 0.25 pct (max) C; 2.00 pct (max) Mn; 1.50 pct (max) Si; 24.00 to 26.00 pct Cr; and 19.00 to 22.00 pct Ni. Normally this grade has some measure of hot ductility, but in many cases proves exceedingly difficult to hot work. A misch metal addition of 4 lb per ton in the arc furnace and 8 lb per ton in the Ajax

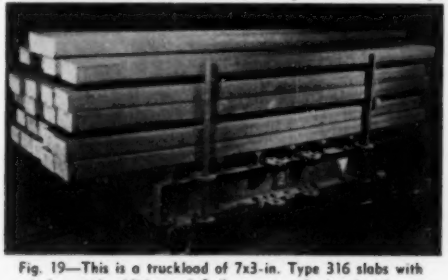

Fig. 19—This is a truckload of 7x3-in. Type 316 slabs with misch metal additions of 2 lb per ton, basic electric-arc furnace metal.

Fig. 20—Hot-rolled strip 7¾x0.148 in., Type 316 stainless, was made from slabs shown in Fig. 19. There are no cracks along the edge of the strip.

furnace increased the average billet yields of square and round bars by 6.7 pct. Slab rolling of this analysis from 9⅝ in. square ingots always has been a troublesome cogging operation. The misch metal additions make it possible to consistently roll slabs free of injurious checks, and as such, the slabs require very little preparation.

Type 308 stainless steel is another grade that will exhibit so-called *in and out* hot working properties. In this case, the problem can either be that of the steel being unbalanced chemically or of the steel having hot-short tendencies because of a particular melting procedure. Experimental and production data have shown that a misch metal addition of 4 lb per ton in the arc furnace will produce metal with consistently good hot working properties and an average billet yield increase of 4.8 pct over heats made without misch metal. In Carpenter Steel Co.'s practice, the most benefit has been obtained by being able to roll cog 9⅝ in. square ingots to billets, rather than cogging 7 in. ingots on a 16-in. mill, which was necessary before misch metal was used as standard practice.

Conclusions

1—The rare-earths are effective in improving the hot-workability of austenitic, or partly austenitic grades of stainless steels containing 4 to 70 pct Ni, and 10 to 60 pct of elements from the group of chromium, molybdenum and tungsten, the amount of any one element of the group of chromium, molybdenum and tungsten not to exceed 30 pct.

2—The nickel content determines the minimum and maximum amounts of cerium and lanthanum needed to obtain improvements in hot working.

3—At any nickel content, a specific alloy can have a critical cerium and lanthanum content narrower than that indicated by the nickel content, but this content will be within the broad range determined by the nickel content and will be influenced primarily by such alloys as molybdenum, copper, tungsten, etc.

4—Alloy additions of cerium and lanthanum in the range of about 0.02 to 0.04 pct are effective in promoting better hot-workability in high frequency Ajax and basic electric arc melted alloys such as Type 316, 310, 308, etc.

5—Alloy additions of cerium and lanthanum in the range of 0.08 to 0.18 pct are effective in achieving hot-workability in such alloys as Carpenter #20 (nickel-chromium-molybdenum-copper) and other high alloyed stainless steels for corrosion resistance and high temperature strength.

Acknowledgment

The authors gratefully acknowledge the cooperation of C. C. Wilson, Superintendent of Melting, and B. T. Lanphier, Metallurgist, and the encouragement of J. H. Parker, Chairman of the Board, Frank Palmer, President and G. V. Luerssen, Vice President of Carpenter Steel Co., without which this work would not have been possible.

Solid Solution Alloys Of Magnesium With Lithium and Indium

by W. R. Hibbard, Jr., A. L. Kearney, W. H. Hawley, Jr., and E. C. Burke

THE unique position of magnesium with respect to zone theory[1] enabling close control of the c/a ratio over a wide range of values by alloying, and the recent developments[2] of low c/a alloys with superior plasticity stimulated experiments on the comparative plasticity, strain hardening, microstructure, and preferred orientation of the metals given in Table I.

Alloys were prepared in an electric resistance muffle furnace with a nitrogen atmosphere using high purity magnesium and low-sodium lithium supplied by the Magnesium Div. of Dow Chemical Co., and 99.97 pct indium purchased from the Indium Corp. Small castings were homogenized in four stages with intermediate cold work. Heating time totaled 10 days at temperatures from 146° to 480°C for the indium alloy, and 186° to 588°C for the lithium alloy. Chemical analyses were made at the Aluminum Research Laboratory, New Kensington, Pa. Major impurities (less than 0.1 pct) were calcium and silicon in the lithium alloy and lithium in the indium alloy. All other elements detectable were in amounts less than 0.01 pct.

Table I. Magnesium Alloys Tested

Metal, Alloy	Weight, Pct	Atomic, Pct	c/a[3] Ratio
Mg-In	44	14.2	1.633
Mg	—	—	1.624
Mg-Li	5.4	16.4	1.606

Table II. Properties of Alloys Tested

Metal, Alloy	Density, G per Cc	D.P.H. No.	Tensile, Kips	Elongation, Pct in 1 In.
Mg-In	2.705	712	26.1	0
Mg	1.734	275	27.0	1.6
Mg-Li	1.574	427	21.4	3.0

Density, diamond pyramid hardness and tensile properties are given in Table II. The elongation values are unexpectedly low for some obscure reason. However, there is no question about the lack of ductility in the magnesium-indium alloy which broke with a flat brittle fracture.

Cylindrical specimens were cold rolled until cracking occurred, using percent elongation as a measure of the deformation, and determining diamond pyramid hardness after each 5 pct increment. Cracking appeared as follows: Mg-In, 20 pct elongation; Mg, 25 pct elongation; Mg-Li, 35 pct elongation. The strain hardening curves are shown in Fig. 1. The addition of 12.4 atomic pct In caused considerably more solution hardening than 16.4 atomic pct Li, but considerably more strain hardening occurred in the latter as shown in Fig. 2. Cylinders were also hot rolled from 600°F, reheating after each pass and determining hardness after each 5 pct elongation. The specimens all were rolled to over 150 pct elongation without significant cracking and without essentially changing the hardness.

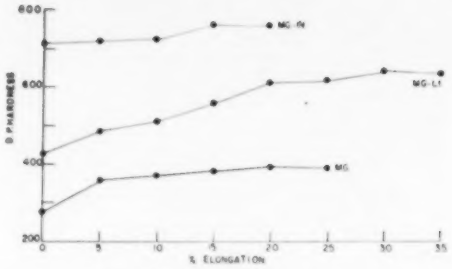

Fig. 1—Cold rolling curves.

Metallographic examination of the cold rolled specimens indicated that the Mg-Li and Mg contained numerous deformation twins, but the Mg-In specimen contained a series of wavy deformation bands or flow layers as shown in Figs. 3a, 3b, and 3c. The latter do not appear to be twins, but etching effects. Similarly, the hot rolled Mg-Li and Mg specimens contained twins, but the Mg-In alloy was apparently free from twins as shown in Figs. 4a, 4b, and 4c. These hot rolled structures appear to be recrystallized.

X-ray examination of the rolled specimens was carried out using the glancing angle technique off the rolling plane in both the rolling and transverse directions at 17°, the θ angle for (0002) diffraction with Cu K-alpha radiation. This method determines the approximate extent of the spread of the basal plane from the rolling plane, since high c/a ratio metals have a preponderant rolling direction spread,[4] while low c/a ratio metals have a wider transverse spread.[5] The orientation of the hot rolled specimens was nearly random, but the grain size was too large for any certainty of definition. For the cold rolled specimens, the transverse spread was greater than

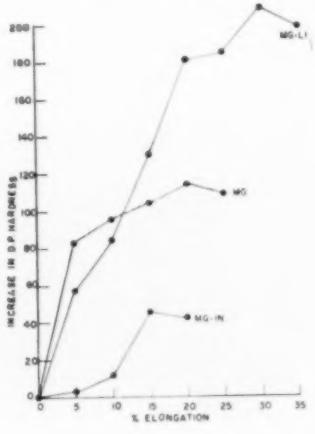

Fig. 2—Strain hardening curves.

W. R. HIBBARD, JR. is Associate Professor, W. H. HAWLEY, JR., E. C. BURKE, and A. L. KEARNEY are Graduate Students, Yale University, New Haven, Conn.

Fig. 3a—Mg-Li cold rolled, 35 pct elongation; 3 pct oxalic acid etch, 500 diam.

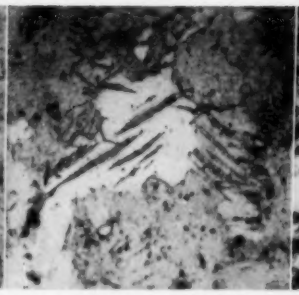

Fig. 3b—Mg cold rolled, 25 pct elongation; picral-acetic acid etch, 500 diam.

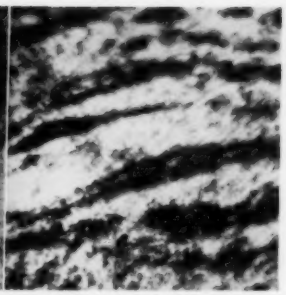

Fig. 3c—Mg-In cold rolled, 20 pct elongation; acetic acid acetone etch, 500 diam.

Table III. Summary of Results

	Mg-In	Mg	Mg-Li
Solution hardening, DPH No.	437	—	152
Strain hardening (20 pct), DPH No.	42	113	180
Microstructure, cold rolled	Deform. Bands	Twins	Twins
Microstructure, hot rolled	No Twins	Twins	Twins
Cold roll texture, trans/long spread	1.16	1.13	1.3
Cold rollability, elongation until cracking, pct	20	25	35
Hot rolling texture	All nearly random		
Hot rollability, elongation without cracking, pct	170	160	195

the longitudinal with the ratios of the angular spreads on the (0002) ring as follows: Mg-In, 1.16; Mg, 1.13; and Mg-Li, 1.30.

The Mg-In alloy was not well defined since the amount of rolling was small. The pronounced transverse spread in the Mg-Li alloy was expected because its c/a ratio approaches that of titanium,[6] beryllium,[7] and zirconium,[8] which show even more pronounced transverse spreads. The indication that pure magnesium showed slightly more transverse spread than longitudinal spread is not in agreement with the results of Bakarian.[9] However, his specimens were rolled at 600°F which is above the temperature where pyramidal slip starts.

The significance of twinning during rolling of magnesium and its alloys is puzzling, since with the basal plane in the rolling plane because of preferred orientation, and a low c/a ratio, twinning would produce an increase in specimen thickness in opposition to the decrease in thickness required by rolling. However, if twinning is considered as the means of placing the basal plane in the rolling plane, the low c/a ratio will favor twinning during rolling. This is illustrated in Fig. 5, where the thickness is reduced from A to B by twinning so as to place the basal plane in the rolling plane. This concept together with both basal and pyramidal slip and a nearly random recrystallized texture may account for the useful hot rollability of these alloys.

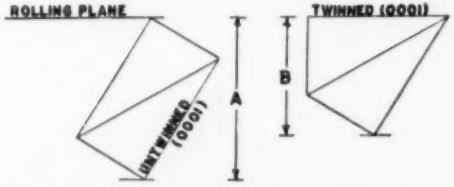

Fig. 5—Schematic movement of basal plane into rolling plane by twinning of low c/a structure. Twinning decreases thickness from A to B and thus is promoted by rolling.

These observations are summarized in Table III. It is hoped that the results will stimulate further investigation of these phenomena.

References

[1] W. Hume-Rothery: Atomic Theory for Students of Metallurgy. Inst. of Metals, London (1946) p. 247.

[2] J. H. Jackson, P. D. Frost, A. C. Loonam, L. W. Eastwood and C. H. Lorig: *Trans.* AIME (1949) **185**, p. 149.

[3] R. S. Busk: *Trans.* AIME (1950) **188**, p. 1460.

[4] V. Caglioti and G. Sachs: *Metallwirtschaft* (1932) **11**, p. 1.

[5] W. G. Burgers and F. M. Jacobs: *Metallwirtschaft* (1935) **14**, p. 285.

[6] H. T. Clark, Jr.: *Trans.* AIME (1950) **188**, p. 1154.

[7] A. Smigelskas and C. S. Barrett: *Trans.* AIME (1949) **185**, p. 145.

[8] P. W. Bakarian: *Trans.* AIME (1942) **147**, p. 266.

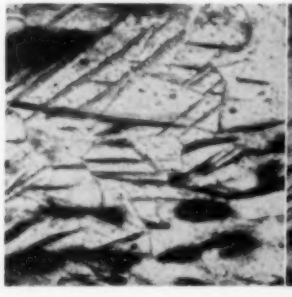

Fig. 4a—Mg-Li hot rolled, 100 pct elongation; 3 pct oxalic acid etch, 500 diam.

Fig. 4b—Mg hot rolled, 100 pct elongation; picral-acetic acid etch, 500 diam.

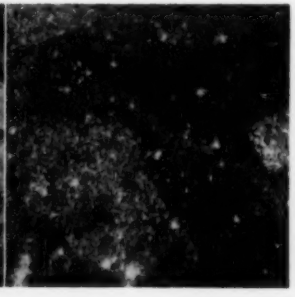

Fig. 4c—Mg-In hot rolled, 100 pct elongation; acetic acid acetone etch, 500 diam.

Nonporous Refractory Coatings Permit Use of Mild Steel for High Temperature Applications

DURING the war a method of upgrading mild steel was used with success for the protection of the mild steel exhaust pipes fitted to the engines of British *Spitfire* and *Mosquito* aircraft. Since the war, the process has been improved, according to *British Engineering*, July 1951.

The latest finish, shown as *Stoneclad*, was developed by Matthews Refractories, Ltd., London, S. W. 17, and is applied by Stewart & Gray, Ltd. It is designed to protect mild steel or cast iron from corrosion at high temperatures and to permit their use in many instances where heat-resisting steel otherwise would be specified. An exception is where the high temperature is accompanied by considerable stress. It consists in carrying, in a boro-silicate matrix, a suspension of insoluble refractories and bonding it to the metal surface by fusion at about 1472°F. The treatment may be a single homogeneous coat 0.004 in. thick where resistance to oxidation only is required; or it may be in two coats, the upper being more refractory than the lower, porous, and 0.020 in. to 0.030 in. thick. The properties of the coating depend upon the proportions of refractory to matrix, the particle size, the number of layers present, and the porosity of the upper face. It is always nonporous at the metal interface.

The process has been applied successfully to the emitting surface of radiant heaters used for space and industrial heating. In an industrial heater in which a mild steel sheet is heated by products of combustion from a bar burner at the bottom of the combustion chamber formed between the steel sheet and a slab of insulating material, a baffle plate is fitted behind the radiating surface. This shields the lower part from overheating due to direct exposure to the products of combustion and radiation from the flames and insulating slab. The panel temperature of this heater originally was limited to 650°F because, at that temperature, the baffle plate was at about 932°F, above which it is not advisable to heat mild steel for long periods if scaling is to be avoided.

The radiant panels and baffle plates of these appliances are now protected by the *Stoneclad* process. The finish of the panels is smooth and black or dark gray in color, its purpose being to prevent rusting; while the baffle plates have a comparatively rough surface brought about by the inclusion of a higher proportion of refractory material. This results in a greater resistance to high temperatures and thermal shock.

The heater with the panel and baffle plate protected by this process has operated for 5000 hr at a panel temperature of approximately 850°F at which the baffle plate is about at 1148°F. On occasions, however, the panel temperature has been as high as 890°F and the baffle temperature 1274°F. The high panel temperature attained in these tests was the result of doubling the normal heat input of the appliance while the panel was radiating on to the surroundings at approximately room temperature.

The tests on the unprotected baffle plate were concluded at 1700 hr because the scaling of the mild steel was having an adverse effect on the performance of the appliance, and the material had failed. In contrast, there was no appreciable change in the appearance of the protected baffle plate after heating for 1700 hr and after 5000 hr heating. It was still working satisfactorily after 7000 hr under the same conditions.

Apart from this application it is used on a number of space heating appliances. A finish similar to that used for the protection of baffle plates has been applied with success to a fabricated mild steel mixing chamber, used in connection with some experiments in which products of combustion at about 1472°F passed through a central tube while comparatively cool recirculated gases were fed into the annulus surrounding the tube before being mixed with the hot gases. Unprotected mild steel had a life of only a few hours, whereas the upgraded mild steel appeared to be in its original condition at the end of the experiments.

The smooth finish as applied to the panels of radiant heaters is claimed to be suitable for use up to a temperature of 1238°F and the refractory finish for baffle plates for temperatures up to 1472°F.

Work Hardening-Reannealing Cycle of Pure Silver

by Marian Balicki and Goldye Leeds

A SURVEY of literature reveals the scarcity of experimental evidence relating to work hardening and reannealing of silver.[1-10] With the exception of the well-known X-ray investigation of silver and other metals by W. A. Wood,[11] the effect of progressive cold working has not been studied. The determination of thermal stability of silver in the work-hardened state by means of isochronal or isothermal annealing has been confined apparently to very high reductions only. In the survey made, no study was encountered which endeavored to produce a complete picture of the changes in various properties due to cold working and subsequent reannealing. To fill these gaps and to assemble data that could be used for the determination of activation energies and of frequency coefficients of primary recrystallization, a systematic experimental approach, which was developed by one of the authors, has been applied to pure silver.

Material and Processing

The silver used was Handy and Harman fine silver, with a spectroscopic analysis at the testing stage of Cu, 0.0001 to 0.001 pct; Te, 0.0001; Pb, Si, Ca, Mg, and Mn, traces. The material was supplied in the form of a rod 0.406 in. diam and was converted into test samples according to the procedure condensed in Table I. It should be mentioned that air annealing was adopted to simulate industrial practice, though it was realized that annealing in a neutral gas or in a vacuum would be preferred.

Table I. Processing of Handy and Harman Silver for Testing

Rod 0.406 in. diam
↓
Air annealing for 1 hr at 600°F followed by air cooling
↓
Swaging to 0.250 in. diam
↓
Air annealing for 1 hr at 600°F followed by air cooling
↓
Drawing to 18 different diameters
↓
Air annealing for 1 hr at 600°F followed by air cooling
↓
Final wire drawing of all wires to 0.032 in. diam to obtain wires with different degrees of cold work. This step was accomplished just prior to testing or heating, followed by marking of the wires for identification.
↓

↓	↓	↓
Testing for the presence and magnitude of strain-age-hardening on storage and handling	Air annealing of selected degrees of cold work for 15 min followed by air cooling	Study at rising temperature of thermoelectric properties (to be described separately)

↓
Determination at room temperature of proof stress, ultimate stress, elongation. Microstructure.

The usual precautions have been taken to eliminate any structural changes and property changes resulting from the storage of the samples prior to annealing or testing. Thus the wires were kept at the fully annealed stage, and the final wire drawing, which produced the desired degree of work hardening, was done just prior to the final annealing or testing. During the short waiting period, the samples were kept in a thermosflask filled with ice. Even with these precautions some strain-age-hardening or self-annealing could occur.

To test such a possibility, wires of different reductions were prepared in the manner adopted and portions of them were immediately tested. The remaining portions were similiarly tested after different periods of storage, both at room and melting-ice temperature. Within experimental error, all samples obtained from a wire of a given percentage of reduction yielded identical values. This result qualified the material for further tests and interpretations, because it showed that either strain-age-hardening and self-annealing were absent, or that these effects fully balanced each other.

The final annealing was carried out in an electric resistance furnace automatically controlled to within $\pm 10°F$. It was realized that the temperature fluctuations were greater than desired for this type of work. To diminish the errors due to fluctuations of temperature, the hot junction of the thermocouple was placed as close to the samples as possible; the time of soaking was reduced to 15 min; and the number of samples annealed at different temperatures was increased.

It will be seen from Table I that some tests were performed on the same material at rising temperature. These will be discussed elsewhere.

Room temperature testing was limited to the determination of some of the mechanical properties that are known to be additive in a degree sufficient to be used for indirect study of the kinetics of the reannealing process. Tensile tests, carried out on a manually operated J. Camillon machine, accurate to within ¼ lb, permitted the determination of the ultimate stress (U.S.) and of the 2 in. elongation, (A_2). The proof stress (σ_b) has been determined from a series of bend tests carried out on a Tinius Olsen Stiffness Tester by using the offset method. This involved accurate determination for each sample of load-angular deflection curves, finding a

M. BALICKI, Member AIME, is Professor of Metallurgical Engineering, Polytechnic Institute of Brooklyn, Brooklyn, N. Y., and G. LEEDS is a Field Engineer, West End, N. J.

Discussion on this paper, TP 3158E, may be sent, 2 copies, to AIME by April 1, 1952. Manuscript, May 7, 1951. New York Meeting, February 1952.

This paper represents part of a thesis by Goldye Leeds submitted in partial fulfillment of requirements for the degree of Bachelor of Metallurgical Engineering to the Polytechnic Institute of Brooklyn.

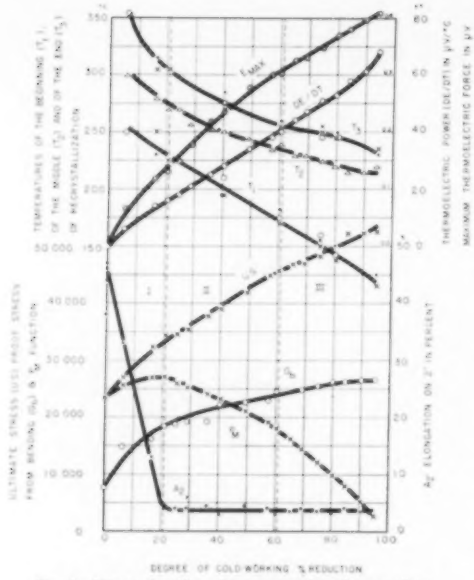

Fig. 1—Effect of cold work on properties of pure silver.

A_2 is the elongation on 2 in., σ_{ts} the proof stress from bending test; U.S., the ultimate stress; p_m, Krupkowski's strength factor; dE/dt, the thermoelectric power of couples Ag cold-worked/Ag annealed; E_{max}, the maximum thermoelectric force developed by the same couples; T_1, T_2, T_3, the temperatures of the beginning, middle, and end of recrystallization respectively, all plotted vs. the percentage of reduction produced by room temperature drawing.

load responsible for 5° deflection, and calculating the corresponding stress from the bending formula. Values of proof stress thus obtained would be somewhat higher than those determined from tensile tests. This difference, which is of no real significance for the main purpose of the work, should be attributed to the adoption of a relatively large angle of permanent set, which brings the most stressed portion of the cantilever test piece well inside the plastic range. There, the bending formula, which is valid within the elastic range only, yields inflated values of stress.

Results

The data obtained have been collected in Appendix 1.* Figs. 1, 2, and 3 represent the findings graphically. Fig. 1 shows how a number of physical properties of fine silver change by cold working from 0 to 95 pct reduction. Elongation on 2-in. gage length A_2, for instance, rapidly decreases from its original value of 46 pct to a constant level of 3 pct, at about 21 pct reduction, z. Ultimate stress, U.S., and proof stress from bending, σ_{ts}, exhibit an almost steady increase, with increasing reduction, though not quite the same in each case. Severe reduction of 95 pct more than doubles the starting values of these properties.

For fuller illustration of the effect of cold working on silver, Fig. 1 contains six additional curves. Two of these, namely, thermoelectric power, dE/dT, and maximum thermoelectric force, E_{max}, shown by thermocouples made of silver wires drawn to different reductions, z, and a standard fully annealed silver wire, show a steady increase as a function of the percentage of reduction. This increase, it will be seen, is very similar to the increase of ultimate and proof stress.

The strength change index, p_m, introduced by Krupkowski[11] has been calculated from ultimate stress data and values of the percentage of reduction z, by means of the relationship $p_m = \text{U.S.} \left(1 - \frac{Z}{100}\right)$. It may readily be shown that $p_m = \frac{P_{max}}{F_o}$, where P_{max} is the breaking load and F_o, the section area prior to final wire drawing. It may be seen in the figure that this index slightly increases for low reductions to reach a shallow maximum at about 21 pct. This is followed by a steady decrease, slightly accelerated after 60 pct reduction.

The last three curves in the figure, namely, T_1, T_2, and T_3, represent, as a function of the percentage of reduction, the characteristic temperatures of primary recrystallization, which is the phenomenon responsible for the main change in properties on reannealing. The data for plotting the T_1 and T_3 curves, illustrating the temperatures of the beginning and of the end of recrystallization, respectively, have been derived from Figs. 2 and 3; while data for the T_2 curve, that is, the temperature of the middle of recrystallization, have been taken from studies of thermoelectric properties at rising temperature. It may be seen that in silver, as in other metals, the temperature range in which the main change in properties takes place on reannealing, is visibly lowered for higher reductions. Unlike other metals studied by this method, however, for reductions greater than 60 pct, silver exhibits an enlargement of the temperature range (vertical distance between T_3 and T_1 curves). It appears that the beginning of recrystallization is decreasing with reduction more rapidly than is the middle and the end of the process (Figs. 2 and 3).

An analysis of all the curves shown in Fig. 1 permits distinguishing three regions of plasticity. The first region between 0 and approximately 21 pct reduction is characterized by rapid increases or decreases in most of the curves. The limit of this region is quite well defined by the percentage of reduction at which elongation reaches its low value and by the maximum in the p_m curve. The second region between approximately 21 and 60 pct reduction shows a steady run in most of the curves. The border between the second and the third region is not easy to locate. This can best be done with reference to Fig. 4, which is a supplementation of Fig. 1. Wood[11] in his work on silver of similar purity to that used in this study, encountered a growing tendency toward self-annealing after 65 pct reduction, i.e., in the third region of plasticity.

Figs. 2 and 3 show the change in mechanical properties of wires with a selected percentage of reduction caused by 15 min reannealing at different temperature levels. All curves in these figures are well determined by suitably spaced experimental points. The proof stress σ_t curves show least deviation of experimental points, and they appear to be more suited for revealing small differences encountered than are the ultimate stress curves. For instance, proof stress and elongation curves for 80.1 and 60.5 pct reductions (Fig. 2) show quite well a small shift of the main change in the direction ex-

* For Appendix 1 order Document 3360 from American Documentation Institute, 1719 N St., N.W., Washington 6, D. C., remitting $1.00 for microfilm (images 1 in. high on standard 35 mm motion picture film) or $1.00 for photocopies (6x8 in.) readable without optical aid.

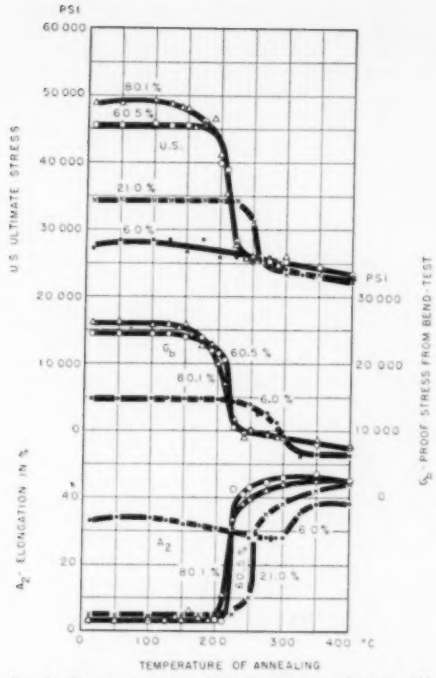

Fig. 2—Change in the mechanical properties of silver cold drawn to 6.0, 21.0, 60.5, and 80.1 pct reduction due to annealing for 15 min at the temperatures indicated.

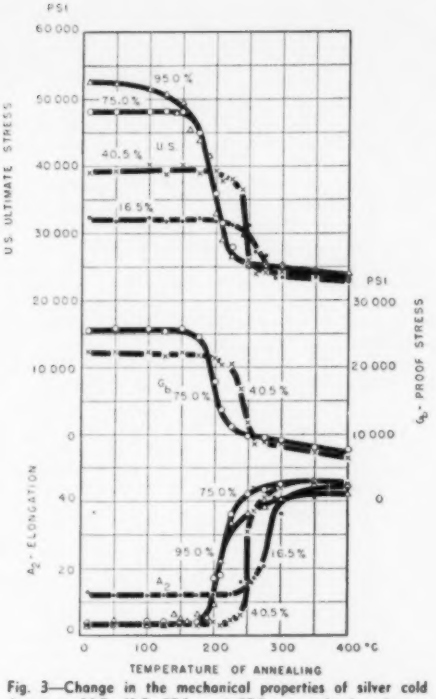

Fig. 3—Change in the mechanical properties of silver cold drawn to 16.5, 40.5, 75.0, and 95.0 pct reduction due to annealing for 15 min at the temperatures indicated.

pected, while the ultimate stress curves exhibit too great a scatter of points to permit any differentiation.

All the curves in Figs. 2 and 3 can be divided into three parts; two almost level and straight portions at low and high temperatures of annealing joined by a third curved portion. The temperature at which the low temperature straight portion joins the curved segment is that of the beginning of primary recrystallization, while the temperature at which the curved segment merges with the second straight portion is that of the end of recrystallization. Observation of the temperatures at which tangents drawn to the straight line portions depart from the curves yields the values of T_i and T_f. The temperatures of the beginning and of the end recrystallization obtained from all reannealing curves in Figs. 2 and 3 have been plotted on Fig. 1, using the same markers as in the curves from which they have been derived. There is some scatter of points, but it is not large. It may therefore be concluded that all three properties of the wire with a given percentage of reduction exhibit the main recrystallization change in the same range of temperature.

Microstructure of silver wires with different degrees of cold working has been studied at a magnification of 500X. In general, the structural changes revealed by this work follow the pattern exhibited by other metals on progressive work hardening and reannealing. Because of that only a very brief summary of results needs to be given. In the first region of plasticity, that is, for reductions lower than 21 pct, the microscope revealed the presence of slip lines, as well as a slight departure from equiaxiality of the original crystals. In the second and third region of plasticity, a progressively better developed fibrous structure was observed. The effect of annealing was studied on wire with 40.5 pct reduction. Small annealed areas were first observed on samples annealed for 15 min at 225°C. The wire annealed at 250°C produced a structure almost completely free of work-hardened state. These results, when considered together with reannealing curves for z = 40.5 pct in Fig. 3, permit a statement that the change in mechanical properties of cold-worked silver, as in other metals, is due to primary recrystallization; that is, the conversion of the work-hardened structure into a fully annealed, stress-and-distortion-free

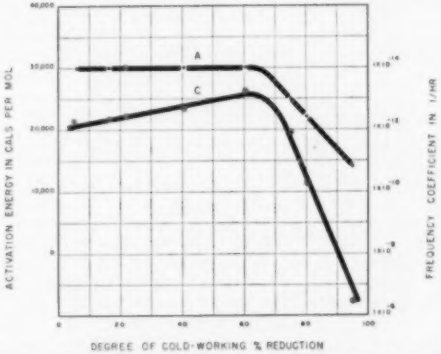

Fig. 4—Activation energies A and frequency coefficients C of primary recrystallization of cold-drawn silver as a function of the percentage of reduction.

one. As the main change in mechanical and physical properties on reannealing has been ascribed to "recovery" or "relaxation," it follows that these phenomena are identical with primary recrystallization.

Activation Energy and Frequency Coefficient

The data secured from isochronal annealing experiments and collected both in Appendix 1 and Figs. 2 and 3 can be used for calculation of two coefficients, namely, the activation energy and the frequency coefficient of primary recrystallization. Since a number of suitably spaced reductions between 5 and 95 pct reduction have been tested, the change of these constants as a function of the degree of cold work (z) can also be determined. The calculations are based on the fact that primary recrystallization is an activated process.[12, 13] In the absence of pronounced side phenomena such as strain-age-hardening and excessive crystal growth, primary recrystallization is described by the expression:

$$x = 1 - e^{-c_z t_z e^{-A/RT}}$$

or

$$\log \frac{1}{1-x} = c_z t_z e^{-A/RT}$$

In this expression, x is the fraction of a unit volume of a work-hardened metal sample which has fully recrystallized on subsequent reannealing. Depending on conditions of reannealing, i.e., on temperature of reannealing, T°K and the time in hours, t, x may acquire any value between 0 and 1. The expression also contains A, the activation energy of the recrystallization process, R, the gas constant, and k, the frequency coefficient.

For a given metal sample, having the same composition and history, the values A and C are constant. To find numerical values of these it is necessary to plot log-log $1/(1-x)$ vs. $1/T$. The numerical values of x required for this step can be secured from reannealing data such as those collected in Appendix 1, if the properties studied are additive to a degree sufficient for the purpose. The properties studied in the present work are considered as adequately fulfilling this condition. The calculation of the amount of the fully annealed state in partially annealed samples x has been obtained from the proportion:

$$x = \frac{(P_z - P_z)}{(P_z - P_z)}$$

when using properties which decrease on reannealing, viz., ultimate stress and proof stress from bending. When a property that increases on reannealing is used, such as elongation, both the numerator and the divisor in the proportion are multiplied by (-1). In the above proportion, P_z designates the value of a property found when testing a fully cold-worked sample without any annealing; P_x, the value of the same property found after annealing for 15 min at temperature T°K; and P_∞, the level of property values found in totally annealed samples.

With the exception of the data for $z = 21.5$ pct all the data assembled in the Appendix have been used and values of log-log $1/(1-x)$ calculated. These, whether derived from the values of ultimate stress, proof stress, or elongation of a given percentage of reduction of the wire, have been plotted on the same diagram vs. the inverse of the absolute temperature of annealing. The points for each percentage of reduction arranged themselves into straight lines. The spread of points present introduced some uncertainty as to the true position of the straight line. To secure straight lines, the slope of which would yield the value of activation energy A, five different observers were asked to determine their version of the slopes of the straight line for

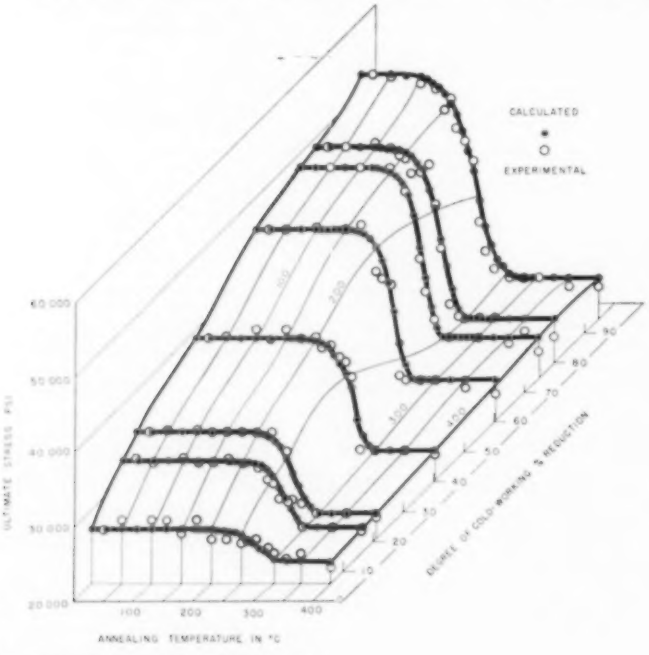

Fig. 5—Space diagram showing the agreement between the experimental and calculated values of the ultimate stress of silver cold drawn to the reductions indicated and subsequently annealed for 15 min at the temperatures indicated. Open circles, experimental; filled in circles, calculated.

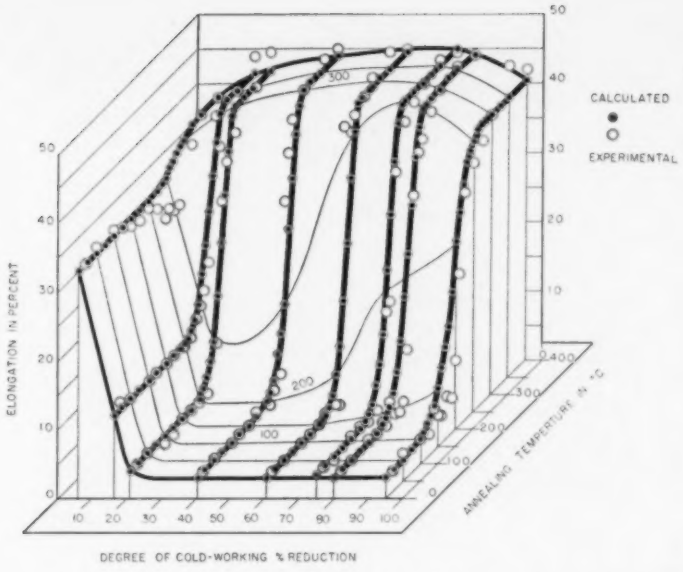

Fig. 6—Space diagram showing the agreement between the experimental and calculated values of 2 in. elongation of silver cold drawn to the reductions indicated and subsequently annealed for 15 min at the temperatures indicated. Open circles, experimental; filled in circles, calculated.

each system of points. The slopes thus obtained resulted in average values of the activation energies and frequency coefficients of each degree of cold work. A plot of these coefficients vs. the corresponding percentage of reduction is given in Fig. 4. The values for 21 pct reduction have been obtained by interpolation. The differences between the different observers, alone, make these points uncertain to within ± 4000 cal per mol. It may be seen in Fig. 4 that the activation energy remains constant up to 65 pct of cold work and diminishes steadily for higher percentages of reduction. The constant level of activation energy is approximately at 30,000 cal per mol, a value found previously for copper, nickel, and iron.

The values of the frequency coefficient, c, are also plotted on Fig. 4. They arrange themselves into a curve which slowly increases up to about 60 pct reduction and subsequently decreases. This decrease is very rapid.

Verification of the Treatment Employed

There are two pertinent questions which demand an answer: 1—how accurately do the equations used in the treatment describe the course of reannealing, and 2—how well are the activation energy and the frequency coefficients determined? A positive answer to both questions can be secured by confronting the experimentally found values of three properties studied after 15 min annealing at different temperatures with corresponding values derived by calculation from the equations used. A reasonably good coincidence of calculated and experimental points should constitute a proof that both the equations employed, as well as the constants used, are sound. Too great a difference between the experimental and calculated values would indicate that either the equation or the constants are wrong. An additional investigation would then be necessary to secure an individual answer to the two questions.

The detailed calculations of the P_x values are omitted here. The steps involved in arriving at the calculated P_x values are as follows: 1—substituting into the main equation numerical values of A and c found for silver with the percentage of reduction examined, together with numerical values of R and t = 15 min; 2—finding numerical values of x from this equation for several assumed values of temperature, T; 3—substituting these values of x into the auxiliary equation, $x = (P_i - P_x)/(P_i - P_a)$, together with numerical values of P_a and P_i; and 4—solving this equation for P_x. The values of ultimate stress, proof stress, and 2 in. elongation thus obtained have been plotted against the assumed temperatures of annealing (filled double circles in Figs. 5, 6, and 7). The experimental data from Appendix 1 have also been plotted on the same diagram (open double circles). As may be seen from these figures, in which all results are collected, the calculated and experimental points lie as closely together as can be hoped for. Because the experimental and calculated curves coincide, a conclusion can be drawn that the equation used truly depicts the course of reannealing of silver, and that the numerical values of the activation energy as well as those of the frequency coefficients have been determined to a satisfactory degree.

Discussion

A few remarks concerning the curves of the activation energy and of the frequency coefficient, Fig. 4, are in order. Up to a 60 pct reduction, both these curves behave like similar curves for iron and nickel tested by this method. Here, the activation energy remains almost constant and at the same 30,000 cal level, while the frequency coefficient increases. Such a run of the curves is quite in conformity with the principles of the activation mechanism, though it is not entirely clear why all three metals should require the same activation energy for primary recrystallization.

Above the 60 pct reduction, that is, in the third region of plasticity, both the activation energy and the frequency coefficient of primary recrystalliza-

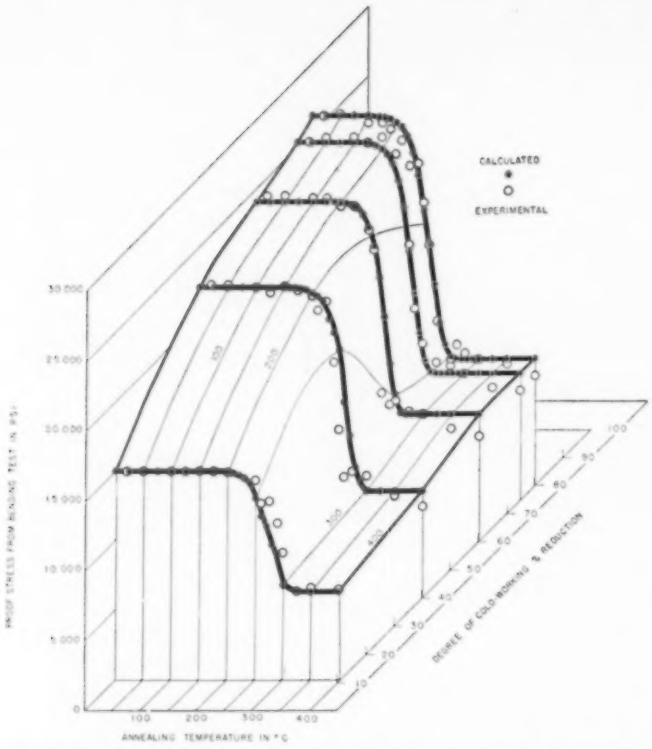

Fig. 7—Space diagram showing the agreement between the experimental and calculated values of the proof stress from the hardening of silver cold drawn to the reductions indicated and subsequently annealed for 15 min at the temperatures indicated. Open circles, experimental; filled in circles, calculated.

tion of silver diminish. This is unexpected, for, with the lowering of the activation energy, it would be reasonable to expect the frequency coefficient to increase. The verification treatment reveals (see Figs. 5, 6, and 7) approximately the same closeness of experimental and calculated points both below and above the 60 pct reduction. This means that the pairs of the frequency coefficients and activation energies, which determine the result of calculation, are quite accurate throughout the whole range of reduction studied. It appears from the above that the lowering of the activation energy and of the frequency coefficient after 60 pct reduction is real and that it is associated with the differences exhibited by reannealing curves after 60 pct reduction is passed. In the region above 60 pct reduction, the drop in properties extends over a longer interval of temperature; the end of recrystallization (T_e) remaining about the same, while the beginning of recrystallization moves rapidly towards room temperature as the percentage of reduction increases, Fig. 1.

The behavior of this kind is no doubt a demonstration of the tendency to self-annealing, to which severely cold-worked silver is known to be prone. The work of Wood[11] reveals that silver, very similar in purity to that used in this work, started to self-anneal when 60 pct reduction was reached.

Thus, the unexpected lowering of the frequency coefficient when the activation energy decreases should be linked with the causes and the mechanism of self-annealing. As our knowledge of self-annealing is limited, the clarification of the issue raised by this work must be left for future research.

In view of the findings presented in this paper, it appears that the recovery of mechanical properties of cold-worked silver on reannealing is caused by primary recrystallization, that is, principally by conversion of the fully work-hardened state into a fully annealed one, and that this process is somewhat affected by the tendency for self-annealing, which occurs at reductions higher than 60 pct.

References

[1] D. H. Ingall: *Journal* Inst. Metals (1924) **32**, pp. 41-64.

[2] R. Glocker and E. Kaupp: *Ztsch. f. Metallkunde* (1924) **16**, pp. 377-379.

[3] R. Glocker: *Ztsch. f. Physik* (1925) **31**, pp. 386-410.

[4] R. Glocker: *Ztsch. f. Metallkunde* (1925) **17**, p. 353.

[5] R. Glocker: *Journal* Inst. Metals (1926) **35**, p. 486.

[6] R. Glocker and H. Widmann: *Ztsch. f. Metallkunde* (1927) **19**, pp. 41-43.

[7] H. Widmann: *Ztsch. f. Physik* (1927) **45**, pp. 200-224.

[8] K. Honda and Y. Shimizu: *Sci. Rep.* Tohôku Univ. (1931) **20**, pp. 460-488.

[9] G. Tammann: *Ztsch. f. Metallkunde* (1934) **26**, pp. 97-105.

[10] E. Osswald: *Ztsch. f. Metallkunde* (1935) **27**, pp. 101-104.

[11] W. A. Wood: *Proc.* Royal Soc. (1936) **172**, pp. 231-241.

[12] A. Krupkowski and M. Balicki: *Acad. Sci. Techn. Varsovie.* (1936) **3**, p. 90.

[13] A. Krupkowski and M. Balicki: *Acad. Sci. Techn. Varsovie.* (1937) **4**, p. 270. Recrystallization chapter.

[14] M. Balicki: *The Physics of Powder Metallurgy.* Chap. 4. (1951) New York. McGraw-Hill Book Co.

Effect of Rare-Earth Metals On the Properties of Extruded Magnesium

by T. E. Leontis

The specific effect of various rare-earth metals on the room- and elevated-temperature properties of magnesium has been evaluated. Alloys containing didymium exhibit the highest tensile and compressive strengths at room and elevated temperatures. All the rare-earth metals increase the creep resistance of extruded magnesium at temperatures in the range of 400° to 600°F, but the degree of enhancement depends on the temperature and on the concentration of the added metal.

THE effects of rare-earth metals on the properties of sand-cast magnesium were discussed in some detail in earlier paper by the author.[1] The present paper deals with the effect of the same alloying elements on the properties of extruded magnesium. This investigation also had as its aim the development of a wrought alloy having a better combination of room-temperature strength and ductility and elevated-temperature strength and creep resistance than is found in magnesium-Mischmetal-manganese alloys, which have been reported earlier.[2-5] The only known attempt to study wrought magnesium alloys containing pure cerium instead of Mischmetal was made by Mellor and Ridley.[6] They found that in the form of rolled bars there is a definite, optimum cerium content for creep resistance at 200°C and that the creep resistance of these alloys at 200°C is significantly improved by heat treatment at 550° to 580°C.

In the present investigation the compositional variation in mechanical properties of the following alloy systems is presented: 1—magnesium-Mischmetal. 2—magnesium-cerium-free Mischmetal. 3—magnesium-didymium. 4—magnesium-cerium. 5—magnesium-lanthanum. Alloys containing predominately praseodymium are not included in this series because of the lack of this material.

Experimental Procedures

The alloying ingredients used in preparing the alloys described herein are the same as those reported in the earlier paper.[1] Cerium-free Mischmetal is the rare-earth mixture remaining when the cerium is removed from Mischmetal, which contains all the rare-earth metals as they occur naturally in monazite sand, the ore from which Mischmetal is produced. Removal of both cerium and lanthanum from Mischmetal leaves what is commonly called "didymium," consisting predominantly of neodymium and praseodymium. Although the composition of the particular batch of each metal used may differ somewhat from the analysis presented previously, these differences are not great enough to warrant repeating the specific composition of each material. The electrolytic magnesium used as the starting material in these alloys has the same typical analysis as that given in the earlier paper.[1]

The alloys were prepared in small laboratory melts applying all the necessary precautions for alloying rare-earth metals with magnesium described by Marande.[7] Most melts were large enough to cast one 3 in. diam billet 10 in. long. In a few cases, particularly the didymium-containing alloys, the lack of sufficient amounts of the rare-earth metal limited the size of the billet to 6 to 8 in. All billets were scalped to a diameter of 2 15/16 in. and faced to a length of 9¼ in. as limited by the size of the extrusion container.

The alloys were extruded into ½ in. diam rod on a 500-ton direct-extrusion press using a 3 in. container. The details of the extrusion step are: billet preheat, 925°F (2 hr); container temperature, 900°F; die temperature, 900°F; extrusion speed, 10 ft per min; reduction ratio, 36:1; and percent reduction, 97.3. The lower melting point of alloys containing didymium[1] necessitated reduction of the extrusion speed to 5 ft per min in order to prevent hot shorting during extrusion. Adequate lengths were cropped from both ends of each extruded rod to assure that all the material used for tests was extruded under uniform conditions.

Tensile and compressive properties at room temperature are reported in the several conditions of heat treatment. The ASTM designations are used to distinguish these conditions as follows:

T5—Direct age at 400°F (16 hr)
T4—Heat treat at 950°F (4 hr) for alloys containing didymium
T4—Heat treat at 1050°F (4 hr) for all other alloys
T6—T4 + age at 400°F (16 hr)

The lower heat-treating temperature for alloys containing didymium is necessitated by the lower melting point of these alloys. All heat treatments were conducted in electrically heated, circulating-air furnaces. A protective atmosphere containing 0.5 to 1.0 pct sulphur dioxide was used for the high temperature heat treatments.

Tension and creep specimens 6½ in. long and compression specimens 1½ in. long were cut from the extruded rod. A reduced section of ⅜ in. diam was machined on the tension specimens, whereas on the creep specimens a reduced section of 0.450 in. diam

T. E. LEONTIS, Member AIME, is associated with the Metallurgical Laboratories, The Dow Chemical Co., Midland, Mich.

Discussion on this paper, TP 3154E, may be sent, 2 copies, to AIME by Jan. 1, 1952. Manuscript, April 16, 1951; revision, Aug. 27, 1951. Detroit Meeting, October 1951.

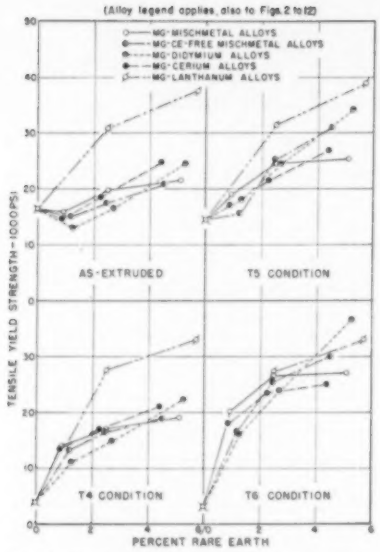

Fig. 1—Tensile yield strength at room temperature.

was used. The ends of the compression specimens were machined square with the cylindrical side, and the tests conducted on the full ½ in. diam without a reduced section. All tension and compression tests were conducted according to standard ASTM testing procedures. Elongation on the ⅜ in. reduced section was measured over a 1½ in. gage length. Yield strengths were determined by the offset method from autographic stress-strain curves at 0.2 pct deviation from the modulus line. Each result is the average of two tests.

Details of the equipment and methods of creep testing have been described elsewhere.[5, 6] Space does not permit the presentation of the complete creep data either in tabular or graphical form. Instead, the creep characteristics of each alloy are defined by the following three parameters:

1—Limiting stress to give 0.1 pct creep extension in 100 hr
2—Limiting stress to give 0.2 pct total extension in 100 hr
3—Limiting stress to give 0.5 pct total extension in 100 hr

These quantities were derived from log stress vs. log extension plots of the original data as described earlier.[7, 8] The total extension figures include the creep extension as well as the initial extension resulting from application of the load. The brevity of these tests prohibits any great significance being ascribed to the measured creep rates, which consequently are not reported in this paper. The method of determining electrical conductivity has been described in an earlier publication.[9]

Discussion of Results

Effect of Extrusion Speed and Temperature: In order to obtain the optimum properties, it is necessary to extrude the alloys under carefully selected conditions. The two most important variables in this process are temperature and speed. Reduction also has some effect on the properties of magnesium extrusions; however, in the case of extruded round rods, the properties are relatively insensitive to reduction over a wide range—as from 16:1 to 144:1. The reduction used in these experiments falls well within this range.

The effect of extrusion speed was determined on an alloy containing 5 to 6 pct Mischmetal + 1.8 pct Mn (according to the ASTM system of designation, this alloy is known as EM62). It was found that in the range of 5 to 25 ft per min, extrusion speed has no significant effect either on the room or elevated-temperature properties of rare-earth containing alloys. Grube, Davis, and Eastwood[3] were able to

Table I. Effect of Extrusion Temperatures and Heat Treatment

Alloy	Composition, Pct: Mischmetal	Composition, Pct: Mn	Extrusion Conditions: Temperature, °F	Extrusion Conditions: Speed, Ft per Min
A	5.7	2.4	700	5
B	5.1	1.8	900	10

Tensile and Compressive Properties

Alloy	Condition	Pct E*	TYS	CYS	TS	Pct E	TYS	CYS	TS	Pct E	TYS	CYS	TS
		Room Temperature											
		As-Extruded				T5 Condition				T6 Condition			
A		10.0	29.2	28.4	38.7	8.0	31.2	30.0	39.5	11.6	19.2	18.0	31.8
B		8.3	24.7	20.4	36.0	6.7	29.3	20.1	38.4	5.7	30.3	18.7	38.7
		400°F				500°F				600°F			
A	T5	35.0	16.6		22.8	72.0	11.0		16.3	222.0	3.9		7.4
A	T6	23.6	14.4		22.3	39.3	12.0		19.4	105.5	6.6		10.6
B	T6	11.5	18.2	17.7	25.0	24.0	14.4	14.4	22.3	72.5	10.1	9.7	15.0

Limiting Creep Stresses

Alloy	Condition	0.1 Pct Creep Ext.	0.2 Pct Total Ext.	0.5 Pct Total Ext.	0.1 Pct Creep Ext.	0.2 Pct Total Ext.	0.5 Pct Total Ext.	0.1 Pct Creep Ext.	0.2 Pct Total Ext.	0.5 Pct Total Ext.
		100-Hr Creep Limits — 1000 psi								
		400°F			500°F			600°F		
A	T5	3.6	4.1	5.3	0.6	0.6	0.7	0.17	0.20	0.30
B	T6	11.0	9.8	12.2	3.4	3.7	4.8	1.5	1.7	2.0

*Pct E — Percent elongation in 1.5 in.
TYS — Tensile yield strength in 1000 psi
CYS — Compressive yield strength in 1000 psi
TS — Tensile strength in 1000 psi

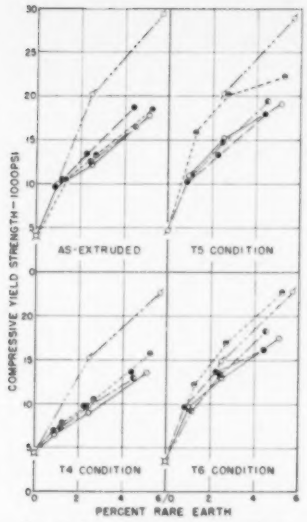

Fig. 2—Compressive yield strength at room temperature.

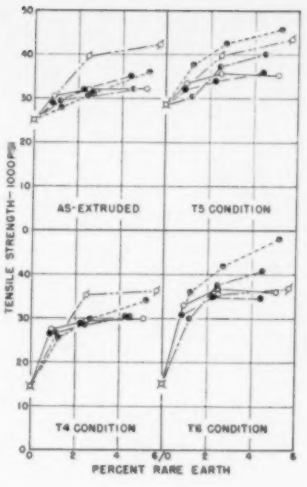

Fig. 3—Tensile strength at room temperature.

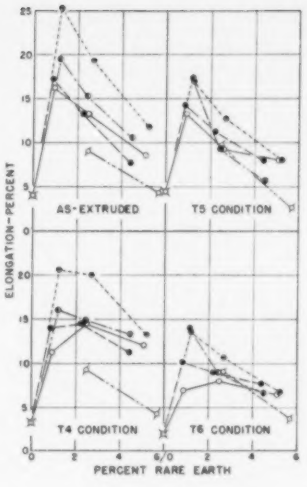

Fig. 4—Elongation at room temperature.

show some increase in strength with decreasing speed in the range of 27.3 to 4.11 in. per min.

Considerable work performed in our laboratory has shown that the maximum strength in magnesium-rare-earth alloys in the heat-treated and aged condition (T6) is developed by extruding at 900°F or higher. Results of one such experiment are presented in Table I. Although the lower extrusion temperature produces definitely higher yield strengths in the as-extruded and in the T5 conditions, significantly higher properties are obtained in the T6 condition by extruding at 900°F. Increasing the temperature above 900°F does not produce an increase in strength large enough to warrant use of such higher temperatures with the attendant greater wear on extrusion equipment and dies. The effect of extrusion temperature is more extensively presented by Grube, Davis, and Eastwood.[5]

Effect of Heat Treatment: The data included in Table I also show the pronounced beneficial effect that heat treating magnesium-rare-earth alloys has on the elevated-temperature strength and creep resistance. Whereas the alloy extruded at 700°F has the best combination of tensile and compressive properties at room temperature in the T5 condition, much higher strengths are exhibited by the same alloy in the T6 condition at elevated temperature. The superiority of the T6 condition is greater the higher the temperature of test. The comparison of creep properties is even more striking, as shown by the appropriate data in the same table.

Thus, it is apparent that in order to develop the maximum creep resistance and strength at elevated temperature in extruded magnesium-rare-earth alloys, the extrusion must be performed at 900°F or higher and the alloys must be heat treated and aged. Lower heat-treating temperatures produce proportionately lower properties. Increasing the heat-treating time beyond 4 hr does not produce any further advantage.

Tensile Properties of Mg-Rare-Earth Alloys: Complete tensile properties at room temperature, 300°, 400°, 500°, and 600°F have been determined on the five magnesium-rare-earth alloy systems as a function of composition. The results are presented graphically in the form of property vs. composition plots in Figs. 1 to 8 inclusive. Because of the small number of compositions investigated, the points have been joined by straight lines.

One of the most significant observations to be made from the room-temperature properties depicted in Figs. 1 to 4 is the marked difference in the degree of age hardening exhibited by the various alloy systems. In the as-extruded and in the heat-treated (T4) conditions, magnesium-lanthanum alloys show a decided superiority over all the other alloy systems, which differ little among themselves. However, magnesium-lanthanum alloys show no age hardening whatsoever, whereas all the other alloys increase in strength upon aging. In general, the degree of aging among the other four alloys increases in the following order: 1—magnesium-cerium. 2—magnesium-Mischmetal. 3—magnesium-cerium-free Mischmetal. 4—magnesium-didymium. This is a direct confirmation of the observations made on the corresponding cast alloys.[1] The result of these marked differences in age hardenability is to give magnesium-didymium alloys the highest strength in the heat-treated and aged condition (T6). In the directly aged state (T5 condition), the full extent of aging is not realized. Thus, magnesium-lanthanum alloys retain their as-extruded superiority in yield strength, but the tensile strength of the magnesium-didymium alloys is significantly higher than all the alloys.

It can be seen from Fig. 4 that the high strengths of the magnesium-lanthanum alloys are associated with relatively low ductility. Magnesium-didymium alloys have, in general, the highest elongation. The ductility of all magnesium-rare-earth alloys goes through a definite maximum at about 1 to 2 pct alloy content. The initial increase in elongation is a result of the marked reduction in grain size effected by the addition of small amounts of rare earths. The elongation decreases with further increases in rare-earth

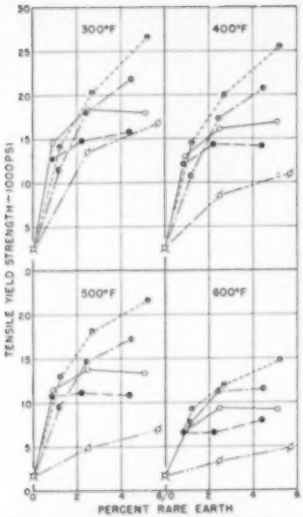

Fig. 5—Tensile yield strength at elevated temperatures T6 condition.

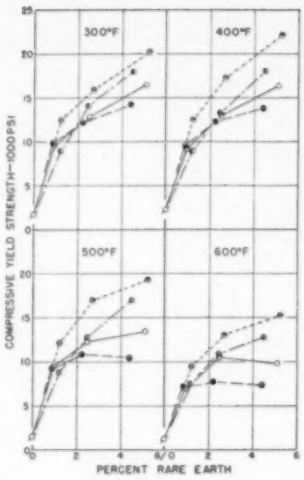

Fig. 6—Compressive yield strength at elevated temperatures T6 condition.

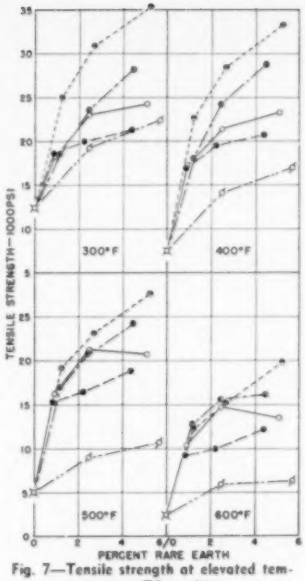

Fig. 7—Tensile strength at elevated temperatures T6 condition.

content because of the increasing amounts of undissolved intermetallic compounds.

The elevated-temperature tensile and compressive properties of magnesium-rare-earth alloys (Figs. 5 to 8) present a more straightforward picture. At all temperatures investigated in the range of 300° to 600°F, the alloys fall in the following order of decreasing strength: 1—magnesium-didymium. 2—magnesium-cerium-free Mischmetal. 3—magnesium-Mischmetal. 4—magnesium-cerium. 5—magnesium-lanthanum. The spread in the strength properties of the alloys increases with increasing alloy content. The low strength of magnesium-lanthanum alloys is associated with very high elongation. The other magnesium-rare-earth alloys do not show very great differences in ductility at elevated temperatures.

Creep of Magnesium-Rare-Earth Alloys: The creep resistance of the various magnesium-rare-earth alloys in the T6 condition at 400°, 500°, and 600°F is shown in Figs. 9, 10, and 11, respectively. The relative effects of the various rare-earth metals on the creep resistance of magnesium depend to a great extent upon the temperature of test and to some extent upon the composition. At 400°F, magnesium-lanthanum alloys are markedly inferior to

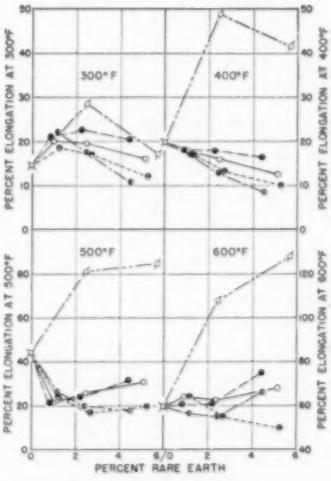

Fig. 8 — Elongation at elevated temperatures T6 condition.

Table II. Tensile and Compressive Properties of Magnesium-Rare-Earth-Manganese Alloys

Alloy	Pct E	TYS	CYS	TS	Pct E	TYS	CYS	TS	Pct E	TYS	CYS	TS	Pct E	TYS	CYS	TS
	Room Temperature															
	As-Extruded				T5 Condition				T4 Condition				T6 Condition			
5.1 Mischmetal + 1.8 Mn	8.3	24.7	20.4	36.0	6.7	29.3	20.1	38.4	11.3	20.0	14.4	31.3	5.7	30.3	18.7	38.7
4.7 Ce-Free Mischmetal + 1.8 Mn	8.7	22.9	19.6	35.0	6.0	32.4	21.4	41.7	11.3	21.6	14.7	31.8	4.7	35.3	19.7	42.4
4.8 Didymium + 1.5 Mn	11.0	25.2	19.3	37.2	7.0	35.7	22.3	45.0	13.0	22.9	16.6	34.4	6.7	38.7	23.0	47.3
4.9 Ce + 1.7 Mn	7.7	26.8	20.9	36.8	7.3	29.2	19.8	37.2	11.0	21.7	14.7	30.7	6.7	27.9	17.3	36.2
1.85 Mn	3.6	26.6	7.1	39.1					4.7	24.0	6.0	38.2	4.7	24.2	5.8	37.6
	T6 Condition															
	300°F				400°F				500°F				600°F			
5.1 Mischmetal + 1.8 Mn	12.3	20.2	17.3	26.2	11.5	18.2	17.7	25.0	24.0	14.4	14.4	22.3	72.5	10.1	9.7	15.0
4.7 Ce-Free Mischmetal + 1.8 Mn	10.4	23.5	17.4	30.0	8.0	22.6	19.5	29.0	14.0	18.9	17.3	25.7	53.0	14.0	13.6	18.9
4.8 Didymium + 1.5 Mn	10.4	27.7	22.7	35.0	9.0	25.6	22.2	31.3	17.0	22.2	20.9	27.7	54.2	15.3	14.9	19.8
4.9 Ce + 1.7 Mn	16.6	16.7	15.6	23.4	13.5	15.0	14.6	23.5	26.2	11.4	11.3	19.7	64.5	8.1	8.8	12.8
1.85 Mn					38.5	6.7	5.3	11.5	52.0	4.2	4.4	7.7	53.5	3.0	3.0	5.3

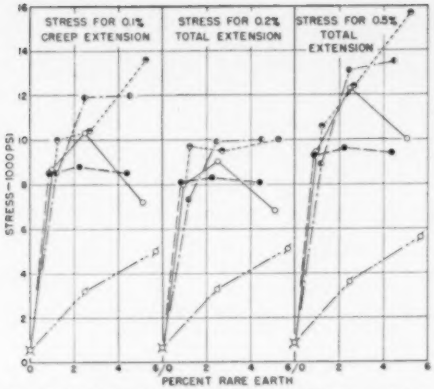
STRESS FOR 0.1% CREEP EXTENSION
STRESS FOR 0.2% TOTAL EXTENSION
STRESS FOR 0.5% TOTAL EXTENSION
STRESS — 1000 PSI
PERCENT RARE EARTH

Fig. 9—100-hr limiting creep stresses at 400°F T6 condition.

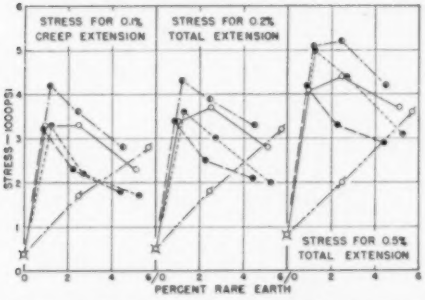
STRESS FOR 0.1% CREEP EXTENSION
STRESS FOR 0.2% TOTAL EXTENSION
STRESS FOR 0.5% TOTAL EXTENSION
STRESS — 1000 PSI
PERCENT RARE EARTH

Fig. 10—100-hr limiting creep stresses at 500°F T6 condition.

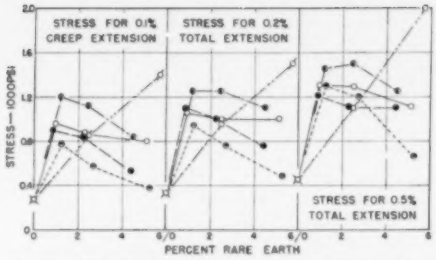
STRESS FOR 0.1% CREEP EXTENSION
STRESS FOR 0.2% TOTAL EXTENSION
STRESS FOR 0.5% TOTAL EXTENSION
STRESS — 1000 PSI
PERCENT RARE EARTH

Fig. 11—100-hr limiting creep stresses at 600°F T6 condition.

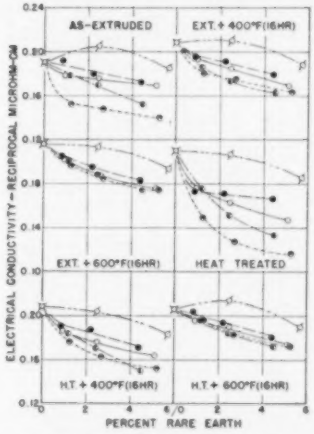

Fig. 12—Electrical conductivity at 95°F.

all the other alloys and magnesium-didymium alloys have the highest creep limits, particularly at the higher end of the composition range investigated. The creep limits of magnesium-lanthanum alloys at 500° and 600°F vary with composition in a strikingly different manner from those of the other four alloy systems. Whereas the creep limits of the magnesium-lanthanum alloys increase regularly with the composition, those for alloys containing Mischmetal, didymium, cerium-free Mischmetal, and cerium rise to a maximum at about 1 to 2 pct rare-earth content and decrease sharply from this value with increasing alloy content. The result of these compositional trends is that the creep resistance of the magnesium + 5.7 pct La alloy is the highest observed at 600°F. Likewise at 500°F this composition tends to show higher creep resistance than is produced by the same quantities of the other solutes studied. The alloys containing cerium-free Mischmetal exhibit the highest resistance to creep at the higher temperatures over the entire composition range. The decrease in creep resistance of all except the lanthanum-containing alloys may be attributed to a decrease in grain size from about 0.005 in. for the 1 pct alloy content to about 0.002 in. for the 5 pct alloy content. Magnesium-lanthanum alloys, on the other hand, retain a much finer grain size of about 0.0006 to 0.0009 over the composition range of 2.5 to 5.7 pct La as a result of the higher proportion of lanthanum in the form of compound. Perhaps the higher creep resistance of the lanthanum-containing alloys at 600°F results from the combination of fine grain size and a large amount of undissolved compound.

Effect of Manganese on Magnesium + 5 Pct Rare-Earth Alloys: In general, the addition of 2 pct Mn to magnesium + 5 pct rare-earth alloys increases

Table III. Limiting Creep Stresses of Magnesium-Rare-Earth-Manganese Alloys

Condition	Alloy	100-Hr Creep Limits — 1000 psi								
		0.1 Pct Creep Extension	0.2 Pct Total Extension	0.5 Pct Total Extension	0.1 Pct Creep Extension	0.2 Pct Total Extension	0.5 Pct Total Extension	0.1 Pct Creep Extension	0.2 Pct Total Extension	0.5 Pct Total Extension
		400°F			500°F			600°F		
T6	5.1 Mischmetal + 1.8 Mn	11.0	9.8	12.2	3.4	3.7	4.8	1.5	1.7	2.0
T6	4.7 Ce-Free Mischmetal + 1.8 Mn	12.8	9.0	15.5	3.4	3.8	5.2	0.94	1.2	1.6
T6	4.8 Didymium + 1.5 Mn	12.0	9.9	15.5	2.3	2.7	4.5	0.52	0.64	0.90
T6	4.9 Ce + 1.7 Mn	8.6	8.1	10.2	3.3	3.5	4.3	1.8	2.1	2.5
As-extruded	1.85 Mn	1.9	2.2	2.8				0.60	0.78	1.0
T6	1.85 Mn	2.3	2.6	3.4					0.94	1.2
Heat treated, water quenched and aged	1.85 Mn	2.3	2.7	3.6				1.2	1.3	1.7

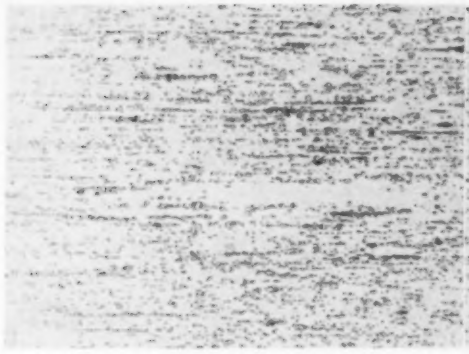

Fig. 13—Mg + 5.08 pct Mischmetal as-extruded. X100.

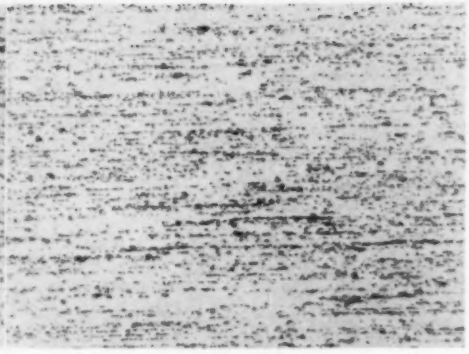

Fig. 14—Mg + 5.23 pct didymium as-extruded. X100.

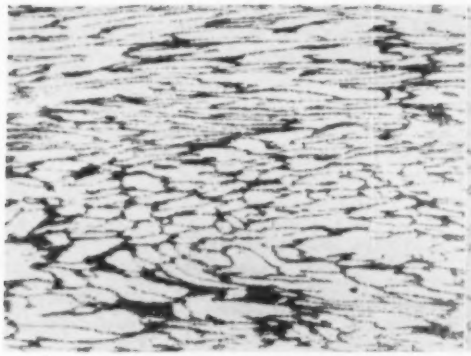

Fig. 15—Mg + 5.69 pct lanthanum as-extruded. X100.

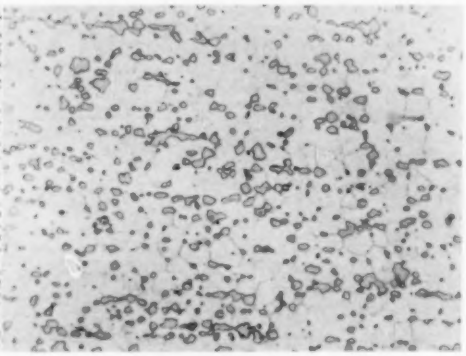

Fig. 16—Mg + 5.08 pct Mischmetal T6 condition. X250.

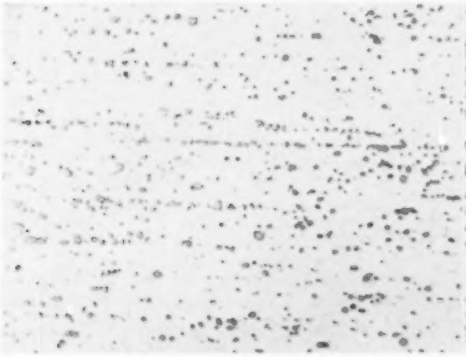

Fig. 17—Mg + 5.23 pct didymium T6 condition. X250.

Fig. 18—Mg + 5.69 pct lanthanum T6 condition. X250.

the strength properties by 1000 to 2000 psi at all temperatures (Table II). The room temperature tensile properties of the binary magnesium + 1.85 pct Mn alloy, extruded under the same conditions as the magnesium-rare-earth alloys, are comparable to those of the latter alloys. However, the compressive yield strength of the binary magnesium-manganese alloy is much lower. Magnesium + 1.85 Mn alloy, however, does not exhibit the same degree of temperature resistance that the rare-earth alloys show.

Manganese also effects a definite improvement in the creep resistance of magnesium-rare-earth alloys (Table III). Much the same order of relative creep resistance is maintained among the various magnesium-rare-earth alloys even with the addition of manganese. This is not true at 600°F, where the alloy containing pure cerium has the highest creep limits and the Mischmetal-containing alloy is second. The creep characteristics of magnesium + 1.85 Mn have been determined in various conditions of

Table IV. Comparison of Optimum Didymium and Mischmetal Alloys

Composition	Tensile and Compressive Properties								Creep Limits (1000 psi) 400°F		
	Room Temperature				400°F						
	1000 psi				1000 psi						
	Pct E	TYS	CYS	TS	Pct E	TYS	CYS	TS	0.1 Pct Creep Extension	0.2 Pct Total Extension	0.5 Pct Total Extension
2.69 Pct Didymium	10.6	23.8	16.9	41.7	13.2	20.0	17.2	28.4	10.4	9.5	12.4
2.47 Pct Mischmetal	8.0	26.4	13.3	37.1	16.0	16.1	13.0	21.4	10.3	9.0	12.3
5.08 Pct Mischmetal	6.7	27.0	17.6	36.0	12.5	16.9	16.3	23.2	7.2	6.8	10.0

heat treatment. Whereas at 400°F this alloy cannot compare with the rare-earth alloys, at 600°F in the heat-treated, quenched, and aged condition, its creep limits are not much lower than those of the magnesium-manganese-Mischmetal alloy. Quenching the magnesium-1.85 Mn alloy from the heat-treating temperature effects a significant improvement in the creep resistance at 600°F. This treatment, however, was not found to have any effect on the tensile properties. Grube, Davis, and Eastwood[2] found the same behavior in this composition. Furthermore, these investigators showed that in alloys containing Mischmetal and manganese, no significant improvement in creep resistance is realized by quenching instead of air cooling from the heat-treating temperature.

Electrical Conductivity: The results of conductivity measurements (Fig. 12) show trends similar to those found in the sand-cast alloys. The low solubility of lanthanum in magnesium is again demonstrated by these data. No special significance should be attached to the maxima in the curves for magnesium-lanthanum alloys. Two possible explanations that might be proposed for this phenomena are: 1—differences in impurity content, and 2—differences in degree of preferred orientation.

Metallography: Selected micrographs of some of the magnesium-rare-earth alloys are shown in Figs. 13 to 18 inclusive. All the structures were revealed by etching with the standard glycol etchant which contains 75 parts ethylene glycol, 24 parts distilled water, and 1 part concentrated nitric acid. The as-extruded structures are given at a magnification of 100 diam. In alloys containing Mischmetal (Fig. 13) and didymium (Fig. 14), as well as cerium-free Mischmetal and cerium, the compound is present in the form of stringers of discrete particles. The magnesium-lanthanum alloy (Fig. 15), however, reveals many characteristics of the cast structure. The compound is present as clusters of small particles resembling a cast eutectic and in many parts of the structure the compound completely outlines the cast grains. These structural differences in the alloys correlate well with the as-cast microstructure. It was shown in the earlier paper[1] that in alloys containing mixtures of rare-earth metals, the eutectics are highly divorced and thus upon extrusion result in stringers of individual particles. Magnesium-lanthanum and magnesium-cerium alloys, on the other hand, form extremely fine eutectics in the cast state with the divorcement tendency being the least in the magnesium-lanthanum alloys. The extruded magnesium-cerium alloys show a slight indication of the eutectic, as in the magnesium-lanthanum alloys, but the slower freezing rate of a 3-in. diam billet as compared to a cast test bar probably leads to considerable divorcement of the eutectic in the magnesium-cerium alloys.

In Figs. 16, 17, and 18 the microstructures of the magnesium-Mischmetal, magnesium-didymium, and magnesium-lanthanum alloys in the T6 condition show that the heat treatment results in considerable solution of compound in the two former alloys and in marked coalescence of the undissolved compound in all three alloys. It is clear from these micrographs and from observations on the other alloys that the order of increasing solid solubility in magnesium of these metals is: 1—lanthanum, 2—cerium, 3—Mischmetal, 4—cerium-free Mischmetal, and 5—didymium. These observations agree well with the conductivity measurements, Fig. 12. All the alloys containing about 1 pct rare earths also have significant amounts of undissolved compound except the magnesium + 1.23 pct didymium alloy. The latter has only a trace, indicating that its solid solubility limit in magnesium must be close to this composition.

Summary

1—Data have been presented to show the specific effects of various rare-earth metals on the room and elevated-temperature properties of extruded magnesium.

2—Alloys may be rated in the following order of decreasing tensile and compressive properties at room and elevated temperatures and creep resistance at 400°F: 1—magnesium-didymium, 2—magnesium-cerium-free Mischmetal, 3—magnesium-Mischmetal, 4—magnesium-cerium, 5—magnesium-lanthanum.

3—Magnesium-didymium alloys do not maintain their superiority in creep resistance over the other alloys at 500° and 600°F. The highest creep resistance over the entire composition range at these temperatures is exhibited by magnesium-cerium-free Mischmetal alloys. High-lanthanum alloys are exceptional in creep resistance at 600°F.

4—It is possible to develop equivalent creep resistance at 400°F with a more favorable combination of strength and ductility at room temperature and higher strength at elevated temperature by using 2 to 3 pct didymium rather than 2 to 5 pct Mischmetal. These effects are illustrated in Table IV.

References

[1] T. E. Leontis: *Trans.* AIME (1949) **185**, p. 968; JOURNAL OF METALS (December 1949). Correction to Table VII, JOURNAL OF METALS (June 1951) *Trans.* AIME, p. 464.

[2] T. E. Leontis and J. P. Murphy: *Trans.* AIME (1946) **166**, p. 295; METALS TECHNOLOGY (April 1946).

[3] K. E. Grube, J. A. Davis, and L. W. Eastwood: *Proc.* ASTM (1950) **50**.

[4] J. C. McDonald: *Proc.* ASTM (1948) **48**, p. 737.

[5] K. Wellinger and E. Keil: *Ztsch. Metallkunde* (1943) **35**, p. 169.

[6] G. A. Mellor and R. W. Ridley: *Journal* Inst. Metals (1949) **75**, p. 679.

[7] R. F. Marande: *Materials and Methods* (1946) **23**, p. 418.

[8] A. A. Moore and J. C. McDonald: *Proc.* ASTM (1946) **46**, p. 970.

[9] T. E. Leontis: *Trans.* AIME (1949) **180**, p. 287; METALS TECHNOLOGY (June 1948).

Preferred Orientation in Zirconium

by R. K. McGeary and B. Lustman

The textures produced in zirconium by cold and hot rolling, and by recrystallization above and below the transformation temperature were determined. Thermal expansivities were measured in the thickness, transverse, and rolling directions of preferentially oriented zirconium and were correlated with the texture scatter in these directions.

PREVIOUS investigations have indicated that minor differences between hexagonal close-packed metals of similar axial ratio may appear with respect to the textures produced both on cold rolling and on subsequent recrystallization. In the case of magnesium, beryllium, and titanium, metals of axial ratio similar to that of zirconium, the ideal orientations produced by rolling are fundamentally the same, although marked variance is reported in the degree and type of scatter about the mean orientation; in those instances where recrystallization textures were observed, they were reported to be similar to the rolling textures. Measurement of the anisotropy of thermal expansion of both rolled and recrystallized zirconium could not be correlated satisfactorily with the textures reported for the above metals, and therefore a study was made of the preferred orientations produced in zirconium. Reported below are the textures produced in zirconium by cold and hot rolling, and recrystallization above and below the transformation temperature, together with the results of thermal expansion measurements.

Determination of Preferred Orientation

Two types of zirconium were investigated: 1—"crystal bar" zirconium obtained from the Foote Mineral Co., produced by the thermal decomposition of zirconium tetraiodide, and 2—zirconium ingot obtained from the Bureau of Mines prepared by melting sponge zirconium in a graphite resistor vacuum furnace in a graphite crucible.

The major impurities present in the two materials used are listed in Table I. Several of the pole figures were later checked with 0.03 pct hafnium crystal bar material and the results were identical with those to be shown for the 1.5 pct hafnium material.

The materials were cold rolled to 0.014 in. in thickness as shown in Table II.

Specimens were cut from the 0.014 in. thick rolled sheets and etched to thicknesses of 0.002 to 0.010 in. Such specimens were used for exposures up to a 50° to 60° angle between the beam and plane of the specimen; for higher angles a wire shape, similar to that described by Bakarian,[1] was formed on an end of the original 0.014 in. sheet. A fine-bladed abrasive cut-off wheel was used to slot the sheet and to form the cylindrical cross-section. The wire shaped ends were then etched to 0.006 to 0.010 in. in diam. Although absorption of X-rays in the wire-shaped specimens does not vary with angle of rotation, the line width around the diffraction rings was not uniform, because the wire was narrower than the X-ray beam, and this condition caused some uncertainty in the estimation of azimuthal intensities. Furthermore, scanning was not practicable with this type of specimen so that spottiness of the rings due to large grain size was excessive for specimens which had been heated above about 650°C. Nevertheless, satisfactory information could be obtained for high angle exposures from the negatives by the use of both types of specimens.

Transmission Laue photograms were taken using unfiltered molybdenum radiation (47.5 kv, 18 ma) and a 0.025 in. pinhole. With the film 8 cm from a 0.005 in. thick specimen exposures of about 30 min were adequate. For specimens with a coarse grain size, a device that scanned about 0.15 sq in. of sheet surface was used.

An attempt was made to plot the pole figures by use of an X-ray spectrometer as described by Norton.[2] However, for the particular technique used, the intensity variations obtained were not considered definite enough to give reliable results, especially for the large grained recrystallized and transformed specimens. This method was therefore abandoned in favor of the standard photographic method.

Nine exposures were taken of each specimen: seven exposures with the beam perpendicular to the rolling direction and at 0°, 10°, 20°, 35°, 50°, 65°, and 80° to the transverse direction, and two exposures with the beam perpendicular to the transverse direction and at 60° and 80° to the rolling direction. Additional exposures were then made where necessary. The intensity variations of the diffraction rings were estimated by eye. It was usually possible to estimate 3 degrees of intensity from the photograms but in some cases 2, 4, or 5 degrees were estimated.

Experimental Results

The preferred orientation was determined for the following treatments: 1—cold-rolled, 2—low temperature rolled, 3—cold-rolled surface layer, 4—cross-rolled, 5—hot-rolled, 6—recrystallized below the transformation temperature, and 7—recrystallized above the transformation temperature.

1—*Cold-Rolled Textures:* The slip plane in hexag-

R. K. McGEARY and B. LUSTMAN, Member AIME, are associated with the Atomic Power Div., Westinghouse Electric Corp., Pittsburgh.

Discussion on this paper, TP 3160E, may be sent, 2 copies, to AIME by April 1, 1952. Manuscript, May 3, 1951. New York Meeting, February 1952.

onal close-packed metals is the basal {0001} plane. During cold rolling this plane would be expected to rotate into the plane of the sheet by slip along the $<11\bar{2}0>$ directions. With such a slip mechanism the principal ideal orientation produced by cold rolling would be expected to consist of basal planes parallel to the rolling plane and either $<11\bar{2}0>$ or $<10\bar{1}0>$ directions parallel to the rolling direction.

For magnesium with an axial ratio (c/a = 1.624) similar to that of zirconium (1.589), Caglioti and Sachs[3] found the {0001}, $<11\bar{2}0>$ orientation, with the scatter greater in the rolling direction than in the transverse direction. Bakarian,[1] using purer magnesium than Caglioti and Sachs, found the same basal plane orientation but no directional orientation of the digonal axes. He showed also that the rolling texture is affected by the presence of certain impurities; 0.2 pct Ca caused a splitting of the central maximum area of the pole figure.

The basal plane pole figure of cobalt by Wasserman[4] indicates a splitting of the maximum area but no directionality of scatter.

Smigelskas and Barrett[5] observed a {0001}, $<10\bar{1}0>$ orientation in the case of beryllium; this is the first observation that the $<10\bar{1}0>$ direction may lie in the rolling direction for close-packed hexagonal metals. Considerably more scatter in the transverse than in the rolling direction is apparent.

The pole figures of Clark[6] for cold-rolled titanium indicate that the hexagonal axis is inclined in the transverse direction about 30° from the rolling plane with the $<10\bar{1}0>$ direction in the rolling direction.

Burgers and Jacobs'[7] pole figures of cold-rolled zirconium show, as do those of beryllium, the major scatter to be in the transverse direction. However, their pole figure of the $\{10\bar{1}0\}$ planes indicates a tendency for the $<11\bar{2}0>$ direction to lie in the rolling direction.

The pole figures of cold-rolled Bureau of Mines zirconium obtained in the present investigation for the three principal planes, {0002}, $\{10\bar{1}0\}$, and $\{10\bar{1}1\}$, are shown in Fig. 1a, b, and c. The pole figures of crystal bar zirconium are fundamentally the same as those of Bureau of Mines zirconium but with less scatter in the transverse direction. The average orientation best describing the maximum intensity areas, shown by the double circle points in Fig. 1, is that shown in the schematic drawing of Fig. 7a, which represents the basal planes parallel to the rolling direction but inclined from the rolling plane about 30° in the transverse direction, and with a $<10\bar{1}0>$ direction in the rolling direction. This orientation is most readily appreciated by consideration of the prism-plane $\{10\bar{1}0\}$, and pyramidal-plane $\{10\bar{1}1\}$ pole figures. The diffraction photograms of Fig. 8a and b also indicate the 30° transverse tilt of the c-axis: four maxima intensity arcs appear at the 7, 8, 10, and 11 o'clock positions of the outer $\{10\bar{1}1\}$ ring of Fig. 8a, while maxima intensity arcs appear only at the 7 and 11 o'clock positions in Fig. 8b where the specimen was rotated 20° about the rolling direction.

2—*Low Temperature Rolling:* It was thought that the slip mechanism of zirconium might change with temperature as is observed in the case of magnesium, and that the change might be reflected in the rolling texture. Therefore, a piece of crystal bar zirconium was rolled 95 pct at liquid nitrogen temperature. The texture of this material is in all respects similar to that of the crystal bar rolled at room temperature.

Table I. Composition of Materials Used

Impurity	In Crystal Bar, Pct	In Melted Bureau of Mines Sponge, Pct
Hf	1.5	1.5
C	0.02	0.09
O_2	0.02	0.08
Fe	0.01-0.05	0.14

3—*Surface-Layer Texture:* It is often the case in wire drawing or cold rolling that the textures observed on the surface are different from those in the body of the metal because of inhomogeneity of the deformation process. The surface texture of Bureau of Mines zirconium was determined on a specimen coated on one side with wax and etched from 0.014 to 0.002 in. in thickness. The pole figures for this specimen did not reveal a new orientation but only a slight sharpening of the cold-rolling texture.

4—*Cross-Rolled Texture:* A square specimen of Bureau of Mines zirconium, which had previously been hot rolled, was cold rolled 90 pct by rotating the square 90° after each pass through the rolls. Each reduction was about 3 pct of the total reduction. The pole figures of Fig. 2 indicate that scatter in the transverse direction has been eliminated and that the cross rolling has resulted in a texture consisting of a basal plane parallel to the rolling plane, a $<10\bar{1}0>$ direction parallel to one rolling direction, and a $<11\bar{2}0>$ direction parallel to the other rolling direction. It would hardly be expected that such an orientation would be stable on cross rolling, but it would rather be expected that a double orientation with some $<10\bar{1}0>$ directions parallel to each rolling direction would be observed. However, if the rolling process is idealized as a combination of tension in the rolling direction and compression in the normal direction, and if a $<10\bar{1}0>$ direction were stabilized in the one rolling direction by duplex slip along $<11\bar{2}0>$ directions, then, in the direction transverse to this, the $<11\bar{2}0>$ direction would similarly be stabilized by duplex slip. To test the effect of orientation prior to cross rolling, a slab of as-cast ingot zirconium, which would not be expected to show any prior orientation, was cross rolled, and also exhibited a $<10\bar{1}0>$ direction parallel to the one rolling direction and a $<11\bar{2}0>$ direction parallel to the other.

5—*Hot-Rolled Texture:* With the exception of beryllium,[5] there is no information on the orientations produced by hot rolling hexagonal close-packed metals. For this metal the type of orientation for rolling temperatures as high as 800°C does not change.

Table II. Rolling Schedule

Material	Type Rolling	Rolling Temperature	Reduction in Thickness, Pct
Crystal bar	Straight	Room temperature	95
Bureau of Mines	Straight	Room temperature	96
Bureau of Mines	Straight	850°C	92
Bureau of Mines	Cross	Room temperature	90

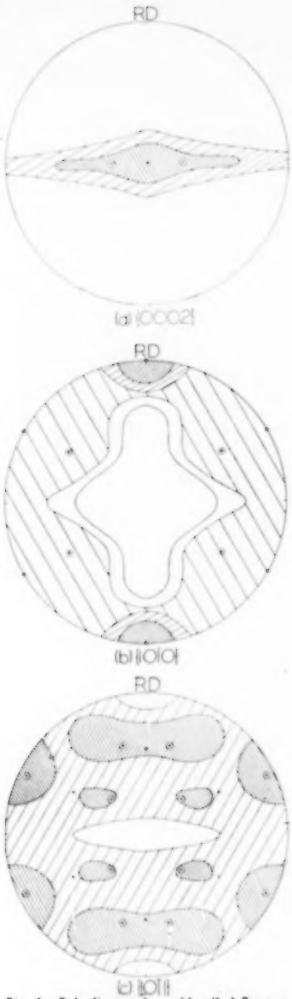

Fig. 1—Pole figures for cold-rolled Bureau of Mines zirconium.
● indicates {0002} || rolling plane and ⟨10$\bar{1}$0⟩ || rolling direction.
○ indicates {0002} rotated 30° about rolling direction.

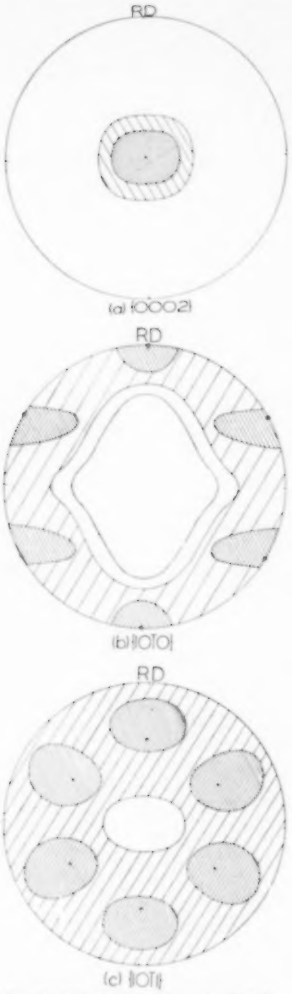

Fig. 2—Pole figures for cross-rolled Bureau of Mines zirconium.
● indicates {0002} || rolling plane and ⟨10$\bar{1}$0⟩ || rolling direction.

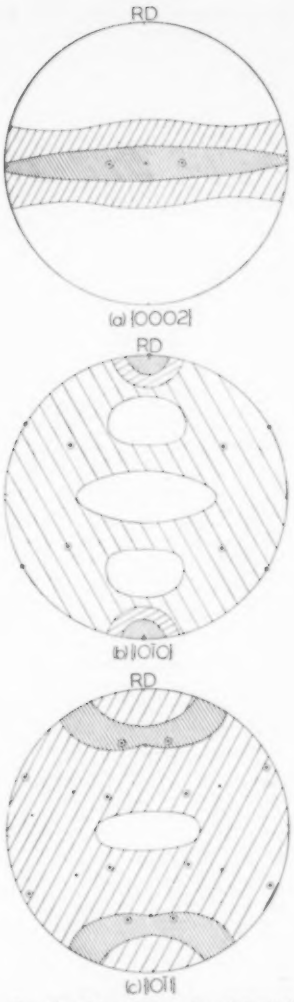

Fig. 3—Pole figures for hot-rolled (850°C) Bureau of Mines zirconium.
● indicates {0002} || rolling plane and ⟨10$\bar{1}$0⟩ || rolling direction.
○ indicates {0002} rotated 30° about rolling direction.

Hot rolling was performed on a specimen of Bureau of Mines zirconium plate, which was placed in a close-fitting steel jacket with $\frac{3}{8}$ in. thick walls, all the seams of which were then welded gas tight. The jacket helped in maintaining the proper temperature of the sample and also in protecting it from oxidation. The total deformation at a temperature of 825° to 850°C was about 92 pct reduction in thickness. The pole figures for this sample, Fig. 3, indicate that the texture is essentially the same as the cold-rolled texture but has much more scatter in the transverse direction.

6—*Recrystallization Textures:* The textures that result when cubic metals are rolled and recrystallized are greatly varied and at present cannot be correlated successfully with any general theory. For these metals the recrystallization textures may be the same as, or may be different from, the deformation texture, or no preferred orientation may result on recrystallization. For hexagonal close-packed metals there has been very little work done on rolling-recrystallization textures or the factors influencing the textures. Zinc and magnesium were found to retain their rolling textures at recrystallization temperatures up to the highest temperatures investigated, 400° and 600°F respectively.[3] The 700°C recrystallization textures of beryllium were also found to be the same as the deformation textures.[3] The basal plane pole figure of Clark[6] for titanium indicates that the recrystallization texture is the same (differing in degree) as the cold-rolled texture. However, a comparison of his photograms for the

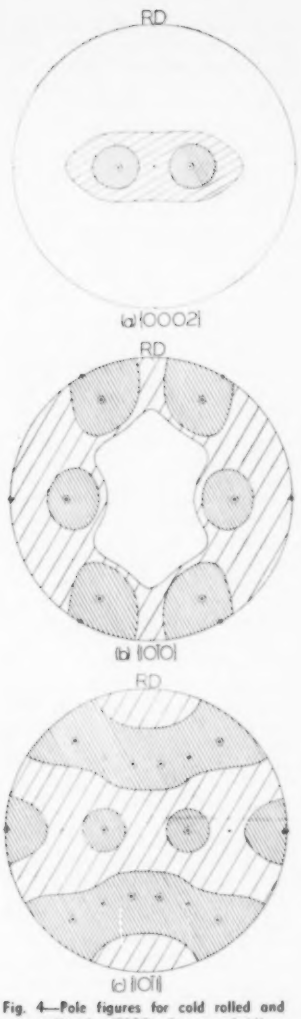

Fig. 4—Pole figures for cold rolled and recrystallized (650°C) Bureau of Mines zirconium.
● indicates {0002} || rolling plane and {11$\bar{2}$0} || rolling direction.
○ indicates {0002} rotated 30° about rolling direction.

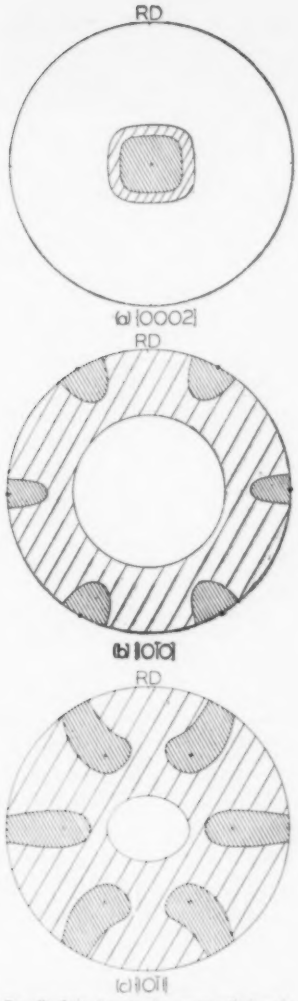

Fig. 5—Pole figures for cross-rolled and recrystallized (650°C) Bureau of Mines zirconium.
● indicates {0002} || rolling plane and {11$\bar{2}$0} || rolling direction.

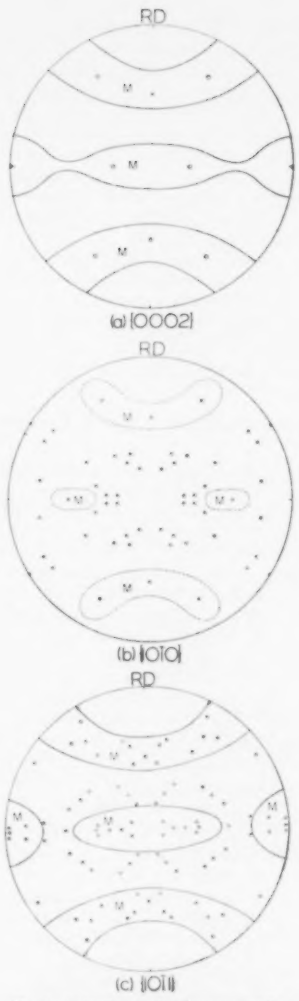

Fig. 6—Pole figures for Bureau of Mines zirconium heated above transformation temperature.
Points indicate calculated pole positions for Burgers' transformation mechanism from an ideal recrystallization orientation. Maximum intensity areas marked *M*.

{10$\bar{1}$0} and {10$\bar{1}$1} rings with the pole figures and photograms obtained in the present case for zirconium indicates that a rotation of the digonal axes about the hexagonal axis has taken place for titanium. Zirconium will be shown to undergo a 30° rotation of this type when recrystallized.

a—*Cold-Rolled Recrystallization Textures:* Specimens of the 0.014 in. thick cold-rolled sheet zirconium were recrystallized at 650°C. The specimens were sealed in evacuated glass tubes and were put into a hot furnace for 5 min (recrystallization was found to be complete in this time). The recrystallization pole figures for Bureau of Mines zirconium are shown in Fig. 4. The pole figures for recrystallized crystal bar are almost identical to those shown for the Bureau of Mines zirconium. A well-defined texture fundamentally different from the rolling texture was observed. A schematic drawing of the average orientation best explaining the maxima areas of the pole figures is shown in Fig. 7b. The basal planes are inclined to the plane of the sheet at an angle of about 30° in the transverse direction and the <11$\bar{2}$0> direction is parallel to the rolling direction.

Pole figures were plotted for a recrystallized sample which was later found to have been overheated. The heating temperature was below the transformation temperature (862°C), since there was no metallographic evidence of a transformation structure, and was estimated to lie between 800° and 862°C. The pole figures of this specimen were very similar to those of the specimen recrystallized at 650°C, so

the recrystallization texture apparently does not vary in this temperature range.

The average orientation described above may also be considered as a twinned orientation with a $\{10\bar{1}1\}$ first-order pyramidal twinning plane perpendicular to the rolled sheet and parallel to the rolling direction. The usual twinning planes for close-packed hexagonal metals are the $\{10\bar{1}2\}$ second-order pyramidal planes. No metallographic evidence of twinning could be found in recrystallized zirconium.

Burgers and Jacobs[7] found the $<11\bar{2}0>$ direction parallel to the rolling direction and the basal plane parallel to the rolling plane, while in a later work Burgers, Fast, and Jacobs reported the following ideal fiber textures for zirconium wire:

Cold drawn wire—$<10\bar{1}0>$ direction parallel to wire axis

Recrystallized wire—$<11\bar{2}0>$ direction parallel to wire axis

If a reasonable correspondence is assumed between the wire axis and the rolling direction of sheet material, the observations for wire coincide with the present observations for rolled zirconium. It is readily apparent that the rotation of axes described above does occur if a comparison of the innermost $\{10\bar{1}0\}$ rings of Fig. 8a and c is made. The former figure, a photogram made with the X-ray beam perpendicular to the plane of the cold-rolled sheet, shows maxima in the 6 and 12 o'clock positions, indicating a $<10\bar{1}0>$ direction parallel to the rolling direction, while the latter figure, a similar photogram of the recrystallized sheet, shows maxima at the 5, 7, 11, and 1 o'clock positions, indicating a $<11\bar{2}0>$ direction parallel to the rolling direction.

For rolled zirconium, the $<10\bar{1}0>$ direction was always found to be parallel to the rolling direction. With flow parallel to the rolling direction by duplex slip on basal planes in $<11\bar{2}0>$ directions, it would be expected that either a $<10\bar{1}0>$ or $<11\bar{2}0>$ direction would be parallel to the rolling direction. Having once established either direction parallel to the rolling direction it would seem impossible to change it by further working. To find if the preferred $<11\bar{2}0>$ direction parallel to the rolling direction observed in the case of recrystallized zirconium could be shifted by further working, the following experiments were performed. The original cold-rolled crystal bar zirconium was recrystallized to place a $<11\bar{2}0>$ direction parallel to the rolling direction as shown in the photogram of Fig. 9c. The specimen was then cold rolled an additional 86 pct and the photogram of Fig. 9d taken. It may be noted that once more the $<10\bar{1}0>$ direction is parallel to the rolling direction. Subsequent recrystallization again caused a rotation of the $<11\bar{2}0>$ into the rolling direction. These direction changes correspond to a 30° rotation about the hexagonal axis. It is interesting to point out the similarity of the above results to those of Beck, Sperry, and Hu[8] who found the maximum rate of growth in the case of recrystallization of aluminum to be at orientations corresponding to a 30° to 45° rotation about a $<111>$ axis with respect to the original orientation.

b—*Cross-Rolled Recrystallization Texture:* It was shown in Section 3 and Fig. 7c that the cross-rolled deformation texture had the following ideal orientations: the basal plane parallel to the rolling plane, a $<10\bar{1}0>$ direction parallel to one rolling direction, and a $<11\bar{2}0>$ direction parallel to the other rolling direction. The pole figures of Fig. 5 showing the recrystallization texture of this specimen indicate a new orientation, shown in the schematic drawing of Fig. 7d: the basal plane is parallel to the rolling plane (as in the deformation orientation) but a $<11\bar{2}0>$ direction is oriented parallel to the rolling direction which in the rolled condition was parallel to a $<10\bar{1}0>$ direction, and a $<10\bar{1}0>$ direction is oriented parallel to the other rolling direction which showed a $<11\bar{2}0>$ direction in the rolled condition. This change corresponds to a 30° rotation about the hexagonal axis.

7—*Texture after Heating above the Transformation Temperature:* The allotropic transformation temperature of zirconium has been established as 862° ± 5°C by dilatometric and thermal analysis.[10] Above this temperature zirconium is body-centered cubic and below it, hexagonal close-packed. Burg-

Table III. Previous Data on Thermal Expansivity of Zirconium

Material	Condition	Treatment	Temperature Range, °C	Coefficient of Thermal Expansion x 10^{-6} per °C	Reference
	CR foil		0-100	2.5 (parallel to c-axis) 14.3 (parallel to a-axis) (by X-ray diffraction)	13
Bureau of Mines	Rolled sheet		25-300	10.3 ± 0.5 (parallel to c-axis) 4.5 ± 0.5 (parallel to a-axis) (by X-ray diffraction)	14
Crystal bar	Drawn wire		Room temp.	6.3	15
	Wire		20-200	5.4	16
			200-300	6.4	
			300-400	6.9	
			400-500	7.9	
			500-600	8.4	
			600-700	8.9	
Crystal bar			20-600	4.69	17
Bureau of Mines	Cold rolled	Rolled 400°-600°C from ingot; cold rolled additional 50 pct	25-300	4.10	18
Bureau of Mines	Hot rolled	Rolled 400°-600°C from ingot	25-500	4.98	18
Bureau of Mines	Recrystallized	Rolled 400°-600°C from ingot; heated 600°C	25-500	5.39	18
Bureau of Mines	Transformed	Rolled 400°-600°C from ingot; heated to 1400°C	25-500	6.60	18
Bureau of Mines	Transformed	Rolled 400°-600°C from ingot; heated to 1400°C; reheated to 950°C	25-500	6.50	18
Bureau of Mines	Recrystallized	Rolled 400°-600°C from ingot; heated to 1400°C; reheated to 950°C; cold worked additional 50 pct; heated to 600°C	25-500	5.20	18
Crystal bar	Recrystallized	Swaged 90 pct R.A.; heated to 600°C	25-500	4.84	18
Crystal bar	Transformed	Swaged 90 pct R.A.; heated to 1400°C	25-500	6.17	18
Powder compact	Transformed	Sintered at 1000°-1100°C	25-500	6.40	18

ers,[11] by X-ray analysis of selected portions of crystal bar zirconium which were single crystals of the cubic modification at the deposition temperature, found the following orientation relationships between the hexagonal close-packed and the body-centered cubic modifications:

BCC β Zr above 862°C		CPH α Zr below 862°C
{110}	planes parallel to	{0001} planes
<111>	directions parallel to	$<11\bar{2}0>$ directions

There are six {110} planes and two <111> directions in each of the planes, hence 12 orientations of α may result from a single β orientation.

With the electron microscope, Burgers and Van Amstel[12] observed that the lamellar crystallites of hexagonal close-packed zirconium form by a crystallographically reversible type of transition, and that nucleation and growth apparently do not take place in the same sense that they occur in diffusion-type phase transformation processes. Observation at high temperature of certain β zirconium grains revealed that the grains retained their shape on transformation to α and then back again to β zirconium, and that after several transformations the α lamellae appear in the same positions with respect to the original β grains that they had previously occupied.

These observations indicate that the orientation existing in recrystallized zirconium should be replaced by a new orientation when heated above the transformation temperature, and that this orientation should not be destroyed by repeated heating above and cooling below the transformation temperature. On heating above the transformation temperature the $\{110\}_\beta$ planes should form parallel to $\{0001\}_\alpha$ planes and a $<111>_\beta$ direction parallel to a $<11\bar{2}0>_\alpha$ direction. On retransformation of the β to α, the old as well as entirely new orientations should appear since there are six $\{110\}_\beta$ planes and two $<111>_\beta$ directions parallel to which the α crystallites may form. Finally, on continued heating and cooling through the transformation temperature no new orientations should appear.

a—*Transformation Texture Arising from Recrystallization Texture:* A specimen of cold-rolled Bureau of Mines zirconium was sealed in an evacuated silica capsule and heated for 1 min at 980°C and then air cooled. Diffraction photograms showing the new positions of the basal planes (compare with recrystallization photogram, Fig. 8c) are shown in Fig. 9a and b. In Fig. 6 the pole figures for the three principal planes are shown with the addition of the positions of the poles that may arise from the ideal orientation by applying Burgers' transformation mechanism.

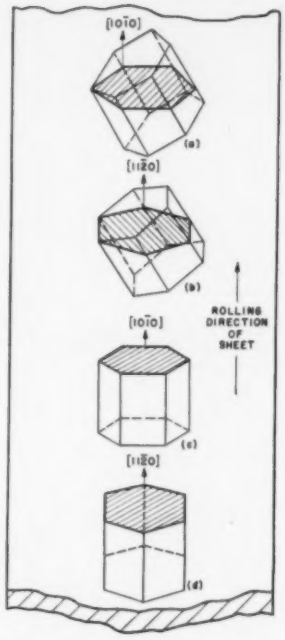

Fig. 7 — Representation of ideal preferred orientation with respect to the rolled sheet (cross-hatched plane is in rolling plane) after: a—cold-rolling, b—recrystallization after cold-rolling, c—cross-rolling, d—recrystallization after cross-rolling.

The areas marked *M* are the maximum intensity areas which would ordinarily be shown as the closest cross-hatched areas, and all other areas are of lesser intensity. The agreement is seen to be good when the following difficulties encountered in interpreting this set of photograms are considered:

1. The transformation orientation seems inherently possessed of more scatter than the recrystallization orientation.

2. The rings are spotty due to a much larger grain size, a condition which was not overcome by the integrating method employed.

3. There are many more orientations with consequent overlapping of scatter regions. For this reason the intensity regions of the $\{10\bar{1}0\}$ plane pole figure of Fig. 6b are shown by dotted lines. The photograms showed very little difference in intensity around the $\{10\bar{1}0\}$ plane rings (cf. Fig. 9a).

b—*Retention of New Texture Despite Repeated Transformation:* It has been shown that no change

Table IV. Thermal Expansivity of Zirconium in Different Sheet Directions for Various Treatments

Condition and Type of Zirconium	Pole Figure Description, Fig. No.	Coefficients of Linear Expansion ±0.4x10⁻⁶ per °C between 200°-300°C: Direction of Sheet Tested — Thickness	Transverse	Rolling	Coefficients Cubical Exp. ±1.2x10⁻⁶ per °C
Cross rolled, recrystallized (600°C), Bureau of Mines	5	8.7 (8.9	5.4 6.3*	5.4 6.3*)	19.5 21.5
Hot rolled (83 pct reduction at 760°C), Bureau of Mines	3	7.4	(With interferometer) 6.4	4.8	18.6
Hot rolled (80 pct reduction at 600°C), Crystal bar	3	8.5	6.2	5.8	20.5
Transformed (heated to 980°C), Bureau of Mines	6	6.7	6.2	5.9	18.8
Cold rolled, Bureau of Mines	1	10.1	4.8	4.6	20.5
Stress-relieved (325°C), Bureau of Mines	1	9.3	6.0	5.1	20.4
Recrystallized (600°C), Bureau of Mines	4	8.6	6.3	5.5	20.4

* Measured in only one of the two rolling directions.

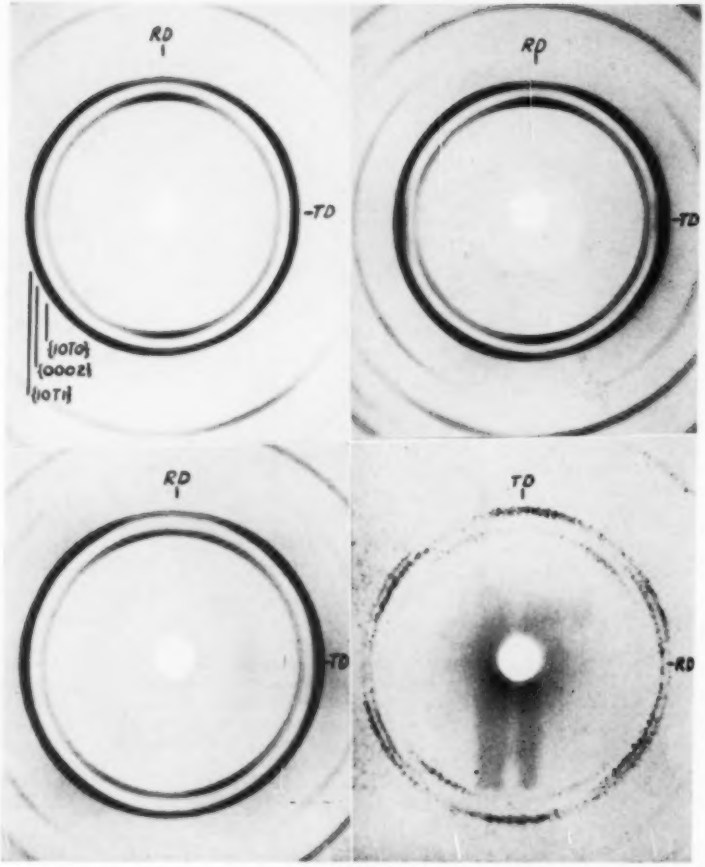

Fig. 8 — Laue transmission photograms of zirconium.

a (upper left)—Cold-rolled Bureau of Mines zirconium, 96 pct reduction. X-ray beam perpendicular to rolled sheet.

b (upper right)—Same as a, but specimen rotated 20° about rolling direction.

c (lower left)—Crystal bar zirconium cold rolled 95 pct reduction then recrystallized at 650°C. Beam perpendicular to rolled sheet. Specimen moving during exposure.

d (lower right)—Same as c, but specimen rotated 75° about transverse direction.

of the transformation texture would be expected on cycling through the transformation range except such due to transformation strains and consequent noncoherent recrystallization. If, however, the mechanism were not exactly that described above but close to it, then repeated transformations would be expected to magnify the difference so that eventually a somewhat different texture or complete randomness might result. A duplicate of the specimen of Section 7a was heated eight times for a minute above the transformation temperature and water quenched after each heating. The photogram of Fig. 9b indicates that the orientation of this coarse grained specimen is entirely similar to that of the specimen of Fig. 9a which was transformed only once.

Anisotropy of Thermal Expansion

The available data on the expansivity of zirconium are listed in Table III. Depending on the treatment received by the material, and hence the differences in texture so produced, expansivities in the rolling direction ranging from about 4 to 6.5 microin. per in. per °C have been reported. The observed variation of expansivity with deformation and annealing treatment in Table III cannot be correlated with the X-ray results of Shinoda[18] who, in the temperature range 0° to 100°C, reported values of expansivity of 2.5 and 14.3 microin. per. in. parallel to the c and *a* axes respectively; a redetermination by X-ray methods of the expansivity revealed values of 10.3 and 4.5 microin. per in. respectively.[14] The correlation of the experimentally observed expansivity anisotropy with the textures described in previous sections and with values derived from X-ray observations will be discussed below.

Experimental Technique

Expansivity was measured in the rolling, transverse, and thickness directions of rolled sheet. Most of the measurements were made by means of a quartz differential dilatometer; the dilatation strain was measured by an unbonded strain gage of about 3 microin. sensitivity. Specimens 0.3 to 0.4 in. in length were used; measurements were made in the thickness directions of rolled sheet by stacking several polished specimens to the proper depth. The specimens were heated at constant rates of 2° to 12°C per min and dilatation measurements made continuously. Results were checked in the case of a cross-rolled specimen by means of a high temperature interferometer dilatometer and were found to agree with those obtained from the differential dilatometer to within the estimated limit of accuracy, $\pm 0.4 \times 10^{-6}$ in. per in. per °C for a 0.3-in. length of specimen. Tabulated in Table IV are the results of expansivity

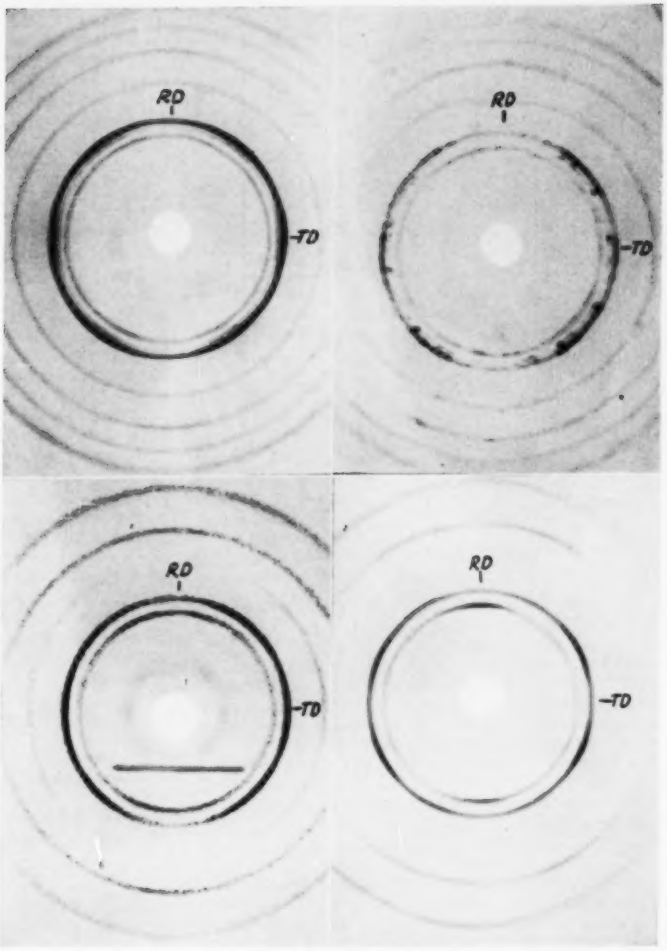

Fig. 9 — Laue transmission photograms of zirconium.

a (upper left)—Cold-rolled Bureau of Mines zirconium heated to 980°C and cooled. X-ray beam perpendicular to rolled sheet. Specimen moving during exposure.

b (upper right)—Treatment for specimen a repeated 8 times; X-ray conditions identical.

c (lower left)—Crystal bar zirconium cold rolled 95 pct reduction and recrystallized. Beam perpendicular to rolled sheet.

d (lower right)—Specimen of c cold rolled an additional 86 pct reduction.

measurements made on sheet with various rolling and annealing treatments.

Experimental Results

It is apparent that a qualitative correlation is possible between the values of expansivity listed in Table IV and the pole figures appropriate for each deformation and annealing treatment if the X-ray values of 10.3×10^{-6} per °C parallel to c axes and 4.5×10^{-6} per °C parallel to *a* axes are assumed for the expansivities of the unit cell axes. Thus the cross-rolled sheet, the texture of which consists of c axes scattered uniformly about the normal to the sheet direction, shows equal expansivities in the rolling and transverse directions and maximum expansivity in the thickness direction. In the case of hot-rolled and recrystallized zirconium the scatter of the c axes is principally in the transverse direction; thus the expansivity here decreases in the order thickness, transverse, and rolling direction. The transformed material exhibits c axes scattered fairly uniformly over the entire projection and correspondingly the expansivity is fairly uniform in the three sheet directions.

Expansivity measurements made on cold-rolled material showed abnormally low expansivity in the transverse direction and high expansivity in the thickness direction, considering the type of scatter for this texture. Presumably these values are abnormal because of stresses in the specimens, since on prior stress-relieving at 325°C more reasonable values for expansivity were obtained.

A more quantitative correlation of texture and expansivity is possible in the case of recrystallized sheet in which the unit cell is inclined with its c axis about 30° from the normal direction in the transverse direction. Scatter about this average orientation is fairly isotropic. The expansivities in the three sheet directions may be calculated from the formula:

$$\alpha_{th,\,tr,\,r} = (\alpha_c - \alpha_a)\cos^2\phi_{th,\,tr,\,r} + \alpha_a$$

where $\alpha_c = 10.4 \pm 0.5 \times 10^{-6}$ per °C (*c* expansivity, Table IV)

$\alpha_a = 4.5 \pm 0.5 \times 10^{-6}$ per °C (*a* expansivity, Table IV)

$\phi_{th,\,tr,\,r}$ = angle between thickness (*th*), transverse (*tr*), or rolling (*r*) direction and mean orientation of c axis.

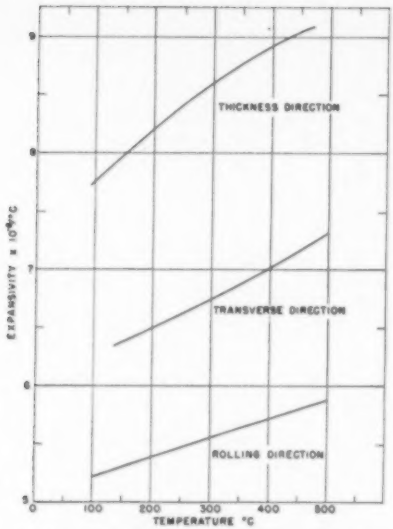

Fig. 10—Expansivity of recrystallized zirconium sheet.

The experimental and calculated expansivities for recrystallized zirconium are shown in Table V.

The uniform scatter for this texture would be expected to increase the experimental rolling direction measurement and decrease the other two measurements. Since the scatter areas of the pole figures are not quantitative no attempt was made to reconcile their resolved contributions. The variations of expansivity with temperature in the three principal sheet directions of cold-rolled and recrystallized (600°C) Bureau of Mines zirconium are shown in Fig. 10.

Summary

1—X-ray diffraction methods were used to determine the preferred orientations of crystal bar and Bureau of Mines zirconium which were subjected to several different rolling and heating treatments. The data were presented as pole figures.

2—The cold-rolling texture indicated an average orientation that can be described as having the basal planes, {0001}, parallel to the rolling direction, but inclined from the rolling plane of the sheet about 30° in the transverse direction, with a $<10\bar{1}0>$ direction in the rolling direction.

3—The recrystallization texture was different from the cold-rolling texture. The average position of the basal planes was the same as for the cold-rolling texture but a $<11\bar{2}0>$ direction was in the rolling direction.

4—The hot-rolling texture was similar to the cold-rolling texture but with more scatter, especially in the transverse direction.

5—A specimen cross rolled at room temperature had a sharp texture with the basal planes parallel to the rolling plane and with the $<10\bar{1}0>$ direction in one rolling direction and the $<11\bar{2}0>$ direction in the other rolling direction.

6—The recrystallization texture of the cross-rolled zirconium showed the same basal plane orientation as the rolled material, but the $<11\bar{2}0>$ direction was in the $<10\bar{1}0>$ rolling direction and the $<10\bar{1}0>$ direction was in the $<1120>$ rolling direction.

7—The texture of surface layers of cold-rolled zirconium was found not to differ fundamentally from that of the interior of the metal.

8—Experimental evidence that the transformation mechanism of β body-centered cubic and hexagonal close-packed α zirconium is of a crystallographically reversible nature was presented. The transformation texture indicates that the orientation relationship is the same as that reported by Burgers, namely $\{0001\}_\alpha \parallel \{110\}_\beta$, $<11\bar{2}0>_\alpha \parallel <111>_\beta$.

9—By X-ray diffraction the thermal expansivity of zirconium in the c-axis direction was found to be $10.3 \pm 0.5 \times 10^{-6}$ per °C and $4.5 \pm 0.5 \times 10^{-6}$ per °C in the *a*-axis direction. The thermal expansivities were measured in the thickness, transverse, and rolling directions of all sheet materials whose textures were determined, and the magnitude of expansion was found to be proportional to the degree of scatter in the three measured directions.

Table V. Linear Expansion Coefficients of Recrystallized Zr ($\times 10^{-6}$ per °C)

	Thickness Direction	Transverse Direction	Rolling Direction	Calculated Volume Coefficient
Experimental	8.6±0.4	6.3±0.4	5.5±0.4	20.4±1.2
Calculated	8.9±0.5	7.3±0.5	4.5±0.5	20.7±1.5

Acknowledgment

The work described in this paper was done under Atomic Energy Commission Contract AT-11-GEN-14. The authors gratefully acknowledge the expansivity data submitted to them by D. M. Wroughton and G. F. Mechlin, of the Westinghouse Atomic Power Div., and Howard Scott and William Mohr, of the Westinghouse Research Laboratories.

References

[1] P. W. Bakarian: *Trans.* AIME (1942) **147**, p. 266.
[2] J. T. Norton: *Journal of Applied Physics* (1948) **19**, p. 1176.
[3] V. Caglioti and G. Sachs: *Metallwirtschaft* (1932) **11**, p. 1.
[4] G. Wasserman: *Metallwirtschaft* (1930) **9**, p. 698.
[5] A. Smigelskas and C. S. Barrett: *Trans.* AIME (1949) **185**, p. 145; JOURNAL OF METALS (February 1949).
[6] H. T. Clark, Jr.: *Trans.* AIME (1950) **188**, p. 1154; JOURNAL OF METALS (September 1950).
[7] W. G. Burgers and F. M. Jacobs: *Metallwirtschaft* (1935) **14**, p. 285.
[8] W. G. Burgers, J. D. Fast, and F. M. Jacobs: *Ztsch. Metallkunde* (1938) **29**, p. 419.
[9] P. A. Beck, P. R. Sperry, and Hsun Hu: *Journal of Applied Physics* (May 1950) **21**, p. 420.
[10] R. Vogel and W. Tonn: *Ztsch. Anorg. Allgem. Chem.* (1931) **202**, p. 292.
[11] W. G. Burgers: *Physica* (1934) **I**, p. 561.
[12] W. G. Burgers and J. J. A. Ploos Van Amstel: *Physica* (1938) **V**, p. 305.
[13] G. Shinoda: Kyoto Imperial University **XVII** No. 1, (January 1934).
[14] G. F. Mechlin: Private communication.
[15] J. D. DeBoer: *Foote Prints* (1930) **3**, No. 2, p. 18.
[16] W. Kroll: *Metallwirtschaft* (1939) **18**, p. 77.
[17] W. M. Raynor: MINING AND METALLURGY (1947) **28**, p. 284.
[18] D. M. Wroughton: Private communication.

Grain-Growth and Recrystallization Characteristics of Zirconium

by F. J. Dunkerley, F. Pledger, V. Damiano, and J. Fulton

Grain-growth and recrystallization characteristics of a commercially pure zirconium prepared by the iodide process are reported. Grain growth from 640° to 800°C was continuous once initiated and obeyed $D = kt^n$. Recrystallization of zirconium occurred at temperatures of 450° to 550°C after deformations of 20 and 50 pct. Hardening from partially soluble inclusions prevented determination of the absolute rates of recrystallization, but the relative rates of recrystallization obtained are useful as a guide in fabrication practice.

BASIC information needed as a guide in the hot and cold working and annealing of metals includes recrystallization and grain-growth data. A search of the literature revealed no such information for pure zirconium. This is a report of practical grain-growth and recrystallization results obtained for a commercial grade of pure zirconium on a project sponsored by the Office of Naval Research. In this work, isothermal grain-growth curves were obtained at five temperatures from 640° to 800°C inclusively; while recrystallization curves have been determined at 450°, 500°, and 550°C for the metal at the deformation levels of 20 and 50 pct. In addition to the usual variables of temperature, time, and deformation, distribution of the second phase found in all commercial grades of iodide zirconium is also treated as an important factor in these grain-growth and recrystallization studies.

F. J. DUNKERLEY, Associate Member AIME, is Assistant Professor of Metallurgy, Dept. of Metallurgy, University of Pennsylvania, Philadelphia; F. PLEDGER, formerly Graduate Student, Dept. of Metallurgy, University of Pennsylvania, is now Metallurgist, E. I. du Pont de Nemours & Co., Orange, Texas; V. DAMIANO, Student Associate AIME, is Graduate Student, Dept. of Metallurgy, University of Pennsylvania; and J. FULTON, Student Associate AIME, formerly Laboratory Assistant and student, Dept. of Metallurgy, University of Pennsylvania, is now Graduate Student, Dept. of Metallurgy, Massachusetts Institute of Technology, Cambridge, Mass.

Discussion on this paper, TP 3144E, may be sent, 2 copies, to AIME by Jan. 1. 1952. Manuscript, Oct. 16, 1950; revision, June 21, 1951. St. Louis Meeting, February 1951.

In conducting this work, two properties of zirconium were particularly pertinent in dictating experimental conditions. First, since zirconium undergoes a transformation from the α close-packed hexagonal form to the β body-centered cubic form at 862°C, no recrystallization or grain-growth studies were made above 800°C. Second, because dissolved gases (oxygen, nitrogen and/or hydrogen) increase the hardness and lower the ductility of the solid metal, all annealing treatments in this investigation were carried out in vacuum or in a helium atmosphere.

Materials and Methods

The zirconium used in this investigation was prepared by the Foote Mineral Co. by deposition from its iodide. A spectrochemical analysis of the metal showed the following composition in weight pct: Hf, 2.1; Mg, 0.012; Fe, 0.035; Si, 0.095; Ti, 0.023; Al, 0.037; Mo, trace; Ni, trace; Cr, trace; Ca, 0.006.

Conventional metallographic procedures involving hand polishing on wet metallographic papers, followed by final polishing on fine, levigated alumina on gamal cloth and a medium speed wheel were used throughout this investigation. Grain boundaries were revealed with modified Tucker's etch containing 20 parts glycerine, 2 parts hydrofluoric acid, and one part nitric acid.

Grain-Growth Procedure: Three lots of zirconium, designated here as series A, B, and C were prepared for the grain-growth studies as follows:

Series A was prepared by cold swaging the ½ in. as-deposited rod to a 3/16 in. final diameter, followed

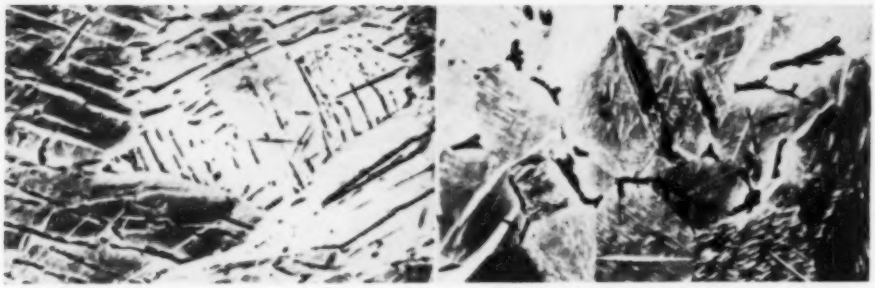

a. α_a structure heated at 950° for 24 hr and air-cooled. b. α_b structure heated at 800° for 72 hr and furnace-cooled.

Fig. 1—Microstructures of deposited zirconium, swaged and heat treated. Etched with 10 pct HF in glycerine. X250.

by annealing for 20 hr at 600°C in an evacuated quartz tube for complete recrystallization. The initial grain size thus developed in the A specimens was 0.009 mm average diameter. These specimens ½ in. long were then sealed in vacuum in quartz tubing and heated for times varying from ½ to 100 hr at the temperatures 640°, 680°, 720°, 760°, and 800°C for grain-growth studies. Series B was prepared by sheathing a small section of rod with an iron pipe, hot rolling at 700°C to a ¼ in. rod and finally cold swaging to a 3/16 in. diam rod. This stock was then heated to 800°C for 1½ hr to develop a grain size of 0.024 mm. Series C was prepared by hot rolling as in the case of the B series and then annealing at 800°C to develop a grain size of 0.023 mm. The usual vacuum-annealing technique was then followed in carrying out grain-growth studies on lots B and C at the temperature levels of 640°, 720°, and 800°C. Temperatures were measured with a calibrated chromel-alumel thermocouple and were always maintained within ±1.5°C of the values reported.

Sections both transverse and longitudinal to the swaging and/or rolling direction were examined and the grain diameters reported are the averages of those on both sections. The usual metallographic grain counting technique was used except paper negatives were made on Kodabromide enlarging paper to facilitate the grain-size measurements. Four to six areas, each containing at least 100 grains, were obtained for each specimen. Grain diameters were calculated from the formula:

$$D = \frac{1.075}{M}\sqrt{\frac{A}{n}}$$

where D is the average grain diameter in mm; A, the area of the field in sq mm; n, the total number of grains; and M, the magnification. In deriving this formula, it was assumed that all grains were regular hexagons and D was equal to the distance between opposite flats of the hexagon.

Recrystallization Procedure: In order to include distribution of the second phase as a variable, the stock metal was prepared and heat treated in the following manner:

The ½ in. deposited rod was cold swaged to ¼ in. diam and a suitable length was sealed in an evacuated quartz tube, heated at 950°C for 24 hr, and air cooled. This produced the structure shown in Fig. 1a, designated hereafter as α_a. The second phase occurs here as coarse lamellar platelets with different orientations in adjacent grains. The second section of ¼ in. rod was heated at 800°C for 72 hr and furnace cooled. Here the second phase is agglomerated in the grain boundaries, as shown in Fig. 1b. Material treated in this way will be designated hereafter as α_b. Portions of the annealed rods were then cold worked on a 5x8 in. flat-roll mill to 20 and 50 pct reductions in cross-sectional area, light passes of about 0.005 in. each being taken to achieve as nearly uniform deformation as possible. The change in length in cold rolling was used in the usual way as the criterion of reduction in area.

Specimens of each structure and reduction were annealed isothermally in vacuum at 450°, 500°, and 550°C. A muffle furnace was used to anneal specimens for ½ hr or longer, while a constant temperature bath was used when the time of annealing was less than ½ hr. Temperature gradients in the muffle furnace were eliminated by placing the tubes in a cavity in the center of a high heat capacity steel bar, 2½ in. in diam x 7 in. in length. Specimens were admitted to the furnace or salt bath at temperature in order to obtain maximum heating rate and to assure accurate time control. Time to attain temperature was experimentally found to be 2 min in the furnace and 3 sec in the salt bath, and this was subtracted from the total time of annealing in each case. The short-time specimens were heated by direct immersion in the salt bath followed by air cooling. The long-time specimens which were sealed in evacuated quartz tubes were air cooled.

Hardness measurements or the rate of softening as a result of recrystallization anneals were used as the major tool for following the progress of recrystallization, since the more classical metallographic[5] technique was difficult to carry out on zirconium. The annealed specimens were thus mounted in bakelite and finish-ground on 600 grit wet metallographic paper in preparation for hardness measurements. The Rockwell Superficial 30-T scale was chosen for hardness measurements because this gave the sensitivity required. An average of seven indentations on specimens reduced 20 pct, and five indentations on those reduced 50 pct were taken as the hardness of the annealed material. A limited number of metallographic determinations of percentage recrystallized were made as checks on the softening data.

Results and Discussion

Grain Growth: Although not all pure metals exhibit a straight line relationship when log D is plotted vs. log t, as suggested by the equation[2,3] $D = kt^n$, where D is the average grain diameter; k, a constant dependent only upon temperature; t, the

time; and n, a constant; the data obtained here conformed closely enough to this formulation to be presented in this way. On this basis, grain-growth data for zirconium, whose initial grain size is 0.009 mm at the temperature levels 640°, 680°, 720°, 760°, and 800°C, are plotted in Fig. 2. The data for 640°, 680°, and 720°C are seen to constitute a family of parallel straight lines over the entire 100 hr of the study. At 760° and 800°C, however, the growth rate shows an abrupt increase after an initial stage, and a new family of curves appears. The grain-growth data for series B and C are given in Fig. 3. Considering first the B series, it is seen that at 640°C, a long incubation period was observed, during which no noticeable change in the average grain diameter was detected. After more than 35 hr, however, grain growth began and proceeded normally. At 720° and 800°C grain growth occurred at the shortest time examined, and it is seen that the data at 640°, 720°, and 800°C form a family of straight lines (Fig. 3). A similar incubation period, followed by normal grain growth was noted for the C specimens which started at the same initial grain size. Also grain growth in this material proceeded consistently, a family of straight lines again expressing the observed behavior.

In Fig. 2, in addition to a plot of the A series, typical curves for series B at 680°C, and C at 760°C are given (there is no need for including all the B and C curves because within each series the curves are parallel). Since the initial grain size for the B and C series was much larger than that of A, the grain-growth curves for the former two series for corresponding temperatures were always shifted to a higher grain-size level. It should be noted, however, that the rate of change of log D with log t for series B at all temperatures is the same as in series A at 760° and 800°C, while the series C curves have a slope or rate of change of log D with log t intermediate between those of series A and C.

These grain-growth results very definitely reflect the effect of the second phase. Cold swaging the deposited rod caused fragmentation of the second phase, which appeared in the deposited rod as parallel platelets (with different orientations in different grains). For the A series, the subsequent recrystallization anneal caused the fine inclusion particles to spheroidize, and the structure shown in Fig. 4a resulted. Further, when the grain-growth anneals were carried out, these dispersed particles inhibited, but did not prevent, grain-boundary migration. Simultaneously, however, the small particles of second phase preferentially dissolved, and diffusion of the second-phase constituents occurred to permit the larger particles of the second phase to grow at the expense of the smaller ones. The inhibiting effect of the particles, especially as long as they remained intragranular, continued but became less effective as the size increased. Temperature, of course, had the effect of accelerating this spheroidizing process as evidenced by the fact that at 720°, 10 hr were required for agglomeration of this second phase into large angular inclusions in the grain boundaries, but within 3 hr at 800°C agglomeration was obtained (Fig. 4b).

The grain-growth curves for metal A at 640°, 680°, and 720°C and the initial part of the 760° and 800°C curves thus represent the rate of boundary migration under the inhibiting influence of the uniformly distributed second-phase particles which were simultaneously undergoing spheroidization and agglomeration. When this spheroidization proceeded to the

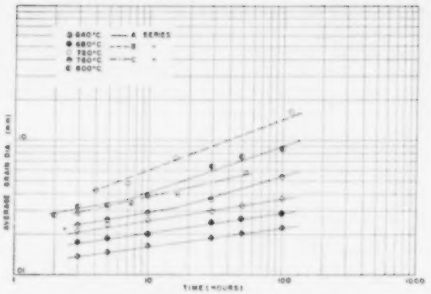

Fig. 2—Isothermal grain-growth curves for A series of zirconium at 640°, 680°, 720°, 760°, and 800°C. Curve for growth of series B, at 680°, and series C at 760°C are superimposed.

point where the intragranular particles had disappeared and large angular second-phase particles appeared in the grain boundary (but not preferentially in the dihedral angles), grain growth became much more rapid. A new family of grain-growth curves was thus obtained.

No indication of a critical temperature below which an equilibrium grain size existed, as found by Beck,[2] is seen in these data. Continuous grain growth in the presence of dispersed second-phase inclusions probably occurred in zirconium of this study because at all the annealing temperatures the second phase was at least partially soluble. This is qualitatively in agreement with Beck's[2, 3] work on aluminum-manganese alloys which showed that when the second phase is soluble normal continuous grain growth occurs.

In the B series however, the second phase was initially agglomerated into large particles at grain boundaries during the recrystallization and preparation anneal as shown in Fig. 5a. At the lower temperatures, then, these particles did not have as pronounced an inhibiting effect as did the finer dispersed particles in the A material; thus a family of curves (Fig. 3) holds over the entire temperature range from 640° to 800°C, instead of only at 760° and 800°C as in series A. In the C series, the second-phase distribution was similar to that in the A series before the grain-growth anneals, except that the particles were initially larger. During the grain-growth anneals, however, these particles did not agglomerate as completely as they did in the A series. An inhibiting effect of intragranular second phase thus persisted during the entire time and at all temperatures. Consequently, the grain-growth curves for the C series are almost parallel to those of the A

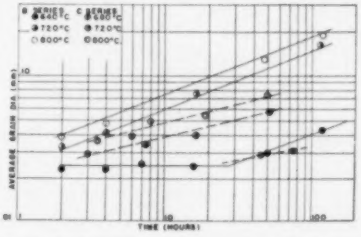

Fig. 3—Isothermal grain-growth curves for the B and C series of zirconium from 640° to 800°C.

series at 680°C, then gradually increased in slope at 720° and 800°C, but never attained the grain growth of the A and B series at 720°, 760°, and 800°C. Thus, since the same degree of agglomeration of the second phase in the grain boundaries was not accomplished in the C series as was always present in the B series throughout and in the latter stages of the A series, the inhibiting effect of the second phase gave grain-growth characteristics which were intermediate between the A and the B series.

Fig. 4—Microstructures of zirconium from grain-growth studies on series A, 10 pct HF in glycerine etch. a (top)—3 hr at 720°C. X300. b (center)—3 hr at 800°C. X300. c (bottom)—50 hr at 800°C. X200.

Dispersed second-phase particles have an inhibiting effect on grain growth either directly or indirectly by obstructing the movement of atoms across grain boundaries. It is noted that, for a given constant amount of second phase, the finer the particles, the greater was the inhibiting effect. This is reasonable if it is accepted that a metal inclusion interface impedes the migration of a grain boundary, because the smaller the particle, the greater is the surface area for a constant amount of second-phase impurities. When the second phase is agglomerated in the grain boundaries, grain growth may be retarded for two reasons: 1—the actual grain boundary or interfacial area across which atoms may migrate may be decreased, or 2—changes in grain-boundary curvature accompanying growth may be prevented by the segregation of second phase in the dihedral angles. That this latter inhibiting effect was present in this work is shown by the fact that the surface of numerous A series specimens, which contained no second phase after being annealed 50 hr at 800°C, grew extremely large and very rapidly, while the internal grains in the presence of the second phase preferentially at the dihedral angles remained comparatively small. It is further noted that the surface grain boundaries are perpendicular to the surface and the dihedral angles are approximately the equilibrium value of 120°C, as predicted by Harker and Parker[4] and others.[5] Also, no additional growth of these surface grains was noted after 100 hr at 800°C, Fig. 4.

The constant slope of the series A growth curves for 640°, 680°, and 720°C establishes that n, in the expression $D = kt^n$, is a constant. This in turn designates that one mechanism of growth is operating at these three temperatures, and thus calculation of the energy of activation of that process can be made. This can be done by means of the relation first proposed by Arrhenius[6] and applied to grain growth by Burke[3] and others; that is, the rate of grain growth $= Ae^{-Q_g/RT}$, where A is a constant (independent of temperature); Q_g, the energy of activation for grain growth; R, the universal gas constant; and T, the temperature in degrees absolute. Using this equation, the energy of activation, Q_g, has been evaluated graphically for series A at 640°, 680°, and 720°C as shown in Fig. 6. The slope of this line divided by R, the universal gas constant, yields the value 68,800 cal per mol. Calculation of Q_g for the higher temperature data and for the B series from

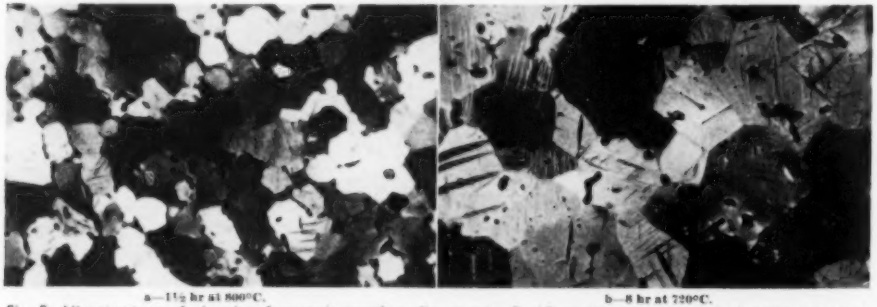

a—1½ hr at 800°C. b—8 hr at 720°C.

Fig. 5—Microstructures of zirconium from grain-growth studies on series B. All specimens were given the initial treatment of 1½ hr at 800°C, as shown in a. 10 pct HF in glycerine etch. X200.

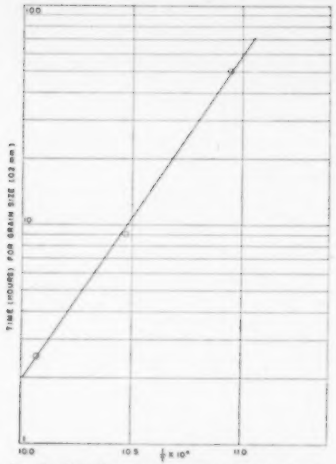

Fig. 6—Plot of time necessary to attain a grain size of 0.02 mm from an initial grain size of 0.009 mm vs. reciprocal of the corresponding absolute temperature.

680° to 720°C, inclusively, yields the value 55,000 cal per mol. These values represent the energies of activation for zirconium containing the second phase, 1—uniformly distributed, and 2—preferentially in the grain boundaries, respectively.

The incubation period in the 640°C curves of the B and C series is now being investigated more completely for zirconium over a wide range of temperatures, and these data will be reported in a later paper. Although commonly observed, present grain-growth theories neither predict nor explain the existence of an incubation or induction period for grain growth subsequent to complete recrystallization, but when a more precise mechanism is established and associated with the energetics of the process, the phenomena should be explicable.

Recrystallization: The isothermal softening curves obtained for zirconium for the temperatures 450°, 500°, and 550°C at 20 and 50 pct reduction levels are found in Figs. 7 and 8. It is seen that for any one distribution of second phase and amount of deformation the rate of softening is principally dependent upon temperature, increasing as the latter increases. The incubation period, however, for the metal deformed 50 pct is appreciably shorter than for zirconium deformed 20 pct. The overall rate of recrystallization increases with the amount of prior deformation. Work hardening as a result of cold work raises the initial hardness level, but the hardness difference in the fully annealed specimens may be either a result of previous annealing treatments or an effect of prior deformation on recrystallized grain size. It is unlikely that the higher final hardness is the residual effect of greater prior deformation, per se.

Definite effects of second-phase distribution and possibly solid solution can also be seen in these data. The α_a form is slightly harder and appears to possess a greater capacity for work hardening than the α_b form, since the hardness differential increases with deformation. This differential is maintained during annealing with the result that the shapes of the softening curves for both temperatures at the same reductions are similar. A considerably longer incubation period is required before softening begins in the α_a structure than in the α_b. In the α_a structure, Fig. 1a, it is seen that the same phase appears as parallel platelets, and this lamellar structure has the effect of retarding softening.

Although the metallographic difficulties encountered with zirconium in the cold-worked state made it impossible to extensively use the classical metallographic approach to the study of recrystallization, some metallographic data have been obtained for correlation of hardness with percentage of recrystallization. These data yielded the correlation between hardness and the fraction recrystallized given by the relationship:

$$x^2 = 1.038 \cdot (h_o - h_x)/(h_o - h_i)$$

where, x is the percentage recrystallized; h_x, the hardness at x pct recrystallized; h_o, the cold-worked hardness; and h_i, the full-annealed hardness. This relationship holds for all but the initial phase of the softening process. This result is to be compared to that of Cook and Richards[5] and others[6] who found that pure copper obeyed the relationship of $x = (h_o - h_x)/(h_o - h_i)$. This latter relationship indicates that softening occurs in direct proportion to the extent of recrystallization. The relationship developed from the present data, however, indicates that softening occurs in this commercially pure grade of zirconium in direct proportion to the square of the percentage recrystallized.

This relation is believed to reflect that a diffusion process associated with and effecting a redistribution of the second phase is occurring simultaneously with recrystallization. This diffusion process continuously changed the solid-solution composition, especially in the early phases of the recrystallization anneal, and a corresponding change in hardness occurred. The hardness change resulting after the various anneal-

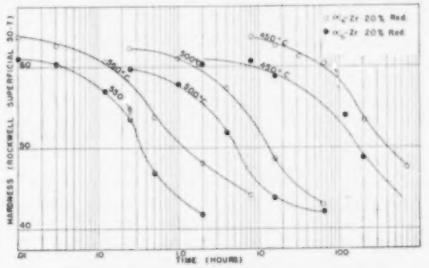

Fig. 7—Softening curves for α_a and α_b zirconium at 450°, 500°, and 550°C for 20 pct reduction.

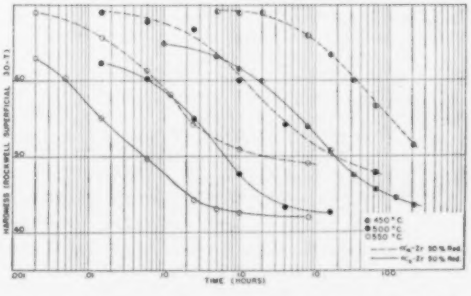

Fig. 8—Softening curves for α_a and α_b zirconium at 450°, 500°, and 550°C for 50 pct reduction.

ing times is thus a composite of softening resulting from recrystallization and hardening resulting from changing the composition of the continuous zirconium solid-solution phase.

Thus, since the parameter (hardness) used to follow recrystallization has also been affected by diffusion of either the second-phase components or residual oxygen in the sample tubes, the absolute rates of recrystallization of zirconium cannot be obtained from the present data. The relative rates of recrystallization revealed by these hardness measurements, however, can be used as a reliable guide to establish fabrication practice of comparable grades of pure zirconium.

No attempt is made to evaluate an energy of activation for recrystallization, since the absolute rates of recrystallization at the various temperatures cannot be ascertained. It is pertinent to point out, however, that the general shape of all the curves is similar, indicating that the same recrystallization mechanism is operative throughout and that this mechanism is independent of prior deformation and prior heat treatment.

Conclusions

1—The isothermal grain-growth data for zirconium follows the relation:

$$D = kt^n$$

2—Second-phase inclusions have pronounced effects on grain growth.

a—In the presence of dispersed second-phase inclusions, grain growth of zirconium was retarded but growth was continuous at temperatures from 640° to 800°C.

b—The retarding effect of the second phase when agglomerated in the grain boundaries was less than when it was dispersed throughout the grains.

c—The entire elimination of the second phase resulted in accelerated grain growth.

3—The energy of activation for grain growth of zirconium in the presence of a dispersed second phase is 68,800 cal per g atom as compared with a value of 55,000 cal per g atom when the second phase is agglomerated in the grain boundaries.

4—Increasing the temperature increases the rate of recrystallization of zirconium independently of prior heat treatment and deformation.

5—The rate of recrystallization increases and the incubation period decreases with increased amount of cold work.

6—Solid solutions of oxygen or the second-phase constituent early in the recrystallization anneal increased the hardness so that appreciable recrystallization occurred before it was revealed by softening. The two structures of zirconium heat treated above and below the transformation temperature contained appreciably different distributions of the second phase, and had different recrystallization characteristics. Heat treating above the transformation temperature results in more work hardening and slightly higher hardness readings than below, and this difference persists throughout the entire annealing period. When the second phase occurs as platelets, recrystallization is retarded.

Acknowledgment

The authors are indebted to the Navy Department, Office of Naval Research, for permission to publish this work. They are also grateful to R. M. Brick and other members of the graduate school and staff of the Metallurgical Engineering Dept., University of Pennsylvania.

References

[1] W. A. Anderson and R. F. Mehl: Recrystallization of Aluminum in Terms of Rate of Nucleation and Rate of Growth. *Trans.* AIME (1945) **161**, pp. 140-166.

[2] P. A. Beck, M. L. Holzworth, and P. R. Sperry: Effect of Dispersed Phase on Grain Growth in Al-Mn Alloys. *Trans.* AIME (1949) **180**, pp. 163-192; METALS TECHNOLOGY (September 1948).

[3] J. E. Burke: *Grain Control in Industrial Metallurgy.* Fundamentals of Recrystallization and Grain Growth. P. 57 (1949) ASM. Cleveland.

[4] D. Harker and E. R. Parker: Grain Shape and Grain Growth. *Trans.* ASM (1945) **34**, p. 156.

[5] Cyril Stanley Smith: Grains, Phases and Interfaces, An Interpretation of Microstructure. *Trans.* AIME (1948) **175**, pp. 15-51; METALS TECHNOLOGY (June 1948).

[6] N. Thorley: Calculation of the Activation Energies of Recovery and Recrystallization from Hardness Measurements on Copper. *Journal* Inst. Metals (1950) **77**, pp. 141-161.

[7] Maurice Cook and T. L. Richards: Observations on the Rate and Mechanism of Recrystallization of Copper. *Journal* Inst. Metals (1946) **73**, pp. 1-31.

[8] S. Glasstone: *Textbook of Physical Chemistry.* P. 1088 (1946) 2nd Ed. New York. D. Van Nostrand.

DISCUSSION, D. Turnbull presiding

H. H. Hausner and H. S. Kalish *(Sylvania Electric Products, Inc., Bayside, L. I., N. Y.)*—We wish to congratulate the authors for their interesting paper and would like to call their attention to our paper.[9] The difference between the authors and our investigations lies mainly in the fact that the authors studied the recrystallization and grain growth of solid, cold-worked material, whereas we investigated the grain growth during sintering and the effect of sintering conditions on the grain size. We found an excellent correlation between grain size and the density of the respective specimen with no respect to whetner this density was achieved by short-time sintering at high temperature, or by long-time sintering at lower temperatures. We found further that the grain size obtained under certain sintering conditions depends on the raw material used for the compact. The rate of grain growth was considerably greater with zirconium hydride powder than with zirconium powder used as a raw material.

F. J. Dunkerley (authors' reply)—The work of Dr. Hausner and Mr. Kalish on grain growth during the sintering of powdered zirconium came to our attention after this work was completed, but it is gratifying to find their results are in good agreement with our data on the wrought metal. We too noted the pronounced inhibiting effect of second-phase impurities on grain growth. In Fig. 4c micrographic evidence of accelerated growth in the absence of the second phase is shown. This phenomena is probably responsible for the more rapid grain growth noted for the zirconium hydride powder.

[9] H. H. Hausner, H. S. Kalish, and R. P. Angier: Powder Metallurgy of Zirconium. JOURNAL OF METALS (August 1951) *Trans.* AIME, pp. 625-633.

In the June 1951 issue, pp. 483 and 484, *Kinetics of Precipitation in Supercooled Solid Solutions* by G. Borelius: the illustration labeled Fig. 21, p. 483, is the illustration for Fig. 22 and belongs on p. 484, while the illustration labeled Fig. 22, p. 484, is the illustration for Fig. 21. The captions are correct as printed and remain where they are.

Chromium-Nickel Phase Diagram

by David S. Bloom and Nicholas J. Grant

An investigation of the Cr-Ni system has revealed that there exists a eutectoid transformation at about 1180°C. The transformation in chromium implied by the eutectoid reaction was detected at about 100°C below its melting point. Associated with the eutectoid transformation, a metastable transition structure has been found.

THE Cr-Ni phase diagram is shown in current literature to be a simple eutectic system in which the high chromium end of the diagram is incompletely determined, Fig. 1. The last investigation of this system was undertaken in 1936.[1] Because of limitations in metal purity, especially of chromium, and temperature measuring techniques, the diagram should be accepted with some reservations, as was indicated by Hansen.[2] For example, the presence of the compound Cr_2Ni, with a tetragonal structure,[3] remains unverified and incompatible with the simple eutectic diagram.

The work reported here began because of discrepancies that appeared in experimental studies in the binary alloys Cr-Ni and in the ternary system Cr-Mo-Ni. The existing binary Cr-Ni diagram failed to provide a complete explanation of observations made by microscope, X-ray, and thermal analyses.

Experimental Methods

The materials employed were of a higher degree of purity than were available to previous investigators. The Mond nickel usec had a nominal purity of 99.87 pct, while the electrolytic chromium analyzed 99.03 pct with the major impurity being 0.5 to 0.7 pct oxygen with some iron. All alloys were melted in a vacuum furnace to remove dissolved gases, sufficient carbon was added to the charge to combine with all the oxygen as CO. Final analysis determined the carbon as about 0.02 pct and the oxygen around 0.06 pct or slightly more. Stabilized zirconia crucibles and thermocouple protection tips were used throughout and contributed no detectable impurity to the melts, as long as the oxygen in the chromium was kept low. Heats averaged about 250 g, which permitted about 2 in. of the thermocouple protection tips to be submerged. The temperature drop across the thermocouple protection tip was determined to be about 3°C, a minor source of error.

The alloys, after removal from the vacuum furnace, were placed in a furnace operating in a purified argon atmosphere for the thermal analyses. Annealed wolfram-molybdenum thermocouples provided the primary means of temperature determination, though a Pt-Pt-10 pct Rh couple was employed for a check when possible. A sensitive, high-speed Leeds and Northrup Speedomax recording potentiometer indicated the thermocouple output.

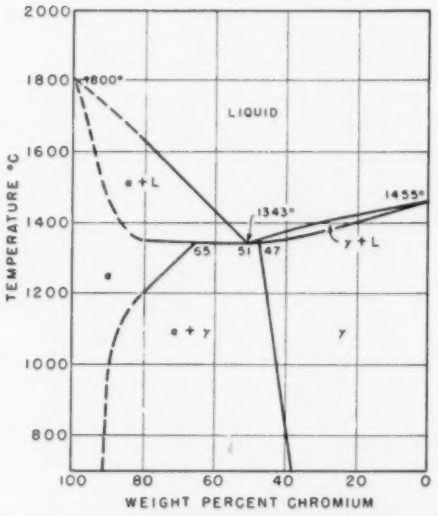

Fig. 1—Cr-Ni phase diagram drawn from the diagram in the Metals Handbook, 1948 Edition.

X-ray diffraction patterns were obtained primarily on a Norelco unit, which permitted diffraction angles only up to 45° ($2\theta = 90°$). In general, either rotated or stationary solid samples were used, because it later evolved that many samples were susceptible to transformation resulting from the cold working involved in pulverizing. It was also noted that rotating a sample sometimes suppressed weak lines, so, usually, samples were not rotated. Later a high temperature camera was adapted for use at temperatures up to 1400°C on the Norelco unit utilizing both solid and powdered samples. Unless otherwise noted, all X-ray patterns were made with a chromium tube and a vanadium filter. Further-

D. S. BLOOM is Research Assistant and N. J. GRANT, Member AIME, is Associate Professor, Dept. of Metallurgy, Massachusetts Institute of Technology, Cambridge, Mass.

Discussion on this paper, TP 3155E, may be sent, 2 copies, to AIME by Jan. 1, 1952. Manuscript, April 18, 1951; revision, Aug. 22, 1951. Detroit Meeting, October 1951.

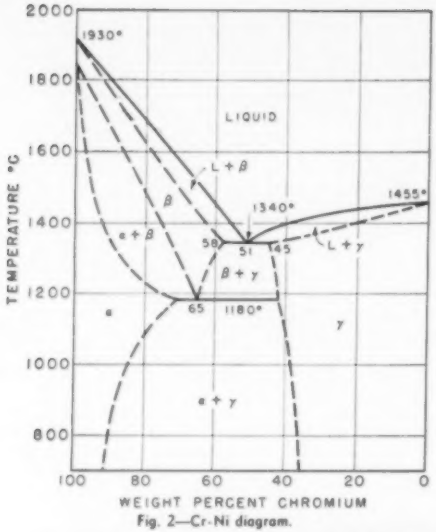

Fig. 2—Cr-Ni diagram.

more, because many samples were sensitive to mechanical polishing, practically all samples were polished and etched electrolytically. The etch generally used was a mixture of concentrated nitric acid, sulphuric acid, and phosphoric acid.

All heat treating was done in a resistance furnace in a purified-helium atmosphere. Inasmuch as the cooling rate turned out to be critical in some alloys, efforts were expended to obtain the fastest quench possible.

Experimental Results

To facilitate the discussion of the experimental results it seems advisable to introduce here the phase diagram, Fig. 2, which resulted from this investigation. The α field is the body-centered cubic chromium solid solution; the γ field is the face-centered cubic nickel phase, while the β phase is a proposed high temperature chromium structure, thought to be face-centered cubic.

In Figs. 3 through 8 are shown the as-cast microstructures of some representative alloys. Fig. 3 shows a 90 Cr-10 Ni alloy in which it can be noted that the grain boundaries do not follow the dendritic structure. This indicates that recrystallization has occurred after solidification. Fig. 4 represents an alloy of 65 Cr-35 Ni, the structure of which cannot

Fig. 3—90 Cr-10 Ni alloy as-cast. Light areas are chromium-rich regions. X500.

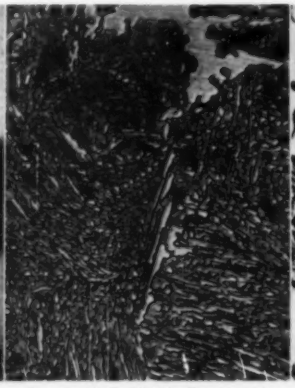
Fig. 4—65 Cr-35 Ni alloy as-cast. X150.

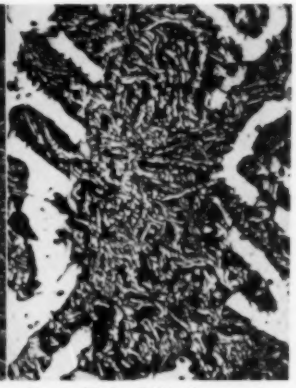
Fig. 5—55 Cr-45 Ni alloy as-cast. The darker regions are the chromium-rich phase. X150.

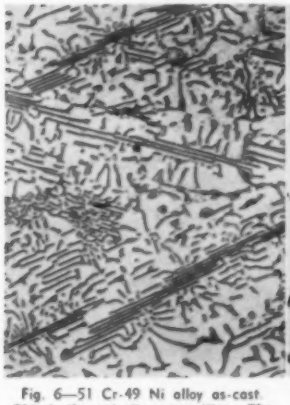
Fig. 6—51 Cr-49 Ni alloy as-cast. This is the eutectic composition. The darker regions are the chromium-rich phases. X150.

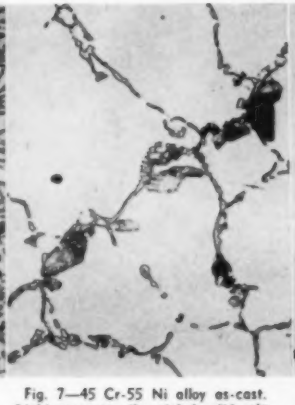
Fig. 7—45 Cr-55 Ni alloy as-cast. Light areas are the nickel solid solution, darker areas are the chromium phases. X150.

Fig. 8—45 Cr-55 Ni alloy as-cast. Light areas are the nickel solid solution, darker areas are the chromium phases. X750.

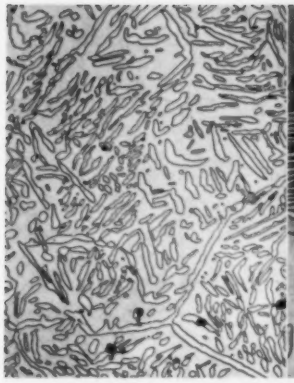

Fig. 9—Composition 60 Cr-39 Ni-1 Mo. Solution treated at 1325°C, furnace-cooled to 1150°C, held for 16 hr, then water quenched. Matrix is α chromium phase, islands are γ nickel. X150.

Fig. 10—Composition 55 Cr-45 Ni. Heat treatment consisted of 5 hr at 1325°C, 36 hr at 1150°C, then water quenched. Darker areas are chromium-rich phase. X150.

Fig. 11—Composition 45 Cr-55 Ni. Heat treatment consisted of 5 hr at 1325°C, 36 hr at 1150°C, then water quenched. X500.

be explained by the existing phase diagram. A 55 Cr-45 Ni alloy is presented in Fig. 5. It can be seen that there is a two-phase structure within the chromium-rich dendrites (the darker regions). This structure does not conform to that expected from the simple eutectic phase diagram, either. Fig. 6 reveals the structure of the eutectic composition (51 Cr-49 Ni); at a higher magnification the chromium-rich phase sometimes reveals an unanticipated internal structure. Figs. 7 and 8 show a 45 Cr-55 Ni alloy, and it will be noticed that there are three phases present. Further, at the higher magnification of Fig. 8, a eutectoid structure can be identified. From these structures alone the correctness of the simple eutectic diagram is subject to doubt.

The next series of microstructures are from specimens quenched from 1150°C, after first being solution-treated at 1325°C and furnace-cooled to 1150°C. Fig. 9 is of a 60 Cr-39 Ni-1 Mo alloy and comparing the structure with that of a 55 Cr-45 Ni alloy (Fig. 10) reveals the relation of the eutectoid structure to the eutectic structure.

A 45 Cr-55 Ni alloy is reproduced in Fig. 11 and shows the interesting form that the precipitate of the chromium-rich phase takes. Fig. 12a is the X-ray diffraction pattern corresponding to the specimen reproduced in Fig. 9, i.e., the 60 Cr-39 Ni-1 Mo alloy. The molybdenum in this alloy was inadvertently picked up from the radiation shield during melting. There was no visible difference between this alloy containing about 1 pct Mo and a similar alloy with no molybdenum, but the presence of the molybdenum permitted the retention of the high temperature phase (yet to be discussed), with no decomposition whatsoever, a condition unobtainable in a binary alloy. The apparent effect of the molybdenum was to stabilize the high temperature phase, fortunately.

There is an important difference between alloys quenched from 1250°C and those quenched from 1150°C as may be seen by comparing Figs. 13 through 15 with those just discussed. Fig. 13 is of the same alloy as shown in Fig. 9 and its X-ray diffraction pattern is shown in Fig. 12b. Comparison of Fig. 12b with Fig. 12a indicates that there is a fundamental difference between the two structures; this is also obvious from the micrographs. Fig. 14 shows the same alloy as in Fig. 10; Fig. 15 is the eutectic composition.

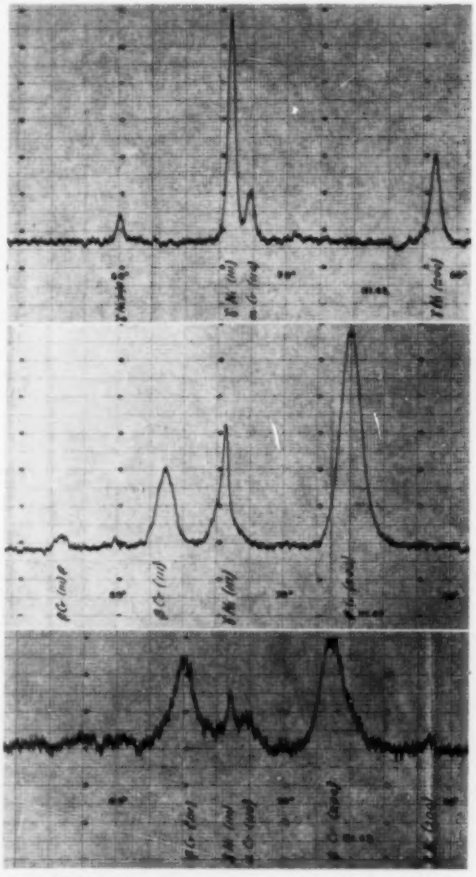

Fig. 12—X-ray diffraction pattern of 60 Cr-39 Ni-1 Mo alloy.
a (top)—As-water-quenched from 1150°C. Sample not rotated so that size of lines is not representative of amount of each phase present.
b (center)—As-quenched from 1250°C.
c (bottom)—As-quenched from 1250°C, electrolytically polished, and then given a slight grinding on 600-grit paper.

Fig. 13—Composition 60 Cr-39 Ni-1 Mo.
Heat treatment 9 hr at 1250°C, water quenched. Light phase γ nickel solid solution, dark phase β chromium solid solution. X750.

Fig. 14—55 Cr-45 Ni alloy as-quenched from 1250°C.
Dark areas are the chromium-rich phase. X150.

Fig. 15—51 Cr-49 Ni alloy (eutectic composition) after quenching from 1250°C.
Darker areas are the chromium-rich phase. X150.

To corroborate the existence of the α to β transformation as shown in the phase diagram, resort was made to a high temperature X-ray camera. The transformation temperature was later determined from dilatometer work to be at 1180°C. In order to obtain all the existing lines, as it was found that solid samples did not always produce all lines, powdered samples were used. These samples were compacted and then placed in the camera, but unfortunately at the temperatures of interest these samples soon sintered into solid specimens. Further, at these temperatures the extremely large thermal gradients in the sample precluded any accurate determination of the transformation temperature.

Figs. 16a and b show that a transformation did occur at a temperature of about 1200°C. Fig 16a shows the room temperature diffraction pattern. Fig. 16b shows the same 2θ range after the transformation has occurred. It is not possible to ascertain the crystal structure of the high temperature phase from this pattern, but it is apparent that a transformation has taken place. The absence of the β-Cr (111) line at about 41° (2θ) can be explained by the sintering of the powder compact into a solid mass.

Inasmuch as the eutectoid transformation implies a crystal transformation in pure chromium, an effort to detect this transformation was made. The transformation in chromium must take place at a temperature above 1700°C, because the specific

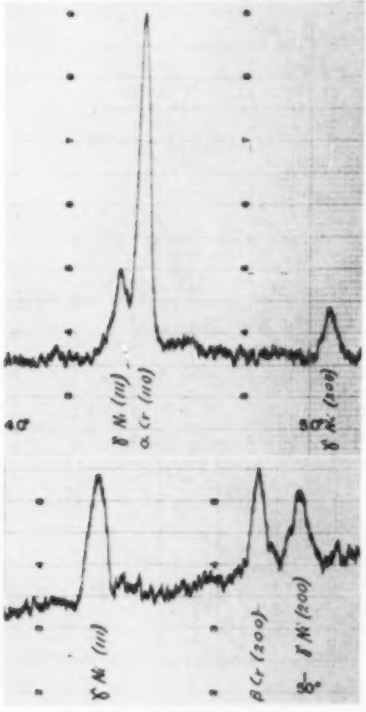

Fig. 16—X-ray diffraction patterns.
a (upper)—Pattern taken at room temperature of 63 Cr-37 Ni alloy showing the α chromium and γ nickel lines. Copper tube, nickel filter.
b (lower)—Pattern taken at about 1200°C of 68 Cr-32 Ni alloy in high temperature camera. Accuracy of lines cannot be better than ±0.2° because of shrinkage due to sintering and expansion of furnace. Comparing Fig. 16a with this figure it can be seen that the γ nickel lines have shifted to the left. Copper tube, nickel filter.

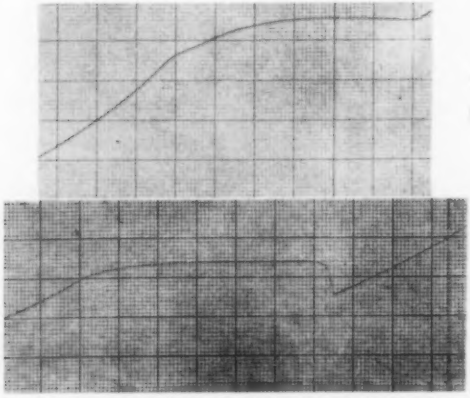

Fig. 17 a (upper)—Cooling curve of chromium. b (lower)—Cooling curve of nickel.
Time is plotted on the abscissa from right to left, temperature is plotted on the ordinate.

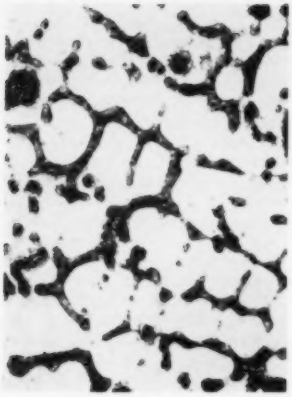

Fig. 18—90 Cr-10 Ni alloy as-drawn-up at about 1900°C into quartz tube and then quenched in water.
The large round body is an oxide inclusion. X500.

resistance has been measured up to this temperature and no anomalies discovered.[4] However, chromium with a small amount of oxygen (1.0 pct) showed a definite discontinuity at about 1600°C, and this discontinuity was ascribed to a eutectic in the Cr-O system. Fig. 17a shows a cooling curve of pure chromium. It will be noticed that there is an unusual change of slope about 100° below the solidification temperature (more accurate values were obtained at lower cooling rates). In Fig. 17b is shown a solidification curve of pure nickel in the same apparatus under similar conditions in order to emphasize the change of slope which exists in the chromium cooling curve. Efforts to retain the high temperature phase by quenching liquid chromium were not successful; however, in Fig. 18 is shown a 90 Cr-10 Ni alloy which was quenched from the liquid. It is evident that here there are two phases present. In Fig. 3 the same alloy is shown as-slowly-cooled, and, as was mentioned before, the fact that the grain boundaries do not follow the dendritic

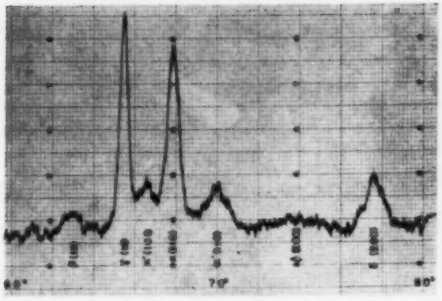

Fig. 19—65 Cr-35 Ni alloy as-quenched from 1250°C, after electropolishing only.
This sample was rotating while pattern was being obtained.

structure is indicative of recrystallization after solidification.

In order to identify the high temperature β chromium it was necessary to use quenched specimens. It had been hoped that by employing a copper-anode X-ray tube and the high temperature camera it would be possible to find additional lines, but it seems that all higher angle lines were so diffuse at 1250°C that they were not recognizable. This same diffuseness of high angle lines was obtained when using quenched specimens in a new Norelco unit which measures 2θ values up to 150°. Consequently, only the lines present in Fig. 12b were available for study. In this connection it is of interest to note that this same diffuseness of lines in this system was reported by Jette and others in 1934.[5]

The available lines fit a face-centered cubic crystal with a lattice constant of 3.76 kx units; considering the metastable structure which exists, and yet to be discussed, the face-centered cubic crystal seems the most likely structure.

If the lattice constant of a face-centered cubic chromium is calculated, taking into consideration the correction in interatomic distance involved in the change in coordination number corresponding to a change from a body-centered cubic to a face-centered cubic, the result is a lattice dimension of 3.68 kx. Remembering that the face-centered cubic struc-

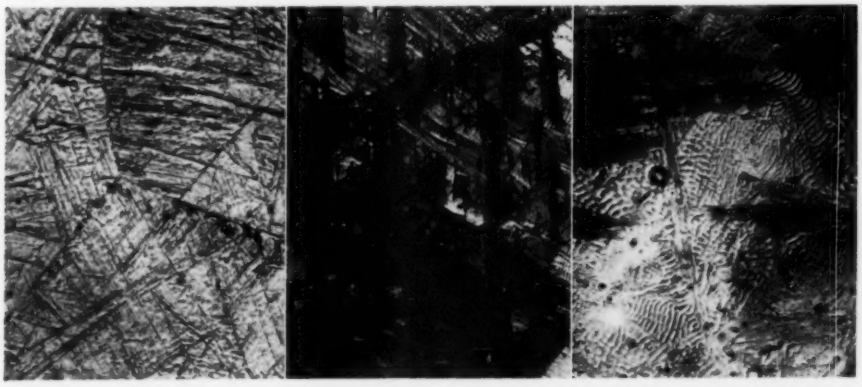

Fig. 20a—66 Cr-34 Ni alloy after quenching from 1250°C, metallographically polished, electrolytically etched. X500.

Fig. 20b—Same as Fig. 20a but with a deeper electrolytic etch. X500.

Fig. 20c—Same as Fig. 20a and b but with a still deeper electrolytic etch. X500.

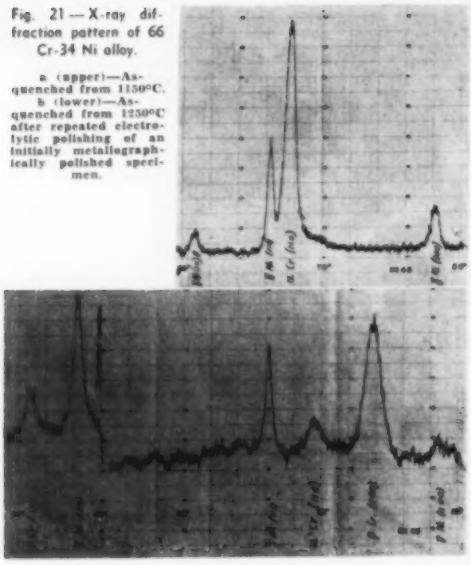

Fig. 21 — X-ray diffraction pattern of 66 Cr-34 Ni alloy.

a (upper)—As-quenched from 1150°C. b (lower)—As-quenched from 1250°C after repeated electrolytic polishing of an initially metallographically polished specimen.

ture depicted in Fig. 12b is saturated with nickel, the disparity in lattice dimensions is not too bad.

Delineation of the fields above the eutectoid temperature, while desirable, is extremely difficult because of the rapidity of quenching which is needed in order to retain the high temperature phase, particularly when in contact with the low temperature α-Cr phase.

Metastable Phase

In Fig. 19 is reproduced the diffraction pattern of a 66 Cr-34 Ni alloy as-quenched from 1250°C. In this pattern can be identified the lines due to low temperature α Cr, γ Ni, high temperature β Cr, and a transition phase α'. From this pattern the α' phase can be tentatively indentified as a body-centered tetragonal structure with an axial ratio of 1.09. However, from comparison with other patterns it has been determined that the axial ratio is not invariable. The presence of this body-centered tetragonal structure accounts for the previous report[3] of such a structure in this system, but the explanation offered of such a structure, that it is a compound Cr_2Ni, now appears to be incorrect.

It is interesting to note that in the similar system, Fe-C, the tetragonality of the transition structure (martensite) is considered to be due to the interstitially located carbon atoms; this effect cannot be presumed to be operative here.

The determination of phases is further complicated by the effect of polishing on the β phase and the metastable structure. Figs. 20a, b, and c are all of the 66 Cr-34 Ni composition quenched from 1250°C. This sample was first mechanically polished and lightly electrolytically etched as shown in Fig. 20a. The effect of a deeper electrolytic polish and etch of the same sample is shown in Fig. 20b. A yet deeper polish and etch resulted in Fig. 20c. It is obvious that mechanical polishing has transformed the alloy. The X-ray pattern of the alloy after repeated polishing is shown in Fig. 21b; the extra lines are due to the metastable phase which is probably a result of the mechanical work. Referring back to Fig. 20c, there is no explanation of the ripple appearing in the matrix of the specimen. Further evidence of the effect of mechanical working on the β phase is given in Fig. 12c, which shows the X-ray diffraction pattern of the same alloy and specimen as shown previously in Fig. 12b, except that the specimen has been polished lightly on 600-grit paper. A change in the location of the lines is evident.

Another facet of interest of the transition structure is its magnetism. If a eutectoid alloy is quenched from above the eutectoid temperature, and then powdered, portions of the powder will be rather strongly ferromagnetic. In Fig. 22 is presented the diffraction pattern of the magnetic portion of such a powder. The sample was separated by collecting the particles adhering to a small permanent magnet which had been inserted into the powder. While the pattern shows the chromium phase to predominate, there are indications of a partially formed nickel phase. The γ (200) line is actually comprised of two lines as confirmed by other patterns.

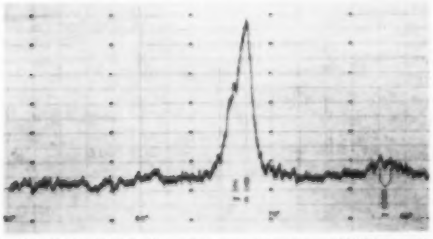

Fig. 22—65 Cr-35 Ni alloy after quenching from 1250°C, powdering, and being separated magnetically. This is magnetic portion.

Conclusions

The investigation of the Cr-Ni system has resulted in the following conclusions:

1—There is a transformation in chromium at about 1830°C tentatively identified as a change from a body-centered cubic to a face-centered cubic structure.

2—The addition of nickel lowers the transformation temperature, until at about 65 Cr-35 Ni a eutectoid temperature of about 1180°C results.

3—In alloys having approximately the eutectoid composition and quenched from above the eutectoid temperature, it is possible to produce a body-centered tetragonal metastable structure.

Acknowledgment

We are grateful to the Bureau of Aeronautics, Department of the Navy, whose sponsorship made this research possible. We are also indebted to Edward LaRocca for his assistance with the high temperature X-ray camera.

References

[1] C. H. M. Jenkins, E. H. Bucknall, C. R. Austin, B. A. Mellor: *Journal* Iron and Steel Inst. (1937) **136**, II, p. 187.

[2] M. Hansen: *Aufbau der Zweistofflegierungen.* (1936) Berlin.

[3] F. C. Blake and J. O. Lord: *Physical Review* (1930) **35**, p. 660.

[4] G. Grube and R. Knabe: *Ztsch. f. Elektrochemie* (1936) **42**, p. 793.

[5] E. R. Jette, V. H. Nordstrom, B. Queneau, and F. Foote: *Trans.* AIME (1934) **111**, p. 361.

Free Energy of Formation of Cementite And The Solubility of Cementite in Austenite

by L. S. Darken and R. W. Gurry

The solubility of cementite in austenite is computed by thermodynamic methods from the observed solubility of graphite. It is found that the solubility of cementite is greater than that of graphite in the entire austenite temperature range. Thus the prior discrepancy between this portion of the phase diagram and the observed metastability of cementite is partially resolved.

FOR several years it has been apparent that a serious discrepancy exists in certain observations pertaining to the Fe-C system. Direct experimental data indicate: 1—That the curve representing the solubility of graphite in austenite[1-4] crosses that for cementite[5] at about 945°C as shown in Fig. 1. 2—That graphite and austenite saturated therewith are stable[1] relative to cementite at all temperatures between the eutectoid, about 723°C, and the eutectic, about 1153°C.

These observations are mutually incompatible in view of a well-known consequence of the second law of thermodynamics, namely, that the stable phase (presumably graphite at all temperatures) has a lower solubility than the metastable phase (presumably cementite). Hence either 1 or 2 above must be in error; either the measured solubility of graphite or of cementite, or the observation as to the stability of graphite, is in error.

Our present purposes are: 1—To collate the available data on cementite and prepare a table of $H^\circ - H_o^\circ$ and of $(F^\circ - H_o^\circ)/T$. This tabular method

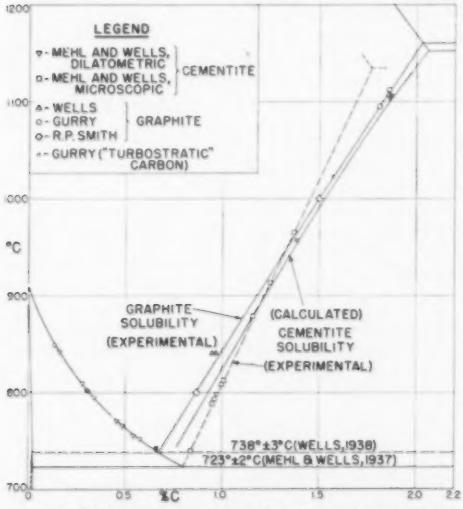

Fig. 1—Solubility of cementite and of graphite in austenite.

Table I. Enthalpy and Free Energy Functions for Cementite

°K	$H^\circ - H_o^\circ$ (Cal)	$\frac{F^\circ - H_o^\circ}{T}$ (Cal per Deg)
0	0	0
273.16	3699	
298.16	4329	10.405
300	4376	10.493
400	7023	15.128
500	9952	19.304
600	12746	23.069
700	15452	26.410
800	18248	29.408
900	21073	32.131
1000	23951	34.627
1100	26939	36.934
1200	30042	39.089
1300	33165	41.113
1400	36315	43.020
1500	39508	44.824
1600	42744	46.536
1700	45970	48.165
1800	49211	49.718
1900	52499	51.204
2000	55798	52.627

seems the best and most convenient way to represent the heat and free energy of formation. 2—To determine whether the measured solubilities of cementite and graphite in austenite are in accord with the above table and the measured thermodynamic properties of austenite, in order to resolve, if possible, the existing paradox of these two solubilities.

Enthalpy of Cementite

The enthalpy of cementite at 273°K, $H_{273}^{cem} - H_o^{cem}$, was computed by integration of the low temperature heat capacity as measured by Seltz, McDonald, and Wells[6] (68° to 298°K) and as given by the Debye functions recommended by them (0° to 68°K); the result is included in Table I. At higher temperature $H^{cem} - H_{298}^{cem}$ is given by Kelley[6] who used the data of Naeser[7] (298° to 1037°K) and of Umino[8,9] (273° to 1923°K).

We have recalculated $H^{cem} - H_{273}^{cem}$ from the data of Umino[8] in the following way. In the equilibrated alloy at temperature the weight fraction of cementite is $\frac{\text{Pct } C - \text{Pct } C^\gamma}{\text{Pct } C^{cem} - \text{Pct } C^\gamma}$, designated $f(C)$, and the

L. S. DARKEN, Member AIME, and R. W. GURRY, are associated with the Research Laboratory, U. S. Steel Co., Kearny, N. J.

Discussion on this paper, TP 3128E, may be sent, 2 copies, to AIME by April 1, 1952. Manuscript, May 18, 1951. New York Meeting, February 1952.

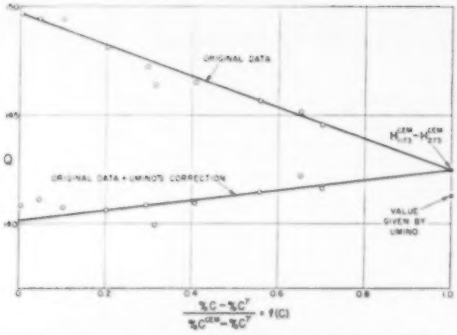

Fig. 2—Determination of the enthalpy of cementite from Umino's data on Fe-C alloys of 1.33 to 5.07 pct C equilibrated at 900°C.

weight fraction of austenite is one minus this quantity. The heat evolved on quenching 1 g of the alloy to 0°C, designated Q, is therefore:

$$Q = Q^{\text{cem}} f(C) + Q^{\gamma} [1 - f(C)]$$

where Q^{γ} is the heat liberated by 1 g of austenite on cooling (perhaps somewhat vague on account of the uncertainties of transformation) and Q^{cem} is $H^{\text{cem}} - H_{273}^{\text{cem}}$. If Q be plotted against $f(C)$ the intercept at $f(C) = 1$ is $H^{\text{cem}} - H_{273}^{\text{cem}}$ and the uncertainty as to Q^{γ} is eliminated by the extrapolation. A typical plot is shown in Fig. 2. It will be noted that the extrapolated value is substantially independent of whether or not the correction (for austenite decomposition) suggested by Umino is used.

The results differ somewhat from those reported by Umino. It is believed that the recalculated values represent more truly Umino's experimental determinations, and these have been plotted along with Naeser's and Umino's original determinations in Fig. 3. The final curve differs only slightly from Kelley's, except in the extrapolated portion which is of no interest for the purpose of this paper, but is included in order that the results may be used at higher temperature if desired. Combination of this with $H_{273}^{\text{cem}} - H_{0}^{\text{cem}}$ from the data of Seltz, McDonald, and Wells permits the evaluation of $H^{\text{cem}} - H_{0}^{\text{cem}}$ over the entire range as given in Table I.

Free Energy of Cementite

Browning, DeWitt, and Emmett[10] have published recently the results of their careful investigation of the equilibrium between cementite, α iron, and mixtures of methane and hydrogen in the temperature range 348° to 468°C. The results are in good agreement with the earlier investigation of Watase[11] (450° to 603°C) on the same equilibrium. The greatest deviation in Browning, DeWitt, and Emmett's experimentally determined equilibrium constant from a smooth curve is about 10 pct, corresponding to a precision of about 150 cal in the free energy of formation. The short temperature range gives rise to a corresponding uncertainty of perhaps 400 cal in their determination of the heat of formation of cementite.

Combination of these recent results of Browning, DeWitt, and Emmett with other information affords an opportunity for an improved evaluation of the free energy of cementite and a precise determination of the relative stability of graphite and cementite. The solubility of graphite and cementite in austenite is generally believed to be known with considerable precision in the vicinity of the eutectoid; however, preliminary calculations indicated that these data are somewhat inconsistent with the other data to be considered and hence no great weight was placed upon them here. The temperature difference (about 7°C) between the graphite eutectic and the cementite eutectic of the Fe-C system permits (in conjunction with thermodynamic data on austenite) an evaluation of the free energy of formation of cementite in the vicinity of 1153°C. The heat of formation and the entropy of formation as evaluated from the low temperature heat capacity are also pertinent. These various data are collated in the following way.

Table II. Measured Eutectic Temperatures

	Cementite Eutectic Temperature, °C	Graphite Eutectic Temperature, °C	Difference, °C
Ruer and Goerens[16]	1146	1153	7
Kasé[17]	1151-1153*	1155	2 - 4
Kasé†	(1130)	(1137)	7

* Rising on repetition. † White and gray irons, data obtained from cooling curves.

The function $\frac{F^{\text{cem}} - H_{0}^{\text{cem}}}{T}$ may be obtained as $\int_{0}^{T} (H^{\text{cem}} - H_{0}^{\text{cem}})\, d(1/T)$ or more conveniently as $-\int_{0}^{T} \frac{H^{\text{cem}} - H_{0}^{\text{cem}}}{T^2}\, dT$. The plot for the graphical integration is shown in part in Fig. 4. Considerable uncertainty is involved in the low temperature portion of the integration; experimental error is greatly magnified here due to the form of the curve which, as usual, contributes a rather large area in this region. In order to eliminate this source of error at higher temperature, this error, which is a constant for temperatures above 25°C, has been represented by δ and an asterisk has been used to denote that the integral is in error by the value of δ. Thus,

$$\frac{F^{\text{cem}} - H_{0}^{\text{cem}}}{T} = \delta - \left[\int_{0}^{T} \frac{H^{\text{cem}} - H_{0}^{\text{cem}}}{T^2}\, dT\right]^{*} \quad [1]$$

The free energy of formation of cementite, ΔF, may be obtained by combining the above function with similar functions for iron[12] and for graphite:[13]

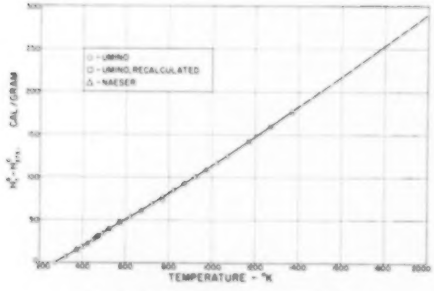

Fig. 3—Enthalpy function for cementite.

$$\frac{F^{cem} - H_o^{cem}}{T} - 3\,\frac{F^{Fe} - H_o^{\alpha\text{-}Fe}}{T} - \frac{F^{gr} - H_o^{gr}}{T} = \frac{\Delta F - \Delta H_o^\circ}{T} \quad [2]$$

Combining eqs 1 and 2:

$$\left[\int_o^T \frac{H^{cem} - H_o^{cem}}{T^2}\,dT\right]^* - 3\,\frac{F^{Fe} - H_o^{\alpha\text{-}Fe}}{T} - \frac{F^{gr} - H_o^{gr}}{T} - \frac{\Delta F}{T} = -\frac{\Delta H_o^\circ}{T} - \delta \quad [3]$$

or, multiplying by T and changing signs:

$$T\left[\int_o^T \frac{H^{cem} - H_o^{cem}}{T^2}\,dT\right]^* + 3\,T\left(\frac{F^{Fe} - H_o^{\alpha\text{-}Fe}}{T}\right) + T\left(\frac{F^{gr} - H_o^{gr}}{T}\right) + \Delta F = \Delta H_o^\circ + T\delta \quad [4]$$

Each of the first three terms on the left of eq 4 is now known as a function of temperature and a knowledge of ΔF at two or more temperatures permits the evaluation of ΔH_o° and of δ. By plotting the left side of eq 4 against T a straight line should be obtained whose intercept and slope are ΔH_o° and δ, respectively. The plot is shown in Fig. 5. The points represent: 1—the data of Browning, DeWitt, and Emmett near the extremes of their temperature range; 2—the data of Watase near the extremes of his temperature range; 3—values obtained from the graphite and cementite solubility lines of Fig. 1* over approximately the range covered by the investigation of Mehl and Wells;[4] 4—a value computed from the observation that the iron-cementite eutectic is 7°C lower than the iron-graphite eutectic;* and 5—crude values at room temperatures from the ΔH_{298} of Naeser[14] and ΔS_{298} from the measurements of Seltz, McDonald, and Wells, and Naeser.

In constructing the line of Fig. 5, it is seen that great reliance cannot be placed on the values from the vicinity of the eutectoid of the Fe-C system, as the corresponding points lie on a curve with slope appreciably different from that drawn; nevertheless the mean value fits well. The most weight has been given: 1—the new measurements of Browning, DeWitt, and Emmett; and 2—the value from the eutectic of the Fe-C system.

Choice 2 requires some justification since the selected line of Fig. 5 implies an error of about 0.08 pct C in the graphite or cementite eutectoid (or distributed between these two points) of the generally accepted temperature-composition diagram, Fig. 1. The previously available data on the temperatures of the two eutectics were discussed by Epstein.[15] Only two determinations are reported in which the two eutectic temperatures were measured on the same specimen. Table II gives the results. An investigation soon to be reported by Darken and Filer of this laboratory indicates a difference of about 6° (1153° and 1147°C). Hence it is considered justifiable to conclude that this temperature difference is undoubtedly 7° ± 2°. As will appear later, a difference of 5° near 1130°C is equivalent to this selected value in so far as Table I is concerned. As a 2° error here corresponds to only 100 cal, in the ordinate of Fig. 5, this figure of 7° difference in the eutectics seems one of the most firm foundations on which to base the calculations. For this reason the line of Fig. 5 is drawn through the corresponding point (on the extreme right).

From the large scale plot from which Fig. 5 was prepared ΔH_o° is found to be 5114 cal and $\delta = 0.952$. This value of δ is added to each of the integrals

Table III. A Comparison of Thermodynamic Functions for the Formation of Cementite from α Iron and Graphite (Cal)

	ΔH_{298}	ΔS_{298}	ΔF_{298}	ΔF_{1000}	ΔF_{1500}	S_{298}^{cem}
This computation	5981	4.10	4760	2916	1477	24.92
Kelley's computation	5500	2.99	4610			23.8
Browning, DeWitt, and Emmett	5453	3.39	4441	2850	1680	
Watase	5756	3.67	4661	2930	1720	
Seltz, McDonald, and Wells						25.7±1
Naeser	5600	(3.08)	(4684)			23.9[16]
Roth[18]	5400±1600					
Andes[20]						23.55

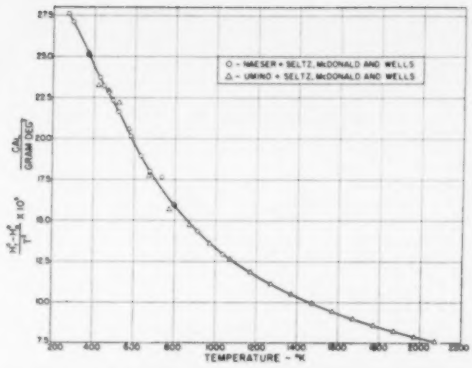

Fig. 4—Plot for evaluating the free energy function for cementite.

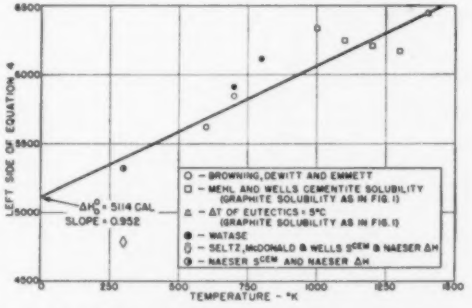
O – BROWNING, DEWITT AND EMMETT
□ – MEHL AND WELLS CEMENTITE SOLUBILITY (GRAPHITE SOLUBILITY AS IN FIG. 1)
Δ – ΔT OF EUTECTICS = 5°C (GRAPHITE SOLUBILITY AS IN FIG. 1)
● – WATASE
◊ – SELTZ, McDONALD & WELLS S^CEM & NAESER ΔH
◑ – NAESER S^CEM AND NAESER ΔH
SLOPE = 0.952
TEMPERATURE – °K

Fig. 5—Plot of a thermodynamic function pertaining to the formation of cementite, for the purpose of evaluating the error in the free energy function for cementite due to inaccuracy in the heat capacity measurements at low temperature.

* This computation involves the use of the activity of carbon and of iron in austenite. These are taken from the work of Smith.[3] The equations employed are:

$$\ln a_c = \ln \frac{N_c}{N_{Fe}} + 6.6\,\frac{N_c}{N_{Fe}}$$

$$\ln a_{Fe} = -\frac{N_c}{N_{Fe}} - 3.3\left(\frac{N_c}{N_{Fe}}\right)^2$$

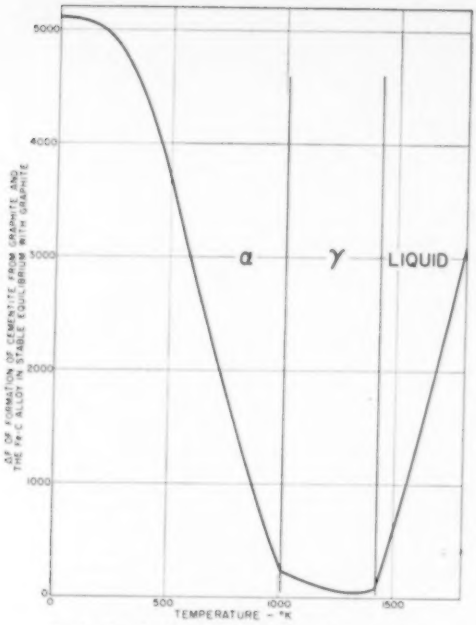

Fig. 6—Plot showing the metastability of cementite.

according to eq 1 to give $\frac{F^{\circ\circ\circ} - H_o^{\circ\circ\circ}}{T}$ which is tabulated in Table I. Of course the error δ also implies an error in $H^{\circ\circ\circ} - H_o^{\circ\circ\circ}$. This, however, is small and no correction is made to the enthalpy table.

A comparison of various thermodynamic functions for the formation of cementite as computed from the tabular values of the free energy function (and $\Delta H_o^\circ = 5114$) with those from other sources is shown in Table III. The agreement of the present computation with experiment is seen to be satisfactory in substantially all respects—a conclusion previously inferred from Fig. 5.

Solubility of Cementite in Austenite

From the free energy function for cementite, Table I, for γ iron[17] and for graphite[18] the activity product $a_c a_{Fe}{}^3$ for equilibrium with cementite was calculated over the range of temperature from the Fe-C eutectoid to the eutectic. Combination of this with the graphite solubility of Fig. 1 and the carbon (and iron) activity data of Smith[3] leads, by successive approximations, to the activity, a_c, of carbon (relative to graphite) in austenite saturated with cementite, and thus to the cementite solubility. Values of these quantities are given in Table IV. The cementite solubility thus calculated, which represents our best estimate, is shown graphically in Fig. 1. Since the activity of carbon for the austenite-cementite equilibrium always exceeds unity (the minimum value is in the vicinity of 1340°K) it is apparent that cementite is metastable over this whole range. In Fig. 6 is plotted against temperature the free energy of formation of cementite from graphite and the Fe-C alloy in stable equilibrium with graphite. Cementite is seen to be metastable in the α and liquid regions as well as the γ.

Table IV. Thermodynamic Functions Leading to the Solubility of Cementite in Austenite

		ΔF of Formation of Fe_3C (Cal)†		Observed Solubility of Graphite in Austenite, Pct C	a_c in γ Fe in Equil. Cementite‡	Calculated Solubility of Cementite in Austenite, Pct C
°K	°C	From Pure γ Fe*	From γ Fe Sat'd with Graphite†			
1000	727	+ 45	244	0.64	1.14$_6$	0.72
1100	827	—183	154	0.95	1.08$_5$	1.01
1200	927	—423	88	1.27	1.04$_6$	1.30
1300	1027	—672	54	1.59	1.02$_7$	1.61
1400	1127	—926	66	1.92	1.03$_2$	1.96

* 3 Fe (pure γ) + C (graphite) = Fe_3C (cementite).
† 3 Fe (γ, saturated with graphite) + C (graphite) = Fe_3C (cementite).
‡ Standard state of carbon is taken as graphite.

Summary and Conclusion

The free energy function and the enthalpy function of cementite have been computed and tabulated from data which are believed to be reliable. The table is based on enthalpy (heat content) determinations, and equilibrium determinations. Other available data are shown to agree (within the experimental error) with the tables and the value 5114 cal for $\Delta H_o^{\circ\circ\circ}$ (the heat of formation of cementite at 0°K). It is concluded that cementite is metastable with respect to graphite and α iron from 0°K to the eutectoid and also with respect to graphite and γ iron saturated with graphite from the eutectoid to the eutectic. The solubility of cementite in austenite computed from the experimentally determined solubility of graphite in γ iron is greater than the latter over the whole temperature range. The computed values differ from the generally accepted direct experimental determinations at both limits of the temperature range covered but are in agreement with them near the center of this range.

References

[1] C. Wells: *Trans.* A.S.M. (1938) **26**, p. 289.
[2] R. W. Gurry: *Trans.* AIME (1942) **150**, p. 147.
[3] R. P. Smith: *Journal* Amer. Chem. Soc. (1946) **68**, p. 1163.
[4] R. F. Mehl and C. Wells: *Trans.* AIME (1937) **125**, p. 429.
[5] H. Seltz, H. J. McDonald, and C. Wells: *Trans.* AIME (1940) **140**, p. 263.
[6] K. K. Kelley: U. S. Bur. Mines *Bull.* 476 (1949).
[7] G. Naeser: *Mitt.* Kaiser-Wilhelm Inst. Eisenforschg. (1934) **16**, p. 207.
[8] S. Umino: *Sci. Repts.* Tohoku Imp. Univ. (1926) Series 1, **15**, p. 331.
[9] S. Umino: *Sci. Repts.* Tohoku Imp. Univ. (1935) Series 1, **23**, p. 665.
[10] L. C. Browning, T. W. DeWitt, and P. H. Emmett: *Journal* Amer. Chem. Soc. (1950) **72**, p. 4211.
[11] T. Watase: *Journal* Chem. Soc. Japan (1933) **54**, p. 110.
[12] L. S. Darken and R. P. Smith: *Industrial and Engineering Chemistry* (1951) **43**, p. 1815.
[13] F. D. Rossini et al.: Nat. Bureau of Standards *Circular* 461 (1947).
[14] G. Naeser: *Mitt.* Kaiser-Wilhelm Inst. Eisenforschg. (1934) **16**, p. 1.
[15] S. Epstein: *The Alloys of Iron and Carbon.* Vol. I (1936) New York. McGraw-Hill Book Co.
[16] R. Ruer and F. Goerens: *Ferrum* (1917) **14**, p. 161.
[17] T. Kasé: *Sci. Repts.* Tohoku Imp. Univ. (1930) Series 1, **19**, p. 17.
[18] C. Schwarz and H. Ulich: *Archiv. Eisenhüttenwesen* (1936) **10**, p. 11.
[19] W. A. Roth: *Ztsch. angew. Chem.* (1929) **42**, p. 981.
[20] R. V. Andes: *Journal of Science.* Iowa State College (1936) **11**, p. 26.

Habit Phenomenon in the Martensitic Transformation

by E. S. Machlin and Morris Cohen

GRENINGER and Troiano[1] were the first to establish the fact that the habit planes of martensitic products are usually planes of high indices. In steels containing 0.55 to 1.4 pct C, the habit plane indices are $\{225\}_A$.* In steels with more than 1.5 pct C and in Fe-Ni alloys, the indices are $\{259\}_A$. The presence of both habits in certain alloy steels has been reported recently.[2]

Several investigators[3-6] have subsequently attempted to provide an understanding of these complex habit relations. Bowles'[3] work is the most recent and the most successful. Like Greninger and Troiano,[1] Bowles concluded that the transformation occurs in two steps, the first, a strain (or displacement) that is homogeneous throughout the volume of the martensitic plate, while the second is a strain that is homogeneous only within relatively small portions of the martensitic plate. The first strain yields the measured tilt of the specimen surface, but does not produce the final martensitic structure. This and the correct lattice orientations are achieved by the second strain. Bowles also reasoned that each strain could be described by the motion of a plane of no rotation and no distortion (hereinafter called the invariant plane) in a direction not necessarily contained in the plane.** In applying these considerations to steels with $\{225\}_A$ habits, Bowles found that the habit plane coincided with the invariant plane of the first strain, a result which signified that the atoms move along certain paths during the transformation. Whether this correlation results from the existence of some sort of a plate nucleus[5] lying along the invariant plane of the first strain, or whether the invariant plane primarily defines the preferred directions of propagation of the first strain, will be discussed in a later section.

There are two obstacles to the general acceptance of Bowles' treatment: 1—it has not been shown that elements of his double-strain analysis are unique, and 2—it is not known whether his treatment applies to transformations yielding the $\{259\}_A$ habit. Unless these two questions are resolved, the correlation between the habit and invariant planes in the $\{225\}_A$ systems might be regarded as coincidental.

Experimental Procedure

Using a 70 pct Fe-30 pct Ni alloy as an example of a $\{259\}_A$ habit system, preliminary attempts were made to obtain a double-strain solution based on a Nishiyama*** set of orientation relations and on a Greninger-Troiano† set, adopting the stereographic technique described by Bowles[3] who used the Kurdjumow-Sachs†† set in connection with the $\{225\}_A$ habit. These attempts were unsuccessful because the method is essentially one of trial and error and requires either exceedingly good luck or a prior knowledge of the results being sought.

Consequently it was decided to measure independently the strain associated with the formation of a martensitic plate as well as the habit-plane indices of the particular plate. By means of matrix algebra, the measured strain was applied to the austenite lattice, whose orientation with respect to the strain was determined, in order to ascertain whether the resultant structure would have the lattice of martensite. This was not found to be the case, and hence it was assumed that the measured strain was the first of two Bowles-type strains, characterized by the motion of an invariant plane. A solution of this displacement was obtained in terms of the invariant-plane indices and the direction of motion of the atoms. Then the second strain

E. S. MACHLIN, Member AIME, formerly with the Dept. of Metallurgy, Massachusetts Institute of Technology, is now associated with the Dept. of Metallurgy, Columbia University, New York; and M. COHEN, Member AIME, is associated with the Dept. of Metallurgy, Massachusetts Institute of Technology, Cambridge, Mass.

Discussion on this paper, TP 3157E, may be sent, 2 copies, to AIME by April 1, 1952. Manuscript, April 24, 1951; revision, Aug. 27, 1951. New York Meeting, February 1952.

This paper is based on a thesis submitted by E. S. Machlin in partial fulfillment of the requirements for the degree of Doctor of Science in Metallurgy to the Massachusetts Institute of Technology, September 1950. The investigation was sponsored by the Office of Naval Research under Contract N5-ori-07814, Task No. XIV, Designation No. NR-031-142.

* The subscript *A* stands for austenite axes, and *M* (to be used later) stands for martensite axes.

** An equivalent description of the Bowles strain is that every point moves, in a fixed direction, by an amount proportional to its original distance from a fixed plane.

*** $(111)_A \parallel (101)_M$; $[1\bar{2}1]_A \parallel [10\bar{1}]_M$.

† $(111)_A$ almost $\parallel (101)_M$; $[1\bar{1}0]_A$ 2½° counterclockwise from $[11\bar{1}]_M$ (looking in the direction of $[111]_A$). This relationship was accurately measured by Greninger and Troiano using a single crystal of martensite of $(259)_A$ habit contained in a single crystal of austenite, and is considered to be more accurate than the Nishiyama orientation relations for the purposes at hand.

†† $(111)_A \parallel (101)_M$; $[1\bar{1}0] \parallel [11\bar{1}]_M$.

Table I. Experimental Values of the Tangents of the Projected Angles Between the Transformed Positions of the Fiducial Markings or Axes and Their Original Positions in the Austenitic State

Strain Matrix*	t_{xy}**	t_{yz}	t_{zx}	t_{yx}	t_{xz}	t_{zy}	Habit of Plate***
T_a'	+0.01±0.01	+0.10±0.02	−0.03±0.02	−0.24 ±0.05	0±0.01	0±0.01	a — $(592)_A$
T_c'		+0.035	+0.15±0.05	+0.08 ±0.02	0±0.01	0±0.01	c — $(295)_A$
T_e'			−0.13±0.05	+0.085±0.05	0±0.01	0±0.01	e — $(259)_A$
T_b''	+0.10±0.02	−0.01±0.01	−0.16±0.02	−0.145 +0.05	0±0.01	0±0.01	b — $(529)_A$
T_d''			+0.17±0.04	−0.095±0.02	0±0.01	0±0.01	d — $(925)_A$
T_f''			0±0.01	+0.21 ±0.02	0±0.01	0±0.01	f — $(952)_A$

* The matrices belong to two sets distinguished by the primes. Each matrix in a set can be obtained from another in the set by a 120° rotation about $[111]_A$. A matrix in one set has a mirror symmetry with one other matrix in the other set across a $(110)_A$ plane. All matrices are crystallographically equivalent.

** The ± values in the table represent the scatter of successive readings on a given plate. Readings for all the plates fell within this uncertainty.

*** See Fig. 2 for the orientations of these plates relative to the parent austenite.

was calculated based on the Greninger-Troiano orientation relations. Finally the elements of both strains were checked using the Bowles stereographic manipulation.

Single crystals of a 70 pct Fe-30 pct Ni alloy[7] were grown from the melt in a molybdenum-wound vacuum furnace using a modified Bridgman technique. Specimens were prepared with three orthogonal faces parallel to $(111)_A$, $(1\bar{1}0)_A$ and $(\bar{1}\bar{1}2)_A$ respectively. Polishing scratches aligned parallel to the three orthogonal axes served as fiducial markings. The crystals were then partially transformed to martensite by cooling to about −40°C. Many plates were formed in a burst.[7]

The specimen was then set into a jig which made it possible to observe microscopically the same martensitic plate on two orthogonal faces. Thus, the habit of the plate as well as the new directions of the fiducial lines within the plate could be measured. Fig. 1 illustrates the parameters that were recorded, and Table I presents a compilation of the results.

In the interpretation of these data the correspondence between subscripts and axes is as follows:

X	$[\bar{1}\bar{1}2]_A$
Y	$[1\bar{1}0]_A$
Z	$[111]_A$

For example, t_{zx} is the tangent of the angular displacement of a scratch parallel to the Z or $[111]_A$ direction in the X or $[\bar{1}\bar{1}2]_A$ direction. The tangent is positive if the positive side of the $[111]_A$ axis moves in the $[\bar{1}\bar{1}2]_A$ direction. It is evident from Fig. 1 that the measurements for t_{xy} and t_{yz} are made on the Z or $(111)_A$ face, for t_{yx} and t_{zy} on the X or $(\bar{1}\bar{1}2)_A$ face, etc. The group of six tangents for a given plate comprise the nondiagonal components of a matrix:

$$T = \begin{pmatrix} t_{xx} & t_{xy} & t_{xz} \\ t_{yx} & t_{yy} & t_{yz} \\ t_{zx} & t_{zy} & t_{zz} \end{pmatrix} \qquad [1]$$

This matrix will be called a T matrix inasmuch as it is composed mainly of tangents of angles. The diagonal components t_{xx}, t_{yy}, and t_{zz} are not tangents; however they are not necessary for this analysis and no attempt was made to measure them. It will be shown later that the T matrix is related to the coordinate-transformation matrix. (Ref. 4 contains a good résumé of the elementary steps of matrix algebra as applied to the present problem.)

Of some 40 observed plates, it was found that to each permutation of the habit-plane indices there corresponded one and only one T matrix, and vice versa. The habit planes corresponding to each of the six matrices given in Table I are shown in Fig. 2 relative to the coordinates used in this study.

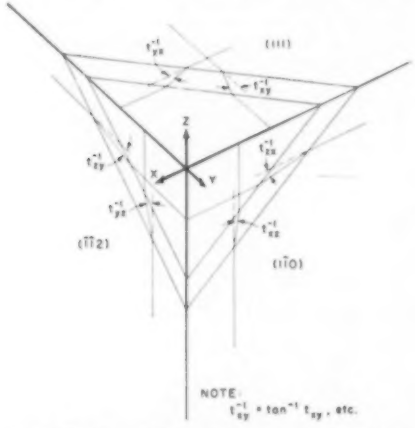

Fig. 1—Showing scribed lines the directions of which change upon traversing a martensite plate.

Meaning of t_{xy}, etc. illustrated with reference to three orthogonal axes.

Analysis of Results

It is first necessary to establish the relationships between the experimental quantities contained in the T matrix and the components of a coordinate-transformation matrix, A. The A matrix simply relates the initial and final positions of points in the transformed region. Thus, if the initial coordinates of a point are x, y, z, its final coordinates are given by:

$$\begin{pmatrix} x' \\ y' \\ z' \end{pmatrix} = \begin{pmatrix} a_{xx} & a_{xy} & a_{xz} \\ a_{yx} & a_{yy} & a_{yz} \\ a_{zx} & a_{zy} & a_{zz} \end{pmatrix} \begin{pmatrix} x \\ y \\ z \end{pmatrix} \qquad [2]$$

or

$$\begin{pmatrix} x' \\ y' \\ z' \end{pmatrix} = A \begin{pmatrix} x \\ y \\ z \end{pmatrix} \qquad [3]$$

The equations relating the T matrix to the required A matrix are derived in Appendix I.

If it is assumed that the transformation can be described by one homogeneous strain, then application of the measured strain to the austenite lattice should generate a body-centered cubic lattice (Fe-Ni martensite). This calculation is performed in Appendix II and the conclusion is reached there that the measured strain does not yield a body-centered cubic lattice. Hence, the single-strain concept of

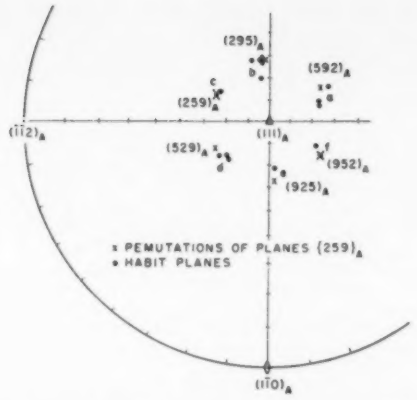

Fig. 2—Habit planes on $(111)_A$ projection, corresponding to the six variations in Table I.

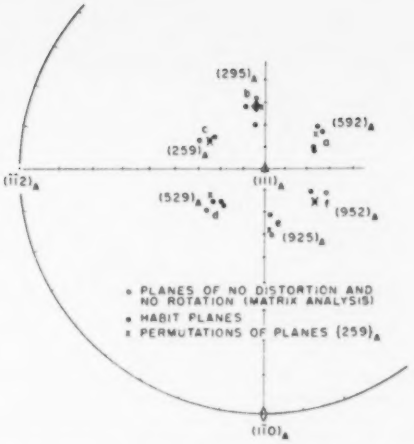

Fig. 3—$(111)_A$ projection of planes of no distortion and no rotation and corresponding habit planes.

Jaswon and Wheeler[4] does not apply to the transformation in this alloy.

The next step in the analysis was to determine whether the Bowles double-strain method is consistent with the data. The procedure was as follows:

1—Assume that an invariant plane of general orientation with respect to the axes used in this investigation (two parameters suffice to describe the position of the pole of the invariant plane with respect to the reference axes) moves in some direction lying in the $(111)_A$ plane.†††

2—Set up a general coordinate-transformation matrix relative to the reference axes on the basis of such motion of the invariant plane. This matrix will then contain as unknowns the two parameters that specify the position of the invariant plane relative to the reference axes, a third parameter that specifies the direction of motion of the invariant plane,†††† and a fourth parameter that specifies the magnitude of the motion. Six equations are obtained by equating‡ the nondiagonal components of the A matrix (as calculated from the measured T matrix) to the corresponding components of the general coordinate-transformation matrix. Two of these equations have already been used because of the fact that the direction of motion of the invariant plane lies in the $(111)_A$ plane. There are four equations left and hence it is possible to calculate the parameters defining the position of the invariant plane and direction of motion of the atoms.

These calculations have been performed in Appendix III. It is found that one and only one invariant plane is associated with a given T matrix, and that this unique invariant plane is closely parallel to the independently measured habit plane associated with the given T matrix.‡‡ The excellent correlation between such experimental habit planes and their respective calculated invariant planes is shown in Fig. 3. The directions of atom motions for the T matrices are given stereographically in Fig. 4. Roughly these directions have the indices $<156>_A$. In each permutation, the direction of motion does not lie in the invariant plane, and hence the first strain is not a simple shear.

Using the matrix method, the elements‡‡‡ of the second strain can be calculated from a knowledge of the first strain and the final orientation of the martensite relative to the austenite. It is assumed that the atoms move to the nearest set of proper positions in the oriented martensite lattice after the first strain.[4] This calculation is performed in Appendix IV. The results are shown in Fig. 5 for the case where the $(259)_A$ permutation is the invariant plane of the first strain. The invariant plane of the second strain is close to $(235)_M$ and the corresponding direction of motion is $[11\bar{1}]_M$. This direction lies in the second invariant plane, and hence the second strain is truly a shear. The elements of the first and second strains are summarized in Table II.

If the above analysis is consistent with the Bowles double-strain analysis, then the assumption of a pair of elements for either one of the strains should yield the pair of elements for the other strain using Bowles' stereographic treatments.§ Figs. 6 and 7 show that, starting with either pair of elements given in Table II, the other pair of elements can be obtained

Table II. Elements of Strains for Martensitic Transformations having $(259)_A$ Habit

	First Strain	Second Strain
Invariant plane	$(259)_A$ within 2°	$(235)_M$
Direction of atom motion	$[\bar{1}56]_A$ within 2°	$[11\bar{1}]_M$

††† The direction of motion must lie in the $(111)_A$ plane because it is found experimentally (Appendix II) that the $(111)_A$ plane does not rotate. Hence only a single additional parameter is necessary to specify the direction of motion.

†††† This is also the direction of motion of all the atoms.

‡ This step implicitly assumes the measured strain is a homogeneous strain.

‡‡ The fact that one and only one invariant plane is found to be associated with a given T matrix can be derived independently from the consideration that the measured T matrix really does correspond to a homogeneous strain.

‡‡‡ Indices of an invariant plane and direction of motion of atoms.

§ Knowing the positions that poles of planes and directions in the austenite take after straining to martensite (this knowledge is based on the minimum displacement hypothesis of Jaswon and Wheeler[4] as well as the final orientation relationships), then it is possible to check the following requirements of the Bowles analysis: 1—initial and final positions of poles of planes that contain the direction of motion of atoms during one strain must lie on the same great circle as the pole of the invariant plane of the other strain, and 2—initial and final positions of directions lying in one of the invariant planes must lie on the same great circle as the direction of the motion of atoms during the other strain.

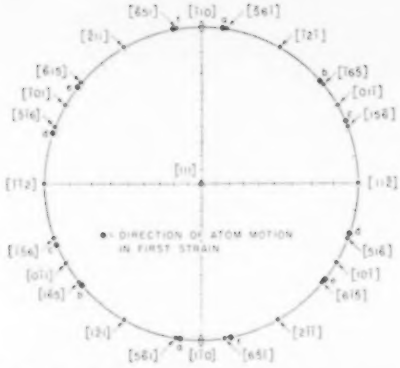

Fig. 4—Direction of atom motion associated with first strain for the six permutations of habit plane indices observed. All directions relate to austenite.

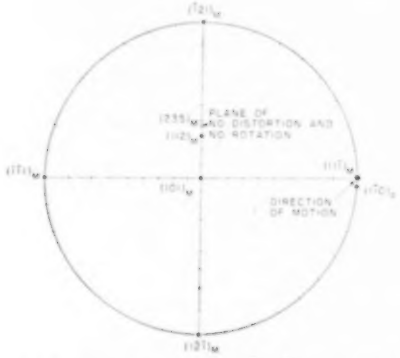

Fig. 5—Stereographic solution showing elements of second strain corresponding to $(259)_A$ habit plane.

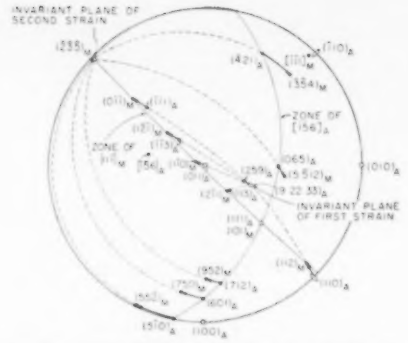

Fig. 6—Stereographic analysis of plane transformations. Initial and final positions of poles of planes that contain the direction of atom motion during one strain lie on the same great circle as the pole of the invariant plane of the other strain.

Fig. 7—Stereographic analysis of direction transformations. Initial and final positions of directions lying in one of the invariant planes lie on the same great circle as the direction of atom motion during the other strain.

from Bowles' stereographic method. It is interesting to note that the first invariant plane in Fig. 6 lies somewhat closer to $(9\ 22\ 33)_A$ than to $(259)_A$. In evaluating these findings, it should be remembered that the probability of securing such consistent results from random choices of pairs of elements is virtually nil. From the correlation between the matrix analysis of the measured strain and the Bowles analysis, it may be concluded that the measured strain is actually homogeneous, otherwise the Bowles analysis would not yield the correct elements of the measured strain.

The matrix analysis also makes it possible to determine the succession of strains in the Bowles analysis. The sequence test performed in Appendix V demonstrates that the two strains must occur in the order already given in Table II. It is shown in Appendix V that the two strains are not commutative: if C is the final strain achieved by application of A followed by B, then application of B followed by A does not result in C. Thus, the correct orientation relation cannot be attained except by the proper sequence of the invariant-plane strains in Table II.

All the results described here hold, in principle, for the $\{225\}_A$ as well as for the $\{259\}_A$ systems.

Discussion of Results

Implications of the Bowles Analysis: The question may now be raised as to the uniqueness of the solutions obtained using the Bowles double-strain analysis: that is, does a knowledge only of the orientation relationship between the austenite and martensite lattices and their structures permit a unique prediction of the elements of the two invariant-plane strains? Consideration of this problem leads to the conclusion that the Bowles double-strain analysis, of itself, does not yield a unique pair of invariant-plane strains.§§ Some additional condition is required to make the solution unique. This condition is, according to the reaction-path concept of the martensitic transformation, that the first strain involving the minimum activation energy, whether it can be predicted a priori or not, is the one that actually operates. Then, the Bowles analysis, on the basis of the final orientation relations, will predict

§§ This fact can be checked as follows: choose one invariant plane such that its pole lies on the great circle connecting either $(9\ 22\ 33)_A$ and $(235)_M$ for the $\{259\}$ case or $(225)_A$ and $(112)_M$ for the $\{225\}$ case. Choose one direction such that it lies on the great circle connecting $[156]_A$ and $[111]_M$ for the $\{259\}$ case or $[112]_A$ and $[111]_M$ for the $\{225\}$ case. This choice of a pair of elements will then determine the other pair of elements having internal consistency with the Bowles analysis, yet will not be the solution experimentally obtained.

a unique set of elements for the second invariant-plane strain. Theoretically, if the potential energy curve as a function of the strain for each possible first strain was known, then a unique pair of invariant-plane strains, and thus their elements, could be predicted.

From the observation that the atom motion in the second strain takes place along the only direction that remains close-packed in the unrotated, but distorted $(111)_A$ plane after the first strain, for both the $\{225\}_A$ case and $\{259\}_A$ case, tentative criteria for predicting the unique invariant plane of the first strain (and hence the habit plane) can be set up using the Bowles stereographic analysis and the final orientation relationship between the austenitic and martensitic structures. Of the two close-packed directions in the $(101)_M$ plane, the direction of motion in the second strain is selected as the one which makes the smaller angle with its original§§§ close-packed $<110>_A$ direction in the $(111)_A$ plane. Thus, poles of planes in the zone of this direction must lie on the same great circle as the pole of the invariant plane of the first strain. By choosing this direction as the second direction of atom motion in the Bowles analysis, a unique prediction for the habit plane is obtained. This procedure might be termed a modified Bowles method.

The foregoing criterion for the habit-plane prediction suggests that different orientation relations will predict different habit-plane indices. In particular, the Kurdjumow-Sachs orientation predicts the $\{225\}_A$ set of habit plane indices, the Greninger-Troiano orientation predicts the $\{259\}_A$ set, and the Nishiyama orientation predicts a $\{5\ 34\ 46\}_A$ set. It should be emphasized that the above criterion for prediction of the habit plane does not mean that the habit plane is controlled physically by the final orientation relationship, rather the reverse is implied: that is, the first strain corresponding to the minimum activation energy path will, according to the criterion, uniquely determine the final orientation relationship as well as the habit plane.

Significance of Correlation between the Habit Plane and the Invariant Plane of the First Strain: It has now been demonstrated that the double-strain mechanism of martensite formation in ferrous alloys can lead to a plane of no distortion and no rotation in the first strain lying close to the $\{259\}_A$ habit when the Greninger-Troiano orientation prevails, and lying close to the $\{225\}_A$ habit when the Kurdjumow-Sachs orientation prevails. These findings strongly suggest that the double-strain mechanism is real, and that the correlation of the habit plane with the first invariant plane is most significant.

There are two possible explanations for this correlation. The first explanation, as indicated by Bowles,[5] assumes the existence of a two-dimensional nucleus lying along the habit plane, having roughly the final radial dimensions of the plate to form. In this picture, the plate grows in thickness in such a way as to maintain the plane of the habit as an invariant plane of the first strain.

The second explanation is based on the very reasonable assumption that the martensitic embryo is quite small compared to the final martensitic plate. Thus, it is necessary to account for the preferential propagation of the transformation along the invariant plane of the first strain. This result follows directly from a consideration of the strain energy developed in the austenite by a platelike region with different orientations of the plate relative to the invariant plane, as illustrated in Fig. 8. The plate has length and width dimensions w, thickness h, and $\frac{w}{h}$ is taken equal to 10. From the assumption that the stress developed at any point is proportional to the displacement of that point, and that the displacement is determined by the first strain only, the strain energy developed in the austenite for the plate lying parallel to the invariant plane turns out to be only 1/50 that for the plate lying normal to the invariant plane. Therefore, it can be concluded that as the first strain spreads out radially from the small embryo, the largest resistance is first encountered in the thickness direction. This resistance to the propagation of strain soon reaches a sufficient magnitude to limit further growth in thickness, probably by the onset of plastic flow.[7] The propagation of the strain along the invariant plane is relatively unhindered, and hence the plate spreads outward from the embryo mainly along the invariant plane of the first strain. The habit plane, as a result, lies parallel to the invariant plane of the first strain.

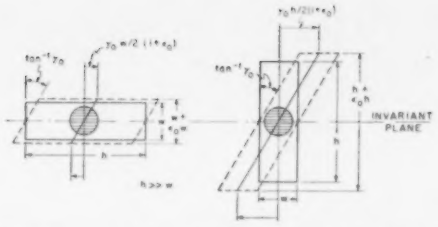

Fig. 8—Illustration of the effect of plate orientation, with respect to the invariant plane of the first strain, on strain energy.

γ_0 is the unit shear strain and w_0 is the unit normal strain relative to the invariant plane. Note that if $h>>w$, the displacements in the austenite surrounding the plate are smallest when the plate lies parallel to the invariant plane.

There are two implications in the latter basis for the choice of the habit plane. 1—Inasmuch as the invariant plane in this Fe-Ni alloy invariably belongs to the $\{259\}_A$ family, then there must be a unique crystallographic first strain that is preferred to all other possible strains (such a unique crystallographic first strain is found experimentally as

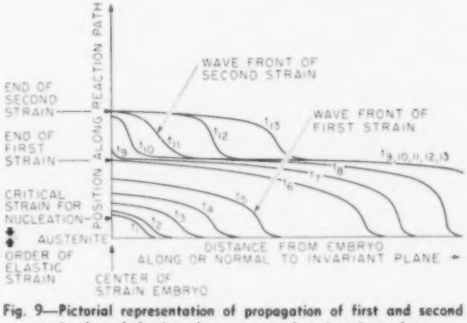
WAVE FRONT OF SECOND STRAIN
WAVE FRONT OF FIRST STRAIN
END OF SECOND STRAIN
END OF FIRST STRAIN
CRITICAL STRAIN FOR NUCLEATION
AUSTENITE
ORDER OF ELASTIC STRAIN
CENTER OF STRAIN EMBRYO
POSITION ALONG REACTION PATH
DISTANCE FROM EMBRYO ALONG OR NORMAL TO INVARIANT PLANE

Fig. 9—Pictorial representation of propagation of first and second strain through lattice along or normal to invariant plane.

§§§ The Jaswon and Wheeler direction-transformation matrix is used for making this selection.

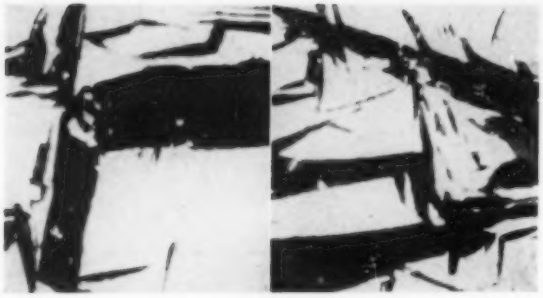

Fig. 10—Martensite plates in a 1.1 pct C, 5.4 pct Ni steel.

Transverse markings on plates appear to be the traces of the invariant planes of the second strain. X1500. Taken by W. J. Harris, Jr., M.I.T., 1948.

shown in Appendix I) and this is synonymous with a unique initial portion of a reaction path.[8] It is readily understandable that one reaction path would be preferred to others because the activation energy along one path is the least of all possible paths. This is the one that operates during the first strain.¶ 2—The other implication of the "least resistance" basis for the choice of the habit plane is that the second strain does not contribute materially to the strain energy developed in the austenite during the time interval when the habit plane is being determined. Otherwise the strain energy would not be a minimum for a plate lying along the invariant plane of the first strain. Thus, either the homogeneous portion of the second strain must be limited to extremely small volumes so as not to affect appreciably the elastic strain energy in the surrounding austenite, or the second strain occurs after the first strain has been completed throughout the entire platelike region. The latter alternative seems improbable. The first possibility is consistent with the requirement derived from the strain measurements, that the second strain must be macroscopically heterogeneous in order not to influence the observed strains.

The mode of plate formation described as the propagation of a transformation strain outward from an embryo can be explained in terms of Fig. 9. The strain wave starts to move when the strain in the embryo just exceeds the critical strain for nucleation. The strain at the embryo then increases as the wave front of the first strain moves away from the embryo. When the magnitude of the first strain at the embryo reaches its final value, the second strain commences. At this time, the wave front of first strain has shifted to a position somewhat removed from the strain embryo. Hence, there exists a phase lag between the wave front of the first strain and that of the second strain. After the wave front of the first strain is stopped at a barrier, the wave front of second strain catches up with it to complete the formation of a martensite plate. This model of plate formation implies that the interface region between the austenite and the martensite during formation is thicker than one atomic spacing. Bowles' model involves the addition of one plane of atoms at a time, and neglects the gradient of second strain up to and beyond the moving interface.

Double-Strain Nature of the Martensitic Transformation: From the fact that the habit-plane predictions of the modified Bowles method are successful, and that the invariant-plane strains must have the proper sequence to yield the correct result, it may be concluded that at any point in the transforming region the reaction actually takes place by the operation of two successive strains in point of time.¶¶ This situation makes it most unlikely that the plate formation could occur via atom-by-atom diffusion across a sharp interface.[8, 10]

Further evidence for the double-strain mechanism is shown in Fig. 10. The subbands within the martensite are brought out by tempering an Fe-Ni-C alloy. In the case of a $(225)_\gamma$ habit, the structure developed by the first strain is altered during the second strain by a shear of $(112)_\gamma$ planes in opposite directions $(11\bar{1})_\gamma$ and $(\bar{1}11)_\gamma$ to form twin-bands of the martensitic structure in two variants of the Kurdjumow-Sachs orientation.¶¶¶ A similar picture holds for the $(259)_\gamma$ habit except that unequal amounts of shear are required and the final orientations are two variants of the Greninger-Troiano set. It is believed that on tempering the carbides tend to precipitate preferentially along these twin-like boundaries, as in Fig. 10, to delineate the banded structure. Hence these subbands provide indepen-

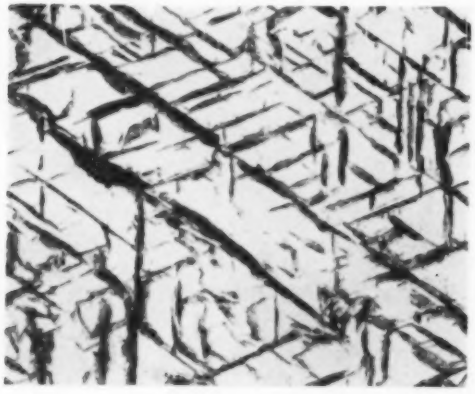

Fig. 11—Martensite plates in a medium carbon steel.

Habit plane indices are $(225)_\gamma$ and the plane of the paper is approximately $(111)_\gamma$. After Greninger and Troiano.[9]

¶ The presence of {225} habits as well as {259} habits in the same alloy system[2] implies the existence of two alternate reaction paths having almost the same activation energy.

¶¶ There is no necessity so far to require each of these strains to be achieved by straight line motions.

¶¶¶ This feature of the double-strain hypothesis is very satisfying intuitively. The first strain produces an unstable structure that is symmetrical with respect to the formation of pairs of twins through motions of $(112)_\gamma$ planes in the same or opposite directions. This situation does not exist until the first strain has been achieved.

dent evidence for the occurrence of a second strain that is macroscopically heterogeneous.

Cooperative Formation of Martensitic Plates: Because the second strain is macroscopically heterogeneous, the direction of motion of the austenite adjacent to the sides of a martensitic plate is given by the direction of motion of the atoms during the first strain. A study of the directions of motion for all the possible permutations of the $\{259\}_A$ habit shows that there are four directions of motion lying on a cone of approximately a 10° half-angle about any $<110>_A$ direction; there are also six motion directions lying within a 28° half-angle cone about any $<111>_A$, eight motion directions lying within a 42° half-angle cone about any $<100>_A$, and twelve motion directions lying within a 43° half-angle cone about any $<111>_A$. An analogous study of the directions of motion for all the possible permutations of the $\{225\}_A$ habit indicates that there are three motion directions on a 20° half-angle cone about any $<111>_A$ direction; there are also four motion directions on a 30° half-angle cone about any $<110>_A$, four motion directions on a 35° half-angle cone about any $<100>_A$, and six motion directions within a 55° half-angle cone about any $<110>_A$.

It may be expected that the strain energy per unit thickness of plate generated by the formation of plates adjoining the same austenitic region will be less if the plates tend to move the intervening austenite in the same direction rather than in opposing directions. In other words, a cooperative action in the martensitic transformation of many plates is predicted if their almost simultaneous appearance helps minimize the resisting strain energy. A rough measure of this cooperation is the number of "common" directions of motion in the first strain, and a comparison of the $\{259\}_A$ and $\{225\}_A$ habits shows that the degree of cooperation expected in the former is about twice that in the latter. The fact that there are twice as many $\{259\}_A$ planes as $\{225\}_A$ planes leads to a similar conclusion.

Pictorial evidence for this measure of cooperation is given in Figs. 11 and 12. Fig. 11, taken from ref. 1, shows a $(111)_A$ plane in a medium carbon steel having a $\{225\}_A$ habit. The triangular configurations of martensitic plates correspond to the three $\{225\}_A$ poles lying on about a 20° half-angle cone around the $[111]_A$ direction. This is the most preferred grouping of plates in the $\{225\}_A$ system according to the above concept of cooperative movements. Fig. 12 shows two $\{259\}$ type plates; specifically the habit planes are $(\bar{5}92)_A$ and $(\bar{9}52)_A$ where the plane of the page is $(111)_A$. The common direction of motion (the half angle is about 10°) is $[110]_A$. This is one of the two most preferred groupings for the $\{259\}_A$ habit systems according to the above criterion of cooperation.

These concepts receive further confirmation in that they account for the observation of Greninger and Troiano[1] regarding the tendency for $\{225\}_A$ systems to show obtuse angles between pairs of adjoining plates, whereas the $\{259\}_A$ systems are characterized by acute angles between such pairs of plates. It turns out that a random section through the $\{225\}_A$ grouping in Fig. 11 will exhibit obtuse angles, while a random section through the $\{259\}_A$ grouping in Fig. 12 will exhibit acute angles.

Twinning and the Martensitic Transformation: Bowles[6] describes the elements of the two strains in the $\{225\}_A$ system as close to those of twinning in

Fig. 12—Martensite plates in a 70 pct Fe-30 pct Ni alloy. Habit plane indices are $(259)_A$ and the plane of the paper is $(111)_A$. X500.

the austenite and martensite respectively. In this study, it is found that the first strain has nothing in common with the twinning crystallography of austenite, whereas the second strain involves an approximation of the twinning elements for the martensitic phase. The second invariant plane is about 5° from the twinning plane of martensite, while the direction of atom motion is the same as in twinning.

Reinvestigation of the results of Bowles as well as those of Greninger and Troiano[6] discloses that the first direction of motion is in the anti-twinning direction. Thus the first strain of the Bowles $\{225\}_A$ solution is not one of twinning in the austenitic phase. The second strain for the $\{225\}_A$ case involves exactly the twinning elements of the martensitic phase. These facts lend credence to the conclusion that the second strain follows the first in any unit of volume undergoing the transformation. The first strain can be said to involve the most favorable reaction path for the transformation in the austenitic structure. The second strain involves the most favorable reaction path in the martensitic structure for the final position along the first strain. Indeed, it now appears that the final position along the first strain is a result of the intercession of a change in the reaction path (the second strain) which is more favorable than a continuation of the first strain.

Magnitude of Strains: It is interesting to note that the magnitudes of the strains associated with the transformation are much larger than elastic strains. For example, the component of strain normal to the invariant plane of the first strain is about 0.05, and the shear component is about 0.20; whereas the respective values for the second strain are 0 and 0.16. Because of the large stresses that must be associated with the normal component of strain during the first strain (the resisting stresses are compressional), it is likely that hydrostatic components of stress would affect the course of the transformation. This prediction, which was pointed out by S. A. Kulin, was recently confirmed by him at M.I.T.

Evaluation of Theories Describing the Formation of Martensitic Plates: There are at least three theoretical descriptions of the formation of a martensitic plate. One can be described as an atom-by-atom diffusion growth under the influence of coherency.[8, 10] Another is the mechanism described by

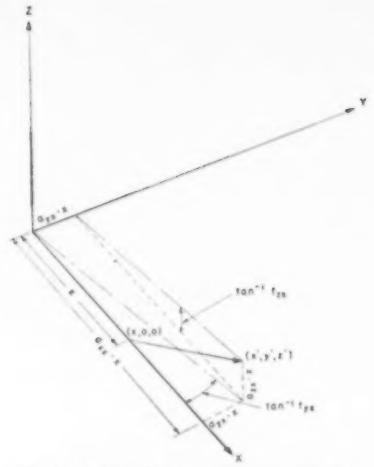

Fig. 13—Relationships between components of T matrix and coordinate-transformation matrix A.

Bowles as the growth by addition of one plane of atoms at a time. Still another is the wave-propagation method described in this paper.

The fact that the measured strain does not yield the martensite lattice, and the probable physical existence of the second strain heterogeneously distributed over the macroscopic plate, both testify against the likelihood of atom-by-atom movements. The requirement of succession in order of application of the two strains and the fact that the measured strain is a consistent invariant-plane strain also point up the improbability of atom-by-atom growth. Furthermore, the diffusion growth process does not seem to be a useful mechanism for the martensitic transformation from the standpoint of interpreting the crystallography involved.

With regard to the second mechanism, the $\{259\}_A$ planes rotate during the second strain, and this means that a plate cannot grow by addition of one $\{259\}_A$ plane at a time, with rotation of the $\{259\}_A$ plane on the martensite side of the interface and no rotation of the $\{259\}_A$ plane on the other side. Also, the requirement in this theory for a plate nucleus of almost final plate length and width lying along the $\{259\}_A$ plane makes the Bowles plane addition mechanism highly improbable.

The remaining mechanism based on the propagation of the transformation strain as a wave has been shown to be a reasonable one in the text of this paper. Of the three mechanisms, it is the only one that yields consistent explanations for the known facts.

Summary and Conclusions

1—All measured transformation strains for the austenite-martensite reaction are crystallographically equivalent in a given habit system. This suggests that, in general, only one reaction path operates in a given habit system.

2—The measured strain does not produce the martensite lattice from the austenite lattice. However, a sequence of two strains can generate the martensite in the correct orientation with respect to the austenite.

3—Each of these two strains can be described as a homogeneous strain involving the motion of an invariant plane, i.e., a plane of no rotation and no distortion. The second strain is (close to) a simple shear, while the first strain is not. The second strain is homogeneous only over small regions compared to the volume of the martensitic plate.

4—The two strains obtained are consistent with the Bowles double-strain analysis for the $\{259\}_A$ as well as the $\{225\}_A$ habit systems. The measured strain is one of the Bowles strains and is therefore a homogeneous, invariant-plane type of strain.

5—From the latter result and the matrix analysis, it is deduced that there is a sequence to the operation of the strains in $\{259\}_A$ systems as follows:

	First Strain (Measured Strain)	Second Strain
Invariant plane	$(259)_A$ within 2°	$(235)_M$
Direction of atom motion	$[\bar{1}56]_A$ within 2°	$[111]_M$

6—The observed habit plane lies parallel to, and is determined by, the invariant plane of the first strain. The parallelism helps minimize the strain energy developed during the formation of the plate.

7—The Bowles invariant-type, double-strain analysis does not yield a unique prediction for the habit plane. However, this prediction becomes possible when the following additional principle is introduced. The second direction of atom motion lies along the only remaining close-packed direction in the unrotated close-packed plane after the first strain.

8—The conclusion is reached that the Kurdjumow-Sachs orientations correspond to $\{225\}_A$ habit planes and the Greninger-Troiano orientations correspond to $\{259\}_A$ habit planes.

9—Metallographic evidence is shown for the existence of a macroscopically heterogeneous strain, corresponding to the predicted second strain.

10—The order of magnitude of the measured strain is quite large, about 0.1.

11—The martensitic transformation in $\{259\}_A$ habit systems should be about twice as cooperative as in $\{225\}_A$ habit systems. This follows from the fact that there are twice as many habit permutations in the former compared to the latter. Also there is a correspondingly greater tendency for groups of martensitic plates to move the intervening austenite in the same direction, thus minimizing the strain energy generated and allowing the plates formed to grow thicker than isolated plates.

12—The reaction-path description of the martensitic transformation is found to be more useful and more likely than the other proposed mechanisms.

Acknowledgments

The authors gratefully acknowledge the support of the Office of Naval Research in this program. The micrographs of Fig. 10 were kindly supplied by W. J. Harris, Jr. of the Naval Research Laboratory.

Appendix I

Derivation of Relations between Measured T Matrices and the Coordinate-Transformation Matrices

Suppose the coordinate-transformation matrix representing a certain strain is A where:

$$A = \begin{pmatrix} a_{xx} & a_{xy} & a_{xz} \\ a_{yx} & a_{yy} & a_{yz} \\ a_{zx} & a_{zy} & a_{zz} \end{pmatrix} \qquad [A\text{-}1]$$

A point (x, o, o) is then transformed by this matrix to:

$$(x', y', z') = (a_{xx}\,x,\ a_{yx}\,x,\ a_{zx}\,x) \qquad [A\text{-}2]$$

Now t_{yz} is the tangent of the angle between the X direction and the final position of this line projected onto the Z plane (Figs. 1 and 13). As shown in Fig. 13, t_{yz} is related to the components of A by the following equation:

$$t_{yz} = \frac{a_{yz} \cdot X}{a_{zz} \cdot X} = \frac{a_{yz}}{a_{zz}} \qquad [A\text{-}3]$$

$$t_{xz} = \frac{a_{xz} \cdot X}{a_{zz} \cdot X} = \frac{a_{xz}}{a_{zz}} \qquad [A\text{-}4]$$

By similarly investigating the transformation of points in the Y and Z axes, the following relations are obtained:

$$t_{xy} = \frac{a_{xy}}{a_{yy}} \qquad t_{zz} = \frac{a_{zz}}{a_{zz}} \qquad [A\text{-}5]$$

$$t_{zy} = \frac{a_{zy}}{a_{yy}} \qquad t_{yz} = \frac{a_{yz}}{a_{zz}} \qquad [A\text{-}6]$$

The diagonal components t_{xx}, t_{yy}, t_{zz} need not be discussed here because they are unnecessary to the analysis and have not been measured. They represent extensions or contractions and are difficult to determine.

Calculation of Equivalence of T Matrices: Because the Z axis is the $[111]_A$ direction (Fig. 1), there exists a three-fold symmetry about this axis. Thus, a counterclockwise and clockwise rotation by 120° should yield crystallographically equivalent matrices; that is, transformations in which the reaction path during the transformation is exactly the same.

In order to ascertain which of the T matrices are equivalent, values of the diagonal components are required. Such values have been approximated in Appendix III. It was found that T_a', T_c', and T_e' are related to one another by 120° rotations about $[111]_A$, and similarly for T_b'', T_d'', T_f''. Furthermore, in investigating the relation between the single-prime matrices and the double-prime matrices, it was also found that any one single-prime matrix has a mirror symmetry with one of the double-prime matrices across a $\{110\}_A$ plane. Thus, it may be concluded that all the matrices are crystallographically equivalent in that they represent the same crystallographic reaction path.

The best choice found for T_a' is:

$$\begin{pmatrix} 1.013 & 0.011 & \overline{0.03} \\ 0.10 & 1.079 & \overline{0.22} \\ 0 & 0 & 1 \end{pmatrix}$$

and for T_b'' is:

$$\begin{pmatrix} 0.99 & 0.11 & \overline{0.16} \\ \overline{0.01} & 1.09 & \overline{0.14} \\ 0 & 0 & 1 \end{pmatrix}$$

Appendix II

Can a Body-Centered Cubic Structure be Obtained From the Measured Strain?

Inasmuch as the nondiagonal components of the T matrices (the only measured components) will yield the final positions of the axes (Fig. 1), the final angles between axes to determine whether the measured strain generates a body-centered cubic structure can be investigated.

From all the X-ray determinations of lattice orientations, it is found that at least one $\{110\}_M$ plane is parallel to a $\{111\}_A$ plane.* From the work of Greninger and Troiano (Fig. 6 of ref. 4), it is also known that the pole of this $\{111\}_A$ plane lies in the same octant on the stereographic projection as the pole of the habit plane. Using this knowledge and the fact that all the habit planes corresponding to the T matrices lie in the same octant as $(111)_A$, it may be concluded that $(111)_A$ becomes $(101)_M$. This means that the final position of the $(111)_A$ plane after the transformation is unrotated with respect to its initial orientation. In addition, the fact that $t_{xz} = t_{zy} = 0$ shows that the $(111)_A$ plane does not rotate during the first strain. Also, the fact that $t_{xy} \neq 0$ and $t_{yz} \neq 0$, shows that the $(111)_A$ is not the invariant plane of the first strain. Hence, the $(111)_A$ must lie in the zone of the direction of motion of the invariant plane.

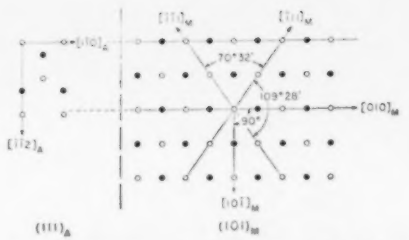

Fig. 14—Arrangements of atoms in $(\bar{1}11)_A$ and $(10\bar{1})_M$ showing the three possible sets of choices of martensite directions derivable from $[\bar{1}10]_A$ and $[\bar{1}\bar{1}2]_A$.
Note: Closed circles lie in next plane above plane of open circles.

The next step is the determination of the angles between the deformed positions of the X and Y axes. According to the convention of sign, the final angle between the X and Y axes, providing $t_{xz} = t_{zy} = 0$, is:

$$90° - \tan^{-1} t_{yz} - \tan^{-1} t_{xy}$$

Inasmuch as $t_{xz} = t_{zy} = 0$ for all the T matrices, this angle can be calculated and for T_a' is:

$$90° - \tan^{-1} 0.01 - \tan^{-1} 0.10 = 83° 40'$$

There exists an experimental uncertainty in both t_{xy} and t_{yz}. Taking the extremes, the uncertainty in this transformed angle is about ± 1° 30′.

Reference to Fig. 14 shows that the most probable choices of angles for this "deformed" angle in the final body-centered cubic martensite are 90°, 70° 32′, and 109° 28′.** All these choices are out of the experimental range found (83° 40′ ± 1° 30′) and hence it may be deduced that the structure corresponding to the measured strain is not martensite. Further calculations assuming the strain to be characterized by an invariant plane (Appendix III) shows unequivocally that the structure corresponding to the measured strain is not martensite.

Appendix III

Calculation of Invariant Planes and Directions of Atom Motion Corresponding to Measured T Matrices

Now that the coordinate-transformation matrix has been related to the measured T matrix, A can be derived on the basis that in the transformation there exists at least one plane of no distortion and no rotation.

Let a set of coordinates be chosen in the following manner: The Z_1 axis is taken perpendicular to this plane of no distortion and no rotation. Then consider the most general motion of this invariant plane; that is, motion in a direction not contained in the plane. The X_1 axis is chosen to lie in the invariant plane and in the plane defined by the direction of motion and the Z_1 axis. The Y_1 axis defined by a right-handed set (as in Fig. 13) then lies in the invariant plane. Relative to these coordinates the most general coordinate transformation matrix which leaves the X_1Y_1 plane undistorted and unrotated is:

* Actually, it can be deduced from the work of Greninger and Troiano that all close-packed planes in the austenite become $\{110\}$ planes in the martensite.

** It should be remembered in considering Fig. 14 that the original positions of the atoms are close-packed. This consideration places a limit on the possible choices of transformed directions corresponding to the original close-packed directions.

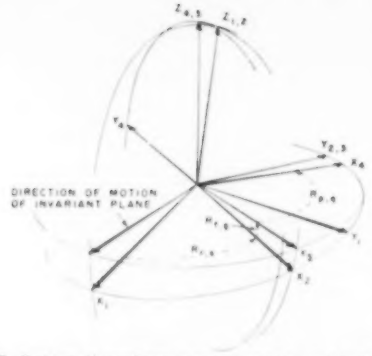

Fig. 15—Positions of coordinate axes and rotations used to illustrate matrix analysis for determining the experimental first invariant plane and direction of atom motion.

$$A_i = \begin{pmatrix} 1 & 0 & m \\ 0 & 1 & 0 \\ 0 & 0 & 1+n \end{pmatrix} \qquad [A\text{-}7]$$

To show that this matrix has the properties claimed for it, operate with this matrix on any X_iY_i plane, i.e. $z = c$:

$$\begin{pmatrix} x_i' \\ y_i' \\ z_i' \end{pmatrix} = \begin{pmatrix} 1 & 0 & m \\ 0 & 1 & 0 \\ 0 & 0 & 1+n \end{pmatrix} \begin{pmatrix} x_i \\ y_i \\ c \end{pmatrix} \qquad [A\text{-}8]$$

or:

$$x_i' = x_i + cm$$
$$y_i' = y_i$$
$$z_i' = c(1+n)$$

Thus, the plane at $z_i = c$ is carried into a plane parallel to itself at $z_i = c(1+n)$. Further, it can be proved that distances and angles in the plane are preserved. Hence, the X_iY_i plane is an invariant plane.

Now, however, the matrix A_i must be converted into an equivalent matrix in the coordinate system used in the measurements because the $X_iY_iZ_i$ axes are arbitrary in these considerations. This calculation can be performed either step-wise or in one operation. Inasmuch as it is easier to visualize the resulting quantities from the step-wise calculation, the discussion will be from this point of view.

The equivalent matrix A_e in the coordinate system used for the measurements can be derived from A_i by a series of three rotations as described in Fig. 15, namely, $R_{r,z}$; $R_{r,x}$ and $R_{p,y}$. The subscripts in the above are respectively the cosine and sine between the axes shown for the respective rotations. Using matrix algebra, the equivalent matrix is obtained as follows:

$$A_e = R_{p,y}^{-1} R_{r,x}^{-1} R_{r,z}^{-1} A_i R_{r,z} R_{r,x} R_{p,y}$$

$$= \begin{pmatrix} 1 + pmn + pqgmns & -pqn - q^2gmns & pmr - qfmns \\ -pqn + p^2gmns & 1 + qmn - pqgmns & -qmr - pfmns \\ 0 & 0 & 1 \end{pmatrix}$$

$$= \begin{pmatrix} a_{xx} & a_{xy} & a_{xz} \\ a_{yx} & a_{yy} & a_{yz} \\ a_{zx} & a_{zy} & a_{zz} \end{pmatrix} \qquad [A\text{-}9]$$

As shown by eq A-9 there are certain relations between the derived experimental quantities a_{ij} and the components of A_e. These relations make the determination of the invariant plane possible and are:

$$-\frac{p}{q} = \frac{a_{yz}\,a_{zz}}{a_{zy}\,a_{yz}} \qquad [A\text{-}10]$$

$$\frac{g}{f} = \frac{a_{zz} - a_{yz}}{qa_{zz} + pa_{yz}} \qquad [A\text{-}11]$$

$$n = -\left(\frac{p}{q}\,a_{xy} + \frac{q}{p}\,a_{yx}\right) \qquad [A\text{-}12]$$

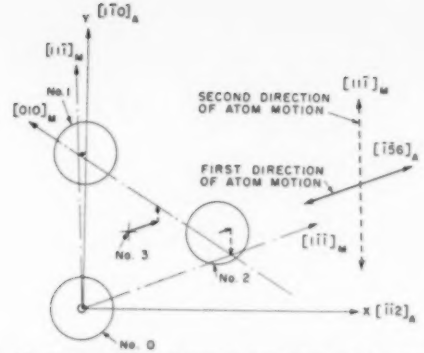

Fig. 16—Motion of atoms of primitive tetrahedral cell of austenite during transformation to martensite.
Motions lie in plane of paper which is $(111)_A \parallel (101)_M$. Atom No. 3 lies in plane above the plane containing atoms No. 0, 1, and 2.

$$\frac{r}{s} = -\frac{fn}{a_{xz} - a_{zx}} \qquad [A\text{-}13]$$

and

$$m = -\frac{fn}{gr} \qquad [A\text{-}14]$$

Because the diagonal components t_{xx}, t_{yy}, t_{zz} have not been measured, it is necessary to use an approximation method to obtain the values of the components of A_e as follows:

1—Assume $a_{ij} = t_{ij}$ and calculate values of p, q; f, g; (gms) and n using eqs A-10 to A-14.

2—With these tentative values of cosines and sines, calculate first approximations of the diagonal components a_{xx}, a_{yy}, a_{zz} using eq A-9.

3—Using these values of the diagonal components, recalculate the second approximations of the nondiagonal components and repeat steps 1 to 3 until the computed values of a_{ij} do not change measurably with further approximations.

It was found that the second approximations of a_{ij} were sufficient since rapid convergence existed.

The second-approximation solutions corresponding to T_a' and T_b'' are:

	p/q	g/f	r/s
T_a'	−1.29	±0.581	±0.878
T_b''	+0.100	±0.685	±0.61

In using these values, care must be taken to be consistent in sign for any particular choice of sign of p and f. Otherwise the solutions are liable to result in rotations in the wrong directions.

On carrying through the calculated rotations for the solutions to T_a', T_b'', and their crystallographic equivalents, the results shown in Figs. 3 and 4 are obtained.

Appendix IV

Calculation of Elements of Second Strain

The elements of the second strain can be determined by the following procedure:

1—Calculate the positions of the atoms defining the primitive tetrahedral cell in austenite after the first strain relative to the austenite lattice.

2—Pick the orientation of the martensite lattice relative to the austenite and transform the positions found in 1 to be relative to the martensite axes.

3—Select the nearest positions of these atoms that would correspond to the martensite structure.

4—Calculate the coordinate transformation matrix required to transform the atoms from the positions found in 2 to their respective positions chosen in 3.

5—Analyze this matrix according to the method outlined in Appendix III.

Carrying through this procedure using T_s' to determine the positions of the atoms after the first strain, the following results are obtained (Fig. 16):

	After First Strain		
Atom	Position Relative to Austenite Axes	Position Relative to Martensite Axes	Nearest Atom Position in Martensite
(1)	$(\overline{0.113}, 2.47, 0)$	(0, 2.475, 0)	(0, 2.477, 0)
(2)	(2.36, 1.33, 0)	(2.42, 1.22, 0)	(2.34, 0.83, 0)
(3)	(1.17, 1.44, 2.06)	(1.24, 1.39, 2.06)	(1.17, 1.65, 2.02)

The matrix relating the atom positions after the first strain to those in the final martensite is found to be:

$$B = \begin{pmatrix} 0.96 & 0 & \overline{0.0113} \\ \overline{0.163} & 1 & 0.224 \\ 0 & 0 & 0.98 \end{pmatrix}^{***}$$

Solving this B matrix according to the method outlined in Appendix III yields the results given in Fig. 5 for the elements of the second invariant-plane strain. The B matrix corresponding to the second strain is also used in Appendix V to test for the sequence of strains.

Appendix V

Non-Commutability of First and Second Strains

If the first and second strains are commutable, i.e., interchangeable in their sequence, then $AB = BA$. Checking with the T_s' case as an example:

$$AB = \begin{pmatrix} 1.109 & \overline{0.045} & 0.205 \\ 0.045 & 0.980 & 0.084 \\ 0 & 0 & 1 \end{pmatrix} \begin{pmatrix} 0.96 & 0 & \overline{0.0113} \\ \overline{0.163} & 1 & \overline{0.224} \\ 0 & 0 & 0.98 \end{pmatrix}$$

$$AB = \begin{pmatrix} 1.070 & \overline{0.045} & 0.199 \\ \overline{0.117} & 0.980 & \overline{0.138} \\ 0 & 0 & 0.98 \end{pmatrix} \qquad [A\text{-}15]$$

*** The '22' component has been taken as equal to 1 in finding the plane of invariance for this matrix. This corresponds to the approximation used by Bowles, namely that of neglecting the change in atom radius due to the change in coordination number.

$$BA = \begin{pmatrix} 1.063 & \overline{0.043} & 0.186 \\ \overline{0.136} & 0.987 & \overline{0.173} \\ 0 & 0 & 0.98 \end{pmatrix} \qquad [A\text{-}16]$$

Thus $AB \neq BA$, and the matrix multiplication is not commutative.

Because A and B are the invariant-plane solutions for the first and second strains, and the order of application of A followed by B (see Appendix IV) yields the correct final orientation, then this sequence must be followed physically.

References

[1] A. B. Greninger and A. R. Troiano: Crystallography of Austenite Decomposition. *Trans.* AIME (1940) **140**, p. 307.

[2] D. Van Winkle: Panel Discussion of the Martensitic Transformation. AIME February 1950.

[3] A. B. Greninger and A. R. Troiano: The Mechanism of Martensite Formation. *Trans.* AIME (1949) **185**, p. 590; JOURNAL OF METALS (September 1949).

[4] M. A. Jaswon and J. A. Wheeler: Atomic Displacements in the Austenite-Martensite Transformation. *Acta Crystallographica* (September 1948) **1**, Part 4, pp. 216-224.

[5] J. S. Bowles: The Crystallographic Mechanism of the Martensite Reaction in Iron-Carbon Alloys. *Acta Crystallographica* (March 1951) pp. 162-171.

[6] C. Crussard: Contribution a la Theorie des Transformations Martensitiques. *Comptes Rendus* de la Semaine d'Etudes de la Physique des Metaux (June 1948).

[7] E. S. Machlin and M. Cohen: The Burst Phenomenon in the Martensitic Transformation. JOURNAL OF METALS (September 1951), *Trans.* AIME, p. 746.

[8] M. Cohen, E. S. Machlin, and V. G. Paranjpe: Thermodynamics of the Martensite Transformation. *Thermodynamics in Physical Metallurgy.* (1950) ASM.

[9] J. C. Fisher, J. H. Hollomon, and D. Turnbull: Kinetics of the Austenite to Martensite Transformation. *Trans.* AIME (1949) **185**, p. 691; JOURNAL OF METALS (October 1949).

[10] G. V. Kurdjumow: Diffusionless (Martensitic) Transformations in Alloys. *Journal of Technical Physics*, U.S.S.R. (1948) **18**, No. 8, p. 1011.

Technical Note

Metallographic Techniques for Austenite Grain Size of Steels in the As-Cast State

by Edward A. Loria

A SERIES of papers on the study of austenite grain size in cast steels has been published recently.[1-3] These studies show that in the as-cast state, the austenite grains are quite large, for they form as the steel freezes at a very high temperature, but a simple reheating above the critical range produces a new set of austenite grains which, in many instances, is finer than ASTM grain size No. 8. Furthermore, there is no apparent relationship between as-cast austenite grain size and subsequent grain size produced by heat treatment.

The as-cast austenite grain size can be determined easily in plain carbon and low alloy steels which produce a continuous grain boundary ferrite envelope in the as-cast structure. In the case of cast steels whose alloy content produces greater hardenability and suppresses the proeutectoid ferrite transforma-

E. A. LORIA, Member AIME, formerly Senior Fellow, Mellon Institute of Industrial Research, Pittsburgh, is now Senior Engineer, Metallurgy, The Carborundum Co., Niagara Falls, N. Y.

TN 88E. Manuscript, July 13, 1951.

Fig. 1a—As-cast macrostructure of alloy cast steel containing 0.25 pct C, 1.05 pct Mn, 0.65 pct Ni, 0.61 pct Cr, and 0.22 pct Mo. Modified nitrosulphuric etch. X2. Area reduced approximately 20 pct for reproduction.

tion, there is no such indicator of the location of the original grain boundaries. Hence it becomes necessary to employ special etching reagents in order to bring out the structure. Perhaps some value for as-cast grain size determinations can be seen if consideration is given to the mechanism of diffusion and its relation to homogenization of structural components during heat treatment. Normally structural equilibrium is more rapidly attained with the smaller grain so that time of heat treatment required for homogenizing cast steels should normally decrease with decrease in austenitic grain size.

In a previous paper[4] the initial results on the use of a modified nitrosulphuric reagent in revealing the as-cast structure and grain size in a few cast alloy steels, which did not show ferrite outlining of the original grain boundaries, were shown. Such work has been continued in an effort to learn the quantitative effects of smaller initial grain size on homogenization of alloy cast steel. For this purpose the polished cross-sections of hardenability test bar castings have been subjected to the action of the modified nitrosulphuric reagent. Fig. 1a shows the excellent grain contrast that is produced across the 1½ in. diam bar of a popular grade of alloy cast steel. Such results can be obtained with this reagent when it consists of 20 ml concentrated nitric acid, 10 ml concentrated sulphuric acid, and 20 ml distilled water. The etching procedure was described previously.[4]

In steels exhibiting temper brittleness, it has been found that the addition of the wetting agent, Zephiran chloride, to a modified picral etch reveals a precipitate not shown by other etching reagents.[5] The excellent delineation of the grain outlines occurring in embrittled steel upon etching with the Zephiran reagent, particularly when the specimen is lightly repolished after etching, indicates that this agent would certainly assist in the search for the interfaces of as-cast grains. Therefore, 1 pct Zephiran chloride has been added to 4 pct nital and has increased the sensitivity of the latter and the speed of etching. Since the as-cast grains are quite large,

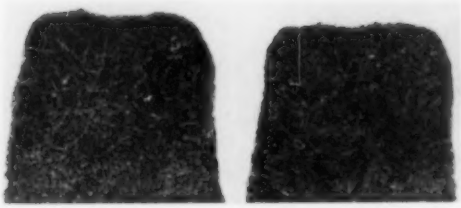

Fig. 1b—As-cast macrostructure of alloy cast steel containing 0.31 pct C, 1.44 pct Mn, 0.26 pct Mo. 6 pct nital-1 pct Zephiran chloride etch. X1.7. Area reduced approximately 20 pct for reproduction.

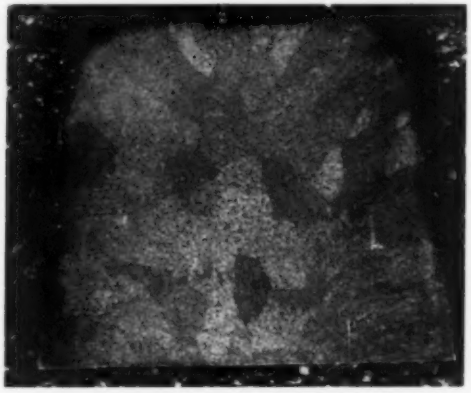

Fig. 1c—As-cast macrostructure of alloy cast steel containing 0.31 pct C, 1.44 pct Mn, 0.26 pct Mo. Modified nitrosulphuric etch. X2. Area reduced approximately 50 pct for reproduction.

a macroetch is really needed, and hence the best results have been obtained employing 1 pct Zephiran chloride in 6 pct nital. An example of the way this grain boundary etchant reveals the as-cast structure in conventional 1⅛x1¼ in. tensile test coupons of alloy cast steel is given in Fig. 1b. Each cross-section was immersed in the reagent until the grain boundaries became apparent visually. A comparison can be made with a similar sized coupon of the same alloy cast steel etched with the modified nitrosulphuric reagent and shown as Fig. 1c. Thus it can be seen that the modified nitrosulphuric reagent as a grain contrast etchant and the 6 pct nital-1 pct Zephiran chloride reagent as a grain boundary delineator are welcome additions to the tools available for the metallography of cast steels.

References

[1] M. F. Hawkes: Austenite Grain Size in Cast Steel. *Trans.* AIME (1947) **172**, pp. 510-530; METALS TECHNOLOGY (June 1947).

[2] E. A. Loria: Detection of As-Cast Austenite Grain Size in Heat Treated Cast Alloy Steels. *Trans.* ASM (1948) **40**, pp. 677-702.

[3] M. F. Hawkes and B. F. Brown: As-Cast Structures in Cast Steels. *Iron Age* (October 1948) **162**, pp. 138-147.

[4] E. A. Loria: Note on As-Cast Structure and Grain Size in Cast Alloy Steels. *Trans.* Amer. Foundryman's Assn. (1949) **57**, pp. 588-596.

[5] M. F. Hawkes and B. F. Brown: The Microstructure and Mechanical Properties of Cast Steels. *Trans.* ASM, (1949) **41**, pp. 519-564.

[6] J. B. Cohen, A. Hurlich, and M. Jacobsen: A Metallographic Etchant to Reveal Temper Brittleness in Steel. *Trans.* ASM (1947) **39**, pp. 109-138.

Low Sulphur Steel from High Sulphur Raw Materials and Fuel

by F. L. Robertson, C. H. Bacon, and J. W. Till

A description is given of the development of a process for making low sulphur steel on furnaces fired with 2½ pct sulphur oil. Slag and metal are analyzed at melt. Slag weight is estimated. A simple method for calculating necessary lime additions for making 0.025 and 0.035 pct sulphur steel is given.

DURING the last 15 years John Summers & Sons have been confronted increasingly by the problem of producing a low sulphur steel from high sulphur materials. The principles adopted, the processes used, the data collected on a furnace specially set aside to study this problem, and speculation on future developments are dealt with in this paper.

This study is limited to two melting shops which make sheet steel only, of the following analysis: C, 0.06 pct; Mn, 0.33; S, 0.04, 0.035, 0.03, and 0.025; and P, 0.02 and 0.015. All the processes described have reference to the manufacturing of this steel and are not necessarily applicable, without modification, to other steels. The raw materials used are given in Table I.

Development of Process

About 1934, Schenck's work on phosphorus was applied to frame quantitative rules for the removal of phosphorus, with great success. We could however, neither in our own work nor in the voluminous literature, find any assistance to frame quantitative furnace rules to remove sulphur. Perhaps, we should have persevered with Schenck's outstanding chapter on sulphur in *The Physical Chemistry of Steelmaking*, but we missed the importance of one sentence on p. 478. "Evidently this ratio $\frac{(\Sigma S)}{[S]}$ is the important quantity to be considered from the point of view of chemical reaction; it is clear that the sulphur content of the steel alone, as frequently given in the literature cannot suffice for judging the success of the reaction unless special details are given regarding the sulphur charge and the amount of slag."[1] We were not however very successful in getting values for Schenck's "η" that agreed with $\frac{(S)}{[S]}$ arrived at by our direct analysis.

In addition to Schenck's work much attention was given to V value. The formula selected for V was:

$$V = \frac{(\Sigma\,CaO) - 1.57\,(\Sigma\,P_2O_5)}{(\Sigma\,SiO_2)}$$

After plotting many charges a curve was obtained, based upon the relationship between the percentage sulphur in the finished steel and V value, Fig. 1. For a long time this was used as standard with about a 60 to 70 pct success on producer-gas fired furnaces, if all uprising scrap was used and no bought scrap used. An inspection of this curve shows clearly that it is not a quantitative manufacturing process, and that it was not sure enough to go to the trouble and expense of doing stage analysis for P_2O_5,

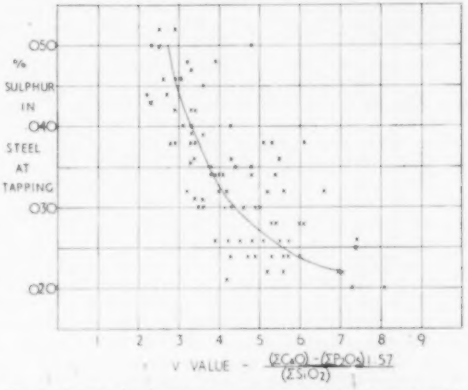

Fig. 1—Relationship between percentage of sulphur in steel and V value for producer-gas fired furnaces. (Coal 1 pct S.)

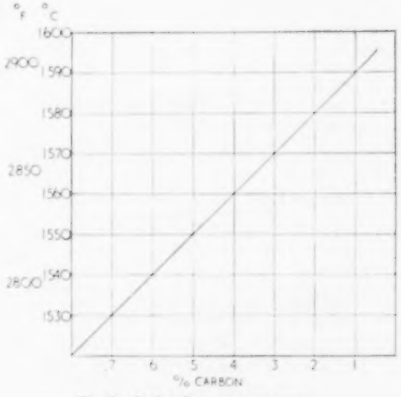

Fig. 2—Carbon/temperature curve.

F. L. ROBERTSON, deceased. C. H. BACON and J. W. TILL are with John Summers & Sons Ltd., Hawarden Bridge Steelworks, Shotton, Chester, England.

Discussion on this paper, TP 3106C, may be sent, 2 copies, to AIME by Jan. 1, 1952. Manuscript, Feb. 26, 1951. St. Louis Meeting, February 1951.

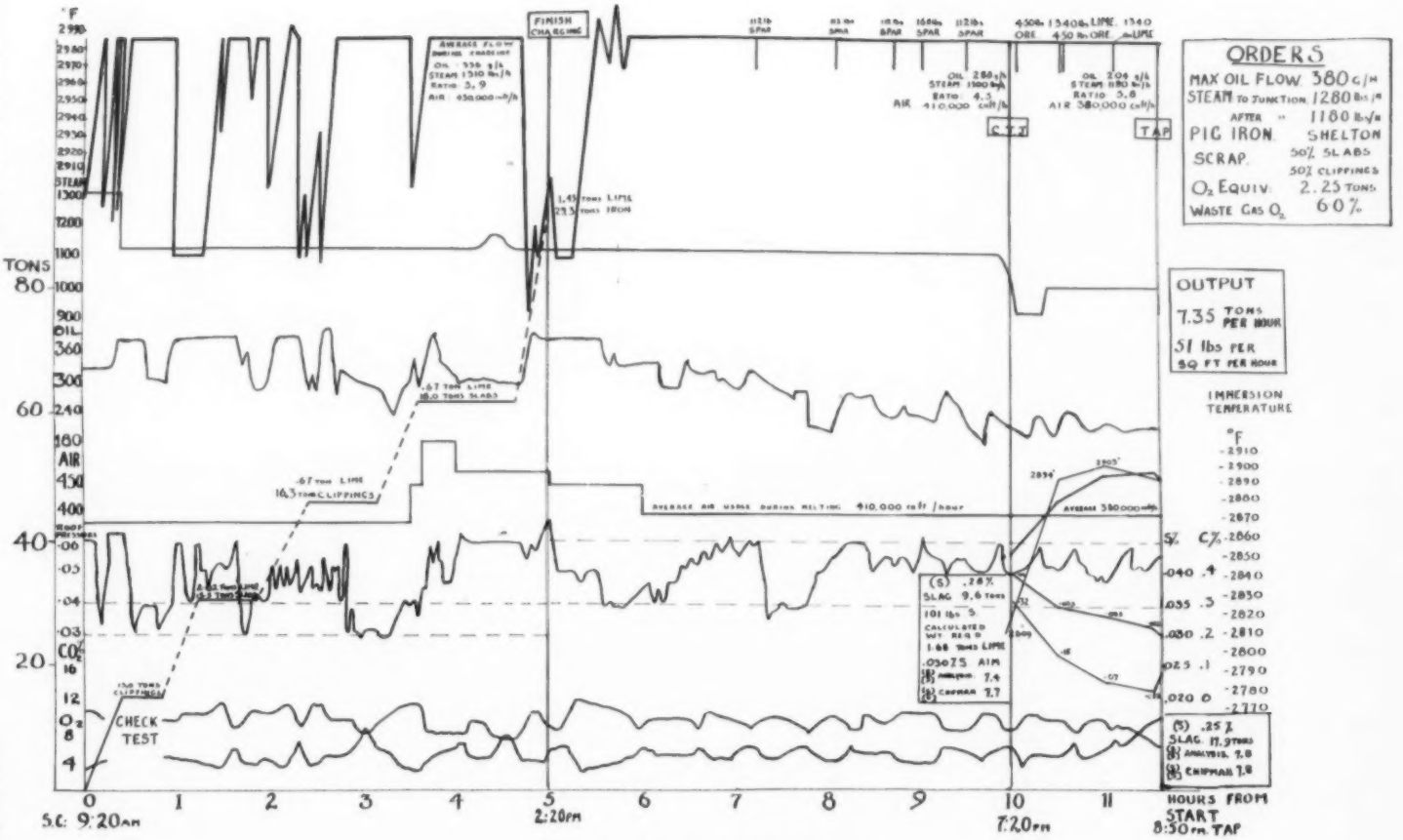

Fig. 3—Master chart, Cast L204, Jan. 26, 1950.

CaO, and SiO_2. At this time there was no problem in making as much 0.025 pct S steel as required, and other matters pressed.

In 1946, four oil (S = 2.5 pct) fired furnaces were introduced and it was found that conditions that had given 60 to 70 pct of 0.025 pct S charges on producer gas firing gave none on oil firing. Generally throughout the works, this was ascribed to the sulphur in the oil but, even yet, this is not proven for certain until more quantitative work is done to insure that the slag weights are equal in both cases. The works position was, however, so serious that the whole question of sulphur passage between the slag and steel was studied anew.

By this time Grant and Chipman's paper had appeared.[2] With this, and with Schenck's older work as a basis, work was started with a view to evolving a process for making steel of any specified sulphur content from the materials available.

With the combined assistance from many departments and Trade Union organization in the Works, a scheme was set up to work one furnace under special supervision and controlled conditions.

Experimental Furnace Trials: The furnace was fully instrumented and was given priority in operation. The object was to reduce the variables to a minimum, so that the relation between furnace practice and rate of output could be studied. This presented an opportunity to study sulphur in a way that had not been possible before. A full report of the furnace conditions and their relation to output is given in a paper by Robertson and Thring.[3] A short description of the conditions of the trial, insofar as they influence the investigation on sulphur, will be presented here.

Three roof pyrometers are fitted and the oil flow is controlled automatically from them. The control system is arranged to operate so that, as soon as one of the three pyrometers reaches the set maximum temperature, the oil flow is reduced. A maximum fuel flow controller is incorporated to operate before the maximum roof temperature is reached.

The furnace is charged with 58 tons of steel scrap and about 31 tons of cold machine-cast pig iron. When possible, the scrap used for these trials was all uprising scrap, consisting of slab crops and sheet clippings, to enable an estimate of the analysis to be made.

The actual weight of pig iron needed to give a carbon of 0.3 to 0.5 pct, when clear melted, is calculated by means of the oxygen equivalent. The oxygen equivalent per ton of iron is the weight of oxygen required to oxidize the C, P, Mn, and Si in one ton of iron to CO, P_2O_5, MnO, and SiO_2. The figure for the total oxygen equivalent is found by experience on the furnace and this figure, divided by the oxygen equivalent per ton, gives the weight of pig iron required.

A standard charging sequence was introduced and processing during refining was controlled. Fig. 2 shows the carbon temperature curve adopted. Feeding of lime and ore was not permitted until the steel temperature, obtained by an immersion pyrometer, reached the figure on the curve corresponding to the carbon in the steel. The time at which this occurs is referred to as "junction," instead of the more commonly used "melt out." Junction is defined in the measurable terms of carbon and temperature and therefore is considered to have more value in control work than melt out, which is not capable of precise definition.

Table I. Analysis of Raw Materials, Percent

Material	C	Si	Mn	S	P
33 pct cold pig	3.5-3.8	0.4-1.2	0.75-1.5	0.03-0.07	0.75-1.5
33 pct uprising scrap	0.06		0.3	0.04	0.02
33 pct bought scrap	0.2		0.5	0.06	0.06
Burnt lime				0.1-0.2	
Spar				0.6-0.8	
Oil				2.3-2.7	
Coal				0.9-1.4	

Fig. 3 is a copy of one of the master charts. The individual furnace charts are copied on to this chart, and the following data is shown: charging sequence, roof temperature, oil flow, steam flow, air flow, furnace pressure, CO_2 and O_2 in waste gas, steel temperature rise, and carbon, sulphur and manganese drop.

The ingoing materials in the form of pig iron, lime, spar and ore are analyzed. Full analyses are also carried out on the metal and slag at junction and tapping. The calculation sheet, Fig. 4, is our approach to the study of the behavior of the carbon, silicon, phosphorus, sulphur, and oxidation during the course of the charge and their distribution between the metal, slag, and furnace atmosphere. The top line in each case represents the percentage of the element present. The second line shows the weight of the element (all weights shown are in tons, except sulphur, which is in pounds. References to tons in this paper have been converted to short tons). The third line gives the weight of oxygen that will combine with the element, and the fourth line gives the weight of the oxide formed. The balances for the oxidation, sulphur, and silicon are shown on the right.

In the case of the sulphur balance, the weight of sulphur introduced through the pig iron and scrap is shown under "Metals," and from the lime and spar under "Nonmetals." The difference between the weight of sulphur in the system at junction and the weight of sulphur in the charge gives the weight of sulphur absorbed from, or lost to, the furnace atmosphere. Analysis of the tapping samples enables a second balance to be made showing the pick up or loss between junction and tapping, after making allowance for any sulphur introduced with the feeds.

This information is set out in a rather different form in Fig. 5. This flowsheet proved to be the most helpful approach to the study of the behavior of sulphur. The important points that emerged from the careful study of a large number of sulphur flowsheets were:

1—That the $\frac{(S)}{[S]}$ value at junction varied greatly.

2—That the $\frac{(S)}{[S]}$ value at tapping varied considerably, but that the bulk of the results were in excess of 6. Fig. 6 shows the range of $\frac{(S)}{[S]}$ at tapping for 250 charges.

3—That the pickup of sulphur from the furnace atmosphere varied within wide limits, but that the average figures could be taken as 30 lb between start charge and junction and nil between junction and tapping.

Figs. 7 and 8 are histograms showing the spread

Fig. 4—Calculation Chart, Cast L204

(Continued→)

Time Operation A.M.	Time from S.C.	Materials Charged and Fed																			
		Pig Iron							Scrap				Lime								
		C	Si	S	P	Mn	Fe	Wt	S	Mn	Fe	Wt	SiO_2	S	CaO	CO_2	Wt				
9:20 Start charging									0.038	0.37	99.6										
									0.0238	0.232	62.5	62.7									
									47.7*	0.067											
		4.02	0.94	0.026	0.92	1.35	93.7						0.60	0.12							
		1.18	0.276	0.0076	0.271	0.397	27.6	29.4					0.028	0.0056			4.7				
		1.57	0.315	15.2*	0.348	0.115								11.2*							
2:20 Finish charging	5.0		0.591																		
4:35 Spar																					
5:25																					
6:00																					
6:25																					
6:50																					
6:50 Temperature																					
7:20 Sampled	10.0	Carbon-temperature junction																			
7:25 Ore																					
7:50 Temperature																					
7:55 Lime and ore																	0.67				
8:20 Temperature																					
8:25 Lime													0.008	0.0016			0.67				
														3.1*							
8:45 Temperature																					
8:55 Tapped	11.58																				
Pit sample																					

* All weights in tons (2000 lb per ton) except sulphur, in lb.

Calculation Chart

(Continued→)

Time Operation A.M.	Time from S.C.	Steel						Oxidation											
								Cumulative					From Junction						
		C	S	P	Mn	Fe	Wt	O_2 Abs*	From Ore	From Flame	Pct Flame	Per Hr	O_2 Abs*	From Ore	From Flame	Pct Flame	Per Hr		
9:20 Start charging																			
2:20 Finish charging	5.0																		
4:35 Spar																			
5:25																			
6:00																			
6:25																			
6:50																			
6:50 Temperature		Analysis																	
7:20 Sampled	10.0	0.31	0.038	0.017	0.165	99.6		5.74	Nil	5.74	100	0.574							
		0.26	0.0319	0.014	0.138	83.5	83.9												
		0.335	63.8*	0.019	0.042														
7:25 Ore																			
7:50 Temperature																			
7:55 Lime and ore																			
8:20 Temperature																			
8:25 Lime																			
8:45 Temperature																			
8:55 Tapped	11.58	0.045	0.032	0.011	0.10	99.6		7.14	0.100	7.04	98.5	0.608	1.4	0.100	1.3	52.8	0.822		
		0.037	0.0261	0.009	0.082	81.4	81.6												
		0.049	32.2*	0.012	0.024														
Pit sample		0.030					84.8												

7.35 tons per hr
50.6 lb per sq ft per hr

Calculation Chart

Materials Charged and Fed—Continued					Swedish Ore				Immersion Temperature, °F	Slag										
Spar																				
SiO_2	S	$CaCO_3$	CaF_2	Wt	SiO_2	P	Fe	Wt		SiO_2	FeO	Fe_2O_3	Al_2O_3	MnO	CaO	MgO	P_2O_5	S	"V"	Wt
16.9	0.30																			
0.052	0.0009 1.8*			0.308						Chipman's calculated										
										(Σ Fe) 19.3 pct				Excess Base = 0.420				$\frac{(S)}{[S]}$ =		7.7
									2809											
										6.2	20.4	4.8	1.93	7.8	48.8	3.84	5.44	0.28	6.5	
										0.597	1.96 0.438	0.462 0.14	0.186	0.751	4.7	0.37	0.524	0.027 54.0*		9.6
					5.9		59.0													
								0.22	2894											
					0.026		0.26 0.100	0.22												
									2903											
										Chipman's calculated										
										(Σ Fe) 23.7 pct				Excess Base = 0.428				$\frac{(S)}{[S]}$ =		7.8
									2885											
										4.8	23.3	8.0	1.84	6.2	46.2	4.53	4.45	0.25	8.2	
										0.86	4.17 0.927	1.48 0.432	0.33	1.11	8.3	0.811	0.797	0.044 89.6*		17.9

7.35 tons per hr
50.6 lb per sq ft per hr

Calculation Chart

	Sulphur Balance						Silica Balance					
	Lb S	Gain Cum.	Gain Per Hr	Gain from June	Gain Per Hr	Non-Met. Add.	Tons SiO_2	Gain Cum.	Gain Per Hr	Gain from June	Gain Per Hr	Non-Met. Add.
Charged in metal	62.9						0.591					
Charged in non-metal	13.0						0.080					
Charged Total	75.9						0.671					
Metal	63.8	+ 0.9	+ 0.1				Nil	− 0.591	− 0.059			
Slag	54.0	+ 41.0	+ 4.1				0.597	+ 0.517	+ 0.052			
Total	117.8	+ 41.9	+ 4.2				0.597	− 0.074	− 0.007			
Metal	52.2	− 10.7	− 0.9	− 11.6	− 7.4		Nil	− 0.591	− 0.051	Nil	Nil	
Slag	89.6	+ 73.5	+ 6.4	+ 32.5	+ 20.6	3.1	0.86	+ 0.746	+ 0.065	+ 0.229	+ 0.20	0.034
Total	141.8	+ 62.8	+ 5.5	+ 20.9	+ 13.2		0.86	+ 0.155	+ 0.014	+ 0.229	+ 0.20	

* O_2 absorbed by charge, exclusive of O_2 used for fuel burning. Allowance is made for 4.48 tons of Fe volatilized as Fe_2O_3 and lost from liquid system.

for these values. Further study of the results gradually led to the conclusion that an understanding of the behavior of sulphur between the liquid phases could not be reached, unless the weight of the slag and the weight of the steel and the total weight of the sulphur in each were taken into account, besides the percentage of sulphur in the steel and the percentage of sulphur in the slag.

The Partition law cannot be used as a foundation for an extraction process, unless the weights of the two liquid phases, together with the total weight of the substance to be extracted, are taken into account, besides the ratio of the percentage concentrations of the substance in the two liquid phases.

This fundamental principle of the proper application of the Partition law, so well and so long understood in other industries, had escaped, not only ourselves, but other workers in the field. Except for one sentence in Schenck, to which reference has been made, no reference has been found in steel sulphur literature to the fact that consideration of percentages of sulphur in slag and steel is not enough without the weights of steel and slag, and weights of sulphur in each.

At this point we wish to give our apologies to Donald E. Babcock for not acknowledging his work in The American Iron and Steel Institute Proceedings of May 1949.[4] We would explain that our process was worked out and in operation on all furnaces in November 1948. We even venture to regret that Mr. Babcock, who clearly agrees with us, has been tempted to assume a constant slag weight in many of his examples.

Sulphur Partition $\frac{(S)}{[S]}$: Most of the literature concerning sulphur in steel is confined to the distribution of sulphur between steel and slag as measured by:

$$\frac{\text{Pct Sulphur in Slag}}{\text{Pct Sulphur in Steel}}$$

Numerous formulas have been evolved giving different degrees of effect upon this partition ratio to the lime, magnesia, manganese, iron oxide, silica, and alumina contents of the slag. Several of these formulas have been tested and compared with the partition figure obtained by direct analysis of steel and slag for sulphur. For our class of steel, closer agreement has been found with Grant and Chipman's Excess Base figures than with any other formula that has been tried.

Fig. 9 is a copy from Grant and Chipman's paper showing the relation between the calculated Excess

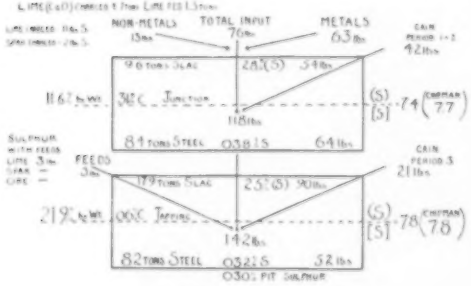

Fig. 5—Sulphur flowsheet, cast L204.

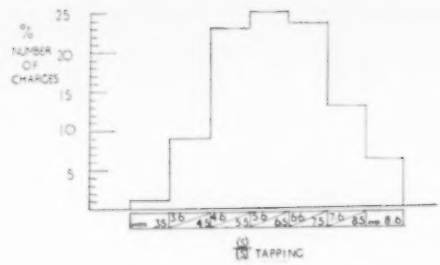

Fig. 6— $\frac{(S)}{[S]}$ at tapping, 250 charges.

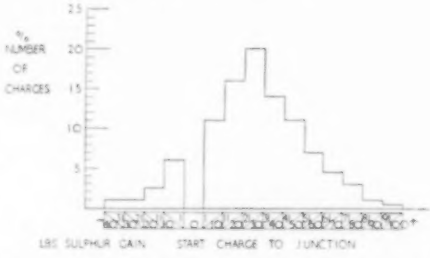

Fig. 7—Sulphur gain. Start charge to junction. 250 charges.

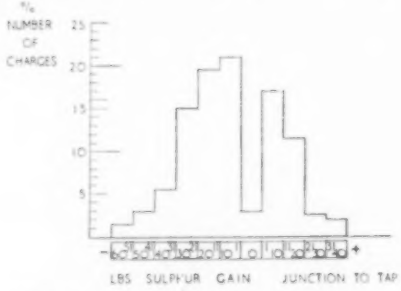

Fig. 8—Sulphur gain. Junction to tap. 250 charges.

Base figure and $\frac{(S)}{[S]}$ by analysis for steel and slag samples from open hearth furnaces. Fig. 10 shows the results for 50 of our charges plotted on the same scale. It will be observed that our results show a very similar pattern to the former with a tendency for the higher $\frac{(S)}{[S]}$ plots to be rather above the standard line.

It is obvious that the higher the $\frac{(S)}{[S]}$ that can be obtained at tapping, the lower will be the slag weight that need be carried for a given sulphur burden and a given desired sulphur percentage in the steel. So, any formula that will give an insight into the factors that are conducive to a high $\frac{(S)}{[S]}$ is valuable as a guide to the slag composition that will give the best possible desulphurization of the metal.

For a process which is based upon the calcula-

tion of the feed lime required for individual charges, however, it has not been regarded as feasible to predict the $\frac{(S)}{[S]}$ for each charge by any basicity measurement. Therefore our process has been based upon an expected $\frac{(S)}{[S]}$ of 6.0 at tapping. Frequently figures are obtained that are considerably in excess of 6, but the process must necessarily be based upon a figure rather below the mean, for safety.

Basis for a Process: At this juncture it became apparent that the basis for a process must consist in increasing the slag weight, so that, at tapping, the percentage of sulphur in the slag is 6 times the percentage of sulphur desired in the metal, and that a means must be found to express this quantitatively in terms of lime additions. A calculation to determine the slag weight necessary for specified sulphur percentage in the steel, in terms of total weight of sulphur in the system and $\frac{(S)}{[S]}$ follows.

W = Weight of steel, lb
w = Weight of slag, lb
P = Percentage of slag weight of steel weight
$[S]$ = Percentage of sulphur in steel
(S) = Percentage of sulphur in slag
TS = Total weight, lb, of sulphur in steel and slag
L = Weight of sulphur in steel, lb
$TS - L$ = Weight of sulphur in slag, lb
$A = \frac{\text{Pct Sulphur in Slag}}{\text{Pct Sulphur in Steel}}$

$$\text{Then } A = \frac{(S)}{[S]} = \frac{\frac{(TS-L) \times 100}{w}}{\frac{L \times 100}{W}}$$

$$= \frac{TS-L}{L} \times \frac{W}{w}$$

$$= \left(\frac{TS}{L} - 1\right) \times \frac{W}{w}$$

$$= \left(\frac{TS}{L} - 1\right) \times \frac{100}{P}$$

$$\text{Therefore, } P = \frac{TS \times 100}{L \times A} - \frac{100}{A} \quad \text{[Eq 1]}$$

For 168,000 lb steel:

$$L = \frac{[S]}{100} \times 168{,}000 = 1680 \times [S]$$

$$\text{And } P = \frac{TS \times 100}{1680 \times [S] \times A} - \frac{100}{A} \quad \text{[Eq 2]}$$

And for $\frac{(S)}{[S]} = 6.0$ and $[S]$ 0.025, 0.030, and 0.035, the calculations are given in the following table:

	For 0.025 Pct Sulphur Steel	For 0.030 Pct Sulphur Steel	For 0.035 Pct Sulphur Steel
Slag wt pct P =	$\frac{TS \times 100}{1680 \times 0.025 \times 6} - \frac{100}{6}$	$\frac{TS \times 100}{1680 \times 0.030 \times 6} - \frac{100}{6}$	$\frac{TS \times 100}{1680 \times 0.035 \times 6} - \frac{100}{6}$
Slag wt pct P =	$\frac{TS}{2.52} - 16.7$	$\frac{TS}{3.02} - 16.7$	$\frac{TS}{3.52} - 16.7$ [Eq 3]

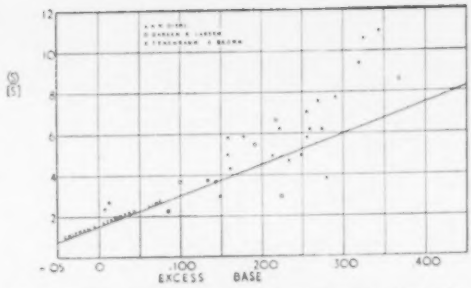

Fig. 9—Sulphur distribution in the basic open hearth. After Chipman and Grant.

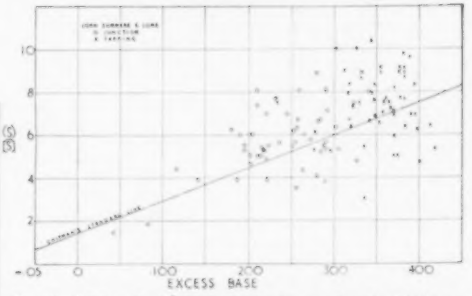

Fig. 10—Sulphur distribution in the basic open hearth. 50 charges. After Chipman and Grant.

Figs. 11a, b, c, and d are charts based upon this calculation, showing the slag weights necessary for 0.025, 0.030, 0.035, and 0.040 pct sulphur steel for differing $\frac{(S)}{[S]}$ values and pounds of sulphur in steel and slag. Figs. 12a, b, c, and d are charts for $\frac{(S)}{[S]}$ values of 4, 6, 8, and 10 showing the slag weights necessary for differing sulphur percentage in the steel and pounds of sulphur in steel and slag. At this stage it only remained to work out simple means to assess the weight of sulphur in steel and slag at junction, and the slag weight increase required between junction and tapping, in order to make the process straightforward enough to be adopted as standard shop practice. Fig. 13 shows the lime additions necessary for the desired slag weight increase.

Slag Weight: It can be seen that in order to work such a process, it is essential to be able to estimate the slag weight with reasonable accuracy. In our early work on the experimental furnace, the slag weights were based upon the percentage of phosphorus in the pig iron and the P_2O_5 percentage in the slag. Calculations based upon manganese and lime were also used.

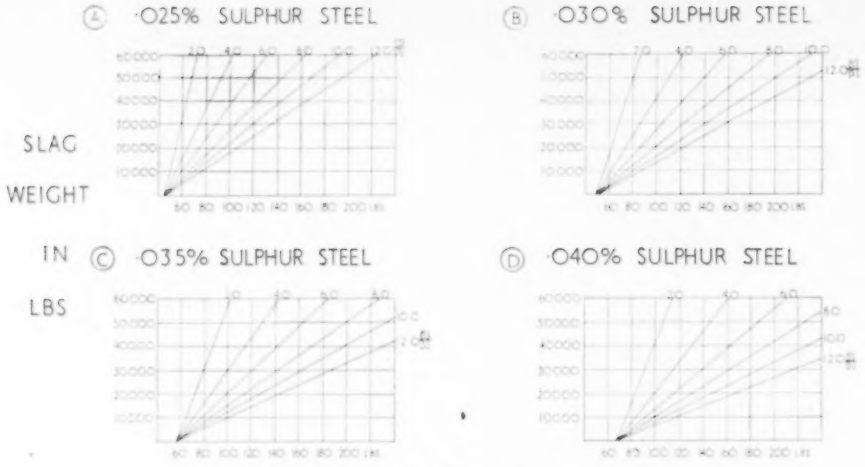
Ⓐ ·025% SULPHUR STEEL
Ⓑ ·030% SULPHUR STEEL
SLAG WEIGHT IN LBS
Ⓒ ·035% SULPHUR STEEL
Ⓓ ·040% SULPHUR STEEL
TOTAL WEIGHT OF SULPHUR IN STEEL AND SLAG

Fig. 11—Slag weight required vs. pounds of sulphur in steel and slag. Steel weight is 168,000 lb. $\frac{(S)}{[S]}$ is 2.0 to 12.0.

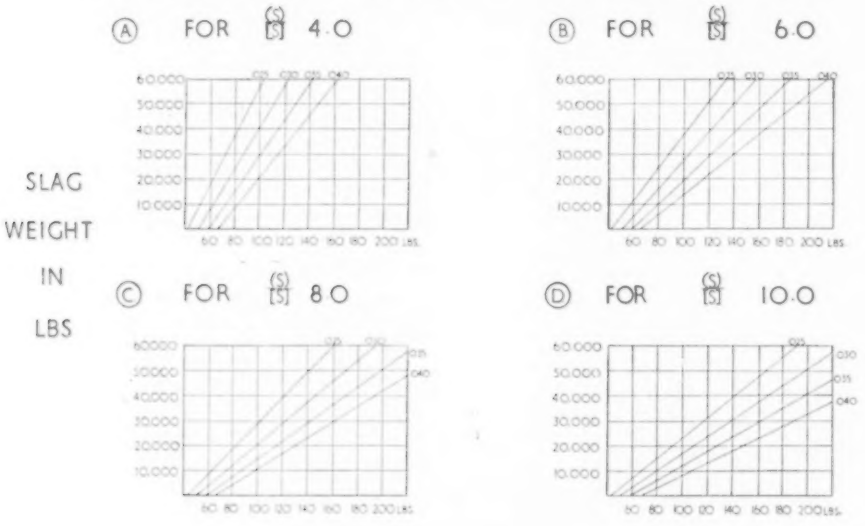

Fig. 12—Slag weight vs. pounds of sulphur in steel and slag. Steel weight is 168,000 lb. Final [S] pct is 0.025, 0.030, 0.035, and 0.040.

Table II* gives the result of a comparison of the slag weights obtained when calculated from P_2O_5 and from lime. Also included in this table is the figure by which the final sulphur percentage in the steel would be affected by the error between the two figures for slag weight at junction. Though the actual difference in slag weight appears to be considerable in some cases, the effect upon the sulphur percentage in finished steel is relatively small, the maximum difference is 0.006 pct S, the average absolute difference is less than 0.002 pct S.

Provided that the slag weight can be estimated to about ± 2 tons, the process can be worked satisfactorily. The slag weight obtained by lime gives results within these limits and has been adopted as a basis for shop practice.

The simple shop rule has been adopted of doubling the weight of lime charged to obtain the slag weight at junction. Fluxing from the banks in this period is not severe and can be ignored. After junction, the bank erosion is severe and is dependent upon the duration of the refining time. Allowance can be

* For Tables II and IV order Document 3361 from American Documentation Institute, 1719 N Street, N.W., Washington 6, D. C., remitting $1.00 for microfilm (images 1 in. high on standard 35 mm motion picture film) or $1.00 for photocopies (6x8 in.) readable without optical aid.

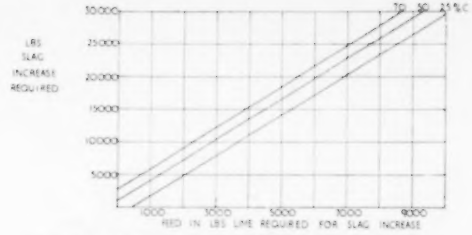

Fig. 13—Lime feed vs. required increase in slag weight.

Furnace capacity is 168,000 lb. Allowance is made for the lime fluxed from the bottom, which is related to the time from junction to tapping. The carbon at junction is used as a measure of the latter.

made for this in calculating the lime addition as shown in Fig. 13 by means of introducing the factor of carbon percentage at junction.

Rules for Making Steel of a Specified S Content: The following represent the rules for shop practice reduced to the simplest possible terms:

1—Calculate the weight of pig iron in the charge to give a carbon of 0.3 to 0.5 at junction. This calculation is based on the oxygen equivalent per ton of pig iron as explained for experimental furnace.

2—Calculate the amount of lime to be charged to give a *V* value of approximately 4 at junction.

3—Weigh the lime charged to within ± ½ ton.

4—Analyze the metal and slag for sulphur at junction and calculate the total weight of sulphur in pounds, assuming the slag weight to be twice that of the lime charged.

5—Calculate the required lime addition from the chart or calculation wheel to give the desired sulphur content at tapping with $\frac{(S)}{[S]}$ of 6. The maximum amount of lime that can be fed economically is found by experience. If the weight calculated for the desired sulphur percentage in the steel exceeds this figure, it is advisable to schedule the steel for a higher sulphur percentage and re-calculate the lime required on the new figure.

6—When the carbon is down, the lime in solution, and the temperature 2895° to 2930°F, check the steel for sulphur percentage and tap the furnace.

Calculation Wheel: Fig. 14 shows the calculation wheel for 0.035 pct sulphur steel, and one of these is fitted on to each furnace. From the steel and slag analysis at junction, the weight of sulphur in pounds in each is obtained. From the sum of these, the amount of feed lime required to give 0.035 pct sulphur in the finished steel is read off. This is given in terms of number of barges, each barge being equivalent to 12 cwt (1350 lb) of lime.

Fig. 15 shows a refinement, by which the weights of lime feed required for 0.025, 0.030, and 0.035 pct sulphur steel can be obtained directly from the percentage of sulphur in steel and slag at junction. It must be stressed that the calculation wheel is only applicable for a standard weight of charged lime. A constant weight of 4.7 tons of lime is now used for charges made with the normal supply of pig iron.

Process in Operation: It is now 27 months since the process was put into operation on all furnaces in the two shops, and over a million tons of steel have been made during this time. The process is welcomed by the melting shop. All sulphur grades can be made without concern, with scrap, as it comes, either on the oil-fired or gas-fired furnaces. Output has gone up and not down, since its introduction.

It has been said that the process is not accurate enough. It is, therefore, worth looking into the accuracy, to which the shop has to work.

The melting shop manager, ordered to make 0.025 pct sulphur steel, is not held to account if his steel ranges from 0.022 to 0.027 pct.

Fig. 16a, b, c, and d show the effect of errors in slag weight at tapping or $\frac{(S)}{[S]}$ upon the final sulphur in the steel for a given sulphur burden on a furnace of 168,000 lb steel capacity.

If the case is considered of 100 lb total sulphur burden on Fig. 16b with 6 $\frac{(S)}{[S]}$, the relative slag weights for 0.022 and 0.027 pct sulphur steel are 46,000 and 34,000 lb. This represents a tolerance of 12,000 lb in the tapping slag weight.

Alternatively, if a slag weight of 42,000 lb is

LBS SULPHUR IN SLAG
FOR ·035% SULPHUR
7 BARGES LIME CHARGED
% SULPHUR IN SLAG FROM % SULPHUR IN STEEL
% SULPHUR IN STEEL
EQUIVALENT BARGES OF LIME TO FEED FROM TOTAL LBS SULPHUR IN SLAG AND METAL

Fig. 14—Furnace calculation wheel for lime to feed for 0.035 pct S steel.

TOTAL SULPHUR BURDEN
lbs AT JUNCTION
JOHN SUMMERS & SONS LTD
FEED LIME CALCULATOR FOR 0.025% 0.030% & 0.035% SULPHUR STEELS
TAPPING 75 TONS STEEL
84 CWTS LIME CHARGED
60% AT TAPPING
CWTS LIME REQUIRED
% SULPHUR IN SLAG
% SULPHUR IN STEEL

Fig. 15—Calculation wheel for lime to feed for 0.025, 0.030, and 0.035 pct S steel.

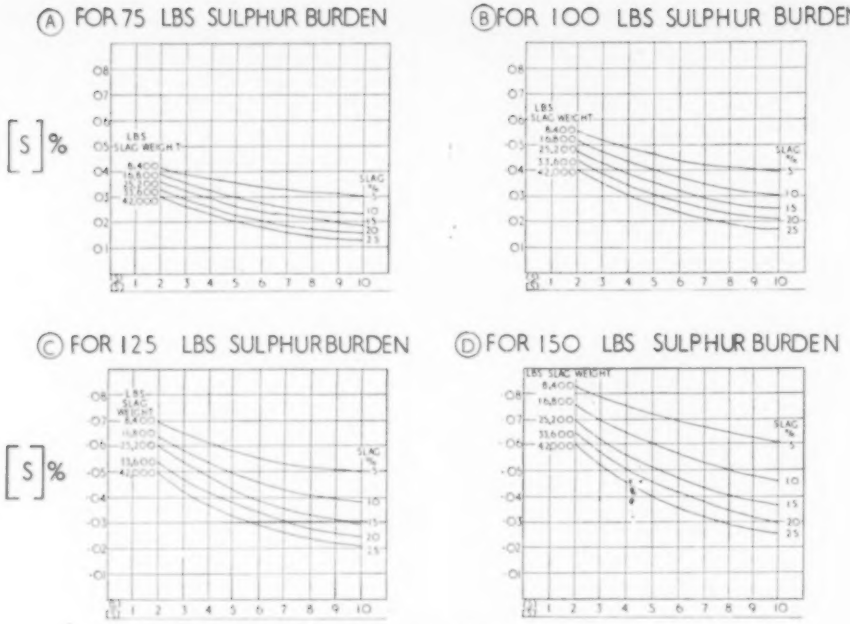

Fig. 16—Effect of varying $\frac{(S)}{[S]}$ and slag weight on final pct [S]. Steel weight is 168,000 lb.

taken, the difference between 0.022 and 0.027 pct sulphur steel represents a tolerance from 6.8 to 4.8 in $\frac{(S)}{[S]}$. The effect of errors of ± 4500 lb in the slag weight at junction is shown in Table III.

The degree of accuracy that can be obtained is, however, best judged by actual results, and for this purpose we have extracted the results from our No. 2 shop for a period of two months, of all casts made, excluding the first cast of each week, and this is shown in Table IV.* The comparison between the sulphur percentage ordered and the pit sulphur percentage actually obtained for the same series of casts is shown in Fig. 17.

It will be noted that there is some discrepancy between the calculated and the actual lime additions in certain cases. Where this occurs, the lime fed is, almost invariably, less than the calculated addition. The calculation for the lime addition is based upon a fixed $\frac{(S)}{[S]}$ at tapping and a fixed amount of lime eroded from the hearth for any particular carbon at junction. If either of these is higher than normal, the amount of lime that need be fed will be less than the calculated figure.

In actual practice in our shops, the latitude allowed in pit sulphur percentage rules the strictness in the pass sulphur percentage before tapping. For instance, when making 0.025 pct sulphur steel, one shop manager allows a furnace to tap after 0.028 pct has been reached with a lapse of 40 min and no further lime addition, provided that the carbon is down to specification even if all the calculated lime has not been added. The manager of another shop feeds all the calculated lime and does no pass tests.

* See footnote on p. 1038.

Things will of course tighten up, when the cost office discovers that a 0.020 pct sulphur steel costs more to make than a 0.025 pct steel. The official complaint will then be that the steel is too good for the job and not that it is not good enough.

Cost of Making Low Sulphur Steel

The relative slag weights required for making 0.025 pct sulphur steel in a furnace tapping 168,000 lb steel at 6 $\frac{(S)}{[S]}$ are shown by reference to Fig. 11b to be as given in Table V.

Reckoning from yearly consumption of lime and dolomite, the slag weight works out at 20 pct of our ingot production for all grades and over two shops. Steel is manufactured from 0.025 to 0.040 pct sulphur according to the order book. The difference in melting cost (i.e. fuel, reduction in steel, output and furnace repairs) in cash, is not known between our 20 pct slag and the common practice abroad of 8 pct. But on materials alone, the cost of the additional

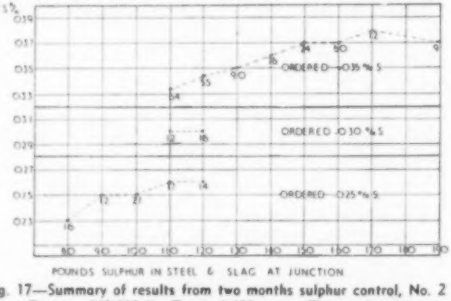

Fig. 17—Summary of results from two months sulphur control, No. 2 shop. Tapping 168,000 lb. Total of 498 casts. The number of casts is averaged under each point.

Table III. Effect of Errors of ± 4500 lb in Slag Weight at Junction

Slag Weight at Junction, Lb	Junction: S in Slag (S), Pct	Junction: S in Slag, Lb	Junction: S in Steel [S], Pct	Junction: S in Steel, Lb	Junction: Total Lb S	Tapping: Slag Wt in Lb	Tapping: Slag Wt, Pct	Tapping: S in Steel [S], Pct
18,800	0.24	45	0.04	66	111	46,000	27.4	0.025
18,800 + 4500	0.24	55	0.04	66	121	50,500	30.0	0.026
18,800 − 4500	0.24	35	0.04	66	101	41,500	24.7	0.024
18,800	0.36	66	0.04	66	132	35,000	20.8	0.035
18,800 + 4500	0.36	84	0.04	66	150	39,500	23.5	0.037
18,800 − 4500	0.36	51	0.04	66	117	30,500	18.1	0.034

lime and iron oxide (which is derived from the metallic iron of the charge) amounts to 8/6 or $1.30 per ton of steel.

The shop man using high sulphur raw materials and high sulphur fuel has to consider whether the yet unknown melting cost of at least 12 pct or 19,500 lb of slag per cast, added to 8/6 ($1.30) per ton for material cost, would not justify the spending of a good deal of money to reduce the weight of sulphur in steel and slag at tapping.

Sources of Sulphur in Steel and Slag

In our cold metal practice, the sources of sulphur weight in the furnace at tapping are as shown in Table VI.

The ways to reduce the weight of sulphur brought in by the pig iron, scrap, lime, spar and dolomite

Table V. Relative Slag Weights for Making 0.025 Pct Sulphur Steel

Wt S in Steel + Slag at Tapping, Lb	Slag Wt, Lb	Pct Slag Wt of Metal Wt
62	13,500	8
82	26,500	15
93	33,600	20

are so well known technologically that it remains merely a comparison of costs to choose, whether this incoming total sulphur weight is made small, or whether it is left large and desulphurized in the Siemens furnace at the expense of high slag weights.

We are fully aware of the technological ignorance on the one hand, and the possible money saving on the other hand, of reducing the weight of sulphur picked up from, or discharged to, the furnace atmosphere. We can but publish here such data as we have collected, in the hope that it may serve others. Up to the present, we have been quite unable to tie it together into any furnace practice rules.

Sulphur Pickup from Furnace Atmosphere

The histograms in Figs. 7 and 8, to which reference has already been made, show the spread of sulphur pickup from, or loss to, the furnace atmosphere, that

Table VI. Sources of Sulphur Weight in Furnace at Tapping

	Average Weight per Cast, Lb	Sulphur, Pct	Sulphur per Cast, Lb
Pig iron	62,800	0.03-0.07	19-45
Uprising scrap	58,200	0.025-0.05	15-29
Bought scrap	58,200	0.04-0.07	23-43
Lime	11,250	0.1-0.2	11-22
Dolomite	6,750	0.1-0.3	7-21
Spar	450	0.6-0.8	3-4
Oil		2.3-2.6	30- + 95
			48-259

had been obtained from charges made in the early stages of adoption of our process. Table VII shows the results for all our controlled charges to date.

It will be noted that the pickup, particularly from junction to tapping, has increased markedly from series V. Though other changes have taken place during the period under review, it is very significant that between series IV and V a change was made in our supply of oil. The sulphur content which was 2.4 to 2.5 pct before rose to 2.6 to 2.8 pct after the change. Table VIII shows the partition of sulphur between slag and metal at junction and tapping. It will be noted that there has been a distinct tendency for the $\frac{(S)}{[S]}$ at tapping to rise in the same way as the pickup of sulphur has risen. Fig.

Table VII. Pounds S Picked Up from (+) or Lost to (−) Furnace Atmosphere from Liquid System Steel and Slag

Series	No. of Charges	Start Charge to Junction: Average	Start Charge to Junction: Range	Junction to Tapping: Average	Junction to Tapping: Range	Start Charge to Tapping: Average	Start Charge to Tapping: Range
I	97	+ 31.6	− 30- + 90	− 8.8	− 50- + 30	+ 22.7	− 40- + 90
II	63	+ 21.5	− 20- + 70	− 9.8	− 50- + 40	+ 11.6	− 30- + 70
III	51	+ 41.3	− 10- + 100	− 13.2	− 60- + 30	+ 28.1	− 30- + 80
IV	38	+ 16.1	− 40- + 50	+ 4.8	− 30- + 40	+ 21.0	− 70- + 70
V	15	+ 35.6	+ 10- + 60	+ 29.0	0- + 70	+ 64.6	+ 40- + 110
VI	22	+ 30.2	+ 10- + 60	+ 22.5	− 20- + 50	+ 52.8	+ 20- + 80
VII	13	+ 43.5	+ 20- + 70	+ 15.4	− 10- + 50	+ 58.8	+ 30- + 90
VIII	32	+ 46.9	+ 10- + 100	+ 18.2	− 30- + 60	+ 65.0	+ 10- + 100

18 shows the relation between sulphur pickup between junction and tapping and $\frac{(S)}{[S]}$ at tapping for a number of individual charges. It can be seen that there is a trend for the high figures for sulphur pickup to be associated with high $\frac{(S)}{[S]}$ at tapping.

It can perhaps be argued that, if the sulphur passes from the furnace atmosphere to the slag, the sulphur in the slag does not necessarily reach equilibrium with sulphur in the metal, whereas, if the sulphur passes from the metal to the slag, then equilibrium is reached. If there is any truth in this

Table VIII. Partition of Sulphur between Slag and Metal

Series	Junction: Average	Junction: Range	Tapping: Average	Tapping: Range
I	5.8	2.3-9.8	5.2	3.9- 8.1
II	5.7	2.2-8.1	6.2	3.3- 9.3
III	5.8	1.9-9.8	6.8	3.0-10.3
IV	5.5	1.4-8.2	7.7	4.7-12.2
V	5.7	2.3-8.9	7.8	5.6- 9.7
VI	5.5	2.3-8.8	8.0	5.0-11.2
VII	6.2	3.2-8.8	7.9	5.7- 9.6
VIII	6.0	2.1-9.8	8.0	4.7-11.0

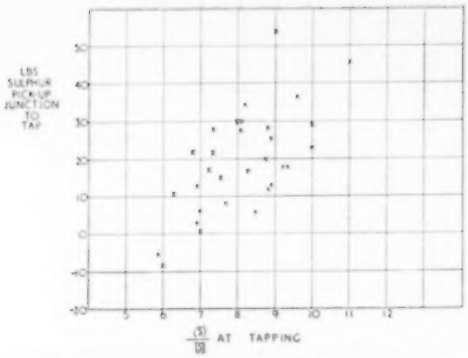

Fig. 18—Relation between sulphur pickup, junction to tap and $\frac{(S)}{[S]}$ at tapping.

explanation, it would help to explain some of the anomalies found between $\frac{(S)}{[S]}$ by analysis and by excess base calculations in the high $\frac{(S)}{[S]}$ range.

It is often stated that reducing conditions tend to favor sulphur pickup, so sulphur pickup has been plotted against factors likely to influence combustion conditions such as oil flow, steam flow, metered air, percent oxygen in the waste gas, etc., but so far no significant trends have been found. The amount of sulphur pickup from start charge to junction, does however, appear to be influenced by the weight of lime charged. Figures from one series of charges, in which a comparison was made between high and low phosphorus iron, with corresponding high and low weights of lime charged are given in Table IX. The reduced pickup is probably due to rather earlier slag formation and to the reduced amount of lime exposed directly to the flame.

Table IX. Influence of Weight of Lime Charged on Sulphur Pickup

No. of Charges	Wt Lime Charged, Lb	Average Sulphur Pickup: Start Charge to Junction	Average Sulphur Pickup: Junction to Tap	Average Sulphur Pickup: Start Charge to Tap
16	9400	50.0	17.8	67.4
16	5380	40.9	21.1	62.3

Fuel Burning to Control Gas Composition

We have read much and done much work on the furnace control necessary to burn fuel so that the gases sweeping the slag or particular geographic areas of the slag have a particular composition. It seems to us that, much as we want scientists to discover the chemistry of the passage of sulphur between specific mixtures of gases on the one hand, and solid pig, and scrap, solid lime, liquid slags, and liquid steel on the other hand, such knowledge will be of little use, until furnace men can reproduce in the furnace what the scientist may find he wants. Our part of the work may take as long and seem more impossible than theirs, but we think that furnace combustion control must precede any real effort the scientist may make. The stimulus to the scientist will become very real when he knows that we have the tools waiting to apply his discoveries. A start has been made on automatic continuous waste gas analyses and on the control of oil-air ratio on the results.

This problem was divided into two parts: 1—sampling, and 2—the invention of recording automatic analyzer. Sampling is considered to be a furnace fitter's problem and therefore we undertook it ourselves. The instruments were handed over to instrument makers and they were given, at the fur-

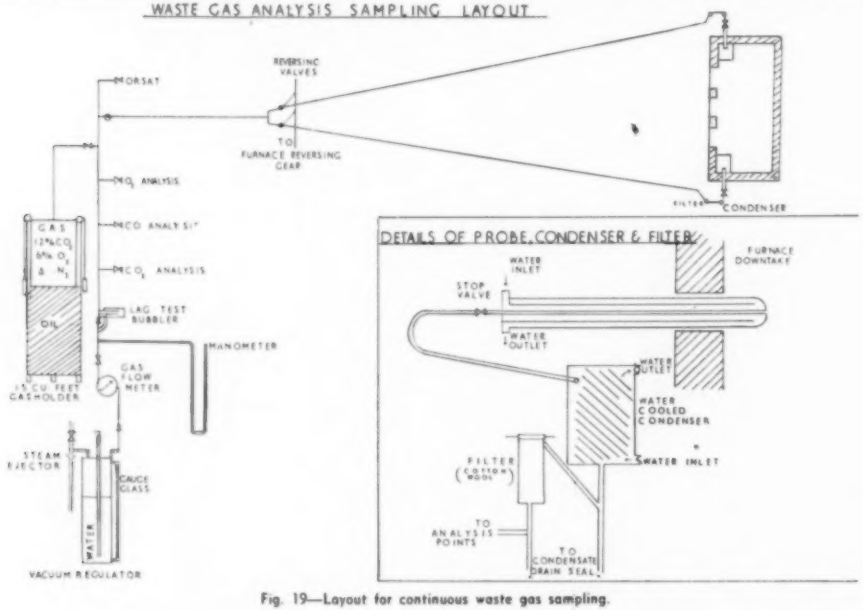

Fig. 19—Layout for continuous waste gas sampling.

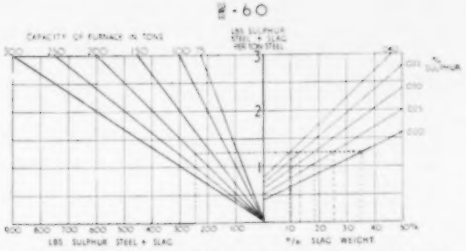

Fig. 20—Slag weights required for varying pounds of sulphur in furnaces of different sizes.

nace, a cool clean place and a pipe through which the gas that was to be analyzed passed at a rapid rate to waste.

The sampling arrangements have been successful for CO_2, CO, and, O_2, for which one sampling tube was used. This is shown in Fig. 19 with the testing apparatus both for the gas tightness of the sampling tube and the testing of the correctness of the gas analysis. These analyses are used on the experimental furnace to control the air screw by human link, but it is hoped that this will be incorporated in the fully automatic furnaces now being built.

A steam-lagged sampling tube for water in gas analysis was built successfully, but the instrument makers have, so far, failed in measuring automatically the water condensed in unit time. A satisfactory sampling method for SO_2 has not been devised and in addition, we are rather doubtful of any recording automatic analysis for SO_2, to operate on an open hearth furnace that has yet come to our notice. The difficulty in sampling is that iron oxide is such a good catalyst for SO_2-O_2 reaction and that water is such an excellent absorber of SO_2. We feel that some day we will have to return to it.

We are very much aware that the waste gases sampled in the downtake at stage level are not representative of the gases sweeping in the hearth at the middle door and much less at the first door. These are the places that count, and we are at a complete loss for the moment as to how to tackle the practical side of any solution that chemists may put forward. We must remember that it is not the chemists' job to give a practical solution. His job is to tell us the chemistry and it is ours to find the practical solution.

Conclusion

The process, which has been described, has provided us with a simple calculation that enables us to make steel to the sulphur specification required, from available raw materials. The process has been worked out specifically to meet our particular conditions. We would, however like to suggest that it forms a logical approach to the study of sulphur in the open hearth furnace. There should be no reason why it could not be modified to suit other conditions, in cases where sulphur governs the slag bulk.

The fundamental principle that we wish to stress is consideration of weights of slag, and steel, and of sulphur in each, in addition to the percentages of sulphur in slag and steel. The tacit assumption of so many workers, that the slag weight remains constant, is one that we cannot accept, and we should like to urge other investigators not to omit taking the weights into consideration. Fig. 20 gives the relation between pounds of sulphur in steel + slag and slag weight percentage required, assuming an $\frac{(S)}{[S]}$ of 6 for different sized furnaces.

Acknowledgments

This paper is presented as the work of John Summers & Sons. Means had to be found to continue to make low sulphur steel on all furnaces, despite increasing sulphur burden. All departments and organizations threw in their weight to achieve this end. The authors were given the job of organizing the work and are only mentioned as three of the gang at whom the technological public might aim their criticisms. Internal acknowledgments are therefore out of place.

We would wish, however, to thank Sir Charles Goodeve, Director of The British Iron and Steel Research Association (and our other friends in The British Steel Industry) for having allowed members of their staffs to give us so much help. They helped us with statistical work and hours of seemingly unprofitable conference, until one day, we found what we have published just lying on our office table.

Finally one of the authors was given much help by a short conversation with John Chipman and C. H. Herty, Jr. at a scientific conference in England.

References

[1] H. Schenck: *Physical Chemistry of Steelmaking.* P. 478.

[2] N. J. Grant and J. Chipman: *Trans.* AIME (1946) **167**, pp. 134-149; METALS TECHNOLOGY (April 1946).

[3] F. L. Robertson and W. Thring: *Journal* British Iron and Steel Inst. (September 1949) **163**, pp. 31-50.

[4] D. E. Babcock: *Yearbook* Amer. Iron and Steel Inst. (1949) pp. 250-321.

DISCUSSION, H. L. Tear presiding

S. L. Case *(Battelle Memorial Institute, Columbus, Ohio)*—What effect does the control of slag weight have on the production? If there is high sulphur in the charge at the start, there will be a high slag weight in order to meet the low sulphur specifications. What effect will this have on production?

C. H. Bacon (authors' reply)—That is rather a difficult question to answer satisfactorily. Production rate has gone up since we introduced the process, and it enables us to make the required lime additions early. We carried out a trial to compare the use of American low sulphur and phosphorus pig iron with our normal supply and we were able to show a reduction in slag weight and an appreciable increase in production rate. I think I can say we could work faster if we could keep the slag weight lower.

H. L. Tear *(Jones & Laughlin Steel Corp., Pittsburgh)*—Our answer to that, Mr. Case, is much different than Mr. Bacon's. It has a great deal of influence on production rates. Fig. 21 shows the lime consumption with the different specifications of sulphur; 80 pct of the heats are in the 0.025 S range and the effect of lower sulphur on lime consumption can be seen. Fig. 22 shows that, with different preliminary sulphur ranges, taking 0.04 as the base, as the first sulphur test goes up there is a loss in production rate, as indicated. With a preliminary sulphur of 0.071 or over, the production rate loss is in the neighborhood of 8 pct, which is much different from that reported by Mr. Bacon.

Mr. Bacon—I should just explain, Mr. Tear, that we have never had an opportunity to work with such low slag weights as you carry over here.

C. R. Funk *(American Locomotive Co., Latrobe, Pa.)*—Will you give us something on the rates?

Mr. Bacon—We have a small furnace and our rate of work is approximately 7.3 tons per hr, or 55 lb per sq ft of hearth area.

Mr. Tear—How many pounds of fluorspar?

Mr. Bacon—We use an average of 2 or 3 cwt of spar with the charge of 84 tons.

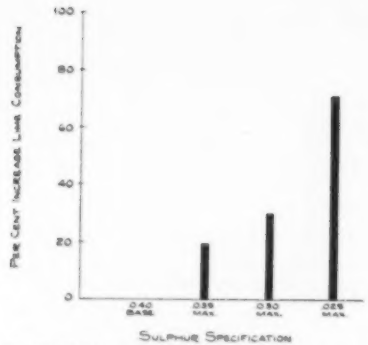

Fig. 21—Sulphur specification vs. lime consumption.

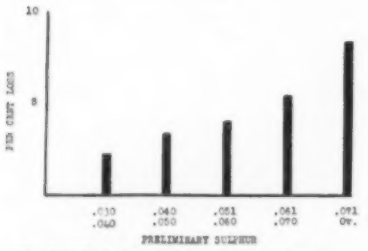

Fig. 22—Preliminary sulphur vs. production loss.

Mr. Tear—You add roughly 330 lb of spar per ton?

Mr. Bacon—No, per charge, about 3 lb per ton.

Mr. Tear—In our case it is around 14 lb of spar per ton of ingots with a slag rate of about 300 lb per ton.

W. A. Peters *(Laclede Steel Co., Alton, Ill.)*—How do you get the higher S over S value. If you want it up higher what do you do about getting it up there?

Mr. Bacon—The higher S over S values that we showed toward the end were our later charges and we assumed it to be due to the fact that we had a higher proportion of sulphur in the furnace atmosphere and a higher pickup of sulphur to the slag from the furnace atmosphere.

L. S. Darken *(U. S. Steel Co., Kearny, N. J.)*—If the sulphur burden is high at junction so that greater lime addition is required, it seems that this would increase the sulphur distribution ratio. The extra time as well as the lime might be expected to increase the sulphur pickup. Thus the correlation between distribution ratio and pickup may be indirect.

Mr. Bacon—I do not think we have any figures to show that the sulphur pickup is greater, when more lime is fed.

C. E. Sims *(Battelle Memorial Institute, Columbus, Ohio)*—Would the fact that the S over S ratio does increase with sulphur pickup indicate you probably did not have equilibrium between metal and slag? You have mentioned that you thought you did have equilibrium. This might indicate you did not.

Mr. Bacon—The suggestion is, that, if the sulphur is coming into the slag from the furnace atmosphere, we probably do not reach equilibrium between slag and metal, but if it is coming from the metal into the slag we are more likely to reach equilibrium.

W. T. Sergy—*(Jones & Laughlin Steel Corp., Pittsburgh)*—This junction seems to be in every correlation that you make and if I understand correctly a definite bath temperature is desirable at a certain carbon. Do you have any limits or range for bath temperature, or do you aim at one particular temperature for a certain carbon content of the bath?

Mr. Bacon—We aim at 0.3 to 0.5 pct C at junction. If we melt out at 0.9 pct C, we want a temperature of 1510°C; at 0.4 pct C, 1560°C.

Mr. Sergy—Does every heat have a junction?

Mr. Bacon—Yes.

Mr. Sergy—Suppose at 38 or 40 pct C you do not have the proper temperature?

Mr. Bacon—We do not call that junction from the point of view of taking samples.

Mr. Sergy—Do you add lime or any other flux on such a basis?

Mr. Bacon—No, we wait until we pick up the temperature and then we take the junction.

Mr. Sergy—And if you never get it?

Mr. Bacon—We have to pick up the temperature to attain a minimum temperature at tapping.

Mr. Sergy—What I am trying to resolve is, do you make any calculations on the amount of lime you would add when you do not have a junction?

Mr. Tear—I think Mr. Sergy means, if you get to the point where you have to refigure a heat do you apply this practice to that heat in the case of a soft melt?

Mr. Bacon—In the case of a very soft melt, we cannot always add enough lime to reach specification.

Mr. Sergy—When junction is not obtained due to too high a bath temperature, do you still make your calculations on that basis?

Mr. Bacon—If the temperature is high at the junction we can feed rapidly.

Mr. Sergy—And if you are low, you do not?

Mr. Bacon—If we melt very soft, we do have to anticipate the junction.

W. O. Philbrook *(Carnegie Institute of Technology, Pittsburgh)*—Have you had time to apply the waste gas analysis, and if so has any trend of variation of the sulphur pickup with the oxidizing potential of the atmosphere been noted?

Mr. Bacon—We have tried to obtain a relation but have failed so far. We have been using an absorption type of analyzer, which is not altogether satisfactory as it involves a delay of about 4 min. We have now installed a paramagnetic type of meter with a quick response. We shall check this on future charges.

T. S. Washburn *(Inland Steel Co., Chicago, Ill.)*—It would be interesting to know whether these relations vary with the carbon content of the bath: for example, 0.60 pct C as compared with 0.10 pct C.

Mr. Bacon—The data are all from low carbon steel.

Mr. Washburn—Consequently, the relations would not be the same for medium or high carbon.

R. L. Long *(Carnegie Institute of Technology, Pittsburgh,* and also from an English steel firm, *The Park Gate Iron & Steel Co., Ltd., Rotherham, England)*—There are two questions I wish to ask. First of all, is your sulphur determination equally rapid, and what is its accuracy? Second, you have mentioned a temperature carbon line for your junction. Is that based on a given superheat, say according to the carbon, or is it based on your own experience as to the suitable stage at which to commence feeding the charge?

Mr. Bacon—As regards the accuracy of the rapid sulphur determination in slag at junction, we consider it to be of the order of 5 or possibly 10 pct. On a slag of 0.22 pct S, the rapid method should give a figure between 0.21 and 0.23.

Mr. Tear—How did you arrive at the origin of the carbon temperature line?

Mr. Bacon—That was arrived at by experience on the furnace.

Mr. Funk—What is the depth of the bath? What do you do when you have a furnace that does not work very well? Is there a difference between a sharp working furnace and a sluggish working furnace?

Mr. Bacon—The depth of the bath is about 2 ft 6 in. for an 80 ton furnace. A sluggish furnace tends to pick up more sulphur than a sharp working one, but the greater part of this occurs before junction, so the analysis at junction should take care of that.

Discussion — Extractive Metallurgy Division*

St. Louis Meeting, February 1951

Sintering Practice at Josephtown Smelter (paper by H. K. Najarian, K. F. Peterson, and R. E. Lund. JOURNAL OF METALS, February 1951, p. 116) 1045

Arc Melting of Titanium Metal (paper by S. F. Radtke, R. M. Scriver, and J. A. Snyder. JOURNAL OF METALS, August 1951, p. 620) 1046

Thermodynamics of Iron-Silicate Slags: Slags Saturated with Gamma Iron (paper by R. Schuhmann, Jr. and P. J. Ensio. JOURNAL OF METALS, May 1951, p. 401) 1046

Metallurgical Reactions of Fluorides (paper by H. H. Kellogg. JOURNAL OF METALS, February 1951, p. 137). 1046

* TP 3173D. Since some of the annual meeting papers had not been published sufficiently in advance of the time this discussion went to press, discussion of these papers will appear when discussion is published next spring.

Sintering Practice at Josephtown Smelter

by H. K. Najarian, Karl F. Peterson, and Robert E. Lund

DISCUSSION, T. H. Weldon presiding

R. E. Powers *(Mellon Institute of Industrial Research, University of Pittsburgh, Pittsburgh)*—Several of the processing methods at the Josephtown smelter might well be considered by plants producing iron blast furnace sinter. In making blast furnace sinter the objectives are much the same as at Josephtown: To produce a strong yet porous agglomerate which has a size consist in a preferred range. The emphasis however is on production rate rather than on the size or other quality characteristics of the sinter. Therefore the technique is entirely different. Blast furnace sinter plants attempt to make their product in one pass with a minimum recirculating load and without sizing treatment after the sinter leaves the machines. Many plants are beginning to feel that more attention paid to quality characteristics would make the product a more desirable blast furnace material.

The pelletizing of very fine material before placing it on the bed is not deliberately done at iron sinter plants, although the installed equipment sometimes gives a similar action. Such pelletizing seems to be a promising way of accommodating the down-draft sintering process to very fine materials.

The recirculating load at Josephtown is extremely high. Two plants[1] producing blast furnace sinter from raw material of comparable size have a recirculating load of about 100 pct of production. At Josephtown it is notable that the size and the rate of feeding of return fines are under control. This is not the case in most blast furnace sinter plants. The sinter slicer appears to be a worthwhile aid in effecting such control. It is similar in action to rakes and plows used at a number of plants, but it has the advantage that the sinter dislodged is positively removed and not left to the inefficient action of a stationary grizzly screen.

Blast furnace size specifications for sinter are not at present so rigid as the Josephtown specifications. If the sizing of blast furnace sinter does become important, then the Josephtown crushing practice, in which a large recirculating load is maintained on the crusher in order that minimum fines be produced, may be of interest.

[1] R. R. Burns: Operation and Practice, Producing Iron Sinter at Ducktown and Copperhill, Tennessee, with Fine Flotation Sulphides. *Blast Furnace Coke Oven and Raw Materials Committee Proceedings.* AIME (1949) 8, pp. 146-150.

Fig. 2—Feed to Dwight and Lloyd sinter machine, Josephtown Smelter.

H. K. Najarian (authors' reply)—We note that Mr. Powers appreciates some points that we tried to emphasize in our paper as being of importance in making zinc sinter of good quality and which may well be applied to iron blast furnace sinter.

Fig. 2 shows the pelletized nature of the feed going on to a Dwight-Lloyd type sintering machine in our plant. Practically, the entire feed consists of more or less rounded particles which permit more uniform air passage through the charge, while the larger particles in the charge roll on to the surface of the grate, which helps to keep the grate openings from being clogged by excessive fines. An agglomerated charge of this character may preferably be made by rolling action while being mixed in a rotating drum and wetted by water sprays to bind the fine particles together and give the charge the desired moisture content. From our observations of several iron ore and blast furnace flue dust sintering operations, we believe that if the fines from the sinter discharged from the machines were to be recirculated and agglomerated with the new feed, not only sinter of better quality but larger capacity from the machines may be realized.

Arc Melting of Titanium Metal

by S. F. Radtke, R. M. Scriver, and J. A. Snyder

DISCUSSION, J. R. Long presiding

R. I. Jaffee *(Battelle Memorial Institute, Columbus, Ohio)*—The authors have written a fine and important paper, and are to be congratulated. I do not entirely follow their discussion of the relationship between the ductility of titanium and its crystal structure. Since high purity titanium is extremely ductile, being capable of cold reductions of over 99 pct, its ductility cannot be unduly restricted by its hexagonal crystal structure. It is true that interstitial solid solutions of nitrogen and oxygen do have a restricting effect on ductility, but this would appear to be an alloying effect rather than a crystal structure effect. The point made by the authors concerning the relative ductility between forged and rolled titanium does not appear to be conclusive, either. It would appear that in the same condition forged material would have equivalent or better ductility than sheet material. The difference between the ductility reported for forged bar and annealed sheet in Table I may be the result of a greater degree of cold work in the as-forged condition.

S. F. Radtke, R. M. Scriver, and **J. A. Snyder** (authors' reply)—We appreciate the discussion by Dr. Jaffee. His point is well taken that the hexagonal structure of titanium does not, in itself, restrict the ductility of iodide material and, therefore, should not be limiting in this case. It is true, however, that the ductility of different grades of titanium is not necessarily related to their hexagonal structure but more likely to their orientation and composition. It is also true that the presence of small amounts of foreign elements in hexagonal metals may have more pronounced influence on ductility than a corresponding quantity in cubic metals.

Average values from a large number of tests might show relatively better ductility for forged titanium than is recorded in Table I. The forged bars used in this work were tested in the annealed condition; little is known concerning the effect of forging practice on ductility in titanium metal.

Thermodynamics of Iron-Silicate Slags: Slags Saturated with Gamma Iron

by R. Schuhmann, Jr. and P. J. Ensio

DISCUSSION, N. Arbiter presiding

John Chipman *(Massachusetts Institute of Technology, Cambridge, Mass.)*—The activity of FeO in silica-saturated slags shown in Table V is about 0.40 in the temperature range 1260° to 1350°C. Recent measurements by N. A. Gokcen at 1600° lead to about the same value. He finds the oxygen content of liquid iron in equilibrium with silica and ferrous silicate slags to be 0.088 pct. Under pure iron oxide slags at the same temperature, it is 0.225 pct. The ratio places the activity at 0.39.

Metallurgical Reactions of Fluorides

by Herbert H. Kellogg

C. M. Decroly *(University of Brussels, Belgium)*—The importance of the fluorides in the process metallurgy of special metals has already been accepted and it will probably increase in the future. Free energy diagrams as such established by Professor Kellogg are therefore very useful.

It is interesting to note that the absolute value of the standard free energy of formation of HF increases with temperature, whereas for almost all the other fluorides it decreases; consequently it should be theoretically possible to reduce all the fluorides of the metals which, at low temperature, have a greater affinity for fluorine than hydrogen by this last element, provided a sufficiently high temperature is used in order to have a good efficiency.

However, with regard to the reduction of UF_6 by hydrogen, I doubt that it will be possible to obtain directly the metal at comparatively low temperatures. There are other uranium fluorides which are more stable than UF_6 and it is very likely that such fluorides will be obtained first. For example, in considering the reaction:

$$UF_{6\,gas} + H_{2\,gas} \rightarrow UF_{4\,solid} + 2\,HF_{gas}$$

it is found, using the thermodynamic data of Brewer et al, that $\Delta H_{298} = -66$ kcal and $\Delta G^\circ_{298} = -65.2$ kcal. As a result, the reduction of UF_6 to $UF_{4\,solid}$ should proceed spontaneously even at ordinary temperature. On the other hand, the standard free energy of formation of $UF_{4\,solid}$ at 298°K is $\Delta G^\circ_{298} = -209$ kcal per mol of F_2. The reduction of UF_4 by hydrogen will be practically difficult and, as it is known, the only practical way of reducing this compound is to use alkaline-earth metals such as calcium or magnesium. I should like to point out, further, that the fluorination of many metal oxides can be carried out very easily by using the ammonium difluoride method of preparation, which renders the use of fluoride gas unnecessary. The first compound formed is generally a double fluoride of the metal and ammonium. This compound can be decomposed by heating either in a vacuum or in an inert atmosphere, ammonium fluoride being volatilized leaving the metal fluoride in a very pure state.

H. H. Kellogg (author's reply)—Professor Decroly is quite right in pointing out that the formation of lower halides of uranium may complicate the reduction of UF_6 by H_2. I was unable to find his reference to the free energy of formation of UF_4 in the compilation of Brewer,[15] however. The value of $\Delta G^\circ_{298} = -209$ kcal for formation of ½ UF_4 seems rather high, and I hope the source of this value may be made clear.

Discussion — Iron and Steel Division*

St. Louis Meeting, February 1951

A Thermodynamic Study of the Reaction CaS + H_2O ⇌ CaO + H_2S and the Desulphurization of Liquid Metals with Lime (paper by T. Rosenqvist. JOURNAL OF METALS, July 1951, p. 535) 1047

Effects of Manganese and Its Oxide on Desulphurization by Blast-Furnace Type Slags (paper by N. J. Grant, U. Kalling, and J. Chipman. JOURNAL OF METALS, August 1951, p. 666) 1048

Effect of Silica Reduction on the Desulphurizing Power of Blast-Furnace Type Slags (paper by N. J. Grant, O. Troili, and J. Chipman. JOURNAL OF METALS, August 1951, p. 672) 1049

Distribution of Sulphur Between Liquid Iron and Slags of Low Iron-Oxide Concentrations (paper by R. Rocca, N. J. Grant, and J. Chipman. JOURNAL OF METALS, April 1951, p. 319) 1050

Desulphurizing Molten Iron with Calcium Carbide (paper by S. D. Baumer and P. M. Hulme. JOURNAL OF METALS, April 1951, p. 313) 1051

Desulphurization of Pig Iron with Pulverized Lime (paper by B. Kalling, C. Danielsson, and O. Dragge. JOURNAL OF METALS, September 1951, p. 732) 1052

Kalling-Domnarfvet Process at Surahammar Works (paper by S. Fornander. JOURNAL OF METALS, September 1951, p. 739) 1052

Low Sulphur Steel from High Sulphur Raw Materials and Fuel (paper by F. L. Robertson, C. H. Bacon, and J. W. Till. Discussion is printed with the paper. This issue, p. 1031).

Solution Loss and Reducing Power of Blast Furnace Gas (paper by T. L. Joseph. JOURNAL OF METALS, January 1951, p. 37) 1053

Oxygen in Liquid Open-Hearth Steel — Oxidation during Tapping and Ladle Filling (paper by T. E. Brower, J. W. Bain, and B. M. Larsen. JOURNAL OF METALS, June 1950, p. 851) 1054

* TP 3172C. Since some of the annual meeting papers had not been published sufficiently in advance of the time this discussion went to press, discussion of these papers will appear when discussion is published next spring.

Thermodynamic Study of the Reaction CaS + H_2O ⇌ CaO + H_2S and the Desulphurization of Liquid Metals with Lime

by Terkel Rosenqvist

DISCUSSION, W. O. Philbrook presiding

J. Chipman *(Massachusetts Institute of Technology, Cambridge, Mass.)*—The fact that the experimental work has been applied to copper rather than iron and that the paper is presented to the Iron and Steel Division, I regard as rather significant. It shows the unity of metallurgy and the fallacy of trying to cut it up by metals. This result for the solubility of sulphur in molten copper correlates with Professor Schuhmann's finding that the published data on the other side of the copper-sulphur miscibility gap are also in error. I should like to ask the author to say a little bit more about the sulphur capacity of the slag.

T. Rosenqvist (author's reply)—I hope that Dr. Chipman will find the derivation of the expression for sulphur capacity more clearly explained in the printed version of the paper than in the oral discussion at the meeting. I feel that this quantity, which actually is the ratio of two activities, can be measured more easily than the individual activities. Even if the ratio CaO/CaS is chosen as the standard state, the expression can be used for any slag, even for slags completely free of lime, and it represents a way to put the desulphurizing power of all slag constituents into one bag.

Some doubt has been expressed as to whether oxygen ions really exist in calcium oxide and in molten slags. From a thermodynamic view point that question is of minor importance. The term oxygen ion activity, or any activity for that matter, is defined rigorously by the equation: activity = $\exp \mu/RT$, where μ is the change in free energy connected with the transfer of one mol of ions from the standard state into the slag. Whatever happens to the ion in the slag is of no concern to the thermodynamicist. Regardless of whether the ion is "free" in the slag or not, or whether it is present in a very small amount, its activity can always be expressed, and for a thermodynamic calculation that is all we need. However, ionic activities will only be of some real value if they are simple functions of the slag composition, or can be measured easily.

Concerning the real nature of the oxygen in the slag, my feeling is that the oxygen atom has a rather multiplex nature depending on how strongly it is tied by covalent forces or polarized by the other atoms or ions present. The oxides of iron, cobalt, and nickel differ from calcium oxide and blast furnace slags as to the amount of free electrons that can give rise to electronic conductivity. In slags we know that the conductivity is mostly ionic. The fact that reversible emf's can be obtained with oxygen electrodes in certain salt melts, indicates a significant amount of oxygen ions in these melts. But extended work, e.g. polaragraphic studies and measurements of transference number, are needed to obtain quantitative information about the real structure of the slags.

D. E. Babcock *(Republic Steel Corp., Youngstown, Ohio)*—With reference to the ion, it might be well to remember Dr. Moses Gomberg. All of his life he had no use for the ionization theory and he contributed greatly to the field of chemistry on the assumption there was no such thing as ions. I do not think we have to worry about whether the oxygen is ionic or not. I think one thing specifically should be brought to your attention and this I think is one of the important contributions of Dr. Rosenqvist. He pointed out what we know as oxygen potentials or what is described as oxygen potentials. I have used this concept for a long period of time and I want to state that if this concept is properly applied, it vitiates much of what we have in the literature, or makes our usual ideas regarding oxidation seem primitive. That one thing is more valuable than almost all the rest of the discussion as a fundamental basis on which to build a reasonable in-

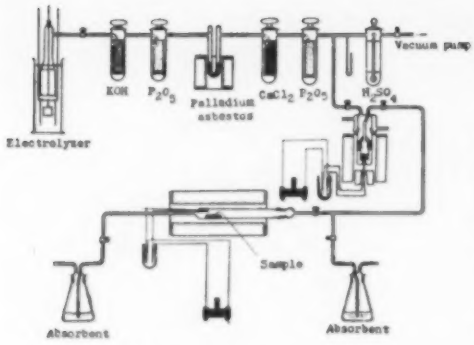

Fig. 9 (above) — Apparatus used in studying the reaction between calcium oxide and hydrogen sulphide.

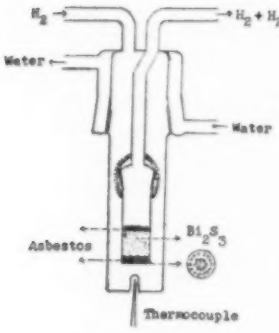

Fig. 10 (left) — Apparatus used to prepare hydrogen and hydrogen sulphide mixed gas.

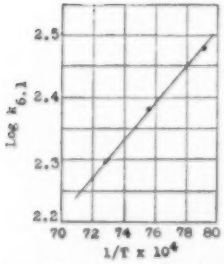

Fig. 11 — Effect of temperature on the equilibrium constant.

terpretation of some of the oxidation phenomena which up to date are poorly interpreted.

It is interesting to bring up another point that Dr. Rosenqvist mentioned about the hydrogen sulphide-water equilibrium, etc. He mentioned the blast furnace in passing. The data of Dr. Darken and some others indicated that as the moisture went up in the blast furnace, sulphurization was somewhat better. I have been told it is a statistical phenomenon, but it stirs up one's curiosity to do a little looking around relative to the reason that this fact has existed. We do not have anything like the whole answer to this.

If you use the concept of the saturation point of slag and compute the kinetics in the blast furnace, you find if the blast furnace is operated like the laboratory experimental runs, it would not produce. It is interesting and there is more to look at than appears on the face of the data. We have looked so long at the slag, many of us are blinded by the fact that from 75 to 90 pct of all the desulphurization occurs before metal is in contact with a liquid slag.

Tatsuji Uno *(Hokkaido University, Sapporo, Japan)* —I have been studying the desulphurization reactions of iron and steel for many years, and finished the study on $CaO + H_2S \rightleftharpoons CaS + H_2O$ several years ago, but had not been able to publish it, because of the difficulty of printing during and after the war. Fortunately, I could publish it in the *Journal* of Iron and Steel Institute of Japan (Tetsu to Hagane), January 1951.

The apparatus used is shown in Fig. 9. Passing the mixture of H_2S and H_2 over CaO and regarding the difference of H_2S content in the gas mixture before and after the reaction as H_2O formed, the equilibrium constant for this reaction was calculated as $K = p_{H_2O}/p_{H_2S}$.

When H_2 gas passes through H_2S producer shown in Fig. 10, a mixture of H_2S and H_2 of desired composition is obtained by heating Bi_2S_3 at the proper temperature. Therefore, it can be said that my experiment was carried out from the opposite side compared to Dr. Rosenqvist's. I obtained following results from 1000°C to 1100°C:

$$\log K = 3231.8/T - 0.060 \text{ (Fig. 11)}$$

As I used transparent quartz tube, it was difficult to make determinations above 1100°C, and the amount of H_2S at 900°C, was so small, that the experimental errors had largely affected the results. For these reasons, my experiment was limited to a small temperature range.

But I am much pleased to find that your results, obtained over a wide temperature range, are in good agreement with mine.

Dr. Rosenqvist—It is a great pleasure to see that Dr. Uno, with a different technique, has arrived at equilibrium values very close to those obtained in my investigation. In the temperature range 1000° to 1100°C the two sets of values differ by 100 cal or less, which is as good as one can expect in work of this kind. The fact that Dr. Uno has approached the equilibrium from the opposite side as compared to my work, shows that true equilibrium has been obtained.

It is only regrettable that the publication of Dr. Uno's work has been delayed so his data were not earlier brought to my attention.

Effects of Manganese and Its Oxide on Desulphurization by Blast-Furnace Type Slags

by Nicholas J. Grant, Ulf Kolling, and John Chipman

DISCUSSION, D. C. Hilty presiding

D. E. Babcock *(Republic Steel Corp., Youngstown, Ohio)*—I would like to know what evidence you have to prove the MnO was pure MnO. I would also like to know whether you might not explain it on the basis of a temperature reversion; and, was it due to the oxidizing power of MnO?

N. J. Grant (authors' reply)—Briefly, we have no proof that pure MnO was used. The manganese oxide was added as chemically pure MnO_2. MnO is assumed as the oxide in the reacted slag following standard molecular slag theories, especially under the reducing conditions of these experiments. The noted sulphur reversion cannot by any means be explained on the basis of a temperature reversion since the temperature effect is shown in this paper to be very small. Until a more logical explanation can be offered, backed I hope by some experimental proof, we propose to explain this sulphur reversion as stated in the paper, namely, that it is due to the oxidizing effect of the added manganese oxide.

Member—How did the oxygen in the slag give you a reversion of sulphur? What was the mechanism there?

Dr. Grant—One of the simpler possible explanations is that the oxygen replaces the sulphur in calcium sulphide, for example. The reaction might be written as follows:

$$CaS\ (slag) + \underline{O} = CaO\ (slag) + \underline{S}$$

Dr. Babcock—This paper was entitled in relation to blast furnaces. The inference was made that it is a laboratory analogy of a blast furnace process.

Dr. Grant—That is exactly what was intended.

Dr. Babcock—I think that is not a good idea because it gives us a notion that some things happen in a blast furnace that just do not happen. For example, we get results in a blast furnace that do not fit this picture. You say calcium oxide is several hundred times or so, as effective as MgO. Is that correct?

Dr. Grant—That is right.

Dr. Babcock—We can, by statistical methods, operate on plant data to determine what the effect is, pretty closely. It is not of that order of magnitude.

The next thing that is of interest is the fact that MgO is in a slag system in which perhaps the physical chemical equilibrium between the associated groups would lead to the conclusion that MgO at any other time could by simple mass effect displace the lime from combination with the other ions or molecules, or whatever you have, so that to discriminate and infer that the effect is only due to lime and not due to lime displacing magnesia in certain systems, I think would be false.

It has been a serious problem to tie together the data of Mr. Hatch, where he figured in his report published by the AIME that the mol for mol excess equivalent effect of magnesia as compared to lime was on the order of two-thirds. Now, we have a ratio of a couple of hundred. The difference of two-thirds effective as lime and a couple of hundred, is a wide gap. Would you put those two things together?

Dr. Grant—Such evidence of the superior desulphurizing power of CaO over MgO, notwithstanding manipulated statistical data, is presented in this paper in graphical form, and was also shown for the Hatch and Chipman[8] data in a recent paper by Sherman and Grant.[9] The results from these two different sets of data are in full agreement. The thermodynamic substantiation of the vastly superior desulphurizing power of CaO compared to MgO is noted in the 1600°C equilibrium constants recently calculated by Chipman (*Basic Open Hearth Steelmaking*, Chap. XVI, 2nd Edition, 1951, AIME), and reported in the work of Rocca, Grant and Chipman.[8]

B. M. Larsen *(U. S. Steel Co., Kearny, N. J.)*—On the practical effect of MgO on sulphur we propounded some data and Kennedy did some work after that, and we found other data later on. All seem to agree that up to around 6 or 8 pct MgO in the slag, the sulphur ratio increased and above that it seemed to fall off again. From that we inferred that the probable effect of MgO was mainly to give more fluidity to the slag and perhaps thus increase the reaction rate.

Dr. Grant—I think that in the case of actual blast furnace work, where the fluidity of the slag and the degree of mixing can be extremely important, that you can ascribe it to the effect of fluidification through the addition of MgO; but if MgO is a good desulphurizer, why should the sulphur ratio fall off after 6 or 8 pct MgO?

Member—The answer to the MgO is that by putting more into the basic slag you get into trouble with the basic slag itself.

Mr. Larsen—There is very likely a wider range of fluid slag compositions with more MgO. But the only point is in respect to the assumption involved here. We do not really know what the liquid constitution of the slag is, and I think maybe the authors might be willing to admit these are rather wild approximations.

Dr. Grant—They may not be exact, but they are hardly wild.

C. L. T. Edwards *(Dept. of Commerce, Washington, D. C. Temporarily with the Industrial Evaluation Board)*—I like everything the speakers have had to say thus far and was particularly impressed with the slight reversion as indicated in the curve.

The heat of combination between magnesium and sulphur is 2481 cal per unit weight of sulphur; the heat of combination between calcium and sulphur is 2947 cal, showing very definitely that calcium, theoretically, has a higher affinity for sulphur than magnesium does and I have found in practice, it has worked out that way in the blast furnace.

Now, in connection with manganese, iron and sulphur, I would like to tell you how, in my very small way, a few simple experiments were made in order to obtain some visible evidence concerning reactions. You scientists might do this on a more thorough scale and come up with something that is really good. Many of you, undoubtedly, have heated a mixture of powdered iron and powdered sulphur. If any of you have not done so, or seen it happen, touch the side of the crucible with a Bunsen flame and as soon as the reaction begins, remove the flame and you will find the heat will progress uniformly across the body of the mixture and, without benefit of a pyrometer, I would say the temperature of the reaction would be somewhere around 1700°F.

The heat of combination between manganese and sulphur is almost exactly double the heat of combination of iron with sulphur. Make up a mixture of manganese and sulphur in atomic proportion. Be very very careful, because the resulting reaction will be dangerous. Move the flame to the side of the crucible and be sure to have a shield for protection, as the reaction is most violent and you are lucky if everything does not fly out of the crucible. What the temperature will be, I do not know, but would guess it to be somewhere around 2700° or 2800°F.

Now, here is where the pay-off comes. Take iron sulphide, FeS, and mix it with powdered manganese; move the flame to the side of the crucible and you will find a reaction that takes place at somewhere around 1700°F. The indications are, of course, that manganese is about twice as potent a desulphurizer as iron, and it might be a good idea to keep that in mind and think about it.

I believe it to be a worthy assumption, that, since manganese sulphide has such a high melting point, there is a strong tendency for it to coagulate in the molten metal and the problem at once becomes one of mechanics, i.e., how to bring these coagulations into contact with the slag under a nonoxidizing, or reducing, atmosphere. Do not make the error of writing off manganese—learn how to use it.

Effect of Silica Reduction on the Desulphurizing Power of Blast-Furnace Type Slags

by Nicholas J. Grant, Olaf Troili, and John Chipman

DISCUSSION, D. C. Hilty presiding

D. C. Hilty *(Union Carbide & Carbon Research Laboratories, Niagara Falls, N. Y.)*—How does this effect of silica compare with the effect of silica in combining with the lime in the slag to reduce the activity of CaO, thereby affecting the first equation?

John Chipman (authors' reply)—That is the object of showing this effect for slags of two different basicities. In the more basic, the silica is more firmly tied up in the slag and is less easily reduced. It is therefore less able to interfere with desulphurization. The important point is that silica is acting in two ways. Of course it is an acid and as an acid it ties up lime and in tying

up lime it interferes with desulphurization; but it also acts as an oxidizing agent as I have shown, and this interferes in a second way with desulphurization.

Alumina, on the other hand, although it may be an acid, does not prevent rapid desulphurization because the alumina is not reduced to any substantial extent.

In the case of MnO, we have a basic oxide which ought to supplement the other oxides in neutralizing silica or taking sulphur out of the metal, but in spite of that it interferes with desulphurization on account of its strong oxidizing power.

D. E. Babcock *(Republic Steel Corp., Youngstown, Ohio)*—On the first equation you have used carbon as a reducing agent and referred to the fact you did not have carbon on the open hearth. Would you not think the iron bath is a pretty powerful reducing agent with a tremendous potential?

Dr. Chipman—The reducing potential of the iron bath depends entirely on the oxygen content and other metals present. In the open hearth it is not a powerful reducing agent, especially at low carbon content.

Dr. Babcock—It is common practice to use a bessemer converter to blow out the manganese and silica, leaving the carbon almost untouched for quite a long time, indicating the carbon is not available for reaction. That is the same experience we had when we desilicized iron in the open hearth. We take out the manganese and silica, direct proportions one to the other, but do not lose the carbon, meaning the carbon in kinetic reaction is extremely slow to react. Why do we have to use carbon when it could just as well be manganese, which reacts more rapidly, or silica alone, which is more powerful and readily available to react with lime?

Dr. Chipman—Not necessarily. We have expressed the equations with carbon as the reducing agent since under our conditions it is the most powerful reducing agent present both in the blast furnace and in most of our experiments. The fact that silicon and manganese are removed by blowing or oreing hot metal has no bearing on the problem. The behavior of these elements is highly dependent on the slag which is entirely different in the two cases.

Dr. Babcock—Then are you not making the assumption that the carbon controls the end limit and does not prescribe the mechanism, because the assumption is based on final equilibria state and not the process in between?

Dr. Chipman—Of course, and the equation represents, as I have said, the simplest possible way we can write the desulphurization reaction. If you wish to write it in kinetic steps (and we do not know what the steps are) the result would be most complex.

C. E. Sims *(Battelle Memorial Institute, Columbus, Ohio)*—We know we can get substantial desulphurization under oxidizing conditions in either the open hearth or electric furnace. Do you think the first reaction illustrates the basic reaction under this condition?

Dr. Chipman—This illustrates the reaction when you have carbon present. If you wish to let the "C" represent dissolved carbon, it still represents the reaction, although at a much lower carbon potential. The whole question of this reaction in intermediate slags of electric furnace type which lie between basic open hearth and blast furnace, is going to be the subject of a paper (Rocca, Grant, and Chipman) and for this reason, I would rather omit the question for the present.

L. S. Darken *(U. S. Steel Co., Kearny, N. J.)*—This general picture that a deoxidation, involving the removal of a relatively small amount of oxygen, is the slow step in the overall desulphurizing reaction seems to fit well the data presented. This automatically raises the question as to how we are to interpret the fact that oxygen is such a stumbling block for desulphurization, and I was wondering what Dr. Chipman would think of the possibility of blaming the slowness on the difficulty of gas nucleation?

We might think that oxygen from the MnO or the SiO_2 would be removed by the carbon as carbon monoxide, but if there is no gas phase in immediate contact with metal and slag, then gas bubble nucleation would be required. Does the difficulty of such nucleation fit your general picture as responsible for the slowness?

Dr. Chipman—I have no picture that is contrary to that. I think it is as good as any other but I had not hoped at this stage of the study to be able to identify the slow step.

Distribution of Sulphur Between Liquid Iron and Slags of Low Iron-Oxide Concentrations

by R. Rocca, N. J. Grant, and J. Chipman

DISCUSSION, D. W. Murphy presiding

D. E. Babcock *(Republic Steel Corp., Youngstown, Ohio)*—With reference to eqs 7 and 8, at what temperature do they apply?

John Chipman (authors' reply)—That was 1600°C.

Dr. Babcock—You have $1x10^{-4}$ as the component for the lime and 1 or $4x10^{-2}$. Now, is it by dividing one into the other you get the 400? That is assuming equivalent activity on the part of oxygen, sulphur, and magnesia.

Dr. Chipman—Yes, they are calculated for 1600. Now, the first one for CaO was calculated before we had a glimpse of Dr. Rosenqvist's paper.[18] If you take his calculation you get 14,000 cal which is very good agreement, but our calculation would be superseded by Dr. Rosenqvist's new data.

Dr. Babcock—The state you assume those to be in is the liquid state, as near as you can measure?

Dr. Chipman—Naturally it is based on the solid CaS, but if you add the effect of fusion on both sides it just about balances out, so the ratio would be about the same.

B. M. Larsen *(U. S. Steel Co., Kearny, N. J.)*—If we knew the activity of sulphur in the slag instead of merely the percentage, we might be able to find some conflicting factors that balance one another out, and find that the FeO or oxygen pressure effect is really present over the whole range.

Dr. Chipman—I am fairly sure we would. The activity of sulphur in the slag and the activity of CaO in the slag, if we just knew those quantities, would enable us to save a lot of this computation and assumption and all the approximations we are doing now.

Mr. Larsen—Two other points perhaps should be included: 1—an independent effect of manganese in helping the desulphurization; and 2—the number of mols of constituents or number of mols of ions or whatever there is in the slag could vary with these compositions in such a way that you get dilution effects.

Dr. Chipman—You can figure all that in if you want to and it might improve the degree of approximation a little bit. Maybe enough to justify the labor of calculation, maybe not, but we did not do it.

L. S. Darken *(U. S. Steel Co., Kearny, N. J.)*—The authors have tackled a very complicated problem in trying to tie together in one picture the desulphurizing problem over the wide range of basicity and oxidation level from that of the open hearth to that of the blast furnace. At the present state of our knowledge of slags such an ambitious undertaking necessarily involves the adoption of numerous hypotheses.

Their formulation (eq 11) for the higher FeO range

[18] T. Rosenqvist: JOURNAL OF METALS (July 1951), *Trans.* AIME, p. 535. Discussion, this issue, p. 1047.

is similar to that presented by Darken and Larsen[19] except that manganese is absent in the present case. This is based on a molecular picture of slag composition, which seems less valid now but is still used because we have no adequate way of expressing the relation otherwise. The principal difference of the present treatment is the bald assumption that the distribution coefficient (L_{FeS}) for iron sulphide varies rather markedly and gives rise to the minimum of the curves of Figs. 6 and 7. The evidence as to the nature of this variation seems rather meager, particularly as K' is apparently assumed constant; K' might reasonably be expected to vary as much as L_{FeS}, or even more, by virtue of the arbitrary nature of the calculated excess CaO. Thus the conclusions as to the effect or lack of effect of FeO (in the higher range) on the desulphurization ratio seem rather questionable. This is emphasized by the fact that the authors reach the conclusion that the sulphur combined with lime becomes negligibly small if FeO exceeds 10 pct. The efficacy of lime as a desulphurizer in this range is well attested by both mill and laboratory experience; the attribution of this effect to secondary factors seems misleading.

Since the melts of this investigation were made in a magnesia lined furnace, the slags were presumably saturated or nearly saturated with magnesia. Hence the activity of MgO is substantially constant and the contribution of MgO to the desulphurizing power of the slag would be difficult if not impossible to detect.

Dr. Chipman—Dr. Darken's remarks as usual are quite correct but apply mainly to the oxidizing ranges of the slag. The treatment here does not differ too much from that of Darken and Larsen.[19] We did not have manganese to put into the equation so that simply makes it easier. We did not know how the FeS distribution would vary with composition. We were a little afraid to assume it was constant as had been done before so we just arbitrarily said that we will suppose it is proportional to the FeO content of the slag. Certainly, we have no evidence one way or the other that this has any merit. That turns out to be a small part of the consideration in the more reducing slags with which we have been here primarily concerned. The introduction of the high FeO slag was brought into the paper mainly to show the relationship between the low FeO slags about which the paper was chiefly concerned and the high FeO slags that had been studied previously. The contribution of the paper lies in the field of the low FeO slags and we claim nothing new with respect to the high FeO.

D. J. Girardi *(Timken Roller Bearing Co., Canton, Ohio)*—I am left with the impression that for reducing slags where FeO values are somewhere around 4 pct and under, the FeO value is much more important than the lime silica ratio; is that correct?

Dr. Chipman—That is correct according to our findings; perhaps not as high as 4 pct, from 2 pct on down, the FeO content is much more important than the lime.

Dr. Girardi—It seems as though the lime silica ratio has an insignificant effect.

Dr. Chipman—Not insignificant, but a small effect compared to the FeO.

Mr. Larsen—You do not see that some of these deviations vary much on a log scale that way. We noticed, for example, that there were large deviations in very basic high MnO slags when we tried to calculate on an excess basis concept. You tend to get ratios up to 13, 14, 15 to 1 (slag sulphur to metal sulphur) yet you cannot very well explain it on a straight excess base.

Dr. Chipman—How do you explain it?

Mr. Larsen—It fits if you consider the MnO and the free CaO as affecting the sulphur activity independently and additively. Of course, I will admit the old formula of ours was very rough.

Dr. Chipman—I think you have something there because MnO in the open hearth is a better desulphurizer than we have given it credit for. We have talked about MnO not being a good desulphurizer in the blast furnace slags because of oxidizing power where you do not want oxygen, but where you are already highly oxidized as in the open hearth slag-metal system, then the MnO no longer has an oxidizing power, it may be at equilibrium with Mn in the bath or substantially so. Eqs 7 and 8 show the values for K for CaO and MgO. I want to show you how MnO fits into this.

The value of K for CaO is about 400 times that for MgO. Comparing CaO with MnO the K is only twice as large. Thus MnO is a much better desulphurizer than MgO and nearly as good as CaO.

Mr. Larsen—Practical experience would indicate that the ratio of effect between CaO and MnO is only 2 or 3 or even less.

Dr. Chipman—Yes, I think it would.

[19] L. S. Darken and B. M. Larsen: *Trans.* AIME (1942) **150**, p. 87.

Desulphurizing Molten Iron with Calcium Carbide

by S. D. Baumer and P. M. Hulme

DISCUSSION, T. L. Joseph presiding

B. M. Larsen *(U. S. Steel Co., Kearny, N. J.)*—Could we have some sort of an estimate on the cost of calcium carbide for this treatment? Also, if you used calcium carbide on carbon-saturated iron, would some effect hold back the reaction?

P. M. Hulme (authors' reply)—As far as I know we have not worked on carbon-saturated iron. About 3½ pct C is the highest we have worked on. As far as cost goes, it depends on how much sulphur you have to take out. It will run anywhere from $0.75 to $2.00 a ton overall cost including the cost of carbide per ton of metal treated. That is, using the efficiencies that we show in this paper. We are getting better efficiencies now.

T. L. Joseph *(University of Minnesota, Minneapolis, Minn.)*—Did you say 2 lb of calcium compound?

Mr. Hulme—That is based on 10 lb of calcium carbide per lb of sulphur removed.

D. E. Babcock *(Republic Steel Corp., Youngstown, Ohio)*—We have run this type of desulphurization process at the blast furnace. We have desulphurized between 100 and 200 at the blast furnace and taken the iron right out of the furnace with an injector system. The process gave us quite varied results; stratified iron, high sulphur on the top and low sulphur on the bottom, and we decided it was impractical.

Mr. Hulme—Just what was the type of injection equipment?

Dr. Babcock—Nitrogen gas for one injection method and we used fairly large gun equipment. We followed the same general type of pattern you show only on a larger scale.

Mr. Hulme—It sounds very much like what we call the gale of wind method. We have very erratic results with that.

Dr. Babcock—We have tried several types, and particle sizes. The operation was not satisfactory.

Mr. Hulme—Of course, we have never tried it on that scale except on a continuous basis. That is the reason we abandoned the idea of working on 35 ton ladles on a batch principle and took it as it came out of the cupola and treated it on the fly on a continuous basis.

Dr. Babcock—When you compare the relative effectiveness of the process as carried out, it does not give a very favorable comparison of that process which is already developed. We did not feel it was worth the

money and effort to go any further, since it did not show the performance and simplicity of the other process.

Mr. Hulme—I am a little doubtful of its value on the blast furnace scale. It seems to have possibilities in the foundry.

Dr. Babcock—That may be true.

John Chipman *(Massachusetts Institute of Technology, Cambridge, Mass)*—There is one question I would like to ask; it has to do with the use of calcium carbide and calcium oxide together in the desulphurization. As I recall, the efficiency of calcium carbide as a desulphurizer was considerably damaged by the presence of calcium oxide. This suggests the possibility that something is going in with calcium oxide, perhaps calcium carbonate or calcium hydroxide or some other impurity of an oxidizing nature. If that is so, perhaps it should be repeated, using dead burned lime along with the calcium carbide.

Mr. Hulme—It was burnt lime and probably had some hydroxide in it.

Dr. Chipman—It might be quite different with freshly burned lime then.

Mr. Hulme—You are right.

Desulphurization of Pig Iron with Pulverized Lime

by Bo Kalling, C. Danielsson, and Ottar Dragge

and

Kalling-Domnarfvet Process at Surahammar Works

by Sven Fornander

DISCUSSION, T. L. Joseph presiding

L. F. Reinartz *(Armco Steel Corp., Middletown, Ohio)*—I would like to know, in the practical application of the Kalling process, what kind of a lining was used, how thick was the lining, and how much metal was treated at one time?

S. Fornander (author's reply)—The rotary furnace is lined with a course of fireclay bricks 6 in. thick. This course is backed by 5 in. of insulation. The furnace has a capacity of about 15 tons.

Mr. Reinartz—How was the ladle preheated?

Mr. Fornander—As pointed out in the paper, the furnace was heated by a gas flame in the beginning of the experiments. During these first tests, however, the desulphurization was inconsistent. We think that this was due to the fact that iron droplets sticking to the furnace walls were oxidized by the gas flame. Now, the furnace is operated without preheating of any kind, and the results are much better.

T. L. Joseph *(University of Minnesota, Minneapolis, Minn.)*—I might add one comment. This furnace was heated with a flame and for a time they had a little difficulty due to some residual metal in the rotating drum that would oxidize in between treatments and they found therefore, that it was very essential to drain the drum completely of metal so that they would not build up any ferrous oxide between treatments and they eliminated some of their erratic heats by maintaining those more reducing conditions.

It was interesting to watch this operation. As soon as the drum started to rotate there was considerable flame, at least, at the time I saw it, that came out around the flanges, indicating there was quite a little pressure on the inside of the drum.

W. O. Philbrook *(Carnegie Institute of Technology, Pittsburgh)*—Is the reaction slag in the Kalling process liquid or solid, and how is it separated from the metal?

Mr. Fornander—In the process there is no slag in the usual sense of the word. The lime powder does not melt during the treatment. After the treatment the lime is still in the form of a fine powder. It is separated from the metal by means of a piece of wood of suitable size placed within the furnace before it is emptied.

D. C. Hilty *(Union Carbide & Carbon Research Laboratories, Niagara Falls, N. Y.)*—Dr. Chipman has given us some of his ideas in connection with a specific effect of silicon and silica on sulphur elimination and how silicon might interfere with desulphurizing in the blast furnace. I wonder if he would like to elaborate on the possibility of a similar effect of silicon in the Kalling process?

J. Chipman *(Massachusetts Institute of Technology, Cambridge, Mass.)*—Silicon does not interfere with the Kalling process. Anything that has strong reducing action is good for desulphurization. In these tests where the temperature was low compared to blast furnace temperatures, the silicon that is in the metal is a better reducing agent than the carbon. At high temperatures, carbon is the better. It is not the silicon in the metal that interferes with desulphurization, it is the silica in the slag.

Mr. Joseph—I might add that the metal that was tapped from the drum after desulphurization was really at quite a low temperature. It was not measured, but I think it was well under 1300°C, probably 1200° or a little above that. That was one of the difficulties, and I think there is no question about the fact that the Kalling process—in that it affects desulphurization between powdered lime, solid and liquid iron—is a reaction definitely between the solid lime and the liquid iron.

E. Spire *(Canadian Liquid Air, Montreal, Canada)*—This Kalling process seems very interesting to us and after all it is only a mixing action that is taking place between the iron and the slag. We have attempted to do the same thing in another way. We have placed at the bottom of the ladle a porous plug through which we injected an inert gas. It can be nitrogen or argon. This plug is placed at the bottom of the conventional ladle and gas injected through the plug. That has appeared in our patent.

To define this new type of treatment, I use the word gasometallurgy. I do not know if you like it, but it is a way of defining methods of treating metal using gases. What we do is exactly what is done in the exchange process in another way. We have a porous plug at the bottom with a high lime slag on top of the metal. Using this method, we have very good agitation of metal and slag, and with a small flow of gas, we can achieve a very strong agitation. For instance, in the 500 lb ladle, we use only 5 liters of gas a minute. We have an agitation compared to very rapidly boiling water in a pail. Moreover, the agitation can be controlled to create any amount of mixing desired.

In a few minutes, with this method, the sulphur dropped from 0.58 to 0.11. These results have been improved since, and we have obtained results like 0.08

to 0.015 in a matter of 10 min, but what is interesting is that we have been able to do that in steel, too.

In steel, we have done exactly the same thing with a high lime slag containing a certain amount of carbon. We have obtained a reduction of 0.5 to 0.25 or, recently, from 0.5 to 0.020. This is interesting because it was done in only 3½ min, and these results, I think, are worth-while because it could be very well used with furnaces where no desulphurization can take place.

All of this work has been done with the help of the Canadian Government and the Bureau of Mines, Ottawa, (now, the Department of Mines and Technical Surveys). I just wanted to point out this new process as having good possibilities in the iron and steel industry where the sulphur problem is such a big one.

Mr. Joseph—Will you tell us about the gas that goes in and the slag that is formed?

Mr. Spire—The gas we are using is either argon or nitrogen. In the case of iron, nitrogen works well. In the case of steel, we started by using nitrogen. This gave us trouble with blowholes in the steel. Using argon, we had perfectly sound ingots. The flow was 5 liters a min and with that we had a strong agitation. We found no difference if the ladle was full or half empty as far as agitation was concerned, and we expect in large-scale developments, which will take place very soon, that the flow of gas will not be very much greater.

For iron, we have to use a fairly liquid slag and we have been trying lime and soda ash. We have been trying sodium carbonate and calcium carbonate and that was probably the best we have used. It worked very well. The weight was around 2 pct. For steel, we have been using various slags. We are planning to use some Perrin slags. The agitation we obtained is similar to the Perrin process, only we have a longer time for reaction taking place. The Perrin slag is a very good slag in connection with that. We have also been using a simple lime mixture with a certain amount of carbon in order to reduce the FeO content to a minimum.

Mr. Larsen—Do you have to have the gas flow on all the time that the metal is in contact with the porous refractor?

Mr. Spire—We prefer to have the gas going on all the time for various reasons. I may say that the refractory problem is not very simple. The way the porous plug is fixed to the bottom gave us trouble for several months, and I think we have straightened out this problem and the porous refractory can be used. We have used the same one for 30 heats in the 500 lb ladle. We do not have any more difficulty, but now we expect to run larger heats to see what we will get.

C. H. Bacon *(John Summers & Sons, Ltd., Shotton, Chester, England)*—What type of refractory is being used for the porous plug for the steel ladle?

Mr. Spire—We have been using brucite-type magnesium oxide.

Solution Loss and Reducing Power of Blast Furnace Gas

by T. L. Joseph

DISCUSSION, A. H. Sommer presiding

S. T. Killian *(Johnstown, Pa.)*—This is one of the finest papers I have read. Tying in stoichiometric calculations with furnace performance and practice is a step which had to be taken sooner or later. The noteworthy difference between Dr. Joseph's type of calculations and regular blast furnace calculations is that the lb mol system is used as a basis. With the lb mol system, weights, volumes, and chemical reactions can all be expressed in the same equation.

In the paper, wind, ore, flux, and fuel are all expressed as lb or lb mols. Probably Dr. Joseph does not realize it, but the vague word coke appears only twice in the entire paper. Lb of C and lb mols of C are followed through reactions but the word coke appears only as 1560 lb coke per ton of pig and 1700 lb of coke per ton of iron. Obviously in order to understand furnace reactions, the coke should be expressed as lb or lb mols of C. Furnaces can also be compared more easily.

In some respects the paper is too thorough and too complete. The effects of the metalloids reduced into the iron upon the top gases represents a difference of less than 3 pct of the CO formed in the bosh. Due to the completeness of the calculations in relation to the CO/CO_2 ratio, this was included and was necessary. However, the exclusion might have enabled more furnace men to follow the lb mol system of calculations through the blast furnace to a better degree. By considering only irons of similar analysis, this part of the calculations might have been omitted. However, if this had been done, total rewriting of the paper later would have been necessary in order to make the work complete as it is now. It also would not have been nearly as authoritative.

In the paper, there appears the reaction:

$$H_2O + CO \rightleftarrows CO_2 + H_2 \qquad [1]$$

Dr. Joseph states that he did not take this reaction into consideration in any calculations pertaining directly to the paper. The probable reason for this is that although it contains all the main reacting top gases except N_2, it is rather inflexible since it is monomolecular in relation to each of the reacting gases and does not tie in with the gasification of C.

Actually the reactions:

$$H_2O + C \rightleftarrows CO + H_2 \qquad [2]$$

$$2H_2O + C \rightleftarrows CO_2 + H_2 \qquad [3]$$

and the solution loss reaction:

$$CO_2 + C \rightarrow 2CO \qquad [4]$$

tend to assume an equilibrium through the reaction:

$$H_2O + CO \rightleftarrows CO_2 + H_2 \qquad [1]$$

which should be considered a balancing or equilibrium reaction. Reactions 2, 3 and 4 permit furnace conditions to balance with the CO/CO_2 ratio and H_2 formation. They tie in with the solution loss. Reaction 1 unites them chemically.

Probably the best calculation to make at this time would be to try to find the relative importance of the CO_2 from the flux and the H_2 in the dilution on an actual furnace gas analysis. For this purpose the Dobscha-Carnegie-Illinois paper—"Effect of Sized and Sintered Mesabi Iron Ores On Blast Furnace Performance" is chosen. This paper was presented before the blast furnace section of the AIME in 1948. This represents the best large scale furnace operation available to me. Unfortunately the changes were brought about by beneficiation of the burden and not by changes on one burden.

In choosing the basis for the calculation in relation to the furnace, 100 mols of dry top gas is chosen. This leaves something to be desired inasmuch as the nitrogen basis is changing but I believe it will be better understood than any other type and it is the easiest to use.

The gas analysis and mols per 100 mol of blast furnace gas of the furnaces compared are:

	Normal Ores		Prepared Ores	
	Pct	Mol	Pct	Mol
CO	26.57	26.57	26.17	26.17
CO_2	12.33	12.33	12.40	12.40
H_2	2.30	2.30	1.60	1.60
CH_4	0.13	0.13	0.13	0.13
N_2	58.67	58.67	59.70	59.70
Total	100.00	100.00	100.00	100.00

Relative Amounts of CO_2 Evolved from Flux

In the paper, the distribution of the lb C per ton of iron in the top gases was given as follows:

	Normal Ores	Prepared Ores
CO	1024	838
Total CO_2	475	397
Flux CO_2	113	76

Since the amount of flux CO_2 in the total CO_2 is given, the flux CO_2 in the gas can be calculated directly:

	Normal Ores	Prepared Ores
Mol CO_2 in gas from flux	113/475 x 12.33	76/397 x 12.40
Mol CO_2 in gas from flux	2.93 mol	2.37 mol

Relative Amounts of H_2 Formed

"Making, Shaping and Treating of Steel" by Camp and Francis contains the following notations on the blast furnace diagram:

875°C—much of the carbon dioxide is reduced by carbon

975°C—Combined water remaining is decomposed

1075°C—limestone is decomposed.

The evolution of CO_2, the driving off of combined water, the H_2 formation, and the solution loss are tied in so closely that it may be impossible to separate them absolutely, but a start should be made. Probably the best way to correlate the H_2 formation from the efficient to the normal furnace would be through an H_2 to flux CO_2 ratio, since the normal furnace would eliminate the cooling and combined water farther down in the furnace with a consequential greater H_2 formation and a greater solution loss.

	Normal	Prepared
Mol H_2 to mol flux CO_2	2.30/2.93	1.60/2.37
Ratio	0.785	0.675

Thus if the furnace using normal ores decomposed as little water as the efficient furnace, the normal top gas would contain:

$$2.93 \times 0.675 = 1.98 \text{ mol } H_2$$

This would leave:

$$2.30 - 1.98 = 0.32 \text{ mol } H_2$$

as excess H_2 decomposed in the normal furnace.

Thus the 0.32 mol of H_2 would not have been formed if the normal furnace had worked as well as the efficient furnace. This excess can not be considered as being independent of the solution loss because it is probably tied in very closely with it. However it does represent excess H_2 in the gas and is so considered.

A breakdown of the calculations shows:

	Normal Ores		Prepared Ores	
	Mol	Pct	Mol	Pct
CO	26.57	26.57	26.17	26.17
Combustion CO_2	9.40	9.40	10.03	10.03
Flux CO_2 (efficient)	2.37	2.37	2.37	2.37
Flux Co_2 (excess)	0.56	0.56	0.00	0.00
H_2 (efficient)	1.98	1.98	1.60	1.60
H_2 (excess)	0.32	0.32	0.00	0.00
CH_4	0.13	0.13	0.13	0.13
N_2	58.67	58.67	57.90	57.90
Total	100.00	100.00	100.00	100.00

In the above table based upon 100 mols of blast furnace gas and comparing the furnace using normal ores with the furnace when using prepared ores, we find 0.56 mol additional due to excess flux CO_2, 0.32 mol additional due to excess water decomposition, and the remainder (with the type of calculations used) of 0.15 mol to be attributed directly to the solution loss reaction with no side reactions. However the solution loss reaction is tied in with the other reactions so closely that nearly 100 pct of the change must be considered as stemming from the carbon going into solution and the resulting interaction with H_2O in the gaseous phase.

The figures seem to show that while the solution loss itself is masked by side reactions, the dilution of the N_2 is not diminished by them but is augmented by the resulting H_2 formation. Basically the principle of N_2 dilution due to the solution loss seems to work out better with the resulting additional water decomposed.

Attention is again called to the fact that the figures used do not represent a change in solution loss with no change in the burden. They represent a change from a burden of normal ores on a normal furnace to a burden of beneficiated ores being reduced more efficiently on the same furnace.

I regret that I can add nothing of value to Dr. Joseph's paper. By all standards it must be accepted as one of the finest papers produced.

Oxygen in Liquid Open-Hearth Steel—Oxidation during Tapping and Ladle Filling

by T. E. Brower, J. W. Bain, and B. M. Larsen

DISCUSSION, R. C. Solomon presiding

John Chipman *(Massachusetts Institute of Technology, Cambridge, Mass.)*—In tapping a heat of steel from the open hearth it is difficult, as the authors have pointed out, to distinguish between oxidation by air and oxidation by reaction with the slag. These effects could be distinguished and the oxidation due to air more closely identified if the same method were applied to tapping electric furnaces. Here the slag can be made reducing and the bath presumably uniform, thus changes due to air oxidation from furnace to ladle should be capable of more exact determination.

It should be pointed out also that if the amount of oxygen picked up from the air is as great as the authors have indicated, there is little incentive to produce an entirely deoxidized bath in the electric furnace. The use of a reducing slag for controlling alloy elements and for desulphurization is understandable. But from the standpoint of deoxidation its effect would be entirely lost in tapping if the reaction with air is comparable with that reported here.

C. H. Bacon *(John Summers & Sons Ltd., Shotton, Chester, England)*—I was particularly interested to see the films of the tapping streams, as we have taken some high speed films of the teeming streams between

the ladle and the mold. The original purpose of taking the films was not connected with oxidation, but we found that the form of the metal streams varied greatly; some of the streams were relatively compact, whereas others were very ragged. I should like to ask Mr. Larsen for his views on the degree of oxidation that takes place between the ladle and the mold, and to what extent this might be influenced by the form of the stream.

N. R. Arant *(Titanium Alloy Manufacturing Co., Pittsburgh)*—The results and motion picture studies in this paper indicate that perhaps a great deal can be learned if the oxidizing and nitrifying effect of air during tapping is accentuated. One way to observe this effect would be to consider the elements which more readily react with air, namely; aluminum, titanium, and zirconium. Since steels containing both titanium and aluminum are in widespread production, these would be the ones to test. The more common grades produced in the arc-electric furnaces are: 321 (18-8 Ti), 17 pct Cr-Ti, 5 pct Cr-Mo-Ti and 19-9DL.

Both titanium and aluminum have a strong affinity for nitrogen as well as oxygen; therefore, if the steels mentioned above can be tapped with a minimum of contact with air, a much cleaner final product might result, with fewer titanium nitride and aluminum oxide nonmetallic inclusions. Furthermore, since ferro titanium and aluminum are expensive, there is the possibility of a considerable saving in the cost of producing the ingots.

In comparing standard tapping methods with the tilted-ladle method while considering the active elements mentioned above, it may be possible to more accurately calculate the volume of air which comes in contact with the steel during tapping.

To obtain accurate data during tapping, I believe it is necessary to obtain representative samples of metal and slag before tap, from the ladle, and during teeming. If good samples are used it seems logical that a clearer picture can be obtained regarding the oxidizing and nitrifying of alloying elements during tapping and ladle filling.

R. K. Kulp *(Electro Metallurgical Co., Division of Union Carbide & Carbon Corp., Pittsburgh)*—Metallurgists have made frequent reference to the problems involved in determining the reactions which occur during the tapping of open hearth heats. The authors of this paper are to be commended for developing the "air oxidation" method of determining the amount of reaction taking place during tapping and ladle filling.

This paper was presented before at the 1950 Open Hearth Conference, and at that time a discussion was presented by Mr. Tenenbaum. He offered data which indicated that the degree of air oxidation was less on heats which were blocked than on heats which were tapped open. In his rebuttal, Brower failed to agree with Tenenbaum's statement that "losses of elements dissolved in steel prior to tap are generally small." Do the authors have any specific information on air oxidation of blocked vs. open heats which would indicate a difference due to initial deoxidation?

B. M. Larsen (authors' reply)—Dr. Chipman's idea of separating slag and air oxidation by using data from electric furnace heats with reducing slags at tap is a logical one. We have obtained data on a few such heats but the method of estimating oxidation by difference, from alloy materials balances, gave inconclusive results. Both the quiet metal bath and the tap stream tend in this practice to be quite inhomogeneous and the sampling problem is an almost impossible one. Thus we feel that such evidence is not nearly as good as that given in the paper, which indicates a relatively negligible effect from reaction with slag. These data on electric steel heats did indicate a large loss by air oxidation, and in spite of the uncertainty caused by variable analyses and the difficulties of representative sampling, we believe that much of this oxidation loss is real, and that with respect to the final ingot, at least, deoxidation is essentially dependent, not on the reducing slag, but on the deoxidizing alloys just as it is in the open hearth. Thus, the tendency for much electric steel to be cleaner than open hearth remains about as much of a mystery as ever from any data we have obtained to date.

We did try to obtain the "representative samples" listed by Mr. Arant. However, the sampling here is a problem at best. Fortunately, the metal in open hearth baths is usually well mixed on heats tapped open. Blocked heats show somewhat more variability in tap stream composition.

We cannot give a definite answer to Mr. Bacon's question about oxidation between ladle and mold, although a few inconclusive indications from inclusion counting vs. various controlled and uncontrolled teeming conditions did indicate the probable existence of a relatively smaller effect which we rather believe did tend to increase inclusion content in the ingot. As noted in our comments on "oxidation effects and steel quality" in the paper, we suspect that certain factors are present which are perhaps not yet even recognized or at least are poorly understood. At least it appears that ragged or spraying teeming streams are worth taking some pains to avoid.

For a really conclusive answer to Mr. Kulp's question about relative alloy losses between blocked and open heats, comparative data on groups of 20 to 30 or more heats in the same grades of steel should be used. The pattern of variability in tapping conditions is so haphazard that results on smaller groups are not very reliable unless the factors involved have a large effect. However, the following data are on three small groups of killed heats, all of them medium to high carbon, mostly around 0.50 to 0.60 pct C at the platform:

	No Block, Tapped on Carbometer-Fine Grain	Blocked Heats	
		Fine Grained	Coarse Grained
No. of heats averaged in group	7	8	10
Loss, lb per ton, Mn	1.67	1.85	1.19
Loss, lb per ton, C	0.30	0.66	0.50
Loss, lb per ton, Si	0.80	0.66	0.97
Loss, lb per ton, Al	0.85	0.68	0.45
Total alloy loss, lb per ton	3.62	3.85	3.11
Lb oxygen per ton, external	2.58	2.55	2.38

Differences here are small, especially in terms of the indicated weight of oxygen reacting (from sources outside of the metal, presumably from air). The coarse grained heats had less aluminum loss, which is reasonable, and less manganese loss most likely because the oxygen happened to react more with the silicon. In total alloy losses, one group of blocked heats was higher, the other lower, than the heats tapped open with no furnace block. As shown by Brower in an earlier discussion* of this same paper that although aluminum and silicon and perhaps manganese (when high in fines) probably are all lost to some extent by floating and burning at the surface (aluminum may also react to some appreciable extent with ladle lining surfaces), yet quite large losses can occur from alloys definitely dissolved in the iron solution by some external effect which, directly or indirectly, would seem to be from atmospheric oxygen. Such an effect, almost obviously, is independent of any blocking or other occurrence in the furnace before tap.

As a purely practical matter, blocked heats with much of the alloy additions made in the furnace before tap probably do have somewhat lower average losses after tap, but the added losses in the bath before tap are such that total alloy loss is generally equal to or greater than in heats tapped open. That blocking improves quality is at least very doubtful, and it is certainly wasteful of alloys and of furnace time. Though sometimes needed for other practical reasons, in the writer's opinion, the blocking of heats should be avoided as much as possible.

* *Open Hearth Proceedings*, AIME (1950) 33, pp. 180-183.

Discussion — Institute of Metals Division*

St. Louis Meeting, February 1951

Metallographic Study of the Martensite Transformation in Lithium (paper by J. S. Bowles. JOURNAL OF METALS, January 1951, p. 44) 1056

Crystal Structures and Transformations in Indium-Thallium Solid Solutions (paper by L. Guttman. JOURNAL OF METALS, December 1950, p. 1472) 1056

Crystallography of Cubic-Tetragonal Transformation in the Indium-Thallium System (paper by J. S. Bowles, C. S. Barrett, and L. Guttman. JOURNAL OF METALS, December 1950, p. 1478) 1057

Grain Growth and Recrystallization Characteristics of Zirconium (paper by F. J. Dunkerley, F. Pledger, V. Damiano, and J. Fulton. Discussion published with the paper, this issue, p. 1003).

Interface and Marker Movements in Diffusion in Solid Solutions of Metals (paper by L. C. Correa da Silva and R. F. Mehl. JOURNAL OF METALS, February 1951, p. 155) 1060

Torsion Texture of Copper (paper by W. A. Backofen. JOURNAL OF METALS, December 1950, p. 1454) 1062

Effect of Ferrite Grain Structure Upon Impact Properties of 0.80 Pct Carbon Spheroidite (paper by M. Baeyertz, W. F. Craig, Jr., and E. S. Bumps. JOURNAL OF METALS, December 1950, p. 1465) 1064

Effect of Alloying Elements on True-Stress True-Strain Flow Curves of Pearlitic Steel (paper by R. Raring, J. A. Rinebolt, and W. J. Harris, Jr. JOURNAL OF METALS, May 1951, p. 395) 1065

Transitions in Chromium (paper by M. E. Fine, E. S. Greiner, and W. C. Ellis. JOURNAL OF METALS, January 1951, p. 56) 1066

Lattice Parameters of Magnesium Alloys (paper by R. S. Busk. JOURNAL OF METALS, December 1950, p. 1460) 1067

Intergranular Energy of Iron and Some Iron Alloys (paper by L. H. Van Vlack. JOURNAL OF METALS, March 1951, p. 251) 1067

Formation of Annealing Twins (paper by J. E. Burke. JOURNAL OF METALS, November 1950, p. 1324) 1068

Atomic Relationships in the Cubic Twinned State (paper by W. C. Ellis and R. G. Treuting. JOURNAL OF METALS, January 1951, p. 53) 1070

Graphite-Rod Hairpin-Resistor Radiation Furnace for High Temperatures (paper by W. J. Kroll, W. W. Stephens, and J. P. Walsted. JOURNAL OF METALS, November 1950, p. 1394) 1074

Ignition Temperatures of Magnesium and Magnesium Alloys (paper by W. M. Fassell, Jr., L. B. Gulbransen, J. R. Lewis, and J. H. Hamilton. JOURNAL OF METALS, July 1951, p. 522) 1075

Mechanical Properties of Stainless Steel Powder (paper by A. H. Grobe and G. A. Roberts. JOURNAL OF METALS, February 1951, p. 125) 1076

Rate of Sintering of Copper Under a Dead Load (paper by F. N. Rhines and H. S. Cannon. JOURNAL OF METALS, July 1951, p. 529) 1076

* TP 3174E. Since some of the annual meeting papers had not been published sufficiently in advance of the time this discussion went to press, discussion of these papers will appear when discussion is published in the spring.

Metallographic Study of the Martensite Transformation in Lithium

by J. S. Bowles

DISCUSSION, M. Cohen presiding

J. W. Christian *(The Inorganic Chemistry Laboratory, Oxford, England)*—I was very interested in Dr. Bowles' results on the suppression of the transformation by solid films of alcohol or propane. The transformation in cobalt, which is also martensitic, can be explained by a mechanism involving the reflection of "half dislocations" down a series of atomic planes.[12] This reflection process is similar to that considered by Frank[13] for plastic deformation on a single slip plane and, as he pointed out, reflection would be impossible if the metal were immersed in a liquid of higher density. It seems possible that solid films of alcohol have a similar effect on the lithium transformation.

Reflection should also be possible at a grain boundary, though a higher kinetic energy of the dislocation, and hence a lower temperature would be required. As Dr. Bowles used coarse grained polycrystalline specimens, transformation on cooling should still have occurred in grains which did not form part of the outside (free surface) of the metal. This may account for the X-ray lines of the low temperature phase which were found. There is thus the interesting possibility that in a polycrystalline specimen a liquid, or in some cases a solid, film of material of comparable or higher density will lower M_s, while in a single crystal it should suppress the transformation completely.

In the case of cobalt it is necessary to find a dense liquid which will not react with the metal at the transformation temperature. The most promising liquid appears to be pure lead, but it is very difficult to devise a method of investigating whether or not this does suppress the transformation.

[12] J. W. Christian: *Proc. Royal Soc.* (1951). In course of publication.

[13] F. C. Frank: Report of Bristol Conference on the Strength of Solids, p. 57. The Physical Society, London.

Crystal Structures and Transformations in Indium-Thallium Solid Solutions

by Lester Guttman

DISCUSSION, M. Cohen presiding

A. H. Geisler and **D. L. Martin** *(General Electric Research Laboratory, Schenectady, N. Y.)*—We were rather interested to note the author's conclusion that the cubic to tetragonal transformation may be of the second order, for we have been able to show that the order-disorder transformation in an analogous alloy system is a first-order transformation with a discon-

tinuous change in composition, rather than the frequently assumed second-order type.[14] Although it seems questionable whether the heterogeneous equilibrium of a martensitic reaction may be described, the author has attempted to define the reaction type, and on this basis we should like to examine the evidence further. In our work we have stressed the importance of establishing equilibrium, which may require hundreds of hours at relatively high temperatures. It is our contention that lack of equilibrium leads to results that suggest the so-called second-order type of transition. Here the author has attempted to attain equilibrium in time intervals of slightly more than a few minutes. We would like to know whether the transformation was studied using any appreciable annealing periods in those cases in which two-phase structures were merely assumed to be nonequilibrium.

In regard to the supposed continuity of volume shown by Fig. 3, if the curve were drawn through the data points for the 12½ and 18 pct alloys, there would be a discontinuity between 18 and 19 pct Tl. This would suggest a first-order transformation with a two-phase field at these compositions and the specified annealing temperatures of 105° to 135°C. These conditions agree with the boundary in the phase diagram, Fig. 9, but require that there should be two boundaries. On the other hand, the data in Table I appear to apply to the structure at room temperature and if this is so, it seems inconsistent to assign any special merit to the data plotted by full circles which are specified as "more thoroughly annealed specimens" where the annealing refers to 105° to 135°C and not room temperature. Thus it is questionable whether these data could support a conclusion regarding the type of reaction.

The author has observed that the data indicate no two-phase region wider than about 0.5 pct Tl at room temperature. This hardly seems an adequate basis for concluding that the cubic-tetragonal transformation is one of the second order rather than of the first order. We are sure that the author considers the liquid to solid transformation in the indium-rich alloys as the first-order type, yet the phase diagram, Fig. 9, fails to show width in the liquid plus solid field for alloys up to 30 pct Tl. Naturally, the minimum accounts for zero width at one point only. In fact there are many binary systems in which the two-phase field between a liquid and solid solution is very narrow or has escaped detection. Similarly the fields between two solid phases such as ferrite plus austenite in most of the γ loop forming systems of the iron-rich alloys are narrow. The A.S.M. Handbook shows a 0.1 pct maximum range for Fe-V. The two-phase fields between the ordered and disordered phases in Co-Pt alloys with 18 to 26 pct Co are less than 0.5 pct Co in width but still are detectable. In this case we found that electrical resistance measurements were most convenient for determining boundaries of the two-phase fields.

Since the two-phase region, if it exists between cubic and tetragonal phases in In-Tl alloys, is narrow, additional evidence is needed before the type of transformation can be definitely established. Perhaps, as the author noted, highly precise measurements of the heat capacity are needed to distinguish a first from a second-order transformation, but there may be some doubt that the sensitivity of thermal methods is as good as that of currently used techniques. Apparently the only practical deciding test for a two-component system is whether or not there is an "unambiguous" two-phase region. The test has not yet yielded conclusive results for many systems including the order-disorder reaction in β brass.

L. Guttman (author's reply)—The comments of Drs. Geisler and Martin are valuable for drawing attention to portions of the paper which are obscure, partly for reasons of language. It is hoped that the following formulation will clarify the basis for my conclusions, which remain essentially unchanged.

The evidence summarized in Table II is that the cubic-tetragonal transformation, both on heating and cooling, is complete in a temperature interval of less than 10° centered on the line drawn in Fig. 9. Hence the equilibrium boundary or boundaries must lie within this region, which is about 0.5 atomic pct wide at all temperatures, the slope of the line being roughly 20° per atomic pct Tl.

The effect of uniform long annealing is to decrease the fluctuations of a few hundredths of 1 pct in the lattice parameters apparently caused by severe deformation, which would otherwise obscure the changes associated with the transformation itself. The choice of the phrase "approach to equilibrium" to describe this process of stress relief was unfortunate. However, aside from the uncertainties due to this effect and to the hysteresis between the direct and reverse transformations, the question to be decided from Fig. 3 is whether there is any discontinuity in volume in the vicinity of 22.7 pct Tl, where the structure changes from tetragonal to cubic at room temperature; the annealing temperature itself is immaterial as long as it is high enough, since the high temperature structures cannot be undercooled more than a few degrees, see also Fig. 8.

Shortly after the present work was submitted, there appeared a similar study by Makarov[15] which agrees in finding no two-phase region between the cubic and tetragonal forms, and places the boundary at about 25 pct Tl at room temperature.

The relevance to the present case of arguments based on other systems is of course questionable; moreover, they should not be allowed to confuse the generally valid criterion that the absence of a two-phase region means that the transformation is of higher order than the first, and vice versa. In particular, examination of the data of Valentiner,[2] which could not be adequately shown in Fig. 9, will reveal definite separation of liquidus and solidus between 0 and 12 pct Tl, even in this very unfavorable case of a minimum melting point only 4° below that of pure In.

Finally, the intention of the comment in the footnote (p. 1477 of the paper) was obviously not to recommend thermal methods for characterization of transformation order in solids.

[14] J. B. Newkirk, R. Smoluchowski, A. H. Geisler, and D. L. Martin: *Journal of Applied Physics* (April 1951).

[15] E. S. Makarov: *Izvest. Akad. Nauk. S.S.S.R. Otdel. Khim. Nauk.* (1950) pp. 485-491.

Crystallography of Cubic-Tetragonal Transformation in the Indium-Thallium System

by J. S. Bowles, C. S. Barrett, and L. Guttman

DISCUSSION, M. Cohen presiding

A. H. Geisler and **D. L. Martin** *(General Electric Research Laboratory, Schenectady, N. Y.)*—The authors have very nicely demonstrated that the observed data agree much better with a proposed double-shear mechanism than they do with an assumed twinning mechanism. Reference is made to our results on an analogous alloy, Co-Pt in which a disordered cubic phase transforms to an ordered tetragonal phase.[16] True, our con-

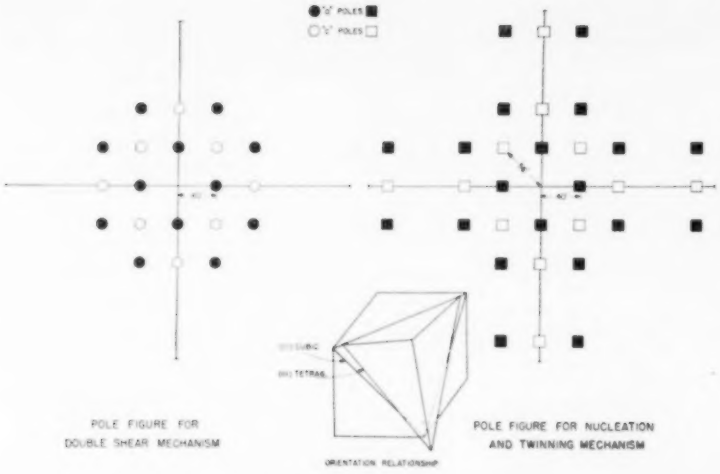

Fig. 14—Array of poles for tetragonal structure formed by transformation mechanism proposed by the authors (left) and that for nucleation and growth on {111} planes with first generation twinning (right).

clusion that the tetragonal lattice has the same orientation as the cubic lattice is only an approximation. Actually coherent platelets on {110} planes require that some of the tetragonal axes make angles of 27' to 43' (depending on c/a ratio) with cube axes according to the orientation relationship $(110)_B$ // $(101)_C$ and $[001]_B$ // $[010]_C$.

We should like to suggest that a better assumption might be made for evaluating the twinning mechanism in In-Tl alloys rather than assuming that the original cubic crystal becomes tetragonal by simple expansion along one cube axis and contraction along the other two, without change of orientation. In this case coherency on {111} planes appears to be promising. That is, a probable mechanism to test the twinning hypothesis would be to assume that the tetragonal phase formed from the cubic phase by growth of platelets on {111} planes with the tetragonal lattice being attained by adjustments in the spacing and atomic positions of {111} cubic planes. It is interesting to note that this

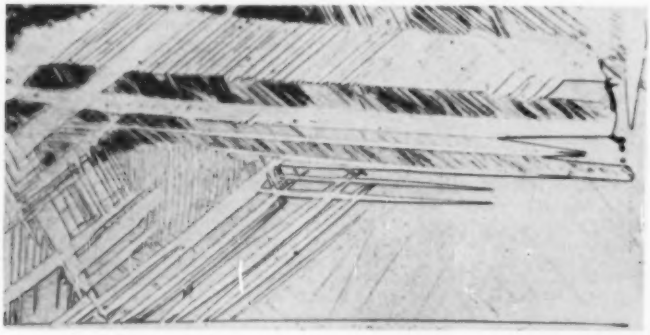

Fig. 15—Banded structure in unrepresentative surface layer of 48 atomic pct Co-Pt alloy disordered at 950°C then cooled to 822°C and held 25 hr and water quenched. Ordered plus disordered phases. X500.

Area reduced approximately 40 pct for reproduction.

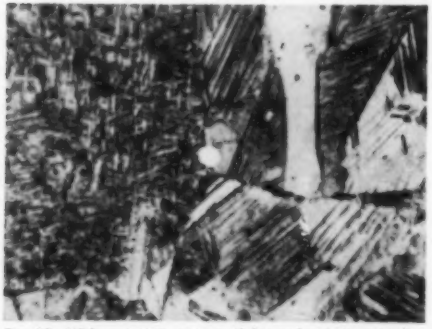

Fig. 16—Widmanstatten pattern (left) and striations (right) in 54 atomic pct Co-Pt alloy held 50 hr at 728°C. Ordered plus disordered phases. X500.

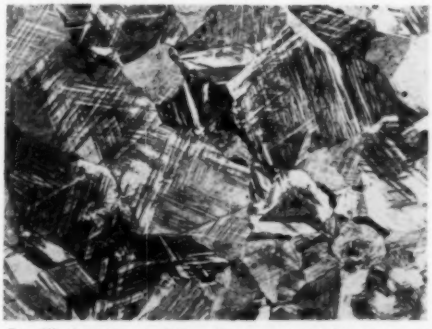

Fig. 17—Striations in fully ordered sample of 54 atomic pct Co-Pt alloy held 1000 hr at 600°C. X100.

Fig. 18—Surface deformation in In-Tl alloy. Oblique illumination. X75.

Fig. 19—Same as Fig. 18, electropolished and electroetched. Area Figs. 18 and 19 reduced approximately 40 pct for reproduction.

mechanism provides a pole figure for the 20.75 pct Tl alloy, Fig. 14, in which the central portion is identical to that for the proposed double shear mechanism. Poles for the initial platelets of the tetragonal phase and first generation twins only are shown. Possibly the outer poles represent twins that do not relieve transformation stresses and thus do not occur. It might be profitable to search for these and for a Widmanstätten pattern of platelets of the tetragonal phase on {111} planes of the cubic phase if samples could be prepared for the two-phase structure with microscopically resolvable particles and without the structure being obscured by the banded markings.

The authors have suggested that the ordering reaction in alloys such as Co-Pt, Fe-Pt, and Cu-Au might progress by a double shear mechanism on the basis that striated microstructures are observed for these alloys also. We should like to examine the comparison further, particularly in regard to Co-Pt where we have made a rather extensive study of the microstructures. In only one sample have we observed the clear-cut main bands with sublamellae shown by Fig. 15 analogous to the structure reported by the authors for In-Tl alloys. Here all bands are parallel to {110} planes and the subbands are on planes at angles of 60° to the plane of the main band, and with evidence of interpretation. The sample which was disk-shaped as cut from ¼ in. diam rod exhibited a transformed zone only around the cylindrical surface (see Fig. 7a, reference 15). The sample had been held at a temperature above the transformation range for the bulk alloy but below the range for the presumably impure surface layer. This sample provides an insight into the mode of lateral growth of the main bands. These usually occurred in pairs with a W-shaped edge possibly due to tilting in opposite senses as for In-Tl alloys, but frequently single main bands were observed to be growing in the untransformed matrix as in Fig. 15. The sloping surfaces at the V-shaped edges are parallel to some high order plane such as {780}. Possibly this should be considered as the "habit" plane rather than the {110} planes to which the irregular edges of the fully developed subbands are parallel.

Usually the striated structures in Co-Pt alloys are not as clearly defined as that shown above. The more prominent striations are apparent when the transformation is conducted at temperatures in or near the equilibrium temperature range. The striations may occur in irregular nodules bounded by no distinct main bands suggesting that the "first shear" is unnecessary. In one sample a banded structure was observed in some grains (Fig. 6d, reference 14) whereas others had a clearly defined Widmanstätten pattern of platelike particles of the ordered phase in the disordered matrix (see Fig. 6c, reference 14 and Fig. 7d, reference 15). It is believed that the latter is the primitive mechanism of the transformation and this is obscured in grains so oriented with respect to their neighbors that the self-deformation process may operate. The two types of structures in adjoining grains are shown by Fig. 16. Recent analyses show that the striations also correspond to traces of {110} planes rather than to the previously reported {111} planes.[14] When ordering is conducted at temperatures such as 700° and 600°C, which are below the equilibrium temperature range, the striated structure is less prominent (see Figs. 7c and 7d, reference 14). Nodules of parallel bands are no longer prominent and the bands appear wavy and intersect each other very frequently as in Fig. 17. The microstructure is more similar to those which have been reported for Cu-Au[6] and Fe-Pt[4] alloys than it is to that reported for In-Tl alloys. In Co-Pt alloys the cubic phase can be retained by quenching and the transformation can be promoted isothermally at subcritical temperatures. Under these conditions the striations appear after the start of the transformation and continue to become more prominent long after completion of ordering according to X-ray data on the same metallographic samples which lend support to the hypothesis that they represent a mode of stress relief rather than the primary transformation. Finally striations are faint or absent on ordering at 500°C where most prominent manifestation of the transformation is the formation and growth

[14] J. B. Newkirk, A. H. Geisler, D. L. Martin, and R. Smoluchowski: *Trans.* AIME (1950) **188**, p. 1249, JOURNAL OF METALS (October 1950).

[15] J. B. Newkirk, R. Smoluchowski, A. H. Geisler, and D. L. Martin: *Journal of Applied Physics* (April 1951).

of recrystallized nodules at grain boundaries (see Figs. 7a and 7b, reference 14).

Thus we are inclined to believe that the major mechanism of the transformation in Co-Pt alloys is by the Widmanstätten type process in which platelets of the tetragonal phase are nucleated and grow parallel to {110} planes of the cubic matrix and that the major source of striations is the self-deformation process by twinning or slipping in which strains are relieved in the course of or subsequent to the transformation.

L. Guttman (authors' reply: Due to the absence from the United States of the other authors, one author is responsible for the reply)—It is difficult to see why an alternative to the double-shear mechanism should be sought, since it appears to account satisfactorily for all the observations. The proposed mechanism is moreover in conflict with several critical features:

1—Presumably, a given colony of main bands consists of the tetragonal material formed by adjustments within a particular (111) plane and one of its first generations twins; but this gives only two orientations of the eight found as shown in Figs. 7 and 8, when a grain has a single set of main bands.

2—The subbands are not explained, since if they were second-generation twins the pole clusters could not correspond to observation.

3—On the proposed mechanism, there is no way to account for the observed mode of development, which is invariably the propagation of a (110) interface into the cubic material. In the paper, it was assumed that the bands appearing on a smooth surface were identical with the "main bands" revealed by electropolishing and etching, and hence represented traces of (110) planes. Although any other possibility seemed unlikely, we have since verified their identity by comparison in several cases of the surface distortion with the microstructure of the material immediately below, as shown by Figs. 18 and 19. It should be noted especially that both members of a pair of main bands are tilted with respect to the original cubic surface (Fig. 5, reference 1), and hence that at least part of the transformation must occur homogeneously.

4—It seems rather perverse to describe the banded markings as "obscuring" the structure when in fact they have served so well in elucidating it.

Apparently the mechanism of ordering in Co-Pt alloys is more complex than suggested by us on the basis of earlier information.

Interface and Marker Movements in Diffusion in Solid Solutions of Metals

by Luiz C. Correa da Silva and Robert F. Mehl

DISCUSSION, A. H. Geisler presiding

A. D. Le Claire and **R. S. Barnes** *(Atomic Energy Research Establishment, Harwell, Didcot, Berks., England)*—This much awaited paper admirably confirms that the Kirkendall effect is a true diffusion phenomenon and likely to be found in all diffusing systems. The most likely explanation put forward so far to account for the shift of interface is that the two components of the system, diffusing in opposite directions, do so with unequal rates so that there is a net loss of material from that half of the diffusion zone rich in the more rapidly diffusing component. This loss is accompanied, and at least partly compensated for, by a closing up or decrease in volume of this latter half of the diffusion zone and an expansion of the other half so as to tend to keep constant the overall volume per atom. This is manifest as a movement of the original interface. If this is a true picture of what is taking place then there are at least two important matters requiring further study.

1—The quantitative relating of the observed shift with the independently measured separate diffusion coefficients of the two diffusing species.

2—A detailed study of the mechanism and characteristics of the closing up process.

We would like first to make a few remarks pertinent to these topics. In connection with the first of these, it is a pity that more and detailed measurements were not made on the Au-Ag system, the only one for which the separate diffusion coefficients of the two species have been measured.[19] One of us (A. D. Le C.) has calculated from Johnson's results the shift to have been expected in samples D.2 and D.3. Darken[4] showed that the velocity v with which the markers move is related to the separate diffusion coefficients D_{Au}, D_{Ag} by the equation:

$$v = (D_{Ag} - D_{Au}) \frac{\partial N}{\partial x}$$

where $\frac{\partial N}{\partial x}$ is the concentration gradient at the markers. Under certain conditions,[4, 20] it can also be shown that:

$$v = \frac{Xm}{2t}$$

where x_m is the total marker shift after time, t:

$$\therefore x_m = 2t\,(D_{Ag} - D_{Au}) \frac{\partial N}{\partial x} \qquad [9]$$

Johnson measured D_{Ag} and D_{Au} in a chemically homogeneous alloy and so his reported figures represent the true or ideal diffusion coefficients[21]; the same quantities in eq 9 represent the actual diffusion coefficients as would be measured in the presence of a chemical concentration gradient, so we need to multiply Johnson's reported values of D_{Ag} and D_{Au} by the thermodynamic factor $\left(1 + \frac{\partial \log \gamma}{\partial \log N}\right)$ before inserting them in eq 9. γ is the activity coefficient of Ag at the concentration prevailing near the markers which we shall assume to be ~ 50 pct. The values of the thermodynamic factor for $N = 0.5$ and the temperatures at which D.2 and D.3 were annealed were obtained from thermodynamic data quoted by Darken.[4]

$\partial N/\partial x$ was computed from the coefficient of interdiffusion of Au and Ag given by Johnson on the assumption that in the samples D.2 and D.3, the concentration distance curve could be represented by the standard equation:

$$N = \frac{N_o}{2}\left\{1 - \phi\left(\frac{x}{2\sqrt{Dt}}\right)\right\}$$

N_o is the original difference in concentration between the two halves of the couple, and ϕ is the error or probability function.

$\partial N/\partial x$ at $x = 0$ is then given by:

$$\partial N/\partial x = \frac{N_o}{2\sqrt{\pi Dt}}$$

and we assume that this represents the concentration gradient at the markers, although it is probable that the figure is slightly high.

When all the appropriate quantities are inserted in eq 9, we find that the expected shifts are: for D.2, 0.0134 cm and for D.3, 0.0119 cm.

The agreement between these results and those

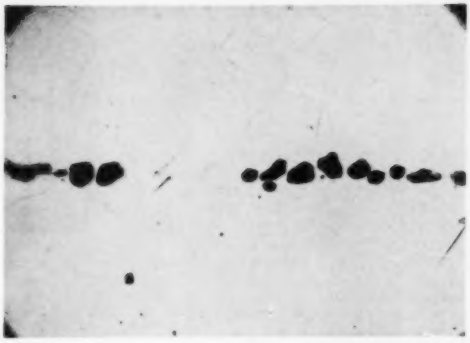

Fig. 62 (above)—Voids in diffusion zone of Cu/Ni couple diffused at 1080°C for 68 hr in hydrogen. Mechanically polished. X270.
Area reduced approximately 75 pct for reproduction.

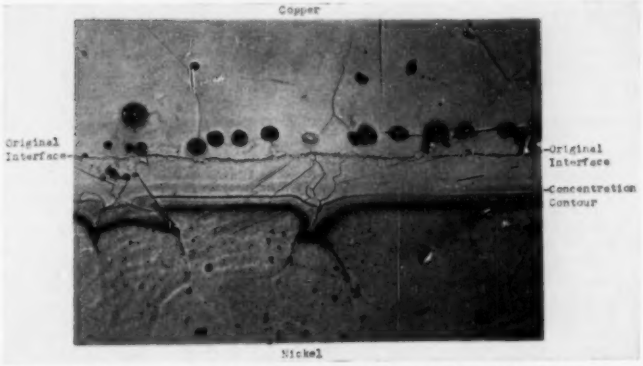

Fig. 63 (right)—Cu/Ni couple diffused at 940°C for 66 hr in argon. Electrolytically polished. X270.
Area reduced approximately 70 pct for reproduction.

actually found by da Silva and Mehl is very satisfactory. It indicates that the marker movement is predominantly determined by the difference in diffusion rates; other possible sources of movement will probably only play a secondary role. Further work along these lines is much to be desired.

An important result which touches upon the closing up process is that "the Matano interface agrees with the original interface." The validity of this statement is important because it is used as evidence that porosity is negligible, although the authors did in fact find porosity. But it seems to be contradicted by the results on samples B 22-I (Fig. 17), B 39-I (Fig. 19), and B 46 (Fig. 22) where the shifts as measured using the diffusion curve method are in the opposite direction to those given in the results for the type of couple concerned. Also in this connection the result of the lateral marker experiment suggests that the shifts obtained by the diffusion curve method should be modified, so spoiling the agreement between Matano interface and original interface positions. The results of the lateral marker experiment is most interesting for not only did these markers not move together as a result of the unequal diffusion flow but, although the lattice parameter in the locality of the markers decreased, their distance apart remained constant. This result can only mean that the number of atomic planes in the direction of diffusion must increase to maintain the distance constant, and as the authors say there must be a restraint to prevent the brass from contracting in directions at right angles to the diffusion flow; this would be expected when the diffusion flow is restricted to one direction as suggested by C. S. Smith in his discussion of the paper by Smigelskas and Kirkendall.[1] In the light of the result of this lateral marker experiment Smith's remarks are more pertinent than before and so the shift due to lattice parameter change should be three times that plotted on the curves relating shift to $\sqrt{t}$ or the Matano area, since the volume changes resulting from the lattice parameter change can only be relieved in the direction of diffusion. If this correction is made then all the points on these plots lie under a line which is the sum of the corrected curve for the lattice parameter shift and the maximum possible shift with the remarkable exception of the results for Cu/Sn couples.

Using the same result that the movements are restricted to the diffusion direction, the lattice plots (Figs. 13 to 24) should be modified, if the effect of the change in lattice parameter is not to be included in shifts obtained by the diffusion curve method. A rough calculation in the case of the sample B 39-I, for example, would move the Matano interface to a position much nearer the ordinate. As the shift given by this diffusion curve as it stands is in the wrong direction, this correction improves the result. In all cases the correction will move the Matano interface toward the small atomic component and so increase all the shifts as calculated from the diffusion curve (apart from those in the wrong direction, already mentioned, which will be reduced). The correction is only of importance in those couples where the Kirkendall effect is small.

It would be interesting to compare figures from the foil bend method and the diffusion curve method, for from the difference the volume occupied by voids can be estimated.

The authors of this paper found porosity in only the diffusion zones of the Cu/α brass and the Cu/Al bronze couples. One of us (R. S. B.) has found quite unmistakable voids occurring in the diffusion zone of Cu/Ni couples on the copper-rich side of the original interface. Similar voids to those reported were also found in Cu/α brass couples on the zinc-rich side of the original interface.

Fig. 62 shows the shape of these voids in a Cu/Ni couple which has been diffused at 1080°C for 68 hr in a hydrogen atmosphere. It may be observed that most of these voids have some straight faces which suggests that the voids are polyhedral in shape. Fig. 63 shows a similar couple, in this case diffused at 940°C for 66 hr in an argon atmosphere and given an electropolish which destroys the shape of the voids but reveals their position relative to the original interface, which is made visible by the impurities occurring in the welded join. Both micrographs show that the voids form in a fairly definite plane at right angles to the diffusion flow and, as reported for the brass couples, at some distance from the original interface, but in the diffusion zone.

In Fig. 63 the technique of outlining a concentration contour on the nickel-rich side of the original interface, as previously described,[20] has been used to show the preferential diffusion of the copper along the nickel grain boundaries, and in these regions where the extra diffusion has taken place the marker interface can be seen to bulge towards the copper-rich side, so giving a larger Kirkendall shift in these regions.

The grain boundaries in the diffusion zone pay little attention to the marker interface in these Cu/Ni couples, but many of them are irregular and suggest strain in this region.

The fact that visible voids are formed in certain cases suggests that the large number of vacancies involved do not necessarily condense only by the mechanism proposed by the authors. There are several possible ways in which the vacancies might condense: 1—by diffusing to the surface, 2—on dislocations with a Taylor-Orowan characteristic (within the crystal or at grain boundaries), 3—on impurities of a macroscopic or even atomic nature, 4—initially probably as platelike voids which soon collapse producing a dislocation ring as the authors suggest, and 5—as voids which do not collapse, probably of a roughly spherical shape.

Mechanisms 1, 2, and 4 do not lead to the formation and growth of visible voids, but it is conceivable that 3 and 5 might do so, and these may be operating in those cases where voids are seen. The presence of gas dissolved in the metal might seriously affect the behavior, subsequent to their formation, of the voids produced by any of the mechanisms 3, 4, or 5 but particularly in cases 3 and 5. Once a cavity is formed by any of these mechanisms, gas present in solution in the metal might diffuse into the cavity and prevent its collapsing, when in the absence of any gas it might have done so. Once stabilized in this way, the cavities might then grow to a visible size by condensation at them of further vacancies. The authors mention the importance of gas reactions as a possible complicating feature of this type of experiment and say that this can be avoided, but without saying exactly how. In view of the existence of a porosity in some samples but not in others, it would be interesting to know if an analysis of the gas content of the samples used by the authors is available. High metallic purity of the samples seems to be no guarantee of the absence of a gas reaction as evidenced by sample C.17. It is possible also that the existence of a porosity in our Cu/Ni samples and its reported absence in those samples used by the authors may be connected with their possible different gas contents.

In connection with Fig. 39, if the values of D previously found by Rhines and Mehl, are "highly approximate," why were they included in this figure? If only the authors present results are used in calculating Q, the values at high zinc concentrations are considerably raised, to about 40,000 cal per mol, and are in much closer agreement with previous measurements of Q in high zinc α-brasses.

L. C. Correa da Silva and **R. F. Mehl** (authors' reply)—The discussion of Messrs. A. D. LeClaire and R. S. Barnes is most interesting, and deserves detailed reply.

Their calculations of marker shift and the agreement of this with the observed shift in the Ag-Au system is encouraging. There are limitations to the application of the calculation, for the data are not quite adequate for the purpose: the data of Johnson are for the 50:50 composition; and the thermodynamic data employed were selected for this composition; the marker, however, surely does not follow this composition, but one at a much higher percentage of Ag,—the agreement found is thus presumably somewhat fortuitous. The "pity" in all research lies in its necessary incompleteness. It would be good to expand the data for the Ag-Au system, for marker shift, as well as for the separate diffusion coefficients by the use of tracers—it is a bit surprising that Johnson's work has not been extended.

Porosity in diffusion samples is often a fugitive, evanescent phenomenon. Although invariably observed in Cu/α brass couples, its occurrence in other couples is sometimes debatable. In most cases it is slight to the point of uncertainty; etching exaggerates it (and may change the geometry of the separate pores, as may polishing), and through the formation of etch pits may deceptively simulate it. Certainly even in Cu/α brass couples the total volume of porosity is small, judging from direct observation, apart from the argument arising in the concurrence of the original interface and the Matano interface. It should be noted in passing that the contradictory results on samples B 22-I, B 39-I, and B 46 should not be given much weight; the concentration range is small, and small errors in chemical analysis disturb the results in these systems; these curves are less reliable than the others. No determinations of "gas" content were, nor could have been made on samples such as those employed. Obvious swelling was observed in some samples (subsequently discarded), originating in the generation of internal blowholes. Inert gas ambients are always to be preferred for this reason. The "foil-bend," the "reference-to-foils," and the "diffusion curve" methods avoid the difficulties which gas or any porosity creates in analysis of marker shift.

The use of lattice units did appear to us to be fundamentally justifiable, apart from any consideration of marker shift; the point which Messrs. Le Claire and Barnes make received much attention in our thinking, but in view of the fact that we have but one measurement of lateral dimensions (made late in our work) it hardly seemed useful further to develop the lattice unit scheme—or any other framework. The matter of changes in lateral dimensions in samples such as ours and in others of differing geometries ought to be studied in detail.

The new observations reported on Cu/Ni couples are most interesting. The greater marker shift near grain boundaries, where diffusion is greater, is of course to be expected. Etching techniques such as those employed have been reported before; several instances were noted in 1936 Institute of Metals Lecture, though the combination of this technique with observation of marker movement is new and might be further exploited. In our case, the grain sizes were so very large that the marker movements recorded must have been near to those for single crystals.

The five possible ways in which vacancies might condense, as suggested, have all been considered. The first seems unlikely for the reasons given in the text. The whole question of mechanism of vacancy condensation is still worthy of thought and resultant experiment; it surely is not yet satisfactorily resolved.

The text with reference to Fig. 39 must have been misread. The expression "highly approximate" was used in reference to the Q-values of Rhines and Mehl; at high temperatures, the D-values, as reported here, agree with those of Rhines and Mehl quite well, as Fig. 38 demonstrates.

[20] A. D. Le Claire: Discussion on reference 4, p. 194.
[21] Chapter 7 of reference 6.
[22] R. S. Barnes: *Nature* (1950) 166, p. 1032.

Torsion Texture of Copper

by W. A. Backofen

DISCUSSION, J. R. Low presiding

W. R. Hibbard, Jr. *(General Electric Co., Schenectady, N. Y.)*—Dr. Backofen's pole figures showing the deformation texture of severely twisted polycrystalline copper are very interesting because of the large shear strains, the difficulty of interpretation, and their correlation with flow.

It is my opinion that the interpretation of the pole figures given in the paper is not self-consistent. It is not reasonable to have one of the four octahedral poles of a given orientation in an area of high intensity, while the others are in areas of low intensity as is the case in Fig. 6. If the texture is (112) [11$\bar{1}$], and a density of eight occurs in the longitudinal direction, then a density of eight must occur in the other positions for the octahedral poles of that orientation, or that is not

Fig. 10—Single crystal of α brass with (111) plane perpendicular to the torsion axis (axis vertical, plane horizontal) given 1.68 shear strain in torsion showing slip lines and deformation bands. Polished prior to twisting. X10.

the orientation involved. The most consistent interpretation of Fig. 6, in my opinion, is a duplex texture as follows:

111 direction parallel to the longitudinal direction with a random orientation of poles perpendicular to that direction (similar to the wire texture)

(110) [001] orientation superimposed

This interpretation will account for the three high density octahedral areas and not require octahedral poles in low density areas. It can be critically evaluated by examining the (002) reflection ring and determining whether or not there are any grains actually oriented with their 001 poles parallel to the longitudinal axis. For both of these orientations slip systems are suitably oriented with slip directions in the direction of maximum shear stress to account for the required flow on the basis of the theory presented in reference 7.

The significance of this duplex texture might be explained on the basis of experiments conducted in 1947 at Hammond Laboratory by Dr. R. E. Swift at the request of Professor C. H. Mathewson. The theory of stable textures described in reference 7 indicates that if a single crystal is deformed in the texture orientation, deformation will occur without changing this orientation. A torsion specimen was prepared from a single crystal of α brass with an octahedral plane perpendicular to the torsion axis (111 direction parallel to the longitudinal direction in accordance with the first orientation listed above) and the specimen was given a shear strain of 1.68 in torsion. Unfortunately, here too, the provision for free torsion did not function and the specimen was also subjected to axial compression. The appearance of slip lines on the surface (Fig. 10) indicated that most of the deformation occurred by shear on the octahedral plane perpendicular to the torsion axis leaving the 111 direction essentially parallel to the longitudinal direction and substantiating the suggestion that this is the stable end orientation or texture for the torsion of face-centered cubic metals. This orientation is the same as the wire texture with a random range of orientations from 110 to 112 normal to the stress axis. In addition to these slip lines there were several deformation bands emanating from the grip ends and extending in a slow helix toward the center of the specimen (also shown in Fig. 10). In these deformation bands the slip lines were about 50° from those in the matrix within 5° of where they should be for a (110) [001] orientation. It was my opinion that these deformation bands were the result of the stress complexity caused by the lack of free torsion or axial compression component, and that they would not have been there under pure torsion. There is the suggestion of the start of such a band in the upper right corner of the left micrograph of Dr. Backofen's Fig. 8.

It is my suggestion, therefore, that the texture for the pure torsional deformation of face-centered cubic metals is the same as the wire texture, namely 111 direction parallel to the torsion axis and a random range of orientations from 110 to 112 normal to it; and that lack of free torsion or the compression component in the torsion axis causes deformation bands to form of the orientation (110) [001].

W. A. Backofen (author's reply)—Dr. Hibbard suggests that the interpretation of the pole figures is not self-consistent because all of the octahedral poles associated with an ideal orientation do not fall in equally dense areas. This is certainly a significant comment, but it seems that it might be extended to other comparably accurate pole figures describing some of the more common cold-working textures. Fig. 11 is a (111) pole figure of cold-rolled copper which was constructed with the technique developed by Norton[12] and discussed in connection with Fig. 6 of the paper. The orientations included in this figure, while they do not position octahedral poles in equally dense areas, constitute the accepted description of the texture.

Dr. Hibbard's interpretation of the pole figures is particularly attractive because of its simplicity. But the writer avoided choosing the [111] wire texture with rotational symmetry about the torsion axis, for if this were developed it would seem that any direction from [110] to [112] in a (111) plane might act as a slip direction.

A slip direction could be expected to coincide with the transverse direction of maximum shear-stress, but it should be unnecessary for active slip planes to be oriented only perpendicularly to the torsion axis as the [111] wire texture would imply. It should be possible to rotate a slip plane originally perpendicular to the torsion axis about the active [110] slip direction without creating an unstable texture. By the rotation, the overall texture is broadened and the (111) [112] and (110) [001] orientations can be derived from the (112) [11$\bar{1}$]. It is not easy to rationalize the ideal texture (112) [1$\bar{3}$1], which can be obtained very nearly from the (11$\bar{1}$) [112] by a 20° rotation about a [110] direc-

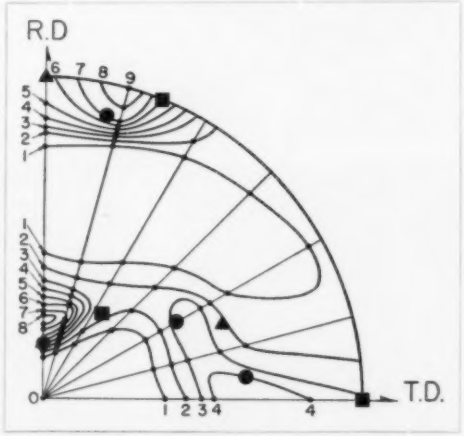

Fig. 11—(111) pole figure of OFHC copper reduced 95.5 pct in thickness by cold rolling.
Ideal orientations: solid square—(110) [112]; solid triangle—(112) [11$\bar{1}$].

tion lying in the plane of Fig. 7 and inclined 30° from the longitudinal direction. It may be that the contribution of this orientation to the description of the torsion texture is not important enough to warrant its use.

The [100] pole distribution was examined by means of a (100) pole figure and also by measurements of the intensity of reflection from (200) planes parallel to the flat surface of disk-shaped specimens removed from some torsion bars. These specimens were prepared so that their flat surfaces were perpendicular to the axes of the bars. It could be concluded from the information obtained in the two ways that there were some grains oriented with their [100] poles parallel to the longitudinal or torsion axis.

It is very interesting to learn that the deformation bands in the twisted single crystal described by Dr. Hibbard are of the orientation (110) [001]. These undoubtedly contribute to the overall texture. However, the pole figure of Fig. 4 was constructed from a specimen that was reasonably free from axial compression during twisting, and it is not different from the others. This suggests that the (110) [001] part of the texture cannot be attributed entirely to deformation bands caused by the restricted torsion. Since this work was published, the axial compressive stress resulting from restricted torsion has been measured. For copper specimens used in this work, the stress rises gradually to a maximum of about 2000 psi, which is 8 pct of the corresponding shear-stress at a shear-strain of 2. It then decreases rapidly as the shear-strain increases. Thus the constraint is relatively small and again it does not seem that it is entirely responsible for the pronounced (110) [001] component of the texture.

Additional work on the torsion texture in polycrystalline α brass has just been completed, but, unfortunately, the pole figures have not yet been prepared for publication. It is interesting to find that the (110) [001] orientation is a necessary, although minor, component of the texture. However, the [111] wire texture does not appear to be an adequate description of the balance of the texture.

Effect of Ferrite Grain Structure Upon Impact Properties of 0.80 Pct Carbon Spheroidite

by M. Baeyertz, W. F. Craig, Jr., and E. S. Bumps

DISCUSSION, J. R. Low presiding

R. M. Fisher and **J. F. Boyce** *(U. S. Steel Co., Kearny, N. J.)*—In recent determinations of ferrite grain size in specimens of AISI-SAE 1060, deoxidized with 0, ½, 1, and 2 lb of Al per ton we found, in agreement with the authors of this excellent paper, that ferrite grain size established by tempering martensite is apparently independent of prior austenite grain size over a considerable range. We felt that others might be interested in our experiences with martensite tempered for shorter times, in which the spheroids were much smaller and much more closely grouped than those in the authors' specimens.

We found it difficult to estimate reliably ferrite grain size with the optical microscope in specimens quenched from 1650°F, tempered for 1 hr at 1250°F, and etched with nital of various concentrations up to 5 pct. A typical micrograph of an aluminum-free specimen after this treatment is shown in Fig. 21a. Austenite grain size was ASTM No. 3 in this steel and No. 7 in those containing aluminum.

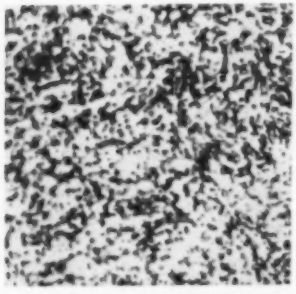

Fig. 21a (left) — Tempered martensite, 1 hr at 1250°F. 5 pct nital etch. X2000.

It was hoped that the X-ray diffraction technique described by Clark[a] would permit accurate measurement of ferrite grain size. However, continuous rings rather than individual spots were formed, which indicated merely that the ferrite grains were finer than ASTM No. 11.

Finally we resorted to the electron microscope and found that by etching these specimens in 2 pct aqueous ammonium persulphate solution for 10 sec, followed by 3 pct nital for 5 sec, we were able to observe ferrite grain size and structure. Collodion replicas, shadowed with uranium, were made of all four specimens. By counting grains in micrographs representing six randomly located areas for each specimen, we found the ferrite grain size of all specimens to be ASTM No. 15, regardless of prior austenite grain size or amount of aluminum addition. A portion of a typical electron micrograph of the replica from the aluminum-free specimen is shown in Fig. 21b. It should be noted that the etchant used shows the ferrite grains primarily because of differences in appearance of the surface of adjacent grains rather than by outlining grain boundaries.

[a] G. L. Clark: *Applied X-rays*. p. 504, 3rd Edition (1940) New York. McGraw-Hill Book Co.

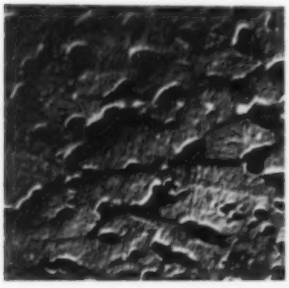

Fig. 21b—Tempered martensite, 1 hr at 1250°F. Ammonium persulphate and nital etch. X9000.

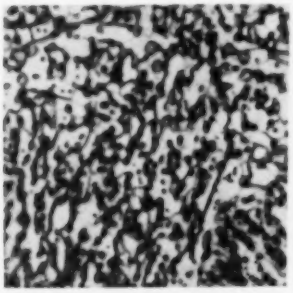

Fig. 21c—Tempered martensite, 19 hr at 1250°F. 5 pct nital etch. X2000.

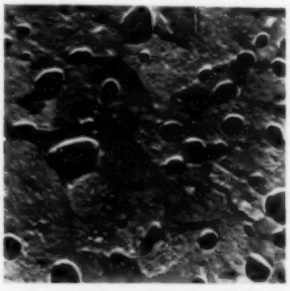

Fig. 21d—Tempered martensite, 19 hr at 1250°F. Ammonium persulphate and nital etch. X7000.

To investigate whether ferrite grain boundary delineation would be improved by longer tempering, the aluminum-free specimen was heated an additional 18 hr at 1250°F (Figs. 21c and d). Ferrite grain size was again determined by counting the number of grains in the known area of electron micrographs and was found to be ASTM No. 13.5, a five fold increase in volume.

The grains in the electron micrograph (Fig. 21d) appear more equiaxed than those in the optical micrograph (Fig. 21c). This seems to indicate that some of the elongated grains, observed with the optical microscope after etching with nital, consist of more than one equiaxed grain, but that nital failed to outline all boundaries adequately.

It was found that altogether 5 pct nital was not as satisfactory with the electron microscope as ammonium persulphate plus nital, ammonium persulphate plus nital was not as satisfactory as 5 pct nital when etching for the optical microscope.

We conclude that ferrite grain size may be measured by using the electron microscope and an ammonium persulphate plus nital etch, when it is difficult to outline grain boundaries satisfactorily for the optical microscope.

M. Baeyertz (authors' reply)—The authors are grateful for the added information on ferrite grain structure presented by Messrs. Fisher and Boyce. When the effect of composition on ferrite grain growth as well as the influences of temperature and period at temperature are taken into account, the evidence in the optical and electron micrographs of the discussers seems to be in agreement with the optical observations of the authors. The ferrite grains in Figs. 21a and b are elongated and of the shape that might be anticipated from a martensite plate structure, but as stated in the discussion, considerable equiaxing and some growth of the ferrite grains was observed after treatment for 19 hr at 1250°F. With the 0.80 pct C-1 pct Ni steel used by the authors, the spheroidization treatment of 54 hr at 1150°F caused but very slight ferrite grain growth, so that the ferrite grain structure after this treatment was essentially the same as that observed with shorter periods of spheroidization at the same temperature. The difference in the rate of ferrite grain growth in the discussers' AISI-SAE 1060 steel and the authors' 0.80 pct C-1 pct Ni steel is ascribed to the differences in composition and spheroidization temperature used in the two cases.

We agree that electron microscopy is a useful tool for study of ferrite grain structures when used with the technique applied in the discussion. Because of the smaller field represented by any one electron micrograph, care must be taken to compare larger fields by light microscopy.

Effect of Alloying Elements on True-Stress True-Strain Flow Curves of Pearlitic Steel

by R. Raring, J. A. Rinebolt, and W. J. Harris, Jr.

DISCUSSION, J. R. Low presiding

G. W. Geil *(National Bureau of Standards, Washington, D. C.)*—The authors state that the degree of accuracy realized in the experimental determination of σ_f is likely rather low. This inaccuracy is attributed to the difficulty in reading the load of the tension machine at the instant of fracture of the test bars. I believe there is another factor which may have added considerably to the inaccuracy in the determination of σ_f, namely, the determination of δ_f. Fracture of a cylindrical tensile specimen of a ductile metal tested in tension at room temperature is generally initiated at the axis and rapidly propagates radially to the periphery of the necked section. During the propagation of the fracture, the metal at the rim of the minimum cross-section extends longitudinally and contracts radially. Thus values of δ_f, based on diameter measurements made after complete fracture of the specimens do not necessarily represent the strain at the initial fracture.[11] Data obtained at the National Bureau of Standards with a 0.3 pct C steel in the condition as-quenched from 1575°F and tempered at 1000°F for 1 hr and tested in tension at room temperature indicated a considerable "rim effect" and as shown in Fig. 13, resulted in an apparent increase in δ_f from 0.90 to 0.98. As the fracture strain of this steel is approximately equal to those of the steels reported by the authors, it seems probable that a similar "rim effect" may have added to the inaccuracies in the reported values of δ_f and accompanying values of E_f.

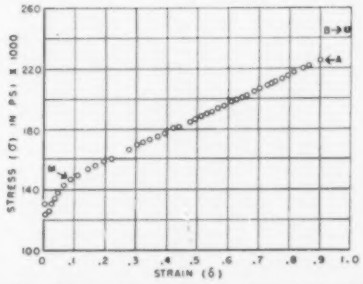

Fig. 13—True stress-strain curve for a specimen of 0.3 pct C steel in the condition as-quenched from 1575°F and tempered 1 hr at 1000°F and tested in tension at 80°F.

M—values at maximum load. A—values based on diameter measurement at initial fracture. B—values based on diameter measurement after fracture.

Table V. Extent to Which Terminal Points Lay Above (+) or Below (—) Flow Curve

Steel	Deviation, psi	Steel	Deviation, psi
C1	—1000	Cu1	—3000
C2	+1500	Cu2	+ 500
C3	+3000	Cu3	+ 500
C4	0	Cu4	+2000
C5	+1000	Cu5	0
C6	0		
C7	0	Cr1	—3500
		Cr2	+7000
Mn1	—2000	Cr3	+10,000
Mn2	—3000		
Mn3	+1000	Ni1	0
Mn4	+8000	Ni2	— 500
		Ni3	+2000
Si1	0	Ni4	+8000
Si2	+ 500	Ni5	0
Si3	—2000		
Si4	—2500	Mo1	—1000
Si5	—5000	Mo2	—1500
		Mo3	—1500
P1	—1000	Mo4	0
P2	0		
P3	0		
P4	—4000	V1	—2500
		V2	— 500
		V3	+ 500
		V4	—1500

R. Raring (authors' reply)—The authors are grateful to Mr. Geil for having called attention to a possible source of uncertainty in the determination of fracture stress, and they are in agreement with the principles upon which his discussion is based.

[11] D. J. McAdam, Jr., G. W. Geil, and R. W. Mebs: *Trans.* AIME (1947) 172, p. 323; METALS TECHNOLOGY (August 1947).

However, it is considered that the "rim effect" in the majority of the pearlitic steels used in the investigation under discussion was negligible, and certainly less than in the quenched and tempered steel cited by Mr. Geil. This consideration is based on the fact that terminal points of the flow curves did not consistently lie above the straight line portion of the curve, as does point *B* in Fig. 13. It would be expected that if a marked "rim effect" occurred, the terminal points calculated from the strain after fracture and the load at the beginning of fracture would lie above the straight line.

In Table V, the extents to which the terminal points were removed from the straight line are listed, and it can be seen that more were low (17) than were high (14), while 10 points were on the curve. Point B of Fig. 13 is approximately 15,000 psi above the extension of the curve. Thus only steels Mn 4, Cr 2, Cr 3, and Ni 4 show a marked upward deviation from the flow curve.

Transitions in Chromium

by M. E. Fine, E. S. Greiner, and W. C. Ellis

DISCUSSION, C. S. Barrett presiding

C. H. Samans and **W. R. Ham** *(Chicago, Ill., and Dixfield, Maine, respectively)*—For several years we have been studying transitions of this basic type in metals, alloys, glasses, etc. Usually, however, they are not so clearly marked as those which the authors have found, and hence are much more difficult to determine accurately. Since our studies indicate that most of them occur virtually unchanged (as far as temperature is concerned) regardless of the form in which the element appears, we believe that they are a characteristic of the atom.

Specifically, we believe that there is an additional rotational degree of freedom possessed by the nucleus which has not been considered heretofore. This nuclear rotation is made up of several components, each related to the several quantum shells of electrons. In chromium there are four of these shells and hence four separate series of characteristic transition temperatures. The lowest temperature at which any transition occurs, based on the present state of our computations, is 125°K, 4° higher than the authors' value of 121°K. A convergence of this series, we believe, shows up at the higher temperature of 2085°K, surprisingly close to the transformation temperature of 2103°K recently announced by N. J. Grant of M.I.T. for a body-centered to face-centered transformation in chromium.

Likewise, our computations indicate a temperature of 311°K for the second transition temperature, reported by the authors as 310°K. A convergence of this series, we believe, shows up at a higher temperature as the melting point at 2163°K.

Although our work on these series must, in a sense, still be regarded as empirical, since we do not understand fully as yet just what the series mean, it is based on a reasonably firm picture. The individual constants, from which the various series are computed for each element, comes directly from the X-ray K absorption limit. Furthermore, the same basic method has accounted for transformation and melting temperatures in about 50 of the chemical elements, which is all we have tried thus far. In many cases the only known transformation is the melting point, but in others the occurrence of transformations or other transitions, equally as well marked as those of the authors, has been pointed out by others. These observations have assisted us greatly. Consequently we were very pleased to see the authors' excellent work in finding these two transitions in chromium. With these confirming data, our picture of this element is clarified considerably, so we expect that at least some of our work can be published in the near future.

R. C. Ruder *(E. I. du Pont de Nemours & Co., Wilmington, Del.)*—The authors' interpretation of these transitions in terms of 3*d* to 4*s* electronic structure transitions is most interesting. It would be interesting to have additional experimental evidence of such transitions from the temperature dependence of the Hall coefficient in the neighborhood of the property changes discussed in this paper. Simple theory[16] suggests the Hall coefficient as a measure of the free electron (or *s* electron) concentration per unit volume. It has been shown that for paramagnetic[16] and ferromagnetic[17] metals the simple theory is in fact too simple. However, the existence of a discontinuity in the Hall coefficient would provide information which should aid both in our understanding of these transitions and the significance of the Hall coefficient in these metals. It was rather surprising that no significant paramagnetic effects were observed. In this connection the recent work of McGuire and Kriessman[18] is cited. They measured the magnetic susceptibility of chromium from 20° to 1460°C. They also observed no large change in the susceptibility although there might be a change in slope in the vicinity of the 40°C transition.

The existence of these 3*d* to 4*s* electronic transitions has been discussed in connection with the paramagnetic susceptibility behavior of nickel and nickel alloys.[19-21] Assuming a correspondence principle between classical and quantum mechanical paramagnetic theory and using classical theory to calculate the effective Bohr magneton number from the Curie constant for substances obeying the Curie-Weiss law,[22] it is found that the effective magneton number is a function of temperature. The process of calculation involves the inverse of the differential of the $1/\chi_A$ vs. temperature curve so that good and numerous data are necessary to obtain significant results. The data of Fallot[23] show a discontinuous increase of about 12 pct in the effective magneton number between 850° and 900°C, followed by a continuous increase up to the melting point. The data of Sucksmith and Pearce[24] show a possible 8 pct increase. The older data of Terry[25] and Weiss and Foex[26] show a continuous increase. It is possible that small amounts of impurity atoms change these electronic transitions significantly. Fallot's[23] data on a nickel alloy with 4.5 atomic pct Fe indicate that the discontinuity occurs around 1300°C.

Systematic investigation of the transition metals for transitions of this nature should provide information which would be very valuable for our understanding of these metals.

The absence of antiferromagnetic structures in chromium has been shown by Shull[27] using neutron diffraction techniques.

M. E. Fine, E. S. Greiner, and **W. C. Ellis** (authors' reply)—The remarks by Drs. Samans and Ham are certainly very interesting, in particular those pertaining to the close agreement between the theoretically calculated values for transition temperatures in chromium and the experimental values reported by a number of investigators. This is a remarkable achievement and we shall look forward to a more detailed presentation of the method followed in their calculations.

We do not believe that the transition in pure chromium near 40°C remains temperature invariant with alloying, as was reported by Samans and Ham for a number of the substances that they studied. We have not done any work with alloys but base our belief on the results of earlier studies in which less pure chromium was included and considerably lower transition temperatures were observed. The transition tempera-

ture, it would be expected, would be changed by solid solution alloying through modification of the electron distribution in the chromium atom by the neighboring solute atoms. The transition is still primarily a property of the chromium atom.

We appreciate Dr. Ruder's discussion of the results of susceptibility measurements on chromium which were not available to the authors at the time the paper was presented. It is gratifying that these measurements support our conclusion that the transition near 40°C is not loss of antiferromagnetism. This seems to be confirmed by the neutron diffraction measurements subsequently reported by Shull. We agree that precise measurements of susceptibility and Hall coefficient would be of great value for filling in some of the details of this transition.

References

[15] Seitz: *Modern Theory of Solids.* (1940) New York. McGraw-Hill Book Co.

[16] I. K. Kikoin: *Journal of Experimental and Theoretical Physics.* (U.S.S.R.) (1940) **10**, pp. 1242-1247.

[17] E. M. Pugh, N. Rostoker, and A. Schindler: *Physical Review.* (1950) **80**, (2) p. 688.

[18] T. R. McGuire and Charles J. Kriessman, Jr.: Pittsburgh Meeting, American Physical Soc. March 1951.

[19] E. C. Stoner: *Reports on Progress in Physics* (1946-1947) **11**, p. 84.

[20] K. E. Keyes: *Physical Review* (1940) **58**, pp. 202-203.

[21] N. Hori: *Bull.* Inst. Phys. Chem. Research (Tokyo) (1940) **19**, pp. 412-423.

[22] R. M. Bozorth: *Review of Modern Physics* (1947) **19**, pp. 29-86.

[23] M. Fallot: *Journal of Physics Radium* (1944) **5**, p. 153.

[24] W. Sucksmith and R. R. Pearce: *Proc.* Roy. Soc. (1938) **167A**, p. 189.

[25] E. M. Terry: *Physical Review* (1917) **9** (2), pp. 255, 394-413.

[26] Pierre Weiss and G. Foex: *Journal Physique* (1911) **1**, (5) pp. 274-288.

[27] C. G. Shull: Pittsburgh Meeting, American Physical Soc. March 1951.

Lattice Parameters of Magnesium Alloys

by Robert S. Busk

DISCUSSION, M. Hansen presiding

William Wilson, Jr. (*Armour Research Foundation, Chicago*)—In his treatment of the relatively soluble group of alloying elements, the author has calculated the regression coefficients, and found that the c/a coefficients for gallium, mercury, and zinc are not significantly different from zero. However, the Student t-test may fail to indicate a significant difference, even if one exists, when insufficient data are tested. The same binary alloys are also those for which the minimum number of observations are available. For these cases, at least, it would be desirable to calculate the fiducial limits of this coefficient. The author's data for magnesium, showing the individual results for each of the five samples, and a knowledge of his weighting procedure in finding these regression coefficients, would be required to calculate the fiducial limits.

Although the work of the previous investigators, reviewed by Raynor,[15] indicates a minimum in the c-spacing vs. atomic pct curves for indium and thallium, and an inflection point in the curves for aluminum and gallium, the author's treatment precludes finding these features of the curves. If a suitable equation for these previous investigations were also tested against the data, then the standard errors of the two might indicate the more exact treatment.

At the first reading, it may appear that the author has tested all of the lattice parameters of the relatively insoluble group with the assumption that the populations were infinite. Actually, in a novel way, the author has corrected the t-values in a way to make this a significant basis for comparison. I wonder if, in calculating the standard errors, the degrees of freedom were considered instead of the "N" defined as the "number of data points."

R. S. Busk (author's reply)—The minimum in the c_o parameter is obtained by combining the data for the c/a ratio and the a_o parameter. The c/a ratio was considered more fundamental and was therefore studied more exactly. In those cases having a minimum in the c_o parameter, the equation does not reduce to the value of pure magnesium at zero concentration. It is therefore evident from this alone that there is a break of some type in the curve. If the a_o parameter is decreasing while the c/a remains constant, then the c_o must also decrease.

The standard errors were calculated by using N rather than N-F.

[15] B. R. Chalmers: *Progress in Metal Physics.* Vol. I, p. 69 (1949) Interscience Pub. Co.

Intergranular Energy of Iron and Some Iron Alloys

by Lawrence H. Van Vlack

DISCUSSION, H. L. Burghoff presiding

C. S. Smith (*University of Chicago, Chicago*)—The author is to be congratulated on his valuable contribution to the extremely meager absolute data on interface energies in metallic systems.

It is interesting to note that the ratio between α and γ iron boundary energies is approximately the same in the quaternary alloy with silicon, carbon, and sulphur as in the binary Cu-Fe alloy. A value for the copper grain boundary energy can be obtained from the author's data, Tables IV and VI, by utilizing the energy ratios of the following pairs of interfaces: copper-sulphide/copper, copper γ iron, γ iron/γ iron, γ iron/copper, and copper/copper. This gives a value of 595 erg per sq cm for the free energy of the copper grain boundary. Despite this circuitous route and the assumption that the γ iron boundary is identical in alloys with and without sulphur and does not change between 1105° and 1000°C, this figure is in remarkably close agreement with other values of the copper boundary energy, obtained by equilibration against lead and against the free copper surface. It therefore appears either that impurities do not greatly affect the grain boundary energies or that boundaries in even nominally pure metals are already sufficiently contaminated so that further change has little effect.

DISCUSSION, H. L. Burghoff presiding

R. G. Treuting *(Bell Telephone Laboratories, Murray Hill, N. J.)*—A growth-accident hypothesis of annealing twin formation raises a question which may deserve clarification. In heavily anneal-twinned material such as α brass, parallel-sided twin bands are by far the predominant form observed. This requires for the present theory that following one growth accident to generate a twin orientation, the most probable subsequent growth accident be on an octahedral plane of the same set, i.e., parallel to the existent composition plane. The implication is twofold: first, that the direction of grain growth remains the same for original and twinned components; and second, that this still advancing octahedral plane (now rotated about its own pole by twinning) remains the most likely to meet an aggregation of atoms suitably disposed for another accident.

The first condition seems to impose little difficulty. The evidence advanced by Dr. Burke indeed supports the choice of <111> as a favored growth direction, and this would not be altered by the twin accident. Yet there are three other <111> symmetrically arranged about that operative in an accident. Although subsequent twinning does occur about one of these alternative poles from time to time, one particular set of octahedral planes is more often consistently favored, as shown by successive parallel twin bands. After a twinning accident, the operative set of planes should have by far the largest area of the four in the twinned material. It may then be that its probability of encountering an orientation suitable to further twinning is correspondingly larger even though growth may be proceeding at the same rate in all four <111> directions. I do not know that this explanation is adequate and would appreciate any comments from the author.

I should like to offer two tentative suggestions with respect to points Dr. Burke considers unresolved:

1—He has already noted grain boundaries as a discontinuity likely to cause twinning during grain growth. The frequency with which a growing grain meets a new orientation that may permit twinning is then a function of the then prevailing grain size. The relative constancy of twin density (twins per grain) throughout grain growth may be related to this. That is, the larger the grain size, the less often a twin accident is likely to occur.

2—It is possible that when a growing grain meets an orientation nearly suitable for a twin accident, whether or not this occurs may be controlled by the states (e.g., the surface energies) of the incident planes. The intensity of twinning may be related in this manner to the presence of solute atoms and so vary among alloys. This, to be sure, is not a crystallographic argument and perhaps does not lie within the intended scope of Dr. Burke's paper.

W. G. Burgers *(Technische Hogeschool, Delft, Netherlands)*—The subject of Dr. Burke's highly interesting paper is one which has been occupying me (and probably other metallographers) considerably during the last years. The two main possibilities, brought forward in the paper to explain the formation of annealing twins, viz: 1—the mechanical nucleation hypothesis, and 2—the growth fault hypothesis, have been discussed.[13, 14] In these papers direct experimental evidence was given by means of the "electron emission loupe" for the fact, mentioned in Dr. Burke's paper, that the width of twin bands bounded by parallel sides remains unchanged. In this investigation by means of the electron emission image a cinematographic record was obtained of the growth, by "exaggerated grain growth" ("secondary recrystallization") of nickel-iron foil, which shows clearly that twin lamellae grow parallel to their straight boundaries (cf. Fig. 8). This fact, which is also clear from Dr. Burke's Fig. 4, seems therefore well established.

The idea that the condition for twins to grow wider is to have a grain boundary as one side, seems to me very stimulating, also the evidence that twins usually form at or near the corner of grains. In this connection the explanation brought forward in a recent note by Fullman[15] is of the greatest interest.

The suggestion given there, due to J. C. Fisher, "that an annealing twin forms in the corner of a growing grain when the orientation relationships between the twin and the grain's neighbor lead to a smaller total interfacial energy than do the orientation relationships between the grain itself and its neighbors," makes it in principle understandable: 1—that twin formation is of necessity related to "lattice faults" (grain boundaries included), which explains why the same metal can "crystallize" without considerable twinning (for example when crystallizing from the melt), 2—that the frequency of twinning depends to a large extent on the "texture" of the matrix in which recrystallization or grain growth takes place, and 3—that different cubic face-centered metals, like copper and aluminum, may differ so much in their twinning frequency as a consequence of a different degree of anisotropy of surface grain boundary energy.

With regard to the above suggestions, I should like to point out that for some time I thought that a somewhat different mechanism, to some extent related to the growth fault hypothesis, might account for them. Although I feel inclined at present to consider a mechanism as proposed by Fisher to be more probable,* yet I cannot give up this idea completely.

The starting point for my considerations[16] was the formation, observed when recrystallizing fine grained aluminum by "primary recrystallization," of "pointed grains" (like B in Fig. 9), the lattice of which appeared to be in exact spinel-twin position (within at least 1

* I must confess that, although grasping the general idea underlying Dr. Fullman's short note, I find difficulty in deducing from the figure given how the atomic processes leading to the twin formation should be visualized.

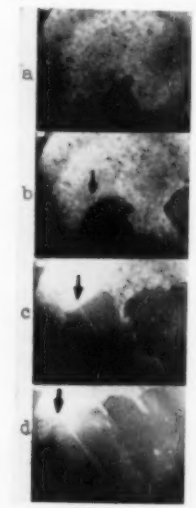

Fig. 8—Electron optical observation of the formation of twin lamellae of constant width during growth of a large crystal in nickel-iron foil by "secondary recrystallization" (from references 13 and 14). X25.

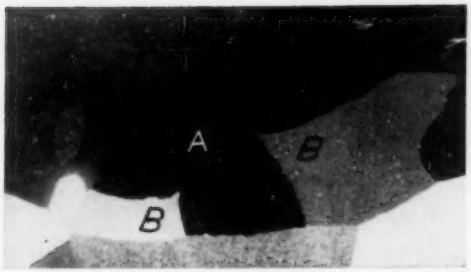

Fig. 9—"Pointed" twins (B) formed by "stimulation" by crystal A. Natural size. Area reduced approximately 40 pct for reproduction.

min of arc[17]) with regard to the lattice of the "surrounding crystal" (A in Fig. 9).

It was shown that the occurrence of such point-shaped crystals can be understood on the assumption that growth of such a "stimulated" crystal starts at the moment that an already growing "stimulating" crystal comes into contact with its nucleus, which was supposed to be a lattice region of the original matrix. In connection with the observed precise twin relationship existing between both crystals, it was thought possible that, on such encounter, "elimination" of a set of dislocations at the plane of contact, by mutual annihilation of dislocations of opposite "sign" (opposite "sense" in case of screw-dislocations) might cause a release of strain energy in the contacted lattice domain, which thus might be transformed into an active nucleus itself. Of course the frequency of such an event would depend largely on the texture of the matrix, as it would be controlled by the chance of a growing crystal to meet a lattice region in "precise" twin position, which it could stimulate to growth. In agreement herewith it was found that even in the same metal, in this case aluminum, the frequency of such twin formation depended very much on the texture of the matrix and varied from case to case.

On the basis of these experimental facts it was thought possible that the frequent twinning in metals like copper, nickel-iron, etc. might be due to the circumstance that the new crystals often develop in a matrix with a fairly pronounced texture, for example the cubic texture in the case of secondary recrystallization of annealed rolled foil. Moreover, as we know from various investigations,[7] these new crystals occupy positions which are related to the matrix texture by rotations about an axis normal to an octahedral plane. Although the amount of rotation, according to most investigators, differs from that observed for exact twinning, it must be kept in mind that these data are deduced by comparing the positions of the new crystals with the "centers" of the pole figures of the matrix. As these latter do generally show a considerable degree of scattering, it seems, a priori, not impossible that the crystals in the course of their growth repeatedly met individual grains of the matrix, which, with regard to them, occupy exact twin positions. In such cases, according to the suggestion given here, stimulation could take place, thus causing a lattice element of the disappearing texture to grow in exact twin position with regard to the already growing crystal, and so forming an "annealing twin." It is evident, however, that this mechanism, when occurring in a pronounced texture, would lead principally to a family of twins corresponding to the matrix-texture; whereas, as Dr. Burke points out, frequently examples of grains with several families of twins are observed.

In annealed rolled aluminum, where, according to Beck and coworkers,[20] similar orientation relationships between matrix and new crystals hold, the fine grained texture is generally less pronounced than in copper or nickel-iron. This, I thought, might explain, why, in aluminum, the "twins" have in general curved boundaries (cf. Fig. 9), as contrasted to copper, etc., where straight edges are generally formed. In fact, the "curved" twins in aluminum grow in matrices with an only slightly pronounced, or even nearly random, texture, so that the boundary-orientation relationship between growing grain and matrix changes from grain to grain; whereas in copper, etc., the texture is generally far more pronounced, possessing for example the "cube-texture," so that growth conditions will remain more constant over longer distances. I must say, however, that I feel not quite clear with regard to this point. In any case, it is a fact that, on recrystallizing a deformed aluminum matrix with a pronounced texture, obtained by rolling a single crystal, "twins" with straight edges are also formed;[21] whereas, on the other hand, the large copper crystals obtained by Cook and Macquarie[22] in cross-rolled copper by "abnormal grain growth" (which has a more random texture than foil rolled in one direction only) show many curved boundaries.

In order to have a direct test that the frequency of twin formation depends upon the orientation relation between growing grain and matrix texture, use might be made of the method of growing a crystal "round the corner," as applied by Tiedema[23] for the preparation of large aluminum crystals with a definite orientation with regard to the surface directions of the test-piece (which method is closely analogous to that applied by Dunn[24] and coworkers for preparing iron-silicon crystals with definite orientations): if in a fine grained matrix with a fairly sharp texture, we start growth of a large crystal at one end by pulling it partly through a heating zone, then bend the not yet recrystallized part and proceed with the growth of the large crystal "round the corner" by now passing the whole test-piece through the heating zone, then we may expect that the frequency of twinning is different at both sides of the "bent," as the relative position of growing grain and to-be-consumed matrix is different before and after passing the "bent." We intend to carry out this experiment. Of course, in case the above expectation comes true, this experimental fact is not exclusively in favor of the "stimulation" theory; it might also be expected on the basis of the views given in Dr. Burke's and Dr. Fullman's papers.

J. E. Burke (author's reply)—I should like to thank Professor Burgers and Dr. Treuting for their kind and stimulating discussion of my paper. In particular, I should like to thank Professor Burgers for calling attention to his earlier discussion of these two mechanisms and to his evidence that parallel-sided twin bands do not grow in width.

The stimulation mechanism for the formation of twins which Professor Burgers has proposed is very ingeneous. It might be pointed out that it cannot operate to form twins during grain growth since the strained fragments or nuclei necessary for the mechanism are not present.

On the other hand, in a deformed metal, either the stimulation or growth accident mechanism could operate. An experimental method of deciding between these mechanisms would be desirable. Professor Burgers suggests an experiment in which the frequency of twinning is observed in a grain as its orientation and growth direction with respect to a textured matrix is observed. Unfortunately, as Professor Burgers points out, a change in twinning frequency with texture could be explained by either mechanism. In fact, some evidence that the direction of growth influences the intensity of twinning was presented in this paper and used to support the growth accident hypothesis. Nevertheless, the results of the experiment will be highly interesting and will certainly help describe the conditions necessary for the formation of twins in greater detail.

I should like to suggest another experiment which might possibly allow a decision to be made between the two possible mechanisms in the formation of the pear shaped "stimulation" grains Professor Burgers shows in Fig. 8. The stimulation hypothesis requires

that the stimulated grain and its stimulator or parent have a (111) slip plane in common, and this (111) plane will, of course, be the twinning plane. In order for the dislocations to move in a proper direction, this (111) plane must be approximately normal to the interface between the two grains at the moment of stimulation. Thus it might be expected that this (111) plane would contain a line which would approximately bisect the angle of the stimulated grains.

On the other hand, if the "stimulated" grain were to have been formed by the growth fault mechanism, the twinning plane should be approximately perpendicular to the line bisecting the apex of the "stimulated" grain, that is, the (111) twinning plane must coincide with the initial interface between the "stimulated" grain and its parent.

The obvious experiment is to determine the position of the twinning plane for a number of cases of stimulation in aluminum. If its position is reproducible with respect to the apex of the stimulated grain it should be possible to draw a conclusion as to mechanism.

If it develops that the position of the twinning plane between the parent and stimulated grain is more or less random, then, unfortunately, no decision will be possible. This could result from the fragment having been partially surrounded before stimulation occurred. It could equally well have resulted from a growth fault occurring on the side of a projection on the parent grain. These should, however, be more or less random, so that if the position of the common (111) plane in a number of stimulated grains are determined, no false conclusion should be drawn.

In reply to Dr. Treuting's first question, I would agree with his explanation. Where a twinning accident occurs it indicates that a grain was growing approximately normal to that (111) twinning plane. Since the twin is in a symmetrical orientation it will probably continue to grow in the same direction, and, as Dr. Treuting points out, the greater part of its advancing front will approximate the (111) twinning plane so that it will be most probable for the next twin to form on that (111) plane and reproduce the original orientation. In further support of this explanation advanced by Dr. Treuting, I can cite Fig. 5 of the paper. Here, on the right hand side, the grain had grown a great deal before any twinning accident occurred, so the condition that the advancing front of the grain is all approximately parallel to a single (111) plane was not fulfilled. Here, twins on two other octahedral planes formed.

To some extent I think the apparent preponderance of parallel-sided twin bands is an optical illusion, however. Many grains have more than one family of twins, and this definitely means that during growth, a grain which formed a twin on one plane at one place formed a twin on a different plane some place else.

As regards Dr. Treuting's suggestion on the constancy of number of twins, it explains the increase in width to twin bands as the grain size increases, but it still seems the number of twins per grain would be expected to increase, because presumably all those formed when the grain size was small would still be there.

It seems very probable that the variation in intensity of twinning from alloy to alloy is controlled by the surface energy of interfaces. Essentially the same argument as Dr. Treuting uses, and supporting evidence for it, has been presented very recently by R. L. Fullman.

References

[12] W. G. Burgers: *Handbuch der Metallphysik*. Vol. III, p. 2, paragraph 141, (1944) Edward Brothers.

[14] W. G. Burgers and J. J. A. Ploos van Amstd: *Metallwirtschaft* (1938) **17**, p. 648.

[15] R. J. Fullman: *Journal of Applied Physics* (1950) **21**, p. 1069.

[16] W. G. Burgers: *Nature* (1946) **157**, p. 76; *Proc.* Acad. Sci. Amsterdam (1947) **50**, p. 858; *Physica* (1949) **15**, p. 92.

[17] W. May: Thesis, Delft (1950).

[18] A. Guinier and J. Tennevin: *Acta Cryst.* (1949) **2**, p. 133.

[19] J. F. H. Custers and G. W. Rathenau: *Physica* (1941) **8**, pp. 759, 771; *Philips Research Rept.* (1949) **4**, p. 241.

[20] P. A. Beck, Hsun Hu, and P. R. Sperry: *Journal of Applied Physics*. (1949) **20**, p. 633; (1950) **21**, p. 420; *Trans.* AIME (1949) **185**, p. 627; JOURNAL OF METALS (September 1949).

[21] V. Ch. Dalitz and W. G. Burgers: *Proc.* Acad. Sci. Amsterdam (1949) **52**, p. 627.

[22] M. Cook and C. Macquarie: *Trans.* AIME (1939) **133**, p. 142.

[23] T. J. Tiedema: *Acta Cryst.* (1949) **2**, p. 261.

[24] C. G. Dunn and F. Lionetti: *Trans.* AIME (1949) **185**, p. 72, 125; JOURNAL OF METALS (February 1949).

Atomic Relationships in the Cubic Twinned State

by W. C. Ellis and R. G. Treuting

DISCUSSION, H. L. Burghoff presiding

D. Whitwham, M. Mouflard, and **P. Lacombe** (*British Council Research Fellow, Labratoire du Professor Chaudron, Vitry-sur-Seine; Ingenieur de Recherches, Labratoire de Vitry; and Maitre de Recherches, Labratoire de Vitry, Professeur Adjoint de Metallurgie, Ecole des Mines, Paris*)—The authors' work is of great interest in bringing out the geometrical relations existing between twinned lattices, and for the notion of a coincidence superlattice developed from this.

We should like to point out that a similar idea was put forward by Friedel[1] in his book on the subject of lattice merohedrism "merihedrie réticulaire:"—When two crystals A and B are twinned with respect to a mirror plane, there exists a common superlattice, "réseau période," which is independent of the contact surface between the two crystals. The volume V of this superlattice is a simple multiple of the volume v of the lattice of crystals A, or B. (Fig. 5). This "multiple cell" is defined by the twin plane $(p\,q\,r)$ and a row of atoms $[h\,k\,l]$ normal to this plane, the base being taken as the smallest unit (two-dimensional) of this plane. Two cases must be considered. First when the multiple cell, as defined, has no atom site at its center nor at the center of its faces other than $(p\,q\,r)$, the twinning index is defined by $\frac{V}{v}$. In the second case, when one of the two above conditions does not apply, then the twinning index is $\frac{V}{2v}$.

A more intuitive definition of the twinning index would be the proportion of atoms of C_2 which would coincide with those of C_1 when the C_2 lattice is imagined to extend on the other side of the contact surface. In the case of cubic crystals, the twinning index

is given by the relation:

$$\Sigma = (p^2 + q^2 + r_0) \text{ if } \Sigma \text{ is odd.}$$
$$= \frac{p^2 + q^2 + r^2}{2} \text{ if } \Sigma \text{ is even.}$$

$(p\,q\,r)$ being the mirror plane.

Thus for the face-centered cubic system with twinning on the octahedral plane (111), $\Sigma = 3$. Similarly for body-centered cubic twinning on (112), we have also $\Sigma = 3$. These results are confirmed by the atomic patterns given by the authors in which it is demonstrated that, parallel to the twinning plane, one plane in every three coincides (two in every six for the diamond lattice).

The concept of "multiple cell" developed by Friedel and analogous to the coincidence superlattice of Ellis and Treuting, though it explains the general stability of the twinned group, does not forecast the position of the boundary surface between the twins. To the metallurgist, such boundary surfaces present a rather exceptional interest in the study of boundary energy. Thus the authors bring out the fact that the (111) plane of contact for face-centered cubic twinning, and (112) for body-centered cubic twinning, corresponds with conditions of minimum distortion of the lattice, though in both cases the two lattices are symmetrical with respect to either a (111) or a $(11\bar{2})$ plane.

For our part, we have tried to extend this idea of minimum distortion in the case of boundaries between multiple twins, and the lateral interfaces noted by the author.

In an earlier paper, Ellis[4] presented an extremely interesting example of multiple twinning in a germanium ingot, and in the following we use a similar system of symbols. Thus if a crystal A has two first-order twins B_1 and B_2 on two different octahedral planes, then B_1 and B_2 are said to be second-order twins. Thus, we have shown that between B_1 and B_2 there exists necessarily a twin relation with mirror planes (221) and $(11\bar{4})$. Fig. 5 clearly shows this relation. In a general way, the Friedel index of a twin of order p can be determined and from it the Miller indices of possible mirror planes deduced. Thus:

Order of Twinning	Friedel Index	Mirror Planes
1	3	(111) or (112) (equivalent)
2	9	(221) or (114) (equivalent)
3	27	(255) or (511) (first possibility)
		(721) (second possibility)

In their theoretical treatment of grain boundary energy as a function of boundary and grain orientation, Shockley and Read[5] have directed attention to the special interest of twinned lattices with the consequent possibility of realizing boundaries of low energy other than the twin plane (energy cusp boundaries). Such boundaries or planes of good atomic fit are the lateral twin interfaces given by the authors. The number of such possibilities is infinite but in practice the surfaces of interest are thought to be limited to planes of high atomic density. Stereographic projections for first, second, and third-order twinning enable the indices of planes which are parallel in the two lattices to be determined; and all such planes are possible lateral interfaces of the twin.

In the first place our attention was directed to the interfaces of second and third-order twins as it was believed that the particularly low energy of the (111) boundary would tend to suppress the appearance of other cusp boundaries in first-order twins. With this in mind, we attempted to interpret the crystal orientations in the micrograph of germanium given by Ellis.[4] The large crystal A (Fig. 6) has contacts only with twins B_1 and B_2 following the lettering, but we have assumed a third contact with B_3 at the top left hand

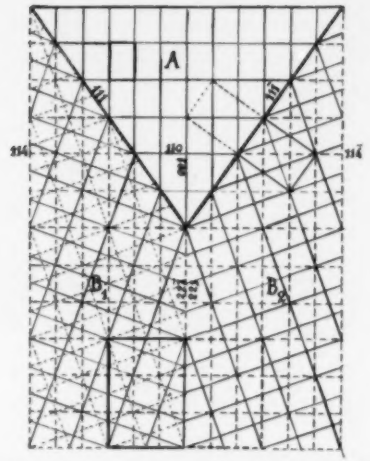

Fig. 5—Diagram showing first-order twinning between lattices A and B_1 (111), A and B_2 $(11\bar{1})$, and the resulting second-order twin B_1B_2 with mirror planes (221) and $(11\bar{4})$.

The section shows the $(1\bar{1}0)$ plane parallel in all three crystals with the multiple cells of Friedel for AB_1 and for B_1B_2 in thick solid lines. The three lattices are shown by solid lines while the prolongation of a lattice is marked by dashed lines.

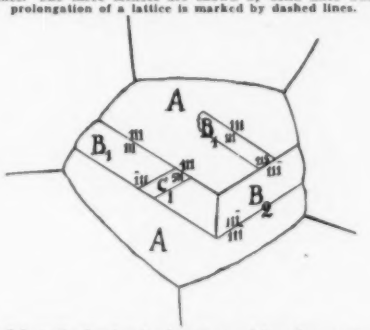

Fig. 6—Schematic drawing to show types of boundary contact between second-order twins.

B_1 and B_2 are first-order twins of A, and C_1 is a first-order twin of B_1; B_1B_2 and AC_1 are thus second-order twins.

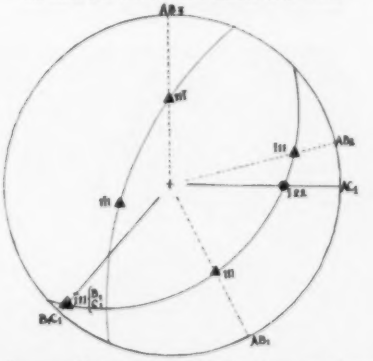

Fig. 7—Stereographic projection to fix the orientation of crystal A in the micrograph of Ellis, from the trace of (111) twin planes between AB_1, AB_2, and AB_3.

The (122) mirror plane of the second-order twin AC_1 is seen to lie on the normal to the boundary between A and C_1. Solid triangle —(111) poles of crystal A. Solid square in triangle—(111) twin plane for B_1C_1.

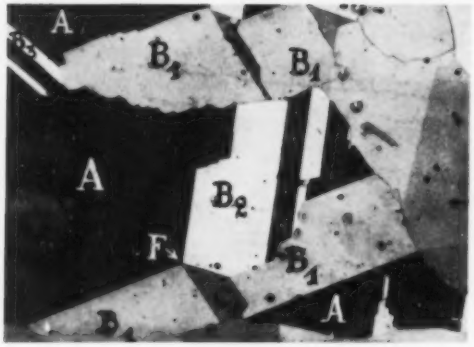

Fig. 8—Multiple twinning in copper sheet specimen recrystallized after a small permanent extension.

B_1, B_2, and B_3 are first-order twins of A, while C_1 is a first-order twin of B_1 (or third-order twin of B_2). Note the point of convergence, F, of the four crystals, A, B_1, B_2, and C_1. X60

side of the photograph, where the similarity of tint and parallelism of boundaries A-B_2 would appear to indicate another part of crystal A. Thus in the stereogram (Fig. 7), we have plotted the (111) poles of crystal A and indicated the three twin planes. It will be remarked immediately that the twin boundary between B_1 C_1 becomes identifiable with the (111) pole of crystal B_1; which encouraged us to believe that the construction used was sound. The crystals A and C_1 are automatically second-order twins with two possible mirror planes (221) and (114). Finally the normal to the boundary A-C_1 has been traced on the stereogram and is seen to pass through the pole of the mirror plane (221) suggesting that the composition plane for this second-order twin is the mirror plane with perfect coincidence of all atoms. We would be very interested to know if our construction is in agreement with the orientations determined by X-rays, and to know whether the boundaries shown have been examined in detail.

The large number of twins found in the germanium ingot has led the authors to suggest that the diamond cubic lattice is particularly favorable for this phenomenon. We should like to point out, however, that numerous twins have also been observed in aluminum, in certain cases of semicontinuous casting.[10] In addition, we have found that the formation of twins of different orders is also demonstrated by the recrystallized structures of face-centered cubic metals such as copper, aluminum, and stainless steel (18/8). One such example is shown in Fig. 8, taken from a copper sheet specimen which had been elongated 1.5 pct and then annealed at 900°C to obtain large crystals, after the method of Carpenter and Tamura.[12] The large crystals so obtained are not immediately evident as they are almost always subdivided into a system of multiple twins. The size of the individual twins was too small for convenient examination by the Laue method, but the problem of determining orientations was considerably simplified by forming a thin sulphide film[13] on the surface. As all grains having a given crystal plane parallel to the surface develop the same interference color, we preferred examination in polarized light because only those grains of the same orientation (in three dimensions) are similarly colored (see Fig. 9). Evidently for a precise determination of orientation relationships it was necessary to choose grain groups in which at least one grain had accompanying twins showing the trace of three different (111) planes.

The stereogram of Fig. 10 has been constructed in this way making use of the (111) twin boundaries between AB_1, AB_2, AB_3. The orientation relationships may thus be represented:

$$\begin{array}{ccccc} B_3 & - & A & - & B_1 & - & C_1 \\ & & | & & & & \\ & & B_2 & & & & \end{array}$$

with boundary contacts between the second-order twins B_1 B_2, the third-order twins C_1 B_3, as well as the remaining first-order twins. The micrograph shows a number of phenomena which are typical in the sense that they occur frequently.

1—The boundary surfaces between twin crystals of the second and third order do not coincide with the possible mirror planes. Whenever the contact is not a plane one, at the magnification used, it is of course not possible to determine the crystal surfaces involved. A number of plane surfaces have nevertheless been observed of which we mention particularly the contact $(111)_A$ $(115)_B$, because of its frequent occurrence and as evidence of a boundary mentioned specifically by the authors, to demonstrate the exact coincidence of atoms possible on a lateral interface though applying to only one third of the atoms, due to the difference in atomic density for the two planes.

2—The surface between first-order twins is in large part the (111) twin plane but a number of other planes of contact were observed. Thus a boundary which at low magnification was apparently curved was often found to consist of series of small steps at a much higher magnification. One such example taken from a twin in aluminum is shown in Fig. 11.

3—Finally, an example is shown of four boundaries meeting in a single point. As this point of convergence was conserved after several successive polishing op-

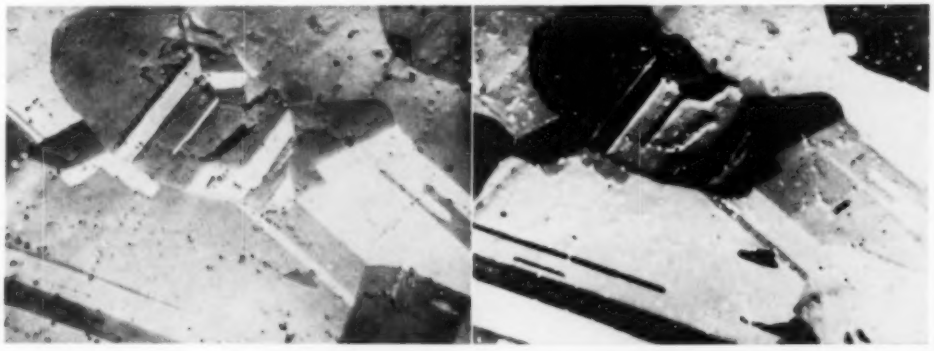

Fig. 9—Micrograph of copper carrying a thin sulphide film for recognition of grains of the same orientation by examination in polarized light between crossed nicols. X60.

Owing to the difficulty of reproducing colored photographs, Fig. 9 was replaced by two black and white photographs of the same grain group as seen in ordinary and polarized light. Difference in contrast is apparent but the wider variety of tints and color sensitivity cannot be appreciated.

erations, it is deduced that the four surfaces must meet in a row of atoms. Knowing that three of the four surfaces are in fact (111) twin planes, it becomes evident that the row of atoms corresponds to a [101] direction which is the zone axis to the three (111) planes. Such an arrangement can therefore only occur when the third-order twin between $C_1 B_2$ is of the type with mirror planes (511) — (255); and not for the alternative (721) twin.

As already noted, our observations were made on specimens which had been recrystallized and thoroughly annealed, suggesting that such structures are comparatively stable. That the boundary between first-order twins so often consists of a series of different plane junctions, which meet in an edge row of atoms, is an interesting confirmation of the theoretical forecast by Shockley and Read[9] that certain boundary positions produce cusps in their energy-orientation curve.

Without specifying any precise mechanism of twin formation, it seems nevertheless probable from the morphology of multiple twin groups that whereas first-order twins are generated directly from a primary crystal *A*, second and higher order twins are the

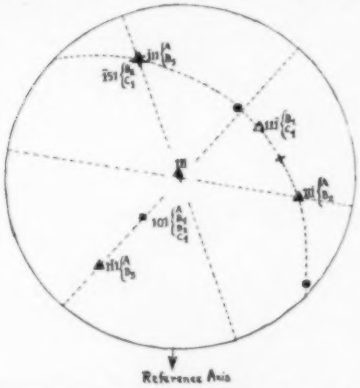

Fig. 10—Stereogram constructed from the traces of twin planes AB_1, AB_2, and AB_3 of Fig. 8.
Solid triangle—(111) poles of crystal A. Open circle in triangle—(111) twin plane of first order twin B_1C_1. Solid circle—Mirror planes (114) and (221) of the second-order twin B_1B_2. Greek cross—Mirror planes (115) and (552) of the third-order twin C_1B_2. Solid square—direction [101] common to the four crystals, A, B_1B_2, C_1.

incidental result of junction between two such twins B_1 and B_2.

In the latter case, the junction surface may or may not have any special orientation as demonstrated by the scheme of Fig. 6. Whether such boundaries can move to some other position, representing lower energy, is not known but is now being studied. This question has already been studied in some detail by Dunn and coworkers[14] for the body-centered cubic system (iron-silicon).

W. C. Ellis and **R. G. Treuting** (authors' reply)—The discussion of Messrs. Whitman, Mouflard, and Lacombe is a valuable addition to the paper, particularly appreciated in that it offers experimental evidence in support of the thesis projected by the authors. We are also grateful to the discussers for making available in English so concise and illuminating a résumé of the earlier exposition of coincidence sites and multiple cell structure in twinned lattices by Friedel. This reference, we regret, was overlooked.

Professor Lacombe and his colleagues are entirely correct in their deductions of the correlations of twin relations and interface traces in the micrograph in an earlier paper[4] by one of the authors. X-ray evidence, not included in the earlier paper, attests to this concordance. The straight portion of the second-order juncture trace, A-C_1, is consistent with a {221} plane, one

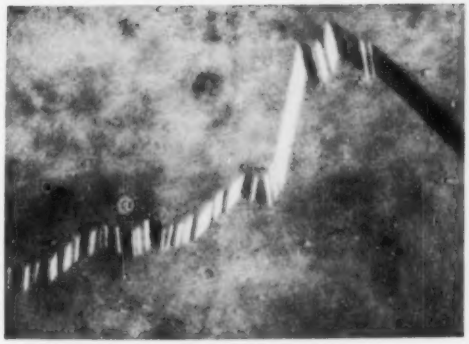

Fig. 11—Boundary between twinned crystals of aluminum, apparently curved at small magnification, but resolved into a series of steps parallel to different crystal planes.
The boundary appears thick under the oblique illumination used because the twin plane lies almost parallel to the surface. X2000.

of the mirror planes of regions A and C_1. We had been discouraged from making a point of this, however, since the A-C_1 juncture appears curved at low magnifications over a considerable portion of its extent. The curved portion conceivably may consist of distinct crystallographic segments to be revealed only by very careful surface preparation and examination at high magnification. This is an attractive possibility; but we have not yet made such examinations.

The discussers have added a welcome reference (reference 10) to the occurrence of twins in semicontinuously cast aluminum. We do not think that this seriously weakens our suggestion that the diamond cubic structure is particularly favorable for twinning, but rather strengthens it. The aluminum ingot referred to appears to be made up in the central portion of long parallel natural grains or crystals each of which is twinned. The slice from the germanium ingot, however, consists entirely of regions in multiple twin relationships. This multiple twin relationship has more recently been confirmed throughout an entire ingot and may quite confidently be presumed general.

In the course of following the interesting deductions of Professor Lacombe and his colleagues with respect

Fig. 12—Stereographic projection constructed from traces in Fig. 8 to illustrate types of coincidence at lateral twin boundaries.

to the twinned copper sheet of Fig. 8, we have reconstructed the stereographic representation of their Fig. 10 employing also normals to additional boundary traces as directly measured on the micrograph. It is evident that the rotations generating B_1 and B_2 from A_1 and C_1 from B_2, can all be taken to be 70°32′ each about the common pole [101], which is the conserved line of intersection of four boundaries pointed out in discussion.

We first directed our attention to the boundary between the third-order twins B_1-C_2, which appears fairly straight. We succeeded in ascertaining only that it coincides with neither the {115} nor the {525} mirror plane between these orientations in agreement with the findings of the discussers. This boundary could be a $(11\bar{1})$ plane of B_2, but seems to have no index pair low for both orientations.

On the other hand, the lateral boundaries between first-order twin pairs A-B_1 and B_1-C_2, the loci of whose normals are shown in Fig. 12, are very closely consistent with, respectively, the planes $(57\bar{5})$ of A and $(13\bar{1})$ of B_2, and the planes $(\bar{1}41)$ of B_1 and $(10\bar{1})$ of C_1. Both these pairs, as well as the {111}:{115} type, lie in the common [101] zone, which thus seems to be experimentally indicated a favorable one for the occurrence of coherent lateral boundaries. The $(575)_1$:$(131)_2$ is a lateral twin boundary also found in copper by Fullman[15] in his extensive examination of grain interfaces, but this is the only pair of low-indexed planes consistent with any of the lateral twin boundaries observed by him.

The statement by the discussers that second and higher order interfaces are incidental junctures between directly generated first order and successive first orders is not to be contradicted by the evidence for copper here presented. The case for germanium may be different: here all orientations in the ingot seem interrelated through sequences of twinning. It is not inconceivable that in the diamond cubic lattice second or higher orders of twins are formed simultaneously or in direct sequence in the course of solidification.

References

[9] G. Friedel: *Leçons de Cristallographie*. Paris 1926. (Edit. Berger Levrault).

[10] W. Shockley and W. T. Read: *Physical Review* (1949) **75**, p. 692; and (1950) **78**, p. 275.

[11] J. Herenguel: *Revue Metallurgie* (1948) **45**, p. 139.

[12] J. Herenguel and P. Lacombe: *Comptes Rendus* Acad. des Sciences (March 1949) **228**, p. 846.

[13] H. C. H. Carpenter and S. Tamura: *Proc.* Royal Soc. London (1927) **113A**, p. 161.

[14] P. Jacquet: *Revue Metallurgie* (1945) **42**, p. 133.

[15] C. G. Dunn, F. W. Daniels, M. J. Bolton: *Trans.* AIME (1950) **188**, p. 368; JOURNAL OF METALS (February 1950).

[16] R. L. Fullman: Private communication.

Graphite-Rod Hairpin-Resistor Radiation Furnace for High Temperatures

by W. J. Kroll, W. W. Stephens, and J. P. Walsted

DISCUSSION, J. P. Nielsen presiding

C. M. Decroly *(University of Brussels, Belgium)*—W. J. Kroll and his collaborators are to be congratulated for the beautiful piece of work they are performing at the Bureau of Mines Experiment Station at Albany, Ore. The furnace they describe in their paper is quite interesting and the use of the hairpin graphite resistor is a very good solution of the problem of heating such a furnace. The use of that kind of resistor is not altogether new. In our researches on the thermal metallurgy of zinc carried out in collaboration with Professor O. Dony[8] before World War II in our laboratory, we systematically made use of such types of resistor. They were made by cutting zig-zag graphite plates of the desired thickness with allowance for an increased area at the contact with the water-cooled connections with the copper conductors.

We used them either for internal or external heating for power input up to 20 kw. One of our furnaces was heated with two resistors about 47 in. long. Providing the thickness of the graphite is sufficient, there is no special danger of breakage. The advantages of such resistors are emphasized by the authors. The increase of resistance that can be obtained is very interesting because it is possible to avoid the purchase of a special high intensity transformer. Fig. 3 shows one of the resistors we used in one of our zinc furnaces.

W. J. Kroll (authors' reply)—Professor Decroly's observation that the use of a slotted graphite resistor to heat electric furnaces, such as the one described by the authors, is not entirely new, is quite true. Such resistors were used some fifty years ago and the early ironing irons, proposed to housewives around the year 1906, i.e., before the arrival of nichrome resistor elements, were heated with graphite grids precisely of the form recommended later by Professor Decroly himself. Whether such resistors are made by slotting plates or tubes does not matter. The Arsem furnace is another typical example of slotting a graphite resistor. The novelty claimed does not reside in the resistor, but in its use for a specific purpose and in the solutions of technical problems concerning its application. Professor Decroly's resistors would probably not perform too well in the high temperature zirconium carbide furnace because of poor contact resulting from the use of plates and high voltage caused by the high resistance. The split rod is simpler, less sensitive, offers better contact opportunities, and has a sufficiently low voltage to prevent arcing in the slot, a very important item when considering the high temperature involved.

Fig. 3—Resistor used in a zinc furnace.

[8] O. Dony and C. M. Decroly: Recherches Théoriques et Expérimentales sur la Métallurgie Thermique du Zinc. Liége (1933).

Ignition Temperatures of Magnesium and Magnesium Alloys

by W. Martin Fassell, Jr., Leonard B. Gulbransen, John R. Lewis, and J. Hugh Hamilton

DISCUSSION, J. P. Nielsen presiding

T. E. Leontis *(The Dow Chemical Co., Midland, Mich.)*—This paper is of particular interest to me because of my own work with F. N. Rhines on the oxidation of magnesium and magnesium alloys a few years ago. The authors are to be complimented on their development of an accurate and reproducible technique for measuring ignition temperatures and on their comprehensive study of the many variables that affect the ignition temperature of magnesium.

It is indeed gratifying to see that they have obtained a good correlation between ignition temperatures and the oxidation rates reported by us. The correlation is valid not only with composition within one alloy system but also between alloy systems; that is, alloying elements which effect the greatest increase in oxidation rate also produce the greatest decrease in ignition temperature.

There are a few points upon which I would like to comment. In attempting to correlate ignition-temperature data, one must be sure that the same definition of this quantity is used by all investigators. It does not appear to me that such is the case in the authors' comparison of their data with the theoretically calculated values of Eyring and Zwolinski. The equation derived by these investigators defines the ignition temperature, T_a, as the temperature at the gas/oxide interface, whereas the present authors use the metal temperature as the criterion for ignition. The contradiction in the effect of oxide-scale thickness on ignition temperature between the predictions of the Eyring-Zwolinski equation and the observations reported in this paper indicate that some variable has not been taken into consideration. Could that be the geometry and size of the specimen? There is a marked difference in the type of specimen used in this investigation and that used in our work which formed the basis of Eyring and Zwolinski's theoretical treatment. Another factor which plays an important role in ignition is the vapor pressure or the rate of vaporization. Combustion can safely be assumed to take place in the vapor phase by the reaction between vaporized magnesium and oxygen. Thus, a more accurate theoretical analysis may be made on the basis of the rate of vaporization which may be the controlling rate of the process.

The effect of a large number of alloying elements on the ignition temperature has been reported in this paper, but beryllium was not included. Practical experience dictates that beryllium markedly decreases the burning tendency of magnesium. I was wondering if the authors plan to study the effect of beryllium in their future work.

The authors predict that concentrations of sulphur dioxide in the furnace atmosphere greater than 5.8 pct would be expected to increase the ignition temperature to values still higher than those they measured. I would like to mention that large concentrations of sulphur dioxide markedly increase the rate of combustion of magnesium once ignition has started. Although it has been shown in the paper that the ignition temperature of magnesium in oxygen increases with increasing sulphur dioxide content up to about 1 to 2 pct, in practice relatively low-melting commercial cast alloys (AZ63A and AZ92A) are being continuously heat treated at temperatures just below the melting point in air containing 0.5 to 0.75 pct SO_2.

In regard to the change in color of the oxide scale observed on magnesium and magnesium alloys just prior to ignition, I would like to mention that in our work alloying elements were found to color the usually white magnesium oxide even though ignition did not occur. For example, the oxide formed on Mg-Al alloys was gray, increasing in intensity with aluminum content in the alloy.

Finally, I might suggest that the authors indicate their source of the value of 0.8 g per cc for the density of MgO as it is formed on magnesium upon oxidation at elevated temperatures.

W. M. Fassell, Jr. (authors' reply)—The comments by Dr. Leontis are very excellent ones and I will attempt to answer them in order.

First, the problem of ignition of magnesium is a rather difficult one since many factors are involved. Concerning the comparison of the T_a in the Eyring-Zwolinski equation, eq 4, with the experimentally determined values, it will be noted that the calculated and experimental values of the ignition temperature in Table I are not self-consistent. In the case of the 1.78 pct Al-Mg alloy the calculated value is 49°C below the experimental value; for the 3.81 pct Al-Mg alloy, 122°C below the experimental value; for Mg with 5×10^{-7} cm film, 19°C above the experimental value; for Mg with 2×10^{-4} cm film, 28°C below the experimental value. Thus, if it were merely a matter of difference of location of temperature measurement the calculated ignition temperature would always be below the experimental value, the difference being due to the thermal gradient through the oxide film.

The possibility of a thermal gradient in the magnesium metal must be considered. From Carslaw and Jaeger,[16] it can be shown that the maximum temperature gradient that could exist between the oxide-metal interface and the center of the sample is of the order of 0.01°C.

The geometry and size of the specimen could certainly have some effect on the ignition temperature. The equation for ignition that has been proposed in reference 14 is of the following type containing terms to account for this and other factors:

$$\Delta H\, v(T) = Cp \frac{M}{A} \frac{dT}{d\tau} + J(T - T_s) + \Sigma \Delta H_i \cdot M$$

where ΔH is the heat of reaction, $v(T)$ is the velocity of the reaction at temperature, Cp is the heat capacity of sample, M is the mass of sample, A is the area of sample, τ is time, J is the total coefficient of heat transfer outward from the reaction zone, T_s is the temperature of the bath or furnace, and ΔH_i is the heat associated with any phase change involved. Prior to the instant of ignition, the vapor pressure of magnesium is of no special significance. After ignition, neither eq 4 nor the above equation is applicable. The actual combination of magnesium cannot safely be assumed to take place in the vapor phase.

While experimental data is lacking to support a hypothesis that ignition does or does not occur in the vapor phase, some observation on the pressure ignition experiments may be of interest. At high oxygen pressures, once ignition has occurred, the reaction of magnesium with oxygen approaches near explosive violence, the entire sample being consumed in probably less than 1 sec. At atmospheric pressure it usually requires 15 to 20 sec. Thus it appears that the oxygen concentration becomes the rate determining factor. Further, if burning magnesium is observed through darkened glass (Lincoln Super-Visibility Shade No. 12) the magnesium sample is very much hotter than the "smoke" and the outline of the sample is retained perfectly. No "flame" is visible above the metal.

No work was done on Mg-Be alloys. We do, however, intend to study this problem in the near future.

[16] H. S. Carslaw and J. C. Jaeger: *Conduction of Heat in Solids*. Oxford (1947), p. 275, eq. 2. Clarendon Press.

Concerning the AZ63A and AZ92A Mg alloys, I assume that you are giving them a solution heat treatment which normally is conducted just below the solidus temperature. Ignition in composition range of AZ62A and AZ92A occurs in oxygen between the solidus and liquidus temperatures. Thus it is understandable that no difficulties are encountered.

The value of 0.8 g per cc for the density of MgO as it is formed on magnesium upon oxidation was calculated from reference 1, Fig. 16.

Mechanical Properties of Stainless Steel Powder

by Arthur H. Grobe and George A. Roberts

DISCUSSION, L. A. Barera presiding

H. H. Hausner *(Sylvania Electric Products Inc., Bayside, N. Y.)*—I tested the 18-8 stainless steel powder described by Grobe and Roberts and the results were excellent. The powder was compacted and sintered in purified hydrogen to a very low density (approximately 20 pct and more porosity). Where the other powders show very little ductility when sintered to such a low density, the described stainless steel was surprisingly high in ductility. I would appreciate it if the authors could give us some data on a similar powder but without silicon and also data on 430 stainless steel powder.

H. S. Kalish *(Sylvania Electric Products Inc., Bayside, N. Y.)*—I should like to verify the excellent results obtained by Grobe and Roberts with their prealloyed stainless steel powder. It seems to me, however, that their data are conservative and that even better densities and higher tensile strength can be obtained with these powders by the selection of proper particle size fractions.

The accompanying data were obtained by sintering compacts pressed from the powder made by Vanadium-Alloys Steel Co. to 0.8 in. in diam about ¼ in. high in a cylindrical double action die without the use of lubricant. The compacts were sintered for 1 hr at 2370°F in hydrogen purified by passing it through a Deoxo unit (palladium catalyst) and a Lectrodryer.

Even the density obtained using the as-received (—100 mesh) compacted at 40 tsi was quite high as was the hardness. This indicates that by increasing the sintering temperature slightly above 2350°F the coining and subsequent secondary sintering operation can be avoided.

With the — 325 mesh fraction, however, very much higher density can be obtained and a high hardness.

Powder Fraction	Compacting Pressure, tsi	Pressed Density, g per cm³	Sintered Density, g per cm³	Hardness Rockwell, F
—100 mesh (As-received)	40	5.94	6.77	86.9
—270 + 325 mesh	40	5.81	6.85	92.3
—325 mesh	40	5.88	7.35	99.6
—100 mesh (As-received)	60	6.51	7.16	97.0
—270 + 325 mesh	60	6.49	7.26	98.9
—325 mesh	60	6.43	7.52	102.3

I have no tensile data to present, but I feel that it is not too optimistic to expect that unusually high tensile strengths and good ductility can be obtained in this sintered material on the basis of the density and hardness data.

The sintered stainless steel made by the above-described methods came out of the furnace very bright and clean. The purified hydrogen atmosphere is important in sintering stainless steel to reduce the oxide present in the powder. The result of such a sintering is good densification and good ductility of the sintered product.

G. A. Roberts (authors' reply)—We are greatly indebted to Messrs. Hausner and Kalish for their discussions of our paper. Their encouraging remarks are greatly appreciated and their confirmatory data will do much to add to the value of the paper. At the present time it is impossible to provide complete data on a similar stainless steel powder without silicon, but we do know that, in general, the properties are slightly inferior. Data on such a powder and on other stainless steel types are to be published in the near future.

Rate of Sintering of Copper Under a Dead Load

by F. N. Rhines and H. S. Cannon

DISCUSSION, L. A. Barera presiding

H. H. Hausner *(Sylvania Electric Products Inc., Bayside, N. Y.)*—The results reported by the authors are interesting because they contribute some information on the principles of sintering and also because of a certain practical value for the manufacture of powder metallurgical parts in production. Pressed powder compacts are frequently sintered in a boat in several layers so that the lower layers are actually sintered under the weight of the upper layers and, therefore, are frequently deformed. The authors gave information on this deformation process by determining the effect of the load on the density. The experimental setup of the authors, however, has a disadvantage—that the sintering occurred in a cylindrical container so that the deformation was stopped in the direction of the diameter. The authors should have rather called this a study of hot-pressing than of sintering.

I want to call the attention of the authors and others interested in sintering under load to the experimental work described by Dawihl and Rix.[1] These authors sintered cylindrical compacts under a lengthwise tensional load of 0 to 25 g and found that the shrinkage in length and diameter changes considerably with the load, but that the volume shrinkage is affected very little by the load.

H. S. Cannon (authors' reply)—We wish to thank Dr. Hausner for calling attention to the experimental work of Dawihl and Rix. The fact that they found volume shrinkage little affected by varying tensional loads during sintering seems to support the contention that the forces due to loading are equivalent to and additive to the forces which cause densification. This contention is the basis of our comparison of sintering and creep.

[1] W. Dawihl and W. Rix: Effect of Tensional Forces on the Shrinkage of Metal Powder Compacts during Sintering. *Ztsch. f. Metallkunde* (1949) 40, pp. 115-119.

AIME OFFICERS:

President—Willis McG. Peirce
Vice-Presidents—A. B. Kinzel, Philip Kraft, R. W. Thomas, J. L. Gillson, M. L. Holder
Vice-President and Treasurer—Andrew Fletcher

AIME STAFF:

Secretary—E. H. Robie
Ass't. Secretaries—E. J. Kennedy, Jr., Ernest Kirkendall, J. V. Beall, J. B. Alford, R. E. O'Brien
Ass't. to Secretary—H. N. Appleton
Ass't. Treasurer—H. A. Maloney

aime NEWS

AIME Dues Bills To Members Staggered To Facilitate Handling

Bills for 1952 AIME dues are being sent out from Institute headquarters by alphabetical groups in the closing three months of 1951. With the exception of the Petroleum Branch, those members whose names begin with "A" through "D" will be mailed their statements in October, "E" through "J" in November, "K" through "P" in early December, and "Q" through "Z" in late December. Bills to Petroleum Branch members were not sent out until after decision had been made at the Fall Meeting of the Branch regarding distribution of the statistical volume.

Although according to the bylaws the annual fee is not payable until Jan. 1, prompt payment will make it possible to issue membership cards promptly and to assure no interruption of the despatch of 1952 publications. Mailing of some 20,000 bills must, of course, be preceded by a careful check to see that the amount of each is correct, which takes some time in the aggregate. Also, the proper crediting of dues payments from the same number of members is a job of no mean magnitude, which can be accomplished much better if checks are received over a period of several months.

The statements are made out with the assumption that each member wishes to receive the same publications in 1952 as he did in 1951. If not, the member should correct the bill accordingly. Transactions volumes are billed to members at $3.50 each; annual subscriptions to one or both of the monthly journals in addition to the member's primary choice are $4 each.

Members are urged to *return the complete bill in making remittances.* When payment is made through a company or bank this is particularly necessary to identify the person to be credited, and the coverage of the payment.

Engineering Societies Library Reports 25 Pct Increase In Income

The report of the Engineering Societies Library covering the fiscal year Oct. 1, 1950 to Sept. 30, 1951 shows a 25 pct increase in income from searching, translating, and photo and microfilm copying over last year. Expenses also increased, but not as much as income. As typical of busy times, the number of non-visitors served increased from 14,618 to 16,783, while the number of visitors served decreased from 22,283 to 18,104.

A new photostat machine has replaced one in use for 26 years, and in the first nine months of operation, a cost savings equal to almost ¼ of the purchase price has resulted from the material saving features of the new machine.

Two new monographs were published during the year: "*Hydraulic Transients*," by G. N. Rich, and "*Theory of Elasticity*," second edition, by S. Timoshenko and J. N. Goodier. The Library has received royalties of $8,214.57 since the Monograph series was started in 1931.

Many local library groups visited the Library as is their annual custom. Groups of foreign librarians, documentalists, and metallurgists sponsored by ECA also paid visits this year. Although fewer periodicals are received as gifts each year, the total number of periodicals by subscription, exchange, and gift, has increased from 1367 to 1392.

AIME Officers for 1952 Election

No supplementary nominations for AIME officers for 1952 having been received by September 1, the nominees of the official Nominating Committee are the only candidates in the field, and balloting of the Institute membership is unnecessary. Official announcement of the elections of those whose names were published in the July issue of JOURNAL OF METALS will be made at the Nov. 14 meeting of the Executive and Finance Committees.

By-Law Changes Approved By Board

All changes in the bylaws published in the August issue of JOURNAL OF METALS, were voted by the Board of Directors at their meeting on Sept. 12 and became immediately effective. The only change made from the printed version is the addition, in Art. I, Sec. 8, of the phrase "without payment of registration fee" immediately after the words: "and be privileged to attend meetings of the Institute." In other words, no registration fee may be charged to Student Associates at any AIME meeting. Other changes voted include: Granting a credit on the initiation fee for Member or Associate Member of $2 for each year of continuous and continuing AIME membership as a Student Associate or Junior Member; standardizing the annual dues of Student Associates at $4.50, including an annual subscription to a journal; and extending the 33-year age limit for Junior Membership for those who have been in military service following World War II.

Canadian Institute Ups Dues

A 33 1/3 pct increase in dues has been voted by members of the Canadian Institute of Mining and Metallurgy, effective with 1952. The new dues are $16 for Members and Associates, and $12 for Junior Members and Junior Associates, except that a Junior Member may pay $5 for the 3-year period immediately following graduation from an approved school. The vote was 1140 for the increase, and 61 against.

Members Urged To Participate In Local Civil Defense Activities

The announcement that Russia has tested her second atomic bomb came as no surprise to many government, military, and civilian leaders. The American public, with an 'it can't happen here' feeling, are reluctant to take the necessary steps to prepare against the possibility of an atomic attack against these shores. Although there is no direct defense against the bomb, a prepared and calm public can greatly reduce the death and chaos that would result from an attack. The Civil Defense Program can only be successful with the wholehearted cooperation of alert citizens.

AIME members are urged to engage actively in the civil defense activities in their communities. Their training should make them valuable for rescue squad training and first aid training. Local Sections can put on programs with the cooperation of Federal and State Civilian Administrations. Information kits and motion picture films are available for instruction.

R. W. Smith, AIME representative at the Civil Defense Conference in Washington, emphasized that Civil Defense is not only for cities or industrial areas. These areas will depend for help in an emergency from areas 100 or 150 miles around. Mining districts could give needed assistance in aiding neighboring cities, in times of necessity and evacuation.

Geological Congress Announced

The First Circular concerning the 19th International Geological Congress, to be held in Algiers in 1952, is now available. The Secretary, AIME, has a small supply of the circulars and will send a copy to any AIME member as long as the supply lasts. Or copies may be secured direct from R. Lafitte, General Secretary of the Algerian Organizing Committee, Faculté des Sciences, Alger (Algeria).

J. F. Myers To Receive Richards Award

J. F. Myers, superintendent of concentration for the Tennessee Copper Co., Copperhill, Tenn., has been selected to receive the Robert H. Richards Award for 1952. The honor will be conferred at the Institute's Annual Banquet, February 20, in New York. The Award recognizes "achievement in any form which unmistakably furthers the art of mineral dressing in any of its branches." Jack has long been active in AIME affairs, and was Chairman of the Minerals Beneficiation Div. in 1948. He is currently a member of the Board of Directors.

Please Specify Branch Affiliations

When notifying AIME headquarters of a change of address, or of company position or affiliation, *please mention the Branch of the Institute to which you belong—Mining, Metals, or Petroleum.* This will make for a more expeditious handling of the change and will facilitate the preparation of various reports.

DeGolyer Elected Honorary Member

Everette Lee DeGolyer was elected an Honorary Member of the AIME at the meeting of the Board of Directors on Sept. 12. Dr. DeGolyer brings the roll of living Honorary Members up to the limit of twenty as provided by the bylaws. He was President of the AIME in 1927 following a six-year term as Vice-President. For years he has headed the firm of DeGolyer & MacNaughton, in Dallas, practically all members of which have been active in AIME affairs. In 1940 Dr. DeGolyer was Anthony F. Lucas Gold Medalist. The formal award will be made at the AIME Annual Banquet at the Waldorf in New York, Feb. 20, 1952.

Cooley Joins Publication Staff

Charles M. Cooley, assistant chief engineer of the Climax Molybdenum Co., Climax, Colo., has been engaged as assistant editor of MINING ENGINEERING. Mr. Cooley reported for duty early in October. He received a degree in metallurgical engineering from the College of Mines and Metallurgy of the University of Texas at El Paso (now Texas Western) in 1947, and was president of the school engineering society. He first worked with Colorado Fuel & Iron at Pueblo before joining Climax 3½ years ago.

Coming Events

Nov. 2, AIME, Pittsburgh Local Section and Open Hearth Local Section, annual off-the-record meeting, William Penn Hotel, Pittsburgh.

Nov. 7, AIME, Chicago Section, Chicago Bar Assn., 29 South La Salle St., Chicago.

Nov. 8-9, ASTM, Joint Engineering Societies' Symposium on Corrosion, Rodger Young Auditorium and Biltmore Hotel, Los Angeles.

Nov. 14, AIME, San Francisco Section, Students' Meeting, Stanford University, Stanford, Conn.

Nov. 25-30, ASME, annual meeting, Chalfonte-Haddon Hall, Atlantic City.

Nov. 26-Dec. 1, Chemical Industries Exposition, Grand Central Palace, New York.

Nov. 28-30, Scientific Apparatus Makers Assn., midyear meeting, laboratory apparatus, optical, nautical, aeronautical, and military instrument sections, Hotel New Yorker, New York.

Nov. 29, AIME, Buffalo Section, Open Hearth Committee, Statler Hotel, Buffalo, N. Y.

Dec. 2-5, American Institute of Chemical Engineers, annual meeting, Chalfonte-Haddon Hall, Atlantic City.

Dec. 3, AIME, Chicago Section, Chicago Bar Assn., Chicago.

Dec. 6-8, AIME, Electric Furnace Conference, William Penn Hotel, Pittsburgh.

Dec. 26-31, American Assn. for Advancement of Science, annual meeting, Philadelphia.

Dec. 27-28, American Chemical Society, Div. of Industrial and Engineering Chemistry, symposium on nucleation, Northwestern University, Evanston, Chicago.

Jan. 9, 1952, AIME, Chicago Section, Chicago Bar Assn., Chicago.

Jan. 16-18, Society of Plastic Engineers, Inc., annual national technical conference, Edgewater Beach Hotel, Chicago.

Feb. 18-21, AIME, annual meeting, Hotel Statler, New York.

Mar. 3-7, ASTM, spring meeting and committee week, Hotel Statler, Cleveland.

Apr. 25-26, AIME, New England Regional Conference, Kenmore Hotel, Boston.

May 6-9, Scientific Apparatus Makers' Assn., annual meeting, Edgewater Beach Hotel, Chicago.

May 22-24, American Society for Quality Control, annual convention, Onondaga County War Memorial, Syracuse, N. Y.

June 23-27, ASTM, 50th anniversary meeting, Hotel Statler, New York.

July 1-Sept. 30, Centennial of Engineering, Chicago.

Personals

JOHN W. HANLEY

ALLEN H. ENGELHARDT

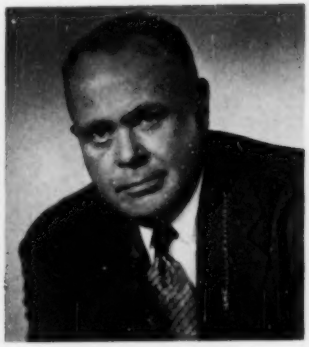

LLOYD R. JACKSON

Allen H. Engelhardt has assumed the post of manager of operations for the Cerro de Pasco Corp. and will be in charge of the corporation's mining, smelting, and refining operations in Peru. He is replacing **A. Russel Merz** who is to undertake new duties at the head office in New York. **John W. Hanley,** superintendent of smelters and refineries of the Cerro de Pasco Corp. since 1949, has been appointed assistant manager of operations succeeding Mr. Englehardt.

Lloyd R. Jackson has been named an assistant director of Battelle Memorial Institute, Columbus and will handle research coordination. Before joining the Battelle staff in 1935, he was a member of the research staff of the Jones & Laughlin Steel Corp.

Kenneth H. Gayle, Jr. has been elected president of Ingalls Iron Works Co., Birmingham, Ala.

Robert M. Lloyd has been elected vice-president, raw materials, U. S. Steel Co.

George D. White has been appointed associate metallurgist by the Oak Ridge National Laboratory, Oak Ridge, Tenn. **Wimmer J Leonard** has been made metallurgist and **Lee S. Richardson** is now junior metallurgist.

R. E. Zimmerman has been named chief preparation engineer in the coal div., U. S. Steel Co., Pittsburgh.

R. P. Bremner has been appointed assistant to the vice-president in charge of operations for Youngstown Sheet & Tube Co.

M. W. Barlow has resigned from his position as sales manager of British Electro Metallurgical Co., Ltd., Sheffield. He has joined Foundry Services, Ltd., as manager of the newly established ferro alloy div.

Richards H. Harrington, for 22 years with General Electric Co., as a research associate in metallurgy, has organized his own company of metallurgical and professional engineering consultants.

William S. Unger has been appointed deputy, U. S. Chairman, Combined Steel Group, in Germany for the U. S. Dept. of State. He will work on the reorganization of the German iron and steel industry.

R. W. Cahn has joined the dept. of metallurgy, University of Birmingham, England. He was formerly engaged in atomic energy research at Berks, England.

P. J. Cutting, formerly with International Engineering Co., is now affiliated with Morrison-Knudsen International Co., at Camp Kue, Okinawa.

Robert F. Schmidt has been transferred to the Ajax metal div., H. Kramer & Co., Philadelphia.

Ernest W. S. Ward is now associated with the Rhokana Corp., Ltd., Kitive, Northern Rhodesia.

Malcolm F. Parkman has accepted a position with Titanium Metals Corp., Henderson, Nev., as shift foreman. He had been associated with the Combined Metals Reduction Co.

Forbes Wilson is with the Freeport Sulphur Co., New York. He had been with Rising & Nelson Slate Co., Inc., West Paulet, Vt.

John E. Bowenkamp has joined the Freeport Sulphur Co., New York.

Thomas L. Hurst has joined the research dept. of Monsanto Chemical Co., Anniston, Ala.

John Naylor has been appointed field engineer on the construction of a new hydroelectric plant on the eastern slope of the Andes for Cerro de Pasco Corp. He is located at Carhuamayo, Peru.

Charles H. Maak, formerly with Aerojet Engineering Corp., Azusa, Calif., has been made standards metallurgist for Sandia Corp., at the Sandia Base, Albuquerque, N. Mex.

Bleecker L. Wheeler has been elected a vice-president of George A. Armstrong & Co., Inc., New York.

John E. Groves has been appointed director of industrial relations and **Ralph L. Ostrander** has been appointed manager of labor relations, Allegheny Ludlum Steel Corp., Pittsburgh.

H. V. Rasmussen has been appointed executive engineer at the Wellsville, N. Y. plant of Worthington Pump & Machinery Corp.

Dennis Ord has joined Sam Tour & Co., New York. He will be located in the research and development laboratories and will specialize in the chemical analysis of titanium and titanium alloys.

Eugene D. Seraphine has joined the Engineering Manpower Commission of EJC in the capacity of assistant executive secretary.

Joseph W. Gray has been appointed division metallurgist for wire at the Joliet, Ill. works of American Steel & Wire Co.

Phillip R. Kalischer, metallurgist and development engineer, has been made associate editor of *Precision Metal Molding.*

Charles F. Pogacar has joined the metallurgical staff of Atlantic Refining Co., Philadelphia.

Edgar A. Rodruan is chief metallurgist for Donegal Mfg. Corp., Marietta, Pa.

Henry M. O'Bryan has been appointed manager of the physics laboratories, Sylvania Electric Products, Inc., Bayside, N. Y. He had been serving as assistant executive secretary of the Research & Development Board, Washington, D. C.

John D. Paulus has been appointed director of public relations for Jones & Laughlin Steel Corp., Pittsburgh.

Leonard Mark Bianchi is now associated with the General Electric Research Laboratory, Schenectady, N. Y.

Donald E. Nulk is resident chief metallurgist for the Solar Aircraft Co., Des Moines, Iowa.

Doyle Geiselman has joined the Westinghouse Electric Corp., atomic power div., Pittsburgh.

George W. Wunder, National Lead Co., has been made plant manager of the Fernald project, AEC, Cincinnati.

Stanley Garfinkel has been promoted to plating engineer for the Stolle Corp., Cincinnati.

B. R. MacKay, formerly with the American Smelting & Refining Co. is now co-owner and secretary-treasurer of the Starr Brass Foundry & Refining Co., Salt Lake City.

Gordon W. Barr has joined the Western Precipitation Corp., Los Angeles as district engineer.

W. E. Sands is now employed as metallurgist for the Black Rock Mining Corp., Bishop, Calif.

Max Hansen, assistant chairman of the metals research dept., Armour Research Foundation of Illinois Institute of Technology, has been promoted to chairman of the department. He succeeds **Carl Swartz,** who has been named metallurgical consultant.

James Boyd, who is resigning as director of the U. S. Bureau of Mines, is joining Kennecott's executive staff. Dr. Boyd was dean of faculty at the Colorado School of Mines, relinquishing that post in March 1947 to become Assistant to the Secretary of the Interior. A few months later he was appointed director of the U. S. Bureau of Mines.

G. Stanley Fergin, development engineer, Kaiser Aluminum & Chemical Corp., has been transferred to the Mead works reduction plant, Spokane. He was formerly affiliated with the metallurgical research div. at Trentwood.

Douglas Alexander has been awarded a Mond Nickel fellowship. These awards enable the recipient to study and gain experience in some chosen metallurgical field.

Obituaries

Morton T. Pawel (Member 1944) died on July 3, 1951. Mr. Pawel was born at Clearfield, Pa. on Sept. 13, 1920. In 1941 he received the degree of AB, chemistry, from Cornell University and then joined the minerals research laboratory of the Tennessee Valley Authority, Morris, Tenn. He remained here for approximately one year and then did research work on nickel for the minerals research laboratory at Muscle Shoals, Ala. for TVA. In 1942 he was engaged in work at the Bureau of Mines' laboratories and also did work at Oak Ridge and the Bureau of Standards on uranium extractions. Mr. Pawel was in the Army during World War II and following discharge he was employed by the Dorr Co., Westport, Conn. as development engineer.

NECROLOGY

Date Elected	Name	Date of Death
1909	Robert M. Black	Sept. 10, 1951
1923	Walter Lyman Brown	Sept. 5, 1951
1918	Alfred Copeland Callen	July 30, 1951
1948	A. F. Connell	Jan. 1, 1951
1945	John F. Gallie	January 1951
1900	Leonidas C. Glenn	Jan. 11, 1950
1940	C. G. Grim	Sept. 8, 1951
1917	Garnett A. Joslin	Sept. 20, 1951
1916	Albert E. Marshall	Sept. 15, 1951
1907	F. O. Martin	June 30, 1951
1917	Hugh Park	Aug. 26, 1951
1926	Earle S. Porter	Unknown
1920	Eijiro Sagawa	1940

Proposed for Membership

Metals Branch AIME

Total AIME membership on Sept. 30, 1951 was 17,234; in addition 2521 Student Associates were enrolled.

ADMISSIONS COMMITTEE

Thomas G. Moore, Chairman; Carroll A. Garner, Vice-Chairman; George B. Corless, F. W. Hanson, Albert J. Phillips, Lloyd C. Gibson, R. D. Mollison, John T. Sherman. Alternates: A. C. Brinker, H. W. Hitzrot, Plato Malozemoff, Ivan Given, T. D. Jones, and W. A. Clark, Jr.

Institute members are urged to review this list as soon as the issue is received and immediately to wire the Secretary's office, night message collect, if objection is offered to the admission of any applicant. Details of the objection should follow by mail. The Institute desires to extend its privileges to every person to whom it can be of service but does not desire to admit persons unless they are qualified. Objections must be received before the 30th of the month on Metals and Mining Branches.

In the following list C/S means change of status; R, reinstatement; M, Member; J, Junior Member; A, Associate Member; S, Student Associate.

Connecticut
Stamford—Hagglund, Erik H. (C/S—J-M)

District of Columbia
Washington—Inouye, Frederick T. (J)

Illinois
Chicago—Hoover, Helen D. (M)
Chicago, Evergreen—Troy, Walter C. (M) (R, C/S—J-M)
New Douglas—Neel, R. Milton (M)
Riverside—Campbell, George V. (M)
Western Springs—Wickenmeyer, Casper (M)

Iowa
Des Moines—Nulk, Donald E. (J) (C/S—S-J)

Massachusetts
Brighton—Haifawy, Mohamed H. (M)

Michigan
Ferndale—Wilson, Gerald D. (M)

New Mexico
Hurley—Mulholland, Lyle E. (M)
Los Alamos—Schonfeld, Fred W. (M) (C/S—J-M)

Ohio
Columbus—Stacy, John T. (M)

Pennsylvania
Bridgeville—Rebholz, Robert W. (M) (C/S—J-M)
Emsworth—Woofter, Robert A. (M)
Irwin—Sansone, Leonard Francis, Jr. (C/S—S-J)
Philadelphia—Romeo, Frank R. (J)
Philadelphia, Chester—Petroskas, John A. (M) (R, C/S—J-M)
Pittsburgh—Blackburn, Felix E. (M). Horne, Gerald T. (J) (C/S—S-J)

Tennessee
Cipperhill—Querry, William Y. (M)

Utah
Tooele—McFarland, Feyette G. (M)

Canada
Ontario—Evans, Howell T. (J)

Egypt
Cairo—Abdel Fattah, Mohamed A. (J)

Japan
Osaka—Akihiko, Koide (M)

Scotland
Glasgow—Carter, P. Thomas (M)

Sweden
Sandvikens Jernverk—Angel, Tryggve G. (J) (C/S—S-J)

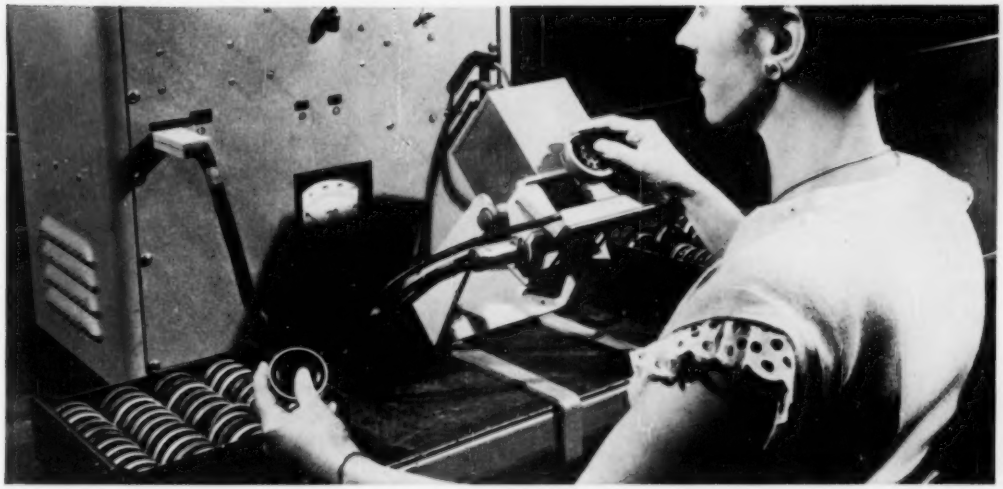

This Western Electric employee mounts a transmitter in the test fixture which is swung down to face an artificial mouth at 45-degree angle, just as transmitters are held in use. More than a million transmitters are tested each year.

This mouth speaks to millions

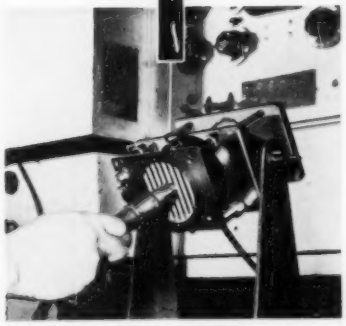

At Bell Laboratories a scientist employs a condenser microphone to check the sound level from another type of artificial mouth, used in transmitter research.

To serve the changing needs of telephone subscribers millions of telephone sets have to be moved each year. Before being put back into service most of them are returned to the Western Electric Company's Distributing Houses where they receive a thorough checkup.

Western Electric engineers needed a rapid method of testing transmitters over a range of frequencies. At Bell Telephone Laboratories, scientists had just the thing—a technique they had devised for fundamental research on transmitters. In co-operation with these scientists, Western Electric engineers developed the practical tester in the illustration.

The transmitter is removed from the handset and put in front of an artificial mouth which emits a tone that swings several times per second over a band of frequencies. A signal lamp tells whether the transmitter is good. Each test takes 5 seconds.

This new tester illustrates how Bell Laboratories research and Western Electric manufacturing skill team up to maintain your telephone service high in quality yet low in cost.

BELL TELEPHONE LABORATORIES

• EXPLORING AND INVENTING, DEVISING AND PERFECTING, FOR CONTINUED IMPROVEMENTS AND ECONOMIES IN TELEPHONE SERVICE

flexible*

accurate*

*Two good words to aptly describe the operation of a *Salem Rotary Hearth Heating Furnace* at work in your plant. Whether your hot-metal operations include piercing, forging, or rolling ferrous or non-ferrous metals, your automatically controlled Salem Rotary will flexibly and accurately adapt itself to large variations in heating and tonnage rates —thus maintaining economy despite downtime for changeover in your metal forming operations. Moreover, you'll reduce scale loss, simplify handling, and save money on labor and maintenance. For greater yield at lower cost, you should be using a Salem Rotary. Write to us.

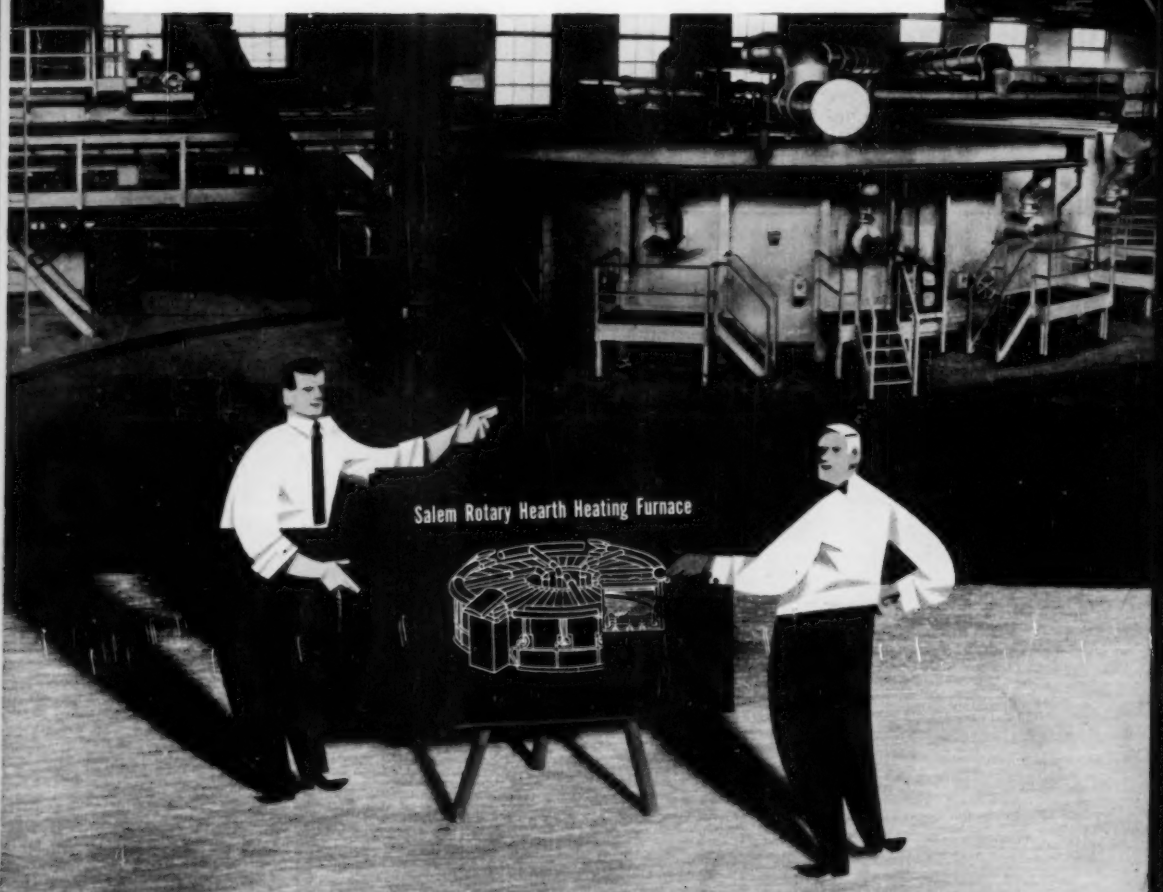

SALEM ENGINEERING DIVISION,

Salem - Brosius, Inc. Salem, Ohio

Affiliates: Brosius Division, Pittsburgh 15, Pa.
Salem Engineering Co., Ltd., Milford nr. Derby, England; Salem Engineering (Canada) Ltd., Toronto, Canada